INVESTIGATION OF DIELECTRIC AND ELASTIC PROPERTIES OF SELECTED DIELECTRIC CERAMICS AND OXIDE GLASSES

THESIS SUBMITTED TO
THE COCHIN UNIVERSITY OF SCIENCE AND TECHNOLOGY
FOR THE AWARD OF THE DEGREE OF
DOCTOR OF PHILOSOPHY

NELSON RODRIGUES

DEPARTMENT OF PHYSICS
COCHIN UNIVERSITY OF SCIENCE AND TECHNOLOGY
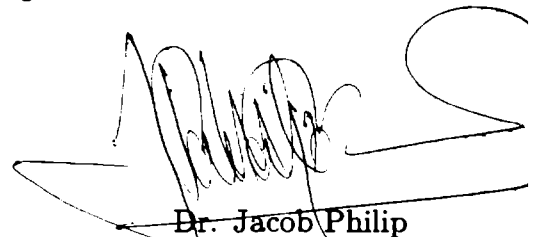COCHIN - 682 022, INDIA

MARCH 1997

DEDICATED TO MY PARENTS

CERTIFICATE

Certified that the work presented in this thesis is based on the bona fide work done by Mr. Nelson Rodrigues under my guidance in the Department of Physics, Cochin University of Science and Technology, Cochin - 22 and has not been included in any other thesis submitted previously for the award of any degree.

Cochin - 682 022

March 15, 1997

Dr. Jacob Philip

Supervising Guide

DECLARATION

Certified that the work presented in this thesis is based on the original work done by me under the guidance of Dr. Jacob Philip, Professor and Head, Department of Instrumentation, Cochin University of Science and Technology, Cochin - 22 and has not been included in any other thesis submitted previously for the award of any degree.
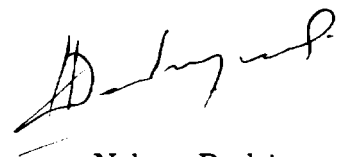
Cochin - 682 022

March 15, 1997.

Nelson Rodrigues

Contents

9 Conclusions 186

Preface

The dielectric and elastic properties are of considerable significance to the science and technology of matter in the solid state. The study of these properties give information about the magnitude of the forces and nature of the bonding between the atoms. Our aim has been to investigate systematically the effect of doping of an appropriate element on the elastic and dielectric properties of selected dielectric ceramics and oxide glasses. These materials have got wide technological applications due to their interesting electrical, optical, thermal and elastic behaviour. Ultrasound propagation and capacitance measurement techniques have been employed for the systematic investigation of the elastic and dielectric properties of selected number of these materials. Details of the work done and results obtained are presented in this thesis.

Among the various techniques available to measure the elastic properties of the solids, the ultrasonic method has proved to be one of the most powerful ones. The ultrasonic technique is nondestructive in nature and the measurements are relatively straight forward to perform. The main advantage of the ultrasonic technique is that both static and dynamic properties can be measured simultaneously. In addition, it is a powerful technique to study elastically driven phase transitions. It enables one to locate transition points, to determine phase diagrams and to make statements about the order of the phase transition. From the temperature variation of the elastic response function, the type of coupling between strain and order parameter involved can be deduced. It is also useful to test the various aspects of modern renormalisation theories like crossover and dimensional effects. The velocity and attenuation coefficients of the ultrasonic waves propagating through a medium are related to the microscopic structure of the materials and they provide valuable information about the structural changes in the system. From their temperature as well as frequency dependence, crucial informations about critical exponents and fluctuations near critical points can be obtained.

The dielectric constant is another important parameter which determines electrical and optical properties of a material. Since the dielectric constant gives information about the nature of the response of a material to an applied electric field at the electronic, atomic and molecular levels, it is one of the first parameters that one measures

i

when a material is prepared. In order to assess the applicability of the dielectric material it is essential to know not only its electrical properties but also its general physical and chemical properties such as mechanical strength, elasticity, conductivity and stability to chemical agents. Studies on the variation of dielectric and elastic properties of dielectric materials with chemical composition and structure will provide clues to synthesise a new material with preassigned properties. Moreover, acoustic and dielectric measurements enable one to investigate the dynamics of low energy excitations in amorphous materials, particularly at low temperatures.

The influence of structure and chemical composition of a material on its elastic and dielectric properties can be studied experimentally by measuring the ultrasonic velocity and dielectric constant as a function of composition. Measurements of these parameters as a function of temperature will give information about the stability, thermodynamics, and related properties which are important from the application point of view.

The samples selected for the present investigations are dielectric ceramics belonging to the groups $Ba_{2-x}Sr_xTi_9O_{20}$, $(Zr_{0.8}Sn_{0.2})Hf_xTi_{1-x}O_4$, $BaLn_2Ti_5O_{14}$ and oxide glasses belonging to the groups $(Bi_2O_3)_{1-x}(CuO)_x$ and $Ba_{1-x}K_xBi\ O_{3-\delta}$ This thesis is divided into nine different chapters as outlined below.

The first chapter provides a general introduction to ultrasonic studies on selected ceramics and glasses and a discussion of elastic wave propagation through isotropic media. A discussion of the dielectric properties and dielectric relaxation are also included in this chapter. General properties of dielectric resonator ceramics and oxide glasses are briefly outlined. The relevance of these measurements at high temperatures to throw light upon the structural transformations in glasses and ceramics are also presented in this chapter. Determination of the dielectric constant of the material from capacitance measurements using parallel plate method, the method adopted to eliminate fringe and stray capacitances are also explained. The general dependence of dielectric constant upon frequency and temperature and their significances are also outlined in this chapter. In addition to these a brief introduction to the nature of the possible transformations in ceramics and glasses with temperature are outlined. Moreover, the

methods of preparation of the samples for ultrasonic and dielectric measurements are included in this chapter.

The second chapter provides a description of the instrumentation used for carrying out the experiments done in this work. Various ultrasonic measurement techniques like the sing around interferometric technique, pulse methods, and continuous wave methods are briefly outlined. The technique used for present ultrasonic velocity and attenuation measurements viz. the pulse echo overlap (PEO) technique for velocity and pulse comparison technique for attenuation are discussed at length along with the details of the transducer bond correction employed during measurements. The experimental set up used for ultrasonic measurements is discussed with the aid of a block diagram. Fabrication and calibration of a dielectric cell in which the temperature can be varied from liquid nitrogen temperature to high temperature (up to 500K) is described in detail. Other details regarding dielectric constant measurements are outlined.

The third chapter deals specifically with the preparation and investigations carried out on the elastic and dielectric properties of $Ba_2Ti_9O_{20}$ ceramics with different levels of Strontium doping. The temperature variation of ultrasonic velocity and dielectric constant of these materials with different Sr concentrations give an insight in to the structural transformation in these materials. Dielectic constant has been found to vary with Sr concentrations with a threshold maximum value at the Sr concentration x=1.5. Elastic constants also increase with Sr doping and are found to exhibit a threshold maximum at the Sr concentration, x=1.5. Occurence of these threshold maxima in dielectric and elastic constants indicate that these samples undergo a change in phase at around Sr concentration x=1.5. Dielectric and elastic constants have been found to decrease with increase of temperature. A detailed discussion of these results are included in this chapter.

The fourth chapter outlines the preparation of Hf doped $Zr_{0.8}Sn_{0.2}TiO_4$ ceramics and the measurements carried out on them. Details of the experimental results obtained from the measurement of ultrasonic velocity and dielectric constant are presented. The influence of Hf doping on the elastic and dielectric properties of the basic $Zr_{0.8}Sn_{0.2}TiO_4$ ceramic are also discussed. $Zr_{0.8}Sn_{0.2}TiO_4$ ceramics have got technolog-

ical importance due to its high value of dielectric constant which makes it a potential material to be used as dielectric resonators in microwave communication. Replacement of some of the Sn ions with Hf ions is very advantageous both from the dielectric and elastic properties' point of view. The features of the temperature dependent variations of the dielectric and elastic constants for these materials are discussed in detail. The material is found to undergo a diffused phase transformation and the temperature at which this phase transformation occurs is found to vary with Hf concentration. This aspect is also discussed in detail in this chapter.

The fifth chapter begins with the method of preparation of $Ba^{2+}Ln^{3+}{}_2Ti^{4+}{}_5O_{14}$ ceramics where Ln stands for Y, La, Pr, Nd, Sm, Gd, Tb, Dy & Er. We have prepared $Ba_2Ti_9O_{20}$ ceramics doped with Y, La, Pr, Nd, Sm, Gd, Tb, Dy & Er and carried out our investigations on them. The room temperature elastic and dielectric constants of these materials have been measured and the influence of dopants on these properties from an application point of view is outlined. The results throw light upon the composition dependence of elastic and dielectric constants of these materials. Influence of Lanthanides on the physical properties of $Ba_2Ti_9O_{20}$ ceramics and its effect on the dielectric relaxation are also discussed in this chapter. The temperature variation of elastic and dielectric properties give an idea about the structural transformation and dielectric relaxation occuring in these materials. The experimental work, results obtained and a detailed discussion of the results are given in this chapter.

The sixth chapter deals with the elastic properties of $Ba_{5-x}Sr_xNb_4O_{15}$ ceramics at different concentrations of Sr. In order to get a clear idea about the structure and physical properties of these materials, the variation of elastic constants and attenuation with temperature at different concentration of Sr have been measured.

The seventh chapter begins with preparation of semiconducting $CuO-Bi_2O_3$ glasses and their important properties. In order to get a clear insight into the structure and physical properties of these materials, the variation of dielectric and elastic constants with varying CuO content have been measured. The variation of these parameters with temperature have also been measured. The details of the results obtained from these measurements are discussed in detail. It is found from the elastic constant measurements

that the addition of higher quantities of CuO to Bi_2O_3 leads to a phase transformation occuring at high temperatures. The increase of dielectric constant with temperature found in these materials is also discussed.

In the eighth chapter we present the work done on $Ba_{1-x}K_xBi\ O_{3-\delta}$ oxide glasses. These glasses have been prepared by the melt quenching technique. Details of the measurements and the results obtained are presented in this chapter. Dependence of the dielectric constant and elastic constants on the concentration of potassium are discussed at length in this chapter.

The last chapter is a concluding one which draws overall conclusions of the work presented in earlier chapters. Scope for doing further work in this direction is also outlined.

The following papers have been published / communicated during the course of these investigations. A couple of more papers are under preparation.

1. Elastic and dielectric properties of Sr doped $Ba_2Ti_9\ O_{20}$ ceramics. *Jap. J. Appl. Phys.* **35**; 673 (1996)

2. Synthesis, characterisation and properties of Hf substituted $(Zr_{0.8}\ Sn_{0.2})TiO_4$ dielectric ceramics, *J. Phys. D: Appl. Phys.* (communicated)

3. Elastic and dielectric properties of CuO doped Bi_2O_3 glasses. *J. Mater. Sci.* (communicated)

4. Elastic and dielectric properties of $BaLn_2Ti_5O_{14}$ dielectric ceramics. *Br. Ceram. Trans. J* (communicated).

5. Elastic properties of K doped $Ba_{1-x}K_xBiO_{3-\delta}$ semiconducting glasses. *J. Mater. Sci.*(communicated).

The following papers have been presented in different conferences during the course of this work.

1. Elastic and dielectric properties of Sr doped $Ba_2Ti_9\ O_{20}$ ceramics. DAE Symp. on Solid State Physics, Jaipur. (Dec. 1994)

2. Elastic properties of Hf doped $(Zr_{0.8} Sn_{0.2})TiO_4$ ceramics. 7 th National Symp.on Ultrasonics, Sivakasi. (Aug. 1996).

3. Elastic and dielectric studies on $(Bi_2O_3)_{1-x}(CuO)_x$ glasses. DAE Symp. on Solid State Physics, Mumbai. (Dec. 1996)

ACKNOWLEDGEMENTS

Chapter 1

Introduction

1.1 Opening remarks

Amorphous solids, because of their irregular microscopic structure, occupy a unique position among the condensed states of matter. Progress in the science of amorphous materials has been considerable on a level comparable to the understanding of crystalline materials during the past two decades due to the discovery of some surprising anomalies in the thermodynamic [1] and acoustic [2] behaviour of these materials. The study of amorphous solids offers new frontiers of research and hopefully, promise for new technological developments. The influence of amorphous materials on the world of science and technology has been so remarkable that they have found a number of applications like electrochemical sensors, electrochromic optic devices, electrophotography, memory and switching elements, optical communications etc.

The interest in amorphous materials is perhaps twofold. First one is the material science aspect, because a wide diversity of materials can be rendered in to amorphous state. The second interest in amorphous materials is in the fundamental physics of such systems. Furthermore, amorphous materials exhibit many properties which are unique to them and are not shared by crystalline solids at all. A translationally periodic array of atoms positions exhibit long range order, while in amorphous solids long range order is absent and an array of equilibrium atomic positions is strongly disordered. For crystals, the atomic scale structure is securely known at the outset from diffraction experiments, and it provides the basis for the analysis of such properties as electronic and vibrational excitations. For amorphous solids, the atomic scale structure itself is one of the key mysteries.

1

In amorphous solids, randomness can occur in several forms, of which topological, spin, substitutional and vibrational disorder are the most important [3]. Topological disorder is that form of randomness in which there is no translational periodicity. Spin disorder is another form of randomness in which underlying perfect crystalline lattice is preserved, but each atomic site possesses a spin or magnetic moment which is oriented randomly. This usually occurs in some dilute magnetic alloys such as Cu-Mn or Au-Fe with from 0.1 to 10 at. % magnetic component. The materials having topological disorder and randomly oriented spin are termed spin glasses. A further kind of randomness is substitutional disorder in which crystalline lattice is preserved but the material is in fact an alloy with one type of atom randomly substituting for the other in the lattice. Vibrational disorder is the final category of randomness which results from the random motion of atoms about their equilibrium positions at finite temperature destroying the perfect periodicity.

Knowledge of structural arrangement of atoms of a solid substance is an essential prerequisite for a detailed understanding of other physical or chemical properties. This is as true for amorphous as well as crystalline materials. Unlike a crystal, determination of the structure of a non-periodic amorphous solid is impossible for which unit cell may be regarded as being infinite in extent. This uncertainty is compounded by the fact that the structure of an amorphous material, at both macroscopic and microscopic levels, often depends on details of the method of preparation. Furthermore, in general, more than one experimental structure probe must be used to obtain as full a picture as possible of the structural arrangement in an amorphous solid. Loss of long range order in amorphous solid eliminated the validity and utility of well known mathematical tools like Brillouin zones, Block functions, k-space, E(k) electronic band structures, ω(k) phonon dispersion curves and elegant uses of symmetry and group theory for the labeling of eigenstates and elucidation of selection rules. Recently Chen and Spaepen [4] have proposed a calorimetric test to distinguish between amorphous and microcrystalline sample.

Although the structure of the amorphous solid is random in statistical sense, we shall find in many cases that the structure of many amorphous solid is infact nonran-

dom, at least on certain length scale. In discussing the structure of amorphous materials, it is useful to consider the types of structural order that can exist in such materials at various length scales. The various experimental probes are generally sensitive to structural correlations at different length scales. One can consider three contiguous length scales [3], short range order (SRO) in the range 2-5Å, medium range order (MRO) in the range 5- 20Åand long range structural order (LRS) at distances $> 20A^o$ Since there is no unique structure for an amorphous material, structural modelling is very useful in determining the structure of the amorphous solids. The structure of the amorphous materials developed by the repetetion of one or more basic molecular units in a way cannot be identified topologically with any known crystalline structure or with any periodic array. But the atomic order within a molecular unit might be similar within small bond angle distortions in both crystalline and amorphous phases. This reveals the importance of short range order in describing structural behaviour of a non-periodic network.

The most important aspects of the short range order are the number and type of immediate neighbours, and their spatial arrangement about a given reference atom. With given short range order and three parameters *viz.* the number of the bonds, the bond length and the bond angle having well defined values in a narrow range, it is possible to construct a model for the amorphous structure. Such models are known as random network models. Zachariasen was the first to model an amorphous solid by random network of atoms with near perfect short range order [5], with particular reference to oxide glasses. There is also possibility of forming isolated microcrystallite regions of large dimensions in some parts of the network. [6, 7, 8]

Since amorphous phase is less thermodynamically stable than the corresponding crystalline form (*ie*, it possesses a greater free energy), the preparation of amorphous materials can be regarded as the addition of excess free energy in some manner to the crystalline polymorph. There are at least a dozen different techniques that can be used to prepare materials in the amorphous state. Among these techniques, solid state diffusional amorphization is the remarkable new technique discovered by Schwarz and Johnson in 1983 [9]. Despite the variety of techniques that can produce amorphous

3

state, only four or five are commercially important. Generally, amorphous solids can be prepared mainly by four processes namely, slow cooling, moderate quenching, rapid splat-quenching and condensation from the gas phase. Materials which can be quenched from a melt to form an amorphous solid are represented by all the major types of bonding interactions found in solids viz. covalent, ionic, metallic, van der Waals, and hydrogen bonds. Inevitably there are some examples like silica glass which do not fit in to any one category, because it has some ionic contribution to the predominant covalent bonding.

When a material is cooled from the normal liquid state, one of two events may occur usually. Either crystallisation may take place at the melting point T_m or the liquid will become highly viscous with decreasing temperature and may ultimately form a glass. The latter is generally termed as glass transition phenomenon. These changes can be readily observed by monitoring the variations in volume as a function of the temperature as shown in the Fig.1.1. The crystallisation process is manifested by an abrupt change in volume at T_m where as glass formation is characterised by a gradual break in the slope. The region over which the change of slope occurs is termed glass transition temperature T_g. Both glass transition region ΔT_g and glass transition temperature T_g depend smoothly on cooling rate [10]. The actual value of glass transition temperature may vary by as much as 10 to 20% for widely differing cooling rates. The ratio $\Delta T_g/T_g$ provides a rough estimate of the non-equilibrium effects occurring at glass transition, so that $\Delta T_g/T_g \ll 1$ is a necessary condition for any thermodynamical approach. In a good glass forming system, the above mentioned condition is usually fulfilled at relatively low cooling rates. Besides, during glass transition, there is no discontinuous changes in first order thermodynamic properties such as volume (V), heat capacity (H) and entropy (S). But discontinuities are observed in derivatives or second order thermodynamic properties such as specific heat capacity and thermal expansivity.

Many theories have been developed to explain this fascinating and complex glass transition phenomenon. But no single theory has been advanced so far is capable of accounting for all aspects of it. In 1965, Adams and Gibbs [11] proposed a theory which links relaxation aspects with entropy considerations of glass transition. Dynamical

4
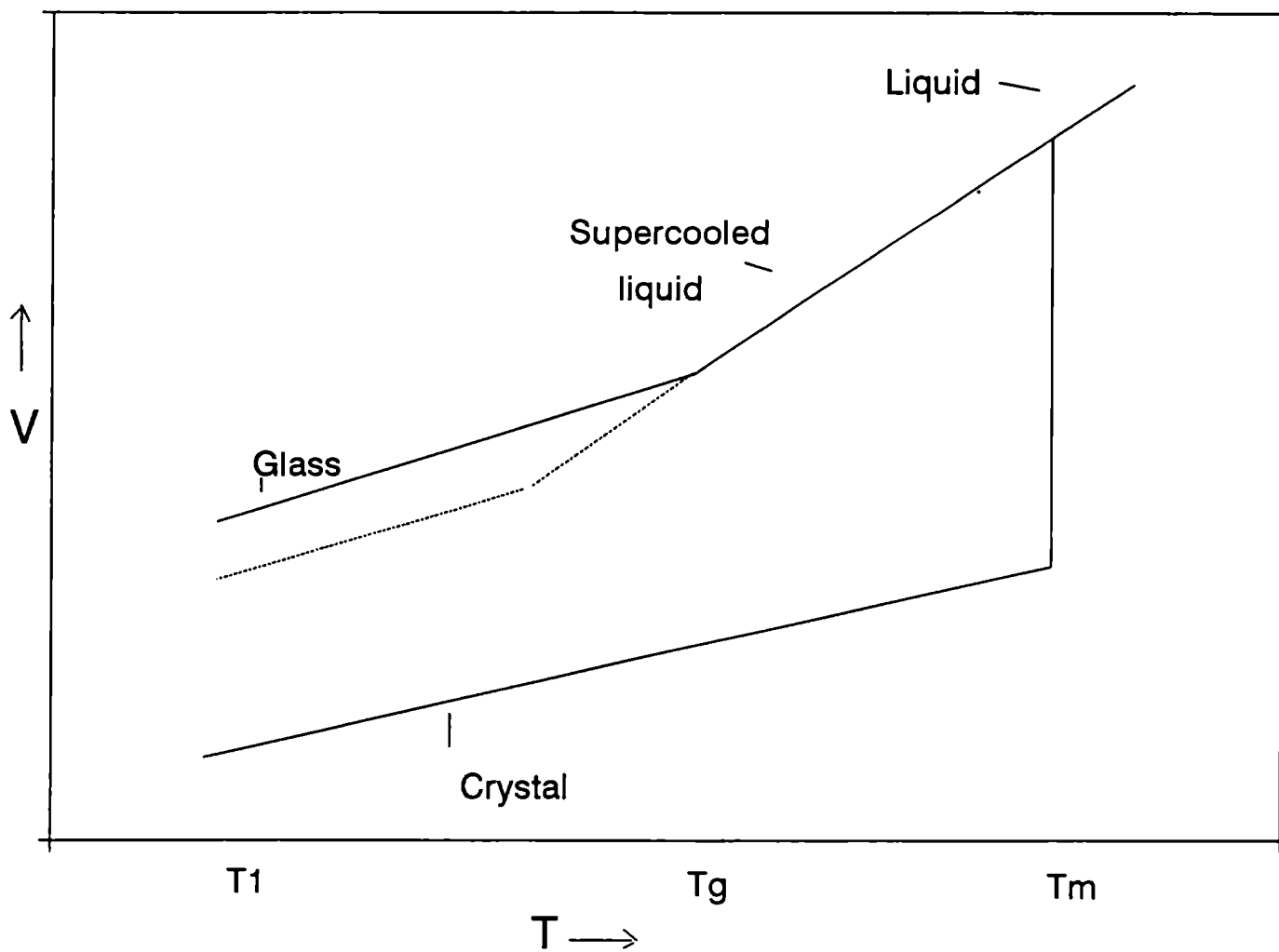
Fig. 1.1

Schematic illustration of change in volume with temperature as a
supercooled liquid is cooled through the glass transition temperature T_g.

theories primarily deal with the dynamical aspects of the transition while the theory connected with free volume describes certain aspects of glass transition that concerned with 'free volume'

The thermal properties of crystalline solids at low temperature are well understood in terms of the Debye theory. But low temperature thermal properties observed in amorphous solids are very different from those observed in crystalline solids. At low temperatures, they exhibit markedly different behaviour from their crystalline counterparts in phonon related properties, such as specific heat capacity, and thermal conductivity. A number of theories have been proposed, to explain low temperature properties of glasses, most succesful being that involving 'two-level systems' (TLSs), proposed independently by Anderson [12] and Phillips [13]. Zeller and Pohl (1) presented clear and unambiguous evidence for this. This paper catalysed new extensive theoretical and experimental research on the low temperature properties of these materials. Measurement of acoustic and dielectric properties of amorphous solids at low temperature show a number of unusual features which have no analogy in crystalline solids [2,14].

In the specific heat measurements, low energy excitations have been detected in amorphous solids over and above the vibrational states already known from crystals. These excitations have been investigated further by Raman and Brillouin scattering [15] and by measurements of infrared and ultrasonic absorption [16-18]. The specific heat of glasses decrease much more slowly with temperature than Debye's T^3 prediction at low temperatures. A number of theoretical models have been proposed to explain the specific heat anomaly in amorphous solids. Among these models, the tunneling model proposed by the Phillips [13] and independently by Anderson et al. [12], and the cellular model proposed by Baltes [19] are the most important. Much of the work connected with specific heat measurements have been reported in various materials in the last few years. This has produced the evidence that at least a part of the anomaly in specific heat variation is not intrinsic in amorphous materials.

Thermal conductivity measurements have been used in an attempt to gain some insight into the physical nature of the localized excitations taking place in the amorphous materials. The following conclusion regarding the thermal conductivity of

6

amorphous materials, have been drawn. Nonelectronic thermal transport below 10 K is provided by phonons. The phonon free path has a magnitude, frequency, and temperature dependence which is characteristic of the glassy state. Phonon scattering responsible for this mean free path is caused primarily by localised excitations. Models based on structural inhomogeneities have also been suggested to explain the variation of the thermal conductivity with temperature. According to this model, density fluctuations [20] and elastic modulii [21] give rise to phonon scattering and limit the phonon free path. The experimentally observed thermal conductivity can be fitted if a suitable distribution of the density fluctuations is assumed.

In addition to the anomalies in specific heat capacity and thermal conductivity of amorphous materials at low temperature, the two level systems have a strong influence on the propagation of sound waves. At low temperatures the one-phonon absorption is the most probable interaction between a phonon and a two-level system. In this process the phonon is absorbed and reemitted by the two-level system after the recombination time τ. This mechanism for sound absorption also leads to an explanation for the power dependence of ultrasonic attenuation. With increasing acoustic intensity, the upper level becomes more and more populated. Therefore, the effective number of two-level systems decrease and which account for the experimentally observed absorption. In this intensity range the magnitude of the attenuation is determined by the dynamic equilibrium between the excitation and recombination rates. The absorption also depends on the number of two-level systems taking part in the resonant absorption process at a given frequency.

Noncrystalline materials have many advantages over their crystalline counterparts while applications are concerned. In general, amorphous solids are relatively easy to prepare in large areas; homogeneous thin films can be prepared for solar cells or thin film transistor applications. Bulk glasses can often be readily formed from melt quenching technique and they are often structurally homogeneous and isotropic on a macroscopic length scale. The absence of structural defects such as grain boundaries or dislocations also have a dramatic effect on the mechanical behaviour and use of amorphous materials in mechanical engineering applications. Furthermore, homogeneous

amorphous phases can often be formed in mixed component systems over rather wide range of compositions,not necessarily restricted to the stoichiometric values. Thus technology stand to benefit enormously, if materials now used in crystalline form could be replaced by amorphous materials having similar properties.

Progress in the theoretical understanding of crystalline solids has been made during the past sixty years. This was achieved by the applications of the quantum mechanics to explain microscopic phenomena in solids and by the band theory which was successful in explaining most of the properties of crystalline materials with periodic lattices [22,23]. On the other hand, proper theoretical understanding of disordered systems remained largely undeveloped mainly because of the mathematical complexities involved in dealing with nonperiodic systems. This was overcome by eminent theorists owing to their expectation that there is an order in all things including things which look disordered. In recent years much attentions has been paid to the search for order in disordered systems and it has resulted in significant advances in the knowledge of the disordered system. This is reflected, for example, by the award of the 1977 Nobel prize in physics to P.W.Anderson, M.F.Mott and J.H.Vanvlek for their contributions to the understanding of disordered system. These materials can be prepared with unique chemical, thermal, electrical, magnetic, optical, mechanical and mass transport properties. Special electrical properties of these materials form the basis for the applications as insulators, dielectric resonators, piezoelectric transducers and ever increasing family of semiconductor devices.

In interpreting the transport properties of amorphous solids, the concept of Anderson localisations [23] and two level system (TLS) tunneling have played key roles. Scaling theories and the ideas of localisation and percolation have been exploited by several authors to solve problems associated with disordered system [24-27]. Pioneering work done by Mott on the various theoretical aspects of the problem [28] have contributed significantly to our understanding of the amorphous state. A complete review on the work done on amorphous materials would be too vast.

Though the progress in amorphous science has been enormous during last few decades, only a few selected topics have been chosen for investigation in this work.

We have studied the elastic and dielectric properties of selected dielectric ceramics and oxide glasses which fall under the category of amorphous materials. Ceramic materials and oxide glasses are of great interest to scientists due to their practical applications. Dielectric ceramics find wide applications as microwave resonators and oxide glasses find a multitude of applications. Applications of these materials call for a study of the properties of resonator materials used in the microwave devices and oxide glasses used in various applications such as switching devices.

Not much work on the mechanical properties of these material have been done before. The studies on the influence of composition on the temperature coefficient of the ultrasonic velocity of glasses have great importance due to their application in acoustical devices such as delay lines, which require glasses with zero temperature coefficient. The structural stability and rigidity of these materials are dependent on their elastic modulii and we have carried out investigations on the elastic properties of these materials. The dielectric constant is an important parameter which determine most of the dielectric properties. We have also carried out detailed study of the dielectric behaviour of several materials belonging to these groups.

1.2   Review of Dielectric Resonators

Ceramic materials are basically inorganic materials containing phases that are compounds of metallic and nonmetallic elements, having definite shape. Since there are many possible combinations of metallic and nonmetallic atoms, there may be several structural arrangements for each combination; it is possible to prepare materials with various properties and hence they form very useful engineering materials. Heating of ceramics enhances diffusion between grains and thus promotes densification. A properly densified ceramic called 'sintered body ' is used for practical purposes. The sintered body is chemically and thermally stable and strong.

Most ceramic phases, like metals, have crystalline structures. Ceramic crystallites are formed by either pure ionic bond, pure covalent, or by bonds that posses ionic as well as covalent characteristics. The crystal structure of ceramics is, however, invariably more complex, since atoms of different sizes and electronic configurations are

9

assembled together. Therefore ceramics are classified in terms of their internal structures. Changes in lattice orientation occur at the interfaces between crystallites, often due to the difference in composition and electric effects. Hence due to the complexities of ceramic microstructures, it turns out to be very difficult to predict and account precisely for the properties of the ceramics. To get a proper insight into the behaviour of ceramics, detailed study of single crystal properties is necessary [29].

Common crystal structures found in crystalline ceramics are caesium chloride structure, rock salt structure, spinel structure, fluorite structure and illmenite structure. However, the growth of single crystals is usually difficult and time consuming that makes them very expensive. Ceramic materials are used as insulators, conductors, semiconductors and dielectrics. Ceramics are also used as ferroelectric and piezoelectric materials. It can be seen that ceramics with perovskite, tungsten bronze, pyrochlore and bismuth titanate layer structure oxides have high dielectric constant and refractive index. The thermal properties of ceramics are quite different from that of metals because they contain relatively few free electrons and ceramic phases are transparent to radiant energy. Heat is conducted through the ceramics mainly by phonon conduction and phonon-phonon interactions. Thermal conductivity decreases with impurity content, porosity and temperature. For maximum thermal conductivity, it is essential to have high density which is found lacking in most ceramic materials.

Although ceramic compounds are normally insulators, they become semiconductors if they contain multivalent transition elements like Ti and Nb. These transition elements form corner-linked octahedral networks in their structure and they are highly polarisable within 'active' ions promoting ferroelectricity [30] and the high permittivities needed for capacitor applications. There are two major groups of active ions with reference to the periodic system. The first group is represented by Ti^{4+}, Nb^{5+} and W^{6+} and second group by Pb^{2+} and Bi^{3+}(10). In both the groups mentioned above different types of atomic orbitals are comparable in energy and hybrid bond formation is prevalent. Ti^{4+}, Nb^{5+} and W^{6+} are characteristic of first group, where d° ions are octahedrally coordinated to oxygen. In Ti^{4+}, the electronic crossover involves in the 3d, 4s, and 4p orbitals which combine with s and p orbitals of its six O^{2-} neighbours to

form a number of molecular orbits for the $(Ti\ O_6)^{8-}$ complex.

The bond energy of the complex can be lowered by distorting the octahedron to lower symmetry. This leads to dipole moments, ferroelectricity and large dielectric constant. In case of the second group elements, the lone pair ions having two electrons outside a closed shell in an asymmetric hybrid orbital contribute to polar distortions. For example Pb^{2+} and Bi^{3+} are present in a number of ferroelectrics like $PbTiO_3$, $Bi_4Ti_3O_{12}$, $Pb_4Nb_2O_6$ forming pyramidal co-ordination with oxygen and hence contribute to the spontaneous polarisation. Although materials with inherent permanent dipoles (polar molecules) posses high ϵ_r at lower frequencies due to dipole relaxation, their ϵ_r decreases sharply at microwave frequencies. Moreover, the permittivity is highly sensitive to temperature.

1.2.1 Dielectric resonators

In the early seventies, when Microwave integrated circuits (MIC) were developed, there were no devices with small size and weight suited to integration in miniature circuits to perform the required function. Bulky metallic cavity resonators, expensive Yttrium Iron Garnet (YIG) and magnetostatic wave (MSW) based devices were used for frequency stabilisation. All these difficulties have been got over with the development of microwave dielectric resonators.

A dielectric resonator (DR) is a piece of unmetallised ceramic which can confine microwave energy at selected discrete frequencies. A good number of reviews are available describing the properties and application of DRs [31-38]. They are commonly used in devices like filters, oscillators and duplexers used in modern microwave communication systems such as cellular telephones. The materials for dielectric resonators are required to have (i) high dielectric constant ($20 > \epsilon_r > 100$) (ii) high Q value (> 2000) (iii) Very small temperature coefficient of the resonant frequency (τ_{f0}). A great deal of research has been done for developing new ceramics and also for improving the dielectric properties of various materials by substitution and additives. The first DR material TiO_2 (rutile) [13] possessed high ϵ_r (≈ 100) and high Q (≈ 1000) but its poor temperature stability ($\tau_f \approx 400$ ppm/K) precludes its use in practical applications. Generally

complex pervoskite oxides have proved to be excellent DR materials (39,40). A number of dielectric materials such as $Ba_2Ti_9O_{20}$, (Zr Sn)Ti O_4, Ba(ZnTa)O_3, BaNd$_{2(1-x)}$ Sn$_{2x}$Ti$_5$ O_{14} etc have been investigated [41-43] as DR materials. Agravovskaya [44] has outlined the dielectric properties of several complex perovskites and suggested the possibility of $A[B_{1/2}^{3+}B_{1/2}^{5+}]O_4$ becoming excellent microwave resonator materials. Several materials belonging to the above class are currently used commercially. BaTi_4O_9 -Ba$_2$Ti$_9$O$_{20}$ and (Zr Sn)TiO_4 [45-47] materials have also gained commercial importance. It is to be noted that there is no single ceramic material that is capable of satisfying the demands of all microwave communication applications. Hence search for new materials is still progressing to develop the ceramics with better and better characteristics.

Quality factor of ceramics are affected by structural and microstructural properties of the material. Therefore the loss is the result of the combination of degree of crystal structure, imperfection and microstructural inhomogeneity. Ceramics with microstructural inhomogeneities such as relaxation of space charge or dipoles which lie between either matrix or at grain boundaries with segregation of concentrated impurities, have high losses [47]. Such inhomogeneities may arise due to secondary phases, impurity segregation, incomplete densification etc. It is found that the quality factor of ceramics is measured with increase of bulk density, provided the densification is promoted by solid state diffusion mechanism. Hence glassy phase formation may be avoided during sintering to get high quality factor.

Because of the natural difficulties involved in getting ceramics with full repeatability in microstructure, it is essential that the ceramic be at least composed of a single phase homogenious microstructure to have as high a Q as possible. The structure factors that are involved in loss mechanisms include lattice defects, distortion of symmetry, mass of ions, cation ordering etc. It is known that the dielectric loss tangent of microwave dielectric is mainly brought about by the effect of anharmonic terms in the potential energy on the mean separation of a pair of atoms and is increased by lattice imperfection of the crystal [48]. The dielectric loss caused by the anharmonic terms increases at higher temperatures. Recently, it has been reported that Q factor of ordered ceramics would be much greater than that of the less ordered ceramics (49-50).

When a material is heated due to thermal energy, its polarisation changes. In normal dielectrics , the polarisability and hence permittivity decreases as temperature increases. Hence the temperature coefficient of permittivity τ_ϵ will generally be a negative quantity. The thermal expansion coefficient (α_T) of dielectric ceramics is positive. Hence it is possible that τ_ϵ and α_ϵ can cancel the effect of each other and gives a perfect temperature compensation effect. In the case of normal ceramics, α_T will be a small negative quantity (-20 ppm/K or less). In certain materials it so happens that either τ_ϵ itself become nearly zero or it assumes a small value so that effect of α_T is cancelled. In both these cases, the DR behaves as a temperature stable resonator. τ_f can be controlled by making solid solutions of similar materials with positive and negative τ_f value. A negative τ_f requires that the dielectric constant should increase with increase in temperature; a behaviour not commonly observed.

Normal dielectrics show a linear decrease or increase of ϵ_r with respect to an increase in temperature depending upon the structure. Therefore the resonant frequency versus temperature curve also shows a linear behaviour. But ϵ_r shows a nonlinear variation with respect to the temperature.

1.3 Review of oxide glasses and their properties

The ever increasing interest in the investigation of glasses is doubly motivated during the last three decades by their widespread practical applications. They exhibit a number of anomalous physical and electrical properties, which suggest specific structural singularities that differentiate the glassy state of matter from the crystalline as well as ordinary amorphous state. Glassy solids exhibit a glass transition which is the phenomenon in which a solid amorphous phase exhibit a more or less abrupt change in derivative of thermodynamic properties (eg: heat capacity or thermal expansivity) from crystal like to liquid like values with change of temperature.

Glassy material have been used in a variety of applications for thousands of years. Until very recently, silicate glasses were the only type of the materials commonly used. The recent discovery is that many types of materials can be produced in amorphous form, either as bulk glasses or as thin films. This development has led to

13

a very rapid increase in the use of such materials in electronic as well as magnetic and optical materials. The important discoveries made on optical memory effects, imaging, photo doping etc. have shown possibilities of new technological applications for these materials. Their electronic applications include use as substrates, delay lines, device passivators, capacitor dielectrics, thick film resistor components, dielectric film layers [51,52] etc. Glassy materials are favoured for many applications because of their wide applicability, low cost and ease of fabrications. Since glassy phase is thermodynamically less stable than the corresponding crystalline form, the preparation of glassy materials can be regarded as the addition of excess free energy in some manner to the crystalline polymorph.

Besides the above general advantages, the glass is optically isotropic with better thermal insulating properties. Both the optical isotropy and low thermal conductivity are the consequences of disorder in a nonmetallic amorphous solid. Isotropy results from the loss of long range order, while low thermal conductivity results because of the disorder induced scattering of thermal phonons. Glassy form of the material has got several advantages over its crystalline form. For example, crystalline silicon photovoltaic cells are used in power equipments on space probe vehicles and they are very expensive for use on large scales.

Generally, glasses are prepared by two different methods, namely vapour condensation technique and melt quenching technique. Vapour condensation technique is employed to prepare thin films while bulk glasses having well defined transition temperatures are prepared by melt quenching technique. Since various techniques differ in degree to which their products depart from equilibrium, mainly as a result of the rate of cooling, vapour deposited material is expected to be less near an equilibrium state than melt quenched material.

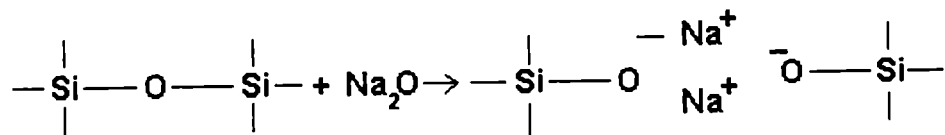The structure of the glass is best described by the radial distribution function (RDF) which gives the probability of finding another at a given distance from an arbitrary central atom. Since RDF is a one dimensional representation of a three dimensional structure, it can carry only a limited amount of structural information. This has led to the necessity of several structural modelling studies.

14

For monoatomic systems, conventional diffraction technique using x-rays, neutrons or electrons yield the maximum amount of structural information about the local and medium range order. For binary compounds, diffraction techniques and their variants like anomalous scattering, magnetic neutron scattering are more suitable. For the systems containing more than two components, only EXAFS is really suitable as a direct structural probe, but it is insensitive to atomic correlation much beyond the second co-ordination shell and it is difficult to deduce co-ordination number qualitatively. Other techniques such as magnetic resonance, Mossbauer and vibrational spectroscopies can supply indirect structural information, usually as an adjunct to other structural probes. The above mentioned experimental techniques can give only limited information about the microscopic structure of amorphous solids only to the first two co-ordination shells. So, systematic structural modeling studies are necessary in order to determine the degree of the medium range order present in it.

Models of the atomic structure of the glassy materials are based upon the ideas expressed by Zachariasen in 1932 [5]. He made successful attempt to categorise materials in to the glass formers and non glass formers. According to him, the strength of glasses is of the same order as the strength of crystals. Besides, materials which form glasses readily, would have an internal energy only slightly larger in the amorphous state than crystalline. The internal energy of a solid is related to its structure (Madelung energy of ionic materials). So the atoms in a glass must be linked by the forces essentially the same as those in crystals. These concepts on the glass structure were strongly conformed by Warren and his coworkers [53]. Later this theory was referred to as the random network theory of glasses. The most important aspect of Zachariasen's approach was that a non periodic arrangement of atoms could be obtained solely as a result of the incorporation of variations in bond angles and dihedral angles. Initially it was believed that an extended three dimensional network must be present if a compound is to form a glass. In certain stoichiometry, glasses have been found in oxide systems where no three dimensional network is possible eg: silicates near orthosilicate composition and many highly stable non-oxide glasses such as, some of the chalcogenides, can not satisfy the three dimensional network criterion.

Recent investigations have shown that certain glasses may develop a granular noncrystalline structure with dimensions in the range of ten to a few hundred Å(1-10 nm). This granular structure has been interpreted as evidence of pure crystalline nuclei which make up a major part of the glass volume. This causes a homogeneous nucleation on a very fine scale in some glasses. Possibly connected with this effect is the existence of metastable phase separation of multicomponent glasses. The analysis of EPR and optical spectra support this concept in semiconducting oxide glasses [54]. Many structural models have been developed from the physical models of 'ball and stick type' (for CRN and other models of covalent materials) or random packing of spheres (metallic solid). Computer methods have also played an important role in the modification or transformation of models, particularly DRP models, as well as monte carlo simulation in which models are constructed by the random positioning of atoms starting from either a crystalline or another amorphous structure.

Generally, glasses can be divided in to two groups, namely, oxide glasses and non-oxide glasses. The chemical formula of an oxide glass may be written generally as $A_m B_n O$ where m and n may not be integers. A represents network forming cations and B is the network modifying cation. An interesting intermediate class of oxides, including TeO_2, WO_3, MoO_3, Bi_2O_3, Ga_2O_3 and V_2O_5 do not by themselves readily form glasses but will form with (modifier) oxides. So they are commonly referred to as network formers. Most oxide glasses are prepared from the fusion of a mixture of various solids. Their basic ingredients are a network former, modifiers, and an intermediate. During fusion, a chemical reaction apparently takes place such that very strong bonds are broken and bridging oxygens are converted in to non bridging oxygen. Such a reaction is conveniently represented as

$$
-\overset{|}{\underset{|}{Si}}-O-\overset{|}{\underset{|}{Si}}- + Na_2O \rightarrow -\overset{|}{\underset{|}{Si}}-O^- \ Na^+ \quad Na^+ \ ^-O-\overset{|}{\underset{|}{Si}}-
$$

It is convenient to divide oxide glasses in to two broad categories. The first group consists of binary glasses such as Na_2O -SiO_2 in which the carriers are alkali ions. The second group consists of binary glasses BaO-SiO_2 and CaO- SiO_2 in which

16

the carriers are divalent ions. The mobility of divalent ions and other high valence ions is usually low relative to alkali ions [55-56]. The addition of network modifiers to glass forming material can result in a very different type of structural change. In borate and germanate systems, the addition of alkali up to a certain limiting amounts causes an increase in co-ordination number of the glass forming cations (from 3 to 4 for B, from 4 to 6 for Ge). In contrast, modification of silicate systems in general causes a depolymerisation of the network, the co-ordination of Si remaining tetrahedral, but doubly co-ordinated bridging oxygen sites are progressively transformed in to singly co-ordinated non-bridging oxygen (NBO) configurations.

Semiconducting oxides in the past had been confined to crystalline materials, but studies on semiconducting oxide glasses offers new scope for research and become technologically as well as scientifically interesting. Most oxides are ionic conductors and their electrical conductivity is insensitive to γ-rays, neutrons and impurities. Electron conduction in oxide glasses usually arises from charge transfer between ions of different valencies. (eg: from Fe^{2+} to Fe^{3+} the activation energy E for conduction, in oxide glasses are usually much less than E_{gap}). The simultaneous presence of the same ion in different valence states is necessary for the conduction in the oxide glasses. The electron migrating from one transition metal ion to another one of different valency is generally considered to induce some polarisation in its surrounding. The effective mass of such hopping electron is larger than electronic mass. So motion of the hopping electrons produce some effect on the network former of the glass. As a result large difference in their properties is observed. Many research workers have reported transport properties of semiconducting glasses (57, 58) but less attention has been given to their elastic or dielectric properties.

The elastic constants of glasses have fundamental importance just as in any solid as they are related to the interatomic forces and atomic vibrations. Ultrasonic propagation studies in these materials enable one to determine these elastic constants. The specific attribute of structure of the oxide glasses are extremely pronounced in the accoustical and dielectric properties and their temperature variations in oxide glasses. The observation of anomalous specific heat [59,60] and thermal conductivity [1,61] of

17

glasses at low temperatures, understanding of the propagation and attenuation [2,62,63], of ultrasonic waves in glasses etc. are of special significance to a better understanding of the glassy nature of condensed matter.

Many acoustical experiments have been conducted in multicomponent optical glasses or in binary and ternary alkali silica systems containing greater than 10% modifying oxides. In this type of glasses, it is possible for the continuity of the glass network to be disrupted for a large number of non bridging atoms to appear and for regions of concentrated inhomogenieties to occur. By studying the acoustical characteristics of such glasses, it is possible to acquire information about the relaxation processes associated with the motion of various ions, [64] the influence of modifying oxides on the elastic modulii [65] and information about the dynamical behaviour of two level systems.

The most interesting peculiarity of glassy state is the anomaly in positive temperature coefficient of velocity of the sound (TCV) and of elastic modulii. In crystals the velocity decreases with increase of the temperature and at very low temperature the velocity is almost constant. Many authors have investigated the temperature dependence of the velocity of the sound and elastic modulii in almost all glasses in various temperature ranges. All glasses show a small increase in velocity with increase of temperature at very low temperature, reaches a peak and then decreases steadily with increase of temperature. McSkimin [66] performed measurement of velocities of longitudinal and shear ultrasonic waves in fused quartz by a pulse method at a frequency of 20.5 MHz and at low temperature from -200 to +40°C observing a decrease in the TCV value. Glasses with tetrahedrally co-ordinated structure like SiO_2, GeO_2, BeF_2 and $Zn(PO_3)_2$ show an increase in velocity with increase in temperature, beyond a peak the velocity decreases, goes through a minimum at some temperature and then begins to increase linearly with temperature. From the technological point of view, the study of the influence of composition on the temperature coefficient of sound velocity is extremely important. With suitable variation in additives, it is possible to obtain glasses with zero TCV in a certain temperature range. Bokin and others [67] obtained TCV value close to zero in small intervals of moderate temperatures for two ratios of the concentration of Na_2O and B_2O_3 in the composition of sodium borosilicate glasses with a fixed SiO_2 content. Acoustic

18

delay lines with zero TCV over the temperature range of application are desirable in computer hardware [68].

Several hypothesis have been put forward concerning the specific mechanism of the structural relaxation of glasses. Anderson and Bommel [71] attribute the low temperature acoustic loss peaks in quartz to the transverse motion of one oxygen atom between two silicon atoms. Strakia [69] also have proposed a some what modified relaxation loss mechanism associated with movement of oxygen atom along the elongated Si-O-Si bonds. Even though both theories conflict with x- ray data for quartz glass, the concept of equivalent state in glass is the generally accepted one so far. Anderson, Halperin and Varma (12) as well as Philips [13] handed this concept in such a way as to treat glassy substance in general with definite atoms that can exist in two slightly non equivalent states. The height of the potential barrier separating the two states, the difference between the depths of their corresponding asymmetrical potential wells, and the distance between them are not constant, rather they are characterised by a certain distribution function. The authors used this model successfully to explain the low temperature anomalies of the specific heat and thermal conductivity of quartz glass on the basis of the resonance tunnelling of the potential barriers and to predict the possibility of resonance absorption of ultrasound due to such tunnelling transition.

Recent work on the frequency dependence of sound absorption in vitreous silica between 10MHz and 35GHz in the temperature range 10-300 K showed that the relaxation process which is predominant in the absorption of ultrasonic waves is not sufficient for describing hyperfine attenuation [70]. Anharmonic three phonon interactions are proposed to explain the excess damping and are seen to be in qualitative agreement with observed temperature dependence above 300K. The magnitude of absorption at the peak is about two orders of magnitude higher than the absortion observed in crystalline quartz at the same temperature and frequency indicating that completely different mechanisms are responsible for attenuation in crystals and their amorphous counterparts. A similar absorption peak has also been observed in other simple glasses and multicompnent glasses. The temperature at which the peak in attenuation appears varies as frequency [71,72]. The magnitude of the absorption per wavelength is found

to be the same for both longitudinal and transverse polarisation [73]. While the height of the maximum increases linearly with frequency, a quadratic frequency dependence of the absorption is found on the high temperature side [74,75]. Plot of frequency with inverse of the absorption peak observed indicates that the orgin of absorption lies in a thermally activated relaxation process.

A behaviour corresponding to that of the ultrasonic absorption can be found in dielectric absorption [76,77]. An important difference is that the magnitude of the ultrasonic absorption and of the dielectric high-temperature peak is only weakly influenced by the impurity content of the material. The magnitude of the dielectric low-temperature peak, however, depends strongly on the presence of OH-groups or polar molecules.

Measurement of ultrasonic velocity at high temperature find important application to study phase transformation and glass transition in glassy materials.

1.4 Dielectric properties of solids

An ideal dielectric is a material which reacts to the sudden application of an electric field by being instantly polarised without the continuous passage of electric current. The dielectric properties of a material are governed by the response of the material to an applied electric field at the electronic, atomic, molecular and microscopic levels. Application of the electric field to a material causes a displacement of electric charges creating and reorienting dipoles in the material. This property, specified by the quantity called polarisation P, which is obtained from the dipole moment per unit volume averaged over the volume of a cell. The total polarisation of a multiphase material containing permanent dipoles will have electronic, ionic, orientational and interfacial contributions. All these can be explained by the intrinsic physical mechanisms of these phenomena in the material.

Electronic polarisation is a consequence of the distortion of electronic distribution with respect to atomic nucleus under the action of external electric field. This is observed in all dielectrics at optical frequencies (10^{15}Hz) irrespective of wheather other types of polarisations are present in the dielectric. At this frequency, dielectric possesing electronic polarisation satisfy the relation $\epsilon = n^2$, where n is the high frequency

refractive index of the material. The ionic polarisation results from the displacement of the positive and negative ions with respect to each other. Ionic polarisation contributes to the dielectric constant only at or beyond the infrared frequencies. A short time of the order of 10^{-13} to 10^{-12}sec, but longer than that for electronic polarisation, is required for ionic polarisation to set in. In highly deformable ionic compounds such as oxides, deformation of ionic polarisation dominates as the oxide ion is large and very deformable.

When a molecule having permanent dipole moment changes orientations in response to an applied electric field, orientational or true dipolar polarisation results. This process can be by the following two mechanisms. (i) In linear dielectrics dipolar polarisation results from the motion of the charged ions between the interstitial positions in ionic structures parallel to the applied field direction. (ii) Molecules having permanent dipole moment may be rotated about an equilibrium position against an elastic restoring force.

The extremely large dielectric constants of oxides arise almost exclusively from the large electronic polarisability of oxygen. Interfacial polarisation is produced due to the piling up of mobile charge carriers at a physical barrier such as grain boundary giving rise to a very large dielectric constant. The extremely large dielectric constant of the oxides arise almost exclusively from the large electronic polarisability of the oxygen. Thus one can conclude that electronic and ionic polarisability are the fundamental microscopic parameters that determine the susceptibility and dielectric constant of a solid.

1.4.1 Frequency dependent polarisabilities.

Fig.1.2 shows various contributions to the real part of the permittivity of typical insulator or semiconductor at different frequencies. Mainly valence band and conduction band electrons contribute at ultraviolet frequencies and above. Dipolar molecules, when they exist in a solid usually contribute only at microwave frequencies and below, while ions typically contribute up to infrared frequencies.

According to the Maxwell's equations, the relation between electric
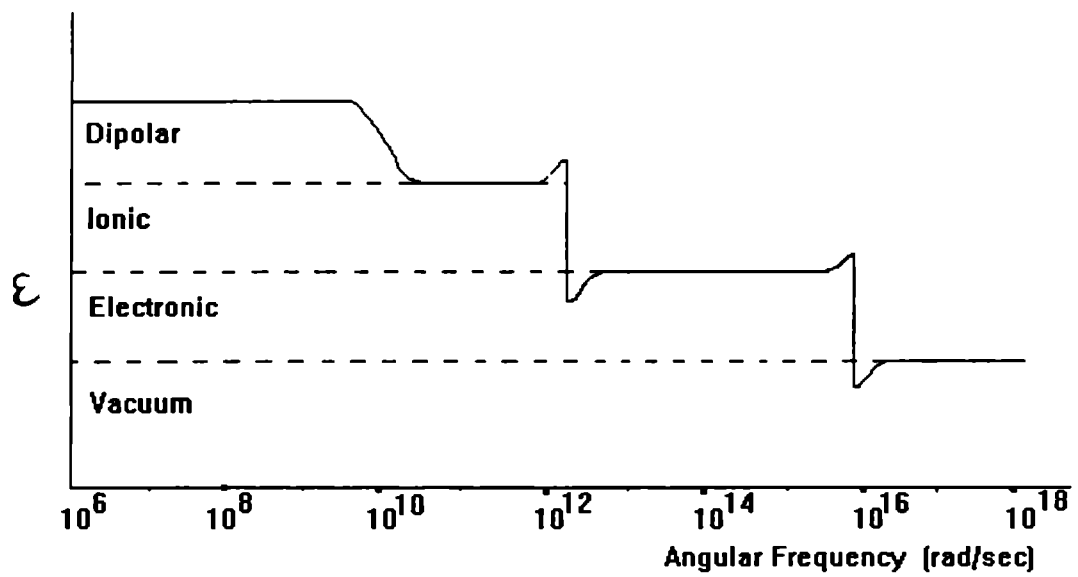
Fig. 1.2

Frequency dependence of polarisation mechanisms in dielectrics.

displacement D and electric field strength E is $D = \epsilon E$, where ϵ is the dielectric constant of the medium, which is defined as the ratio of the permittivity of the material to that of air or vacuum. When a material is subjected to an external electric field, dipole moments are induced inside the material by the electric field. Total polarisation P can be expressed in terms of dipole moment μ as $P = N\mu$ Where N is the number of dipoles per unit volume and $\mu = \alpha E$, α being the polarisability.

The total polarisation of multiphase material containing permanent dipoles will have electronic, ionic, orientational and interfacial contributions. $P = P_e + P_i + P_o + P_s$ where P_e is the electronic contribution, P_i is the ionic contribution, P_o is the orientational contribution and P_s is the interfacial contribution. In the case of solid dielectrics, the polarisation of the surrounding medium substantially reflects in the magnitude of the local field. The local field E/ is calculated assuming a spherical contribution of charges and is given by

$$E\prime = E + \frac{P}{3\epsilon_o} \tag{1.1}$$

where E is the applied field.
Since

$$N_i\alpha_i = \frac{P}{E\prime} \tag{1.2}$$

and

$$N_i\alpha_i = \frac{P}{E + P/3\epsilon_0} \tag{1.3}$$

substituting E and ϵ_o from the above equation, we get

$$N_i\alpha_i = \left[\frac{1}{(\epsilon_r - 1)} + \frac{1}{3\epsilon_o}\right]^{-1} \tag{1.4}$$

Rearranging terms we get

$$\frac{\epsilon_{r-1}}{\epsilon_{r+2}} = \frac{1}{3\epsilon_0}N_i\alpha_i \tag{1.5}$$

This above equation is known as the Clausius - Mossotti equation. If an electric field is created in a dielectric medium, the dipole moments of separate kinetic elements or atomic group will tend to orient in the field direction. If the external field is now removed after a certain time, the polarisation of the sample will diminish to zero as a

result of the thermal motion of separate kinetic elements and system will return to its previous equilibrium state. Such a process of transition to equilibrium is called dielectric relaxation. At the alternating voltage, dielectric properties of the material will depend on the relation between the frequency of the applied voltage ω and dielectric relaxation time τ.

The dielectric properties of a material are characterised by the complex dielectric constant

$$\epsilon* = \epsilon' - i\epsilon'' \qquad (1.6)$$

The ratio

$$\frac{\epsilon''}{\epsilon'} = tan\delta \qquad (1.7)$$

is the dielectric loss tangent. It characterises the phase shift between the alternating voltage applied to the capacitor between the plates in which the sample is placed and current passing through the capacitor. If dielectric relaxation is described by a single relaxation time, then

$$\epsilon' = \epsilon_\alpha + \frac{\epsilon_o - \epsilon_\alpha}{\left(1 - \omega^2\tau^2\right)} \qquad (1.8)$$

$$\epsilon'' = \frac{(\epsilon_o - \epsilon_\alpha)\omega\tau}{\left(1 + \omega^2\tau^2\right)} \qquad (1.9)$$

where ϵ_o is the dielectric constant at $\omega = 0$, ϵ_α is the dielectric constant at $\omega = \alpha$ and loss factor

$$tan\delta = \frac{\omega\tau(\epsilon_o - \epsilon_r)}{\left(\epsilon_o + \omega^2\tau^2\right)} \qquad (1.10)$$

1.5 Elastic properties of isotropic solids

The elastic properties of a solid material is closely related to the propagation behaviour of high frequency elastic waves propagating through it. Measurement of the velocity and attenuation of elastic waves is now a well established technique as an effective means for measuring elastic constants and investigating physical properties which are related to elastic forces between atoms in materials.

The elastic properties of a medium are studied in terms of its response to an applied stress. According to Hooke's law strain is directly proportional to applied stress

24

for small deformations [78]. When a material is subjected to a stress it will deform or get strained. The amount of strain developed for a given stress is characteristic of the medium. If the applied stress is reduced, the strain reduces and upon removal of the stress the strain goes to zero. At sufficiently low levels of stress, the strain is linear, but at high values of stress, the strain is no longer simply linear resulting in a permanent deformation. The ratio of stress to strain is the elastic constant or elastic modulus of the medium for small deformations.

In an elastic solid two types of elastic waves can be propagated. One type of wave is the compressional or longitudinal wave in which the particle motion in a plane wave is along the direction of propagation. The second type of wave called transverse or shear, has the particle motion in a plane normal to the direction of propagation of the wave. Stress and strain are second rank tensors and since they have three components each along the directions of the co-ordinate axes, they have altogether nine components each. The stress tensor represents a force which can be applied along any arbitrary direction of the system and is called a field tensor.

The components of the stress tensor are given by

$$\sigma_{ij} = \begin{bmatrix} \sigma_{11} & \sigma_{12} & \sigma_{13} \\ \sigma_{21} & \sigma_{22} & \sigma_{23} \\ \sigma_{31} & \sigma_{32} & \sigma_{33} \end{bmatrix} \tag{1.11}$$

In the absence of torques $\sigma_{ij} = \sigma_{ji}$ or stress tensor is symmetric. So the above array gets simplified to six independent stress components. The strain tensor is given by

$$c_{ij} = \begin{bmatrix} e_{11} & 1/2(e_{12} + e_{21}) & 1/2(e_{13} + e_{31}) \\ e_{12} + e_{21}) & e_{22} & 1/2(e_{23} + e_{32}) \\ 1/2(e_{13} + e_{31}) & 1/2(e_{23} + e_{32}) & e_{33} \end{bmatrix} \tag{1.12}$$

is also symmetric ($\epsilon_{ij} = \epsilon_{ji}$) and represents the displacement of a point in the deformed body. The generalised Hook's law states that stress is directly proportional to strain within the elastic limits. This can be related as

$$\sigma_{ij} \propto \epsilon_{kl} \tag{1.13}$$

The constant of proportionality is known as elastic stiffness constants C_{ijkl} which is a fourth rank tensor. The inverse of elastic stiffness is the elastic compliance S_{ijkl}. Hence,

25

Hook's law can be written as

$$\sigma_{ij} = \sum C_{ijkl}\epsilon_{kl} \tag{1.14}$$

or

$$\epsilon_{ij} = \sum S_{ijkl}\sigma_{kl} \tag{1.15}$$

The elastic coefficients of a solid can be obtained from the wave velocities and the density of the material and these elastic coefficients are in turn connected to the interatomic binding forces.

In general, C_{ijkl} and S_{ijkl} have 81 elements each, relating 9 stress components to 9 strain components. In the absence of rotation, the stress and strain tensors obey the symmetry $\sigma_{ij} = \sigma_{ji}$ and $\epsilon_{ij} = \epsilon_{ji}$. This reduces the number of independent stress and strain components from 9 to 6, leading to 36 independent components for the elastic constants. To avoid the difficulty in representing elastic constants with full subscript, Voigt notation can be used in which the tensor form of C_{ijkl} (i, j, k, l = 1, 2, 3) is replaced by the matrix C_{ij} (i, j =1, 2, 3, 4, 5, 6) according to the following convention.

Tensor notation	11	22	33	23,32	31,13	12,21
Matrix notation	1	2	3	4	5	6

ij → m = i   if i = j

ij → m = 9 - i - j   if i ≠ j

Using this notation the stress and stain tensors are

$$\sigma_i = \sum_{j=1}^{6} C_{ij}\epsilon_j \tag{1.16}$$

and

$$\epsilon_i = \sum_{j=1}^{6} S_{ij}\sigma_j \tag{1.17}$$

and in matrix form , this can be written as

$$
\begin{bmatrix} \sigma_1 \\ \sigma_2 \\ \sigma_3 \\ \sigma_4 \\ \sigma_5 \\ \sigma_6 \end{bmatrix} =
\begin{bmatrix}
C_{11} & C_{12} & C_{13} & C_{14} & C_{15} & C_{16} \\
C_{12} & C_{22} & C_{23} & C_{24} & C_{25} & C_{26} \\
C_{13} & C_{23} & C_{33} & C_{34} & C_{35} & C_{36} \\
C_{14} & C_{24} & C_{34} & C_{44} & C_{55} & C_{56} \\
C_{15} & C_{25} & C_{35} & C_{45} & C_{55} & C_{56} \\
C_{16} & C_{26} & C_{36} & C_{46} & C_{56} & C_{66}
\end{bmatrix}
\begin{bmatrix} \epsilon_1 \\ \epsilon_2 \\ \epsilon_3 \\ \epsilon_4 \\ \epsilon_5 \\ \epsilon_6 \end{bmatrix} \tag{1.18}
$$

26

When the crystal symmetries of the medium are taken into account, the total number of elastic constants reduce to 21. The number of independent elastic constants will again be reduced depending upon the symmetry class of the medium. As the symmetry of the system increases, the number of independent elastic constant decreases.

In the case of an isotropic solid the elastic coefficient must be independent of the particular set of rectangular co-ordinate axes chosen. This simplification leads to

$$C_{12} = C_{13} = C_{23}; \quad C_{44} = C_{55} = C_{66}; \quad C_{11} = C_{22} = C_{33}; \quad (1.19)$$

and all the other coefficients are zero. Further isotropic medium satisfies the Cauchy relation given by

$$C_{44} = \frac{1}{2}(C_{11} - C_{12}) \quad (1.20)$$

Therefore, the number of independent elastic constants are further reduced to two. They are C_{11} and C_{12}. Then the elastic constant matrix for an isotropic medium is reduced to

$$\begin{bmatrix} C_{11} & C_{12} & C_{12} & 0 & 0 & 0 \\ 0 & C_{11} & C_{12} & 0 & 0 & 0 \\ 0 & 0 & C_{11} & 0 & 0 & 0 \\ 0 & 0 & 0 & \frac{1}{2}(C_{11} - C_{12}) & 0 & 0 \\ 0 & 0 & 0 & 0 & \frac{1}{2}(C_{11} - C_{12}) & 0 \\ 0 & 0 & 0 & 0 & 0 & \frac{1}{2}(C_{11} - C_{12}) \end{bmatrix} \quad (1.21)$$

To define the elastic properties of an isotropic solid completely, two constants known as Lame constants λ and G are defined. They can be expressed as

$$\lambda = C_{12} \qquad G = \frac{1}{2}(C11 - C12) \quad (1.22)$$

G is the shear modulus and $\lambda+2G$ is the longitudinal modulus. Then the elastic constant matrix interms of λ and G becomes

$$\begin{bmatrix} \lambda + 2G & \lambda & \lambda & 0 & 0 & 0 \\ 0 & \lambda + 2G & \lambda & 0 & 0 & 0 \\ 0 & 0 & \lambda + 2G & 0 & 0 & 0 \\ 0 & 0 & 0 & G & 0 & 0 \\ 0 & 0 & 0 & 0 & G & 0 \\ 0 & 0 & 0 & 0 & 0 & G \end{bmatrix} \quad (1.23)$$

27

All the important elastic parameters of isotropic solids are expressed in terms of λ and G in the following manner.

$$\text{Longitudinal modulus} = \lambda + 2G$$
$$\text{Young's modulus} = G\frac{3\lambda + 2G}{\lambda + G}$$
$$\text{Bulk modulus} = \lambda + \frac{2G}{3}$$
$$\text{Poisson's ratio} = \frac{\lambda}{2(\lambda + G)} \tag{1.24}$$

Considering plane wave propagation in isotropic media and considering the symmetry conditions, we get the Christoffel's equation for the propagation of an elastic wave with velocity V in anisotropic solid as

$$\begin{bmatrix} C_{11} - \rho V^2 & 0 & 0 \\ 0 & \frac{1}{2}(C_{11} - C_{12}) - \rho V^2 & 0 \\ 0 & 0 & \frac{1}{2}(C_{11} - C_{12}) - \rho V^2 \end{bmatrix} = 0 \tag{1.25}$$

Where ρ is the density of the medium. From this we get three solutions in which one is for longitudinal and two are for transverse modes. But in the case of an isotropic sample, direction of polarisation does not have any significance and so we get the two elastic constants as

$$\rho V_{long}^2 = C_{11}$$
$$\rho V_{trans}^2 = \frac{1}{2}(C_{11} - C_{12}) \tag{1.26}$$

from this C_{11} and C_{12} can be calculated. So by measuring the velocity of longitudinal and transverse elastic waves, one can determine the elastic constants of an isotropic medium.[79]

1.6 Work reported in this thesis

In this thesis, we report the results of our work on the dielectric and elastic properties of selected dielectric ceramics and oxide glasses.

A general background of these materials and the parameters we have investigated are already given in this chapter. The subsequent chapters describe the instrumentation and experimental techniques we have used, the work done on the various materials, results obtained and detailed discussion of results in each case. The samples selected for the present investigation are (i) dielectric ceramics belonging to the groups $Ba_{2-x}Sr_xTi_9O_{20}, Zr_{0.8}Sn_{0.2}Ti_{1-X}Hf_xO_4$ and $BaLn_2Ti_5O_4$ and (ii) Oxide glasses belonging to the groups $(Bi_2O_3)_{1-x}$ $(CuO)_x$ and $Ba_{1-x}K_xBi$ $O_{3-\delta}$.Solid state ceramic preparation route has been followed to prepare dielectric ceramics and melt quenching technique has been adopted to prepare oxide glasses.

For the study of elastic properties of these selected samples, we have measured longitudinal and transverse ultrasonic velocity and attenuation as a function of composition and temperature using ultrasonic technique. Parallel plate capacitance method has been used for the measurement of dielectric constant of selected samples as a function of the temperature and composition. A home-made cell has been used for these measurements employing an Impedance Analyser for capacitance measurements. All the details of the work done are given in the following chapters of the thesis, devoting a chapter to each of the sample groups cited above.

1.7 References

[1] R. C. Zeller, R O. Pohl, *Phy. Rev.* B4, 2029 (1971)

[2] W Heinicke, G. Winterling and K. Dransfeld, *J. Acoust. Soc. Am.* 49, 954 (1971).

[3] S. R. Elliot, *Physics of Amorphous material* Second edition.

[4] L. C. Chen, and F. Spaepen, *Nature (Lond.)* 336, 366 (1988).

[5] W. H. Zachariasen, *J. Am. Chem. Soc.* 54, 3841 (19832).

[6] R. J. Bell, P. Dean, *Phil. Mag.* 25, 1381, (1972).

[7] S. R. Herd and P. Chaudhuri, *Phys. Status. Solidi* A 26, 627, (1974).

[8] D. E. Sayer, E . A. Stern and F. W. Lytle, *Phy. Rev. Lett* 35, 584 (1974).

[9] R. B. Schwarz, W. C. Johnson, *Phy. Rev. Lett.* 51, 415, (1983).

[10] N. H. Ritland, *J. Am. Ceram. Soc.* 37, 370 (1954).

[11] G. Addam and J. H. Gibbs, *J. Chem. Phys.* 43, 139 (1965).

[12] P. W. Anderson, B. I. Halperin and C. M. Varma, *Philos. Mag.* 25, 1 (1972).

[13] W. A. Phillips, *J. Low. Temp. Phy.* 7, 351 (1972).

[14] R. E. Jaeger, *J. Am. Ceram. Soc.* 51, 57 (1968).

[15] S. Suker, R. W. Gamon, *Phys. Rev. Lett.* 25, 222 (1970).

[16] A. S. Pine, *Phy. Rev.* 185, 1187 (1969).

[17] L. Piche, R. Maynard and R. Hunklinger and J. Jackle, *Phy. Rev. Lett.* 32, 1426 (1974).

[18] J. Jackle, *Z. Phys.* 257, 212 (1972).

30

[19] H. P. Baltes, *Solid State Commun.* **13**, 225 (1973).

[20] D. Walton, *Sol. State. Commun.* **14**, 335 (1974).

[21] G. J. Morgan and D. Smith, *J. Phys. C* **7**, 649 (1974).

[22] J. V Fitzgerald, *J. Am. Cer. Soc.* **34**, 314 (1951).

[23] P. W. Anderson, *Phys. Rev.* **109**, 1492 (1958).

[24] A. H. Wilson, *Theory of metals (Cambridge University press, NewYork,)* (1936).

[25] A. Abrahams, P. W. Anderson , D C. Licciardello and T. V. Ramakrishnan, *Phy. Rev. Lett.* **42**, 673 (1979).

[26] P. A. Lee and T. V. Ramakrishnan, *Phy. Rev. Lett.* **42**, 673 (1979).

[27] D. J. Thouless in *Condensed Matter ed: R. Balian, R. Maynard and G. Toulose* (North Holland, Amsterdam, 1978) p-5.

[28] N. F. Mott and E. A. Davis, *Electronic procesess in Non crystalline Materials* (Clarendon press, 1971).

[29] L. A. Trinogga, G. Kaizhou and I C. Hunter, *Practical Microstrip Design* (Ellis HorWood, 1991).

[30] R. E. Newnham, *Rep. Prog. Phys.* **52**, 123 (1989).

[31] W. Wersing, *Electronic ceramics   Edited by B.C.H. Steele*, Elsevier Pub. Co. Inc. 67 (1991).

[32] D Kajfez and P. Guillon, " *Dielectric Resonators* ", Artech House, Massachusettes (1986).

[33] J. K. Plouride and C. L. Ren, *IEEE Trans. Microwave Theory Tech.*,MTT **29**, 754 (1981).

[34] R. Freer, *Silicates Industrials*, **9-10**, 191 (1993).

[35] S. Nomura, *Ferroelectrics* **49**, 61 (1993).

[36] K. Wakino, T. Nishikawa, Y. Ishikawa and H. Tamura, *British Ceram. Trans. J.* **89**, 39 (1990).

[37] K. Wakino and H. Tamura, *Ceramic. Trans.* **15**, 305 (1990).

[38] Y. Konishi, *Proc.* **IEEE 79**, 726 (1991).

[39] M. Takata and K. Kageyama, *J. Am. Ceram. Soc.* **72**, 1955 (1985).

[40] H. Kagata and J. Kato, *Jpn. J. Appl. Phys.* **33**, 5463 (1994).

[41] H. M. O'Bryan Jr., J. Thomson Jr. and J. K. Plourde *J. Amer. Cer. Soc.* **57**, 450 (1974).

[42] K. Wakino, K. Minai and H. Tamura, *J. Amer. Cer.Soc.* **67**, 278 (1984).

[43] M. Takata and K. Kageyamma, *J. Amer. Cer. Soc.* **72**, 1955 (1989).

[44] Aagranovskaya, *Bull. Acad. Sci. USSR Ser. Phys.* **24**, 1271 (1960).

[45] G. Wolfram and H. E. Gobel, *Mater. Res. Bull.* **16**, 1455 (1981).

[46] K. Wakino, M Minai and H. Tamura, *J. Am. Ceram. Soc.* **67**, 278 (1984).

[47] J. Takahashi, K. Kageyama and K. Kodaira, *Jpn. J. Appl. Phys.* **32**, 4327 (1993).

[48] H. Tamura, H. Matsumoto and K. Wakino, *Jpn. J. appl. Phy.* (supplement) **28-2**, 21 (1989).

[49] H. Tamura, T. Konoike, Y Sakabe and K. Wakino *J. Am. Ceram. Soc.* **67**, C 59 (1984).

[50] K. H. Yoon, B. J. Jung and E. S. Kim, *J. Mater. Sci. Lett.* **8**, 819 (1989).

[51] M. Spector, *Insul. & Circuits*, **25**, (1979).

[52] *Insul. & Circuits* (Directory/ Encyclopedia) 19(7), 194-208 (1973).

[53] W E. Warren, *X-ray diffraction* (Addison-Wesley) (1969).

[54] L. D. Bogomolova, T .F Dolgolenko, *Fiz. Tv. Tela* 16, 1486 (1974).

[55] K. K. Evstrop'ev and V A. Khar'yuzo V, *Dokl. Akad. Nauk SSR*, 136, 140 (1961)

[56] M. Schwartz and J .D Mackenzie, *J. Am. Ceram. Soc.*, 49, 582 (1966).

[57] A. Ghose and B. K. Chaudhuri, *Indian J. Phy.* 58A, 62 (1984).

[58] A. R. Kulkarni, H. S. Maithi and A. Paul, *Bull. Mater. Sci.* 6, 216 (1984).

[59] S. Hunklinger and W. Arnold in *Physical Acoustics ed: R. N. Thurston and W. P. Mason*, Academic press, NewYork 12, 155 (1975).

[60] D. Nag and R. J. Sladek, *Phy. Rev.* B11, 4017 (1975).

[61] A. A. Antoniou and J. A. Morrison *J. Appl. Phys.* 36, 1873 (1965)

[62] O. L. Anderson, H. E. Bommel, *J. Am. Ceram. Soc.* 38, 125 (1955).

[63] G. K. White, *Cryogenics* 4, 12 (1964).

[64] L. Hopkins and C. R. Kurkjian, *Physical Acoustics* ed: W. P. Mason, Vol II B Academic Press, NewYork (1995) p91.

[65] P. Ya Bokin, *Mechanical properties of silica glass*, Nanka, Leningrad (1970).

[66] H. J. McSkimin, *J. Appl. Phy.* 24, 988 (1953).

[67] P. Ya Bokin, N. S. Yuritsyn, E. N. Stepanov and G. N. Samsonkina, *Fiz. Khimi, Slekla* 2, 176 (1976)

[68] M. N. Kulbitskaya, V P. Romanov, E. O. Chernysheva, and V A. shutilov, *Fiz. Khim. Stekla* 2, 183 (1976).

[69] O. L. Anderson and H. E. Bommel, *J. Am. Ceram. Soc.* **24**, 12 (1955)

[70] R. E. Strakna, *Phy. Rev.* **123**, 2020 (1961)

[71] R. Vacher and J. Pelous, *Phy. Lett. A* **53**, 233.

[72] J. T. Krause *Phys. Lett.* **43A**, 325 (1973).

[73] C. K. Jones, P. G. Klemens, J. A. Rayne, *Phy. Lett.* **8**, 31 (1964).

[74] R. E. Strakna, H. T. Savage, *J. Appl. Phy.* **35**, 1445 (1964).

[75] C. Krischer, *J. Acoust. Soc. Am.* **48**, 1086 (1970).

[76] D. B. Fraser, J. T. Krause, A. H. Meitzler, *Appl. Phy. Lett.* **11**, 308 (1967).

[77] S. M. Mahle, R. D. McCammon, *Phys. Chem. Glasses* **10**, 222 (1969).

[78] G. Frossati, J. Le (Gilchrist, J. C. Lasjaumas, W. Meyer, *J. Phys.* **C10**, L 515 (1977).

[79] B. A. Auld in *Acoustic fields and waves in solids* bf Vol II, John Wiley and sons, New York (1973).

Chapter 2

Instrumentation

2.1 Introductory remarks

The study of interaction of acoustic waves and electric fields with matter provide a great deal of information about their elastic and dielectric properties and the associated relaxation effects. Accurate values of these constants are necessary to determine characteristic model parameters as tests of various atomic models of solids. The quantitative study of elastic constants and their variation with temperature and pressure give information about the interactions of lattice vibrations with other elementary excitations in solids. They also provide a sensitive probe of structural phase transitions. The study of the variation of dielectric constant of a solid with density and temperature are also of fundamental and applied interest. Insight into the nature of solid and molecular modes of excitation may be gained by viewing the dipolar coupling to an externally applied electric field.

Many advanced and sophisticated methods have been developed to give the precise information about the dielectric and elastic properties of materials. Ultrasonic techniques are the best and most popular method for the measurement of elastic properties of solids because of their accuracy and nondestructive nature. They are also useful to probe structural transitions taking place in solids. Among the several techniques developed for the measurement of ultrasonic velocity and attenuation, the pulse echo overlap (PEO) method is found to be the most used one. This is the technique used by us to measure elastic properties of dielectric resonator ceramics and oxide glasses. Details of this method along with the McSkimin Δt criterion for selecting properly overlapped echoes and method of making bond correction are explained in this chapter.

35

The details of all the associated experimental setup used for the pulse echo overlap technique are discussed in detail in this chapter.

The parallel plate capacitance method has been used for the measurement of dielectric constant of the different materials presented in this work. The design and fabrication details of the homemade dielectric constant cell for parallel plate capacitance method for the measurement of dielectric constant and its variation with temperature are described in this chapter. Details of the experimental setup are also outlined

2.2   Dielectric constant measurements

In recent years, the techniques for measuring dielectric properties accurately have improved very much, accompanied by the availability of accurate instruments to undertake measurements. There are so many methods and techniques for the measurement of dielectric properties that it is difficult to choose one of them for a specific case. They also often require many troublesome procedures like applying electrodes on the specimen and setting it between the electrodes, applying edge correction, series resistance and inductance correction etc. Several authors have published different measuring methods which have attempted to eliminate such troublesome procedures by combining several well known methods [1,2]. The simplest method to obtain the dielectric constant of a given material is to construct a parallel plate capacitor with the sample forming the dielectric medium. By measuring the capacitance value, the dielectric constant can be calculated using the equation

$$C = \frac{\epsilon A}{d} \qquad (2.1)$$

where C is the measured capacitance value, ϵ is the dielectric constant of the specimen, A is the area of cross section of the plate and d is the thickness of the specimen. The main disadvantage of this technique is that it is very difficult to isolate the capacitance due to the dielectric medium from the measured capacitance, as the total capacitance contains a component of lead and fringe capacitances. The accuracy of the dielectric constant attainable by this method is thus determined by the uncertainties associated with the values of C, A and d. The capacitance can be measured to within 1% by procedures.

36

and this error is insignificant compared to that incurred by the area and thickness measurement of the specimen. In addition to these uncertainties, it has been pointed out that [3] in certain cases, electrode - specimen interaction can lead to capacitance enhancement.

In the present investigations we have accounted for the effect of lead and fringe capacitances [4]. By measuring the total capacitance of a number of samples with varying A/d values and plotting a graph with A/d along the x axis and the measured capacitance along y axis, a straight line will be observed and the intercept of this line gives the sum of lead and fringe capacitances. For capacitance measurements, we have used an HP 4192A Impedance analyser with which measurements can be carried out in the frequency range d.c. - 13 MHz. The main advantage of this instrument is that it is provided with an offset adjustment by which lead capacitance can be completely eliminated. This instrument has a maximum sensitivity of 0.001 pF. For temperature measurement and control, a Lake Shore Cryogenics (USA) Model DRC 82C temperature controller has been used. A block diagram of the capacitance measurement set up is shown in Fig.2.1.

The dielectric constant cell used is specially designed and fabricated for measurements at low temperatures with liquid nitrogen used as the cryogen and also at higher temperatures. The details of this dielectric cell is discussed separately in the next section.

2.3   The fabricated dielectric constant cell

For low temperature as well as high temperature dielectric constant measurements we have designed and fabricated a dielectric constant cell. It is a cold finger type cell provided also with optical windows on diametrically opposite sides to perform experiments on the effect of light on different properties, if necessary.

A schematic diagram of the cell is shown in Fig.2.2. The metallic outer case is half meter long. The top and bottom lids are removable and are made vacuum tight by using rubber 'O' rings of 24 cm diameter. The 30 cm long nitrogen reservoir is welded to the top lid of the cryostat. The liquid nitrogen reservoir has a thick copper bottom
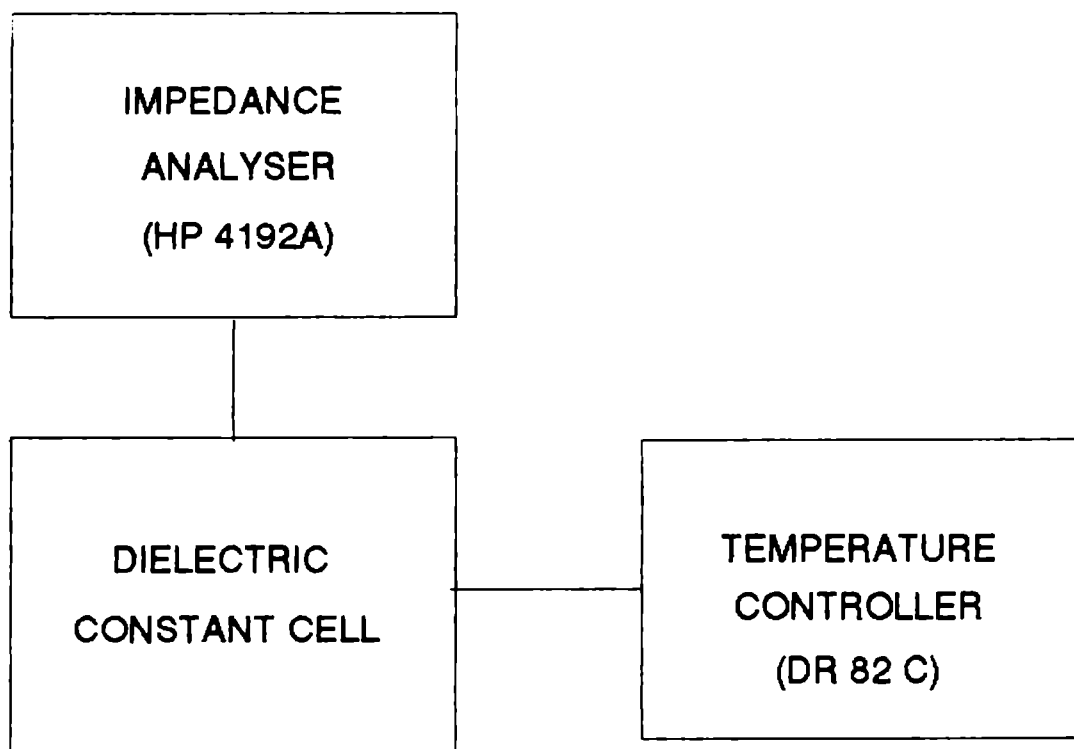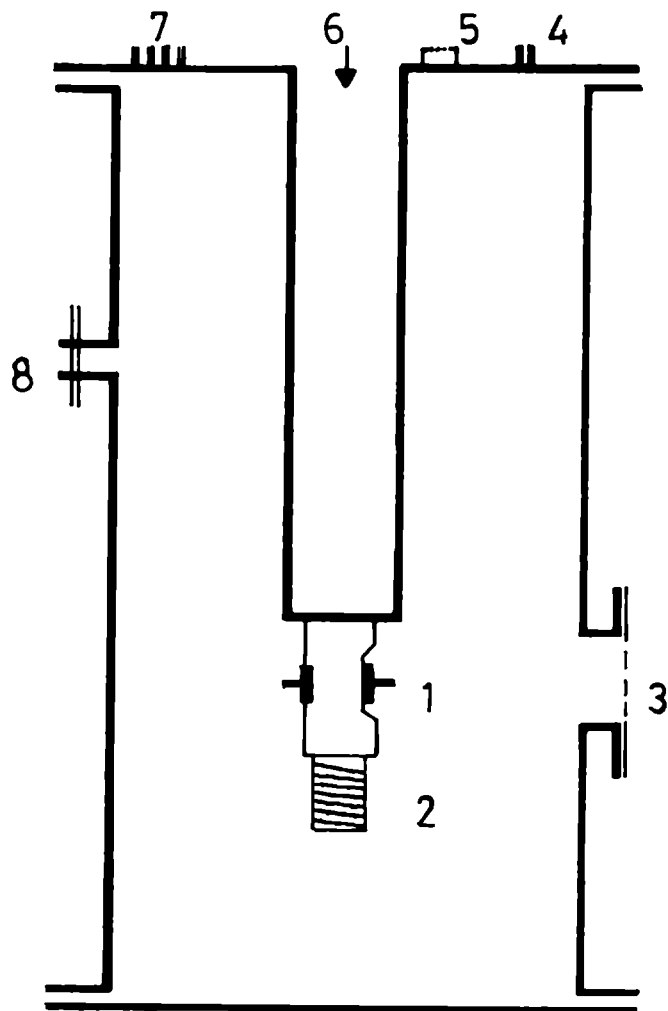
Fig. 2.1: Block diagram of the experimental setup for dielectric constant measurements.

1. Sample Holder   5. D-Type connector

2. Heater   6. Liquid nitrogen reservoir

3. Window   7. BNC connectors

4. Power supply for heater   8. Connector to vacuum pump

Fig. 2.2: Schematic diagram of the dielectric constant cell.

to which the sample holder assembly is tightly fixed by threading. An extra mass can be attached to this copper bottom in order to increase the thermal mass of the cell for efficient control and stabilisation of temperature. The sample holder assembly is 10 cm long, made from thick solid copper cylinder with 1.5 cm diameter grooves at the centre in which two circular platforms along with the sample can be inserted. The sample is kept between these two parallel plates by means of spring and screw arrangement. A thin heater wire is closely wound on the sample holder just below the grooves. This heater wire acts as a heater element for temperature control. A platinum resistance sensor is inserted on the sample holder close to the sample to monitor the temperature of the sample very accurately. Four probe methods is used on the temperature sensor in order to minimise the error in the measurement. Cables with 50 ohm impedance are used for the electrical connections in order to carry out the measurement at high freqencies and terminated at the BNC connector at the top. The terminals of the sensor are taken out through a 9 pin D type connector and the heater power from the temperature controller is applied through a 3 pin connector on the top lid of the cell. Fig. 2.3 shows the photograph of the equipment used for the dielectric constant measurement.

2.4   Elastic properties using ultrasonic technique

The propagation of high frequency elastic waves in solids is a well established technique to study elastic properties and their variation with external parameters of the material by measuring their velocity and attenuation as function of the variable of interest. Such measurements enable one to analyse any property of solid which is related to the dynamics of the lattice. The measurement of acoustic parameters like ultrasonic velocity and attenuation are very useful in studying material properties.

Measurement of ultrasonic velocity in solids is usually carried out in two different ways; depending upon the different purposes. On one hand, one needs highly accurate absolute measurement of velocity in order to determine the properties related to lattice vibrations of the solid. On the other hand, one gets very important information about the changes in a solid when parameters like temperature, pressure etc are varied by measuring the corresponding changes in the wave velocities. In this
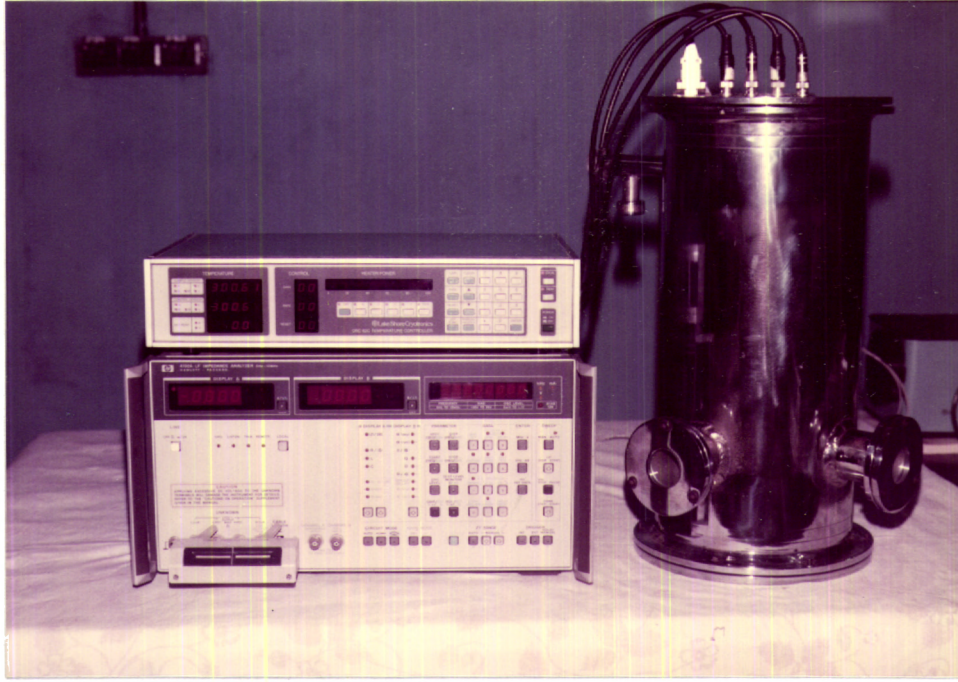
Fig. 2.3: Photograph of equipment used for the dielectric constant measurement.

case, velocity changes are of interest and absolute accuracy is not usually necessary. A high sensitivity of the measurement to such changes is important because they are quite small. Thus the systems for the measurement of ultrasonic velocity naturally fall into two classes. One in which absolute accuracy is the main objective and other case in which sensitivity is the main objective. According to this, a number of methods have been developed for such measurements and they can be classified into three categories as follows.

1. Low frequency methods

2. Continuous wave method

3. Pulse echo method

2.4.1 Low frequency method

In this method, the elastic modulii of solids are determined from their mechanical resonance frequencies. This dynamic method, first originated from the early measurement done by Ide in 1935 [5] is based on standing wave phenomenon in the medium. When the specimen is undergoing longitudinal or torsional vibration, the length of the specimen contains an integral number n of half wave lengths, so that

$$l = \frac{n\lambda}{2}$$

The velocity of wave is then given by

$$V = \lambda \; f = \frac{2lf}{n} \qquad (2.2)$$

where f is the resonant frequency of any mode of vibration. In this case the elastic compliances (Youngs modulus Y and shear modulus G) are determind by measuring flexural and torsional oscillations. These techniques are described by Read et al [6]. These methods are particularly suitable for piezo electric materials which can be excited into mechanical resonance by an electric field directly without transducers [7]. Other non-piezoelectric materials can be measured in a similar way with additional dc bias field using the electrostrictive effect [8]. The various low frequency dynamic resonance methods are described by Schreiber et al [9].

42

2.4.2 Continuous wave methods

In this method, when an acoustic excitation is applied to a sample with piezoelectric transducer, standing waves are set up between the opposite faces of the sample. For a sample of length L, the number of excited resonances of frequency f is given by

$$n = \frac{2Lf}{v} \tag{2.3}$$

whereby the sound velocity v can be determined [10]. A major source of uncertainty in this method is the possibility of erroneous readings due to reflection of the wave from discontinuous surfaces rather than end faces   The consequence of such a reflection is two waves, shear and longitudinal wave travelling at different velocities. The CW method is seldom used for low temperature work, because of sample heating due to large input power to the sample. The CW technique is most suitable in the KHz range. Details of this method are given in a number of references [11,12].

In the continuous composite wave oscillator method [12], the specimen and transducer act as a two terminal electrical network whose characteristics depend on the rapid variation of impedance at each acoustic resonance of the system. The impedance is measured by balancing a bridge [13,14]. If there is a small change in the velocity of the sound in the sample, there is a change in resonant frequency which produces an imbalance of the bridge which can be counteracted by a frequency or bridge capacity readjustment. The accuracy of the measurement using this technique is ± 0.1ppm.

2.4.3 Pulse methods

The pulse methods have become very popular and are the most widely used nowadays. Improvements in both precision and accuracy by this method have been achieved first by Birch [15]. In a pulse echo method, an ultrasonic pulse of short duration is generated using a piezoelectric transducer which is bonded to the sample under investigation. Piezoelectric transducer is usually made of quartz or materials like $LiNbO_3$, $BaTiO_3$, $SrTiO_3$, PZT etc. The samples for the experiment are cut with diamond wheel saw and polished so as to have plain parallel faces perpendicular to the desired direction of wave propagation. The sound waves excited in this direction get multiply reflected from the

end faces and produces an electric signal each time it hits the transducer. These electric echo pulses are amplified and displayed on an oscilloscope as a series of echoes. Because of multiple reflections, each time the stress wave passes through the sample a fraction of energy is absorbed or scattered. The result is an exponentially decaying echo pattern. A typical pattern is shown in Fig.2.4.

The measurement of sample thickness can be accomplished by comparator devices to an accuracy of about $\pm 10^{-5}$ m. From the length of the sample, the transit time of the pulse in the sample and the decay rate of the pulse amplitude of the successive echoes, the velocity and attenuation can be determined. The absolute accuracy of such measurements is generally about 1%. Details of the pulse technique have been described by several authors [16-31].

Considering the plain attenuated wave as represented by equation

$$A(x,t) = A_o e^{-\alpha x} e^{(\omega t - kx)} \tag{2.4}$$

where α is attenuation coefficient which is the imaginary part of the complex propagation vector and the phase velocity v_p is the real part. Then the attenuation can be expressed as

$$\alpha = \frac{1}{(x_2 - x_1)} 20 log_{10} \frac{A(x_1)}{A(x_2)} \text{ dB/unit length} \tag{2.5}$$

where $A(x_1)$ and $A(x_2)$ are the amplitude of two echoes and $(x_2 - x_1)$ represent the distance travelled by the echoes. The attenuation α can be determined by comparing the amplitude of the two echoes or by making use of a calibrated pulse echo pattern on the oscilloscope.

Using phase sensitive method the absolute accuracy can be increased and very high precision of 0.1% can be obtained in the measurement of changes in the velocity. The popular phase sensitive methods are pulse superposition, phase comparison and pulse echo overlap.

2.4.4   Pulse superposition method

The pulse superposition method first proposed by McSkimin [18-20] is highly accurate for measuring the ultrasonic wave velocity in materials. In this method a single
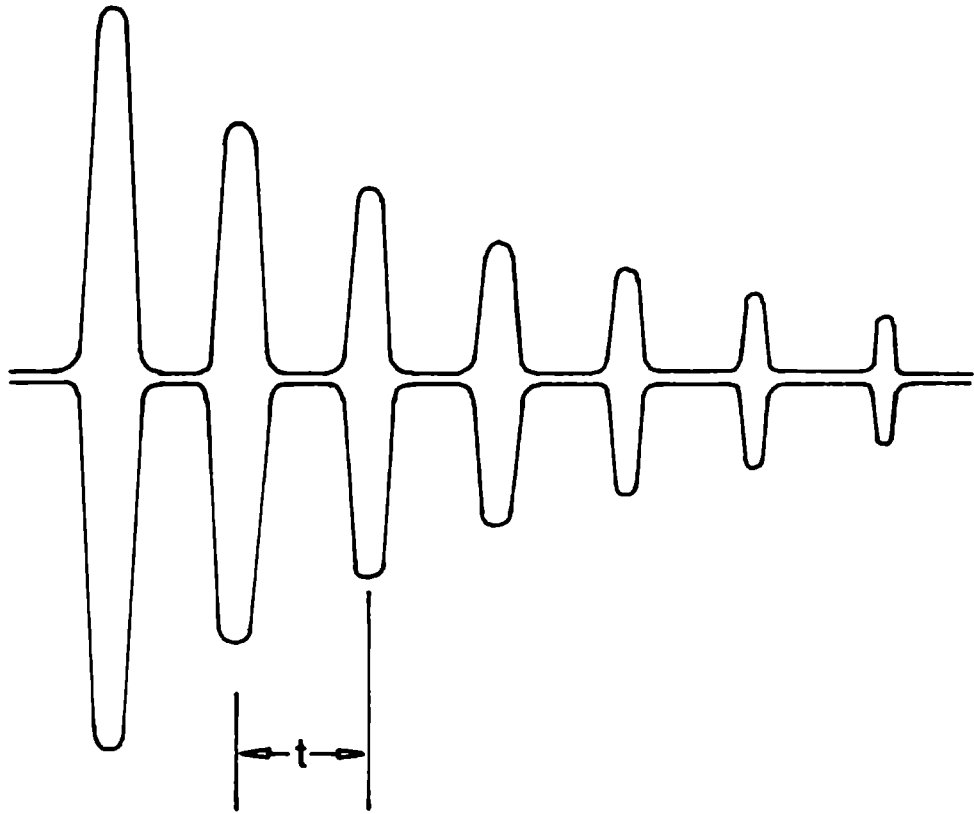
44

Fig. 2.4: A typical exponentially decaying echo pattern.

45

transducer is used on the specimen and multiple echoes are obtained. In the normal mode of operation, the rf pulsed oscillator pulses the transducer once per round trip of the waves in the specimen. Generally pulse sequences are produced every T sec with T approximately equal to some multiple of (p) of the round-trip delay of ultrasonic wave in the specimen. When the pulse repetition frequency (PRF) is critically adjusted, the applied pulse is superimposed on the echo and continuous wave in the applied pulse will be phase adding with continuous wave in the echo. The measured delay time in this specimen is then given by [22]

$$T = p\delta - \frac{p\gamma}{(2\pi f)} + \frac{n}{f} \qquad (2.6)$$

where T is the measured period of the PRF in the interference condition, δ is the true time delay in the specimen, p is the integer discussed as above and γ is the phase shift introduced by the bond. f is the frequency of the CW oscillator and n is an integer associated with the phase difference between continuous wave within the applied pulse and within the return echo. The reciprocal of the time of travel of the wave within the sample is equal to CW oscillator frequency which can be measured using a frequency counter. This method requires a very stable PRF. From the time of travel of the wave, the velocity of ultrasonic wave in the sample can be determined.

The absolute accuracy of this technique arises from the fact that the method is capable of measuring accurately from any cycle of one echo to the corresponding cycle of the next echo. However, it is not certain as to which of the crests are involved because of the lack of resolution or the distortion of the leading edge of the pulses, due to reflection within the transducer and the finite bandwidth of the acoustic system. In precision high resolution measurement, one has to take into account the diffraction effects [21] and the coupling between the transducer and the specimen . Even though the dimension of the transducer and the specimen may be known precisely, the dimension of the bonding material are known only approximately and properties of the bond may also change slightly with temperature and pressure. The second important problem is the location of the start of the echo signal, since the finite band width of the acoustic system gives a finite rise time to the signal. However, this method is not as versatile as

46

the pulse echo overlap method due to the following drawbacks. The precise detection of the maxima or minima of the pulse coherence is limited due to low precision in finding echo superposition on the oscilloscope screen. This method cannot accommodate buffer rods or broad band pulses. The pulse superposition technique has been discussed in detail by many authors [18-20,22].

2.4.5 Sing around system

This method is an automated method for measuring ultrasonic velocity with moderate accuracy. It is highly sensitive to ultrasonic velocity changes [23].

In this method, the measurement is carried out with two transducers. A triggered transmitter sends an electrical pulse to the transmitting transducer, which generate a mechanical wave in the specimen. Second transducer receives these waves and amplifies the signal. The leading edge of the received and amplified signals is used to generate a trigger signal that produces a new pulse from the transmitter. This process repeats continuously. The frequency of trigger signal is measured by a frequency counter. The travel time through the loop is the reciprocal of the trigger signal frequency.

Due to the delays connected with electrical circuits and rise time of the amplified pulse, the travel time through the loop is greater than the travel time through the specimen. This method is very useful for relative measurements such as measurement of changes in velocity with change in temperature or pressure, but it is not good for making absolute velocity measurements.

2.4.6 Phase comparison method

In this method [24] coherent wave packets are generated by gating an oscillator. A comparison signal is superimposed on one of the echo signals from the specimen. The oscillator frequency is adjusted till the comparison signal and the echo are in phase. The frequency then will correspond to an integral number of half wave lengths within the sample. The adjustment of the phase and amplitude of the comparison signal can lead to cancellation of two pulses. This method gives rise to accuracies of 1 part in 10^4. Errors due to bonding can be minimised by reducing the thickness of cement

as nearly as possible to an odd number of quarter wavelengths at the frequency of measurement. Hydemann [25] designed a fringe counting pulse interferometer which is capable of measuring large changes in transit time of the order of 1 to 20 micro seconds with an accuracy of 2.5 x10^{-4} sec.

2.4.7 Pulse echo overlap method

The pulse echo overlap method (PEO) is a highly accurate technique for measuring velocity of ultrasonic waves through solid materials[22,26-29]. This method was invented by John. E. May [26] in 1958 and Papadakis [28] modified this technique into the present form in 1964 with the McSkimin calculation of correct cycle for cycle superposition (overlap in PEO method) incorporated into the technique. The correct overlap obtained by using McSkimin calculation permits travel time with high absolute accuracy of the order of 0.001%. This arises from the capability of measurement of any cycle of one echo to the corresponding cycle of the next echo. The pulse echo overlap method is able to handle diffraction phase corrections properly [21,29].

The PEO method has several advantages compared to other methods. This method can operate with transducer bonded directly with the specimen or with a buffer rod introduced between the specimen and transducer. The PEO method may be operated with broad band pulses [30] or rf bursts. One advantage of broad band pulse is that proper overlap can be setup with the broad band echoes. Simultaneous measurement of attenuation and velocity of ultrasonic wave is another advantage of PEO method. The group velocity [31] as well as phase velocity [27] can be measured with PEO method by using envelope of moderately narrow band rf pulses. The drawback of this method is that it is difficult to automate it as its echoes are overlapped by making observations in the scope time and not in real time.

2.5 The PEO system

The block diagram of the PEO system in present work is as shown in Fig. 2.5. The CW oscillator supplies the frequency which is equal to the reciprocal of the delay time between the echoes of interest. The CW signal supplies signal to the x-input of the
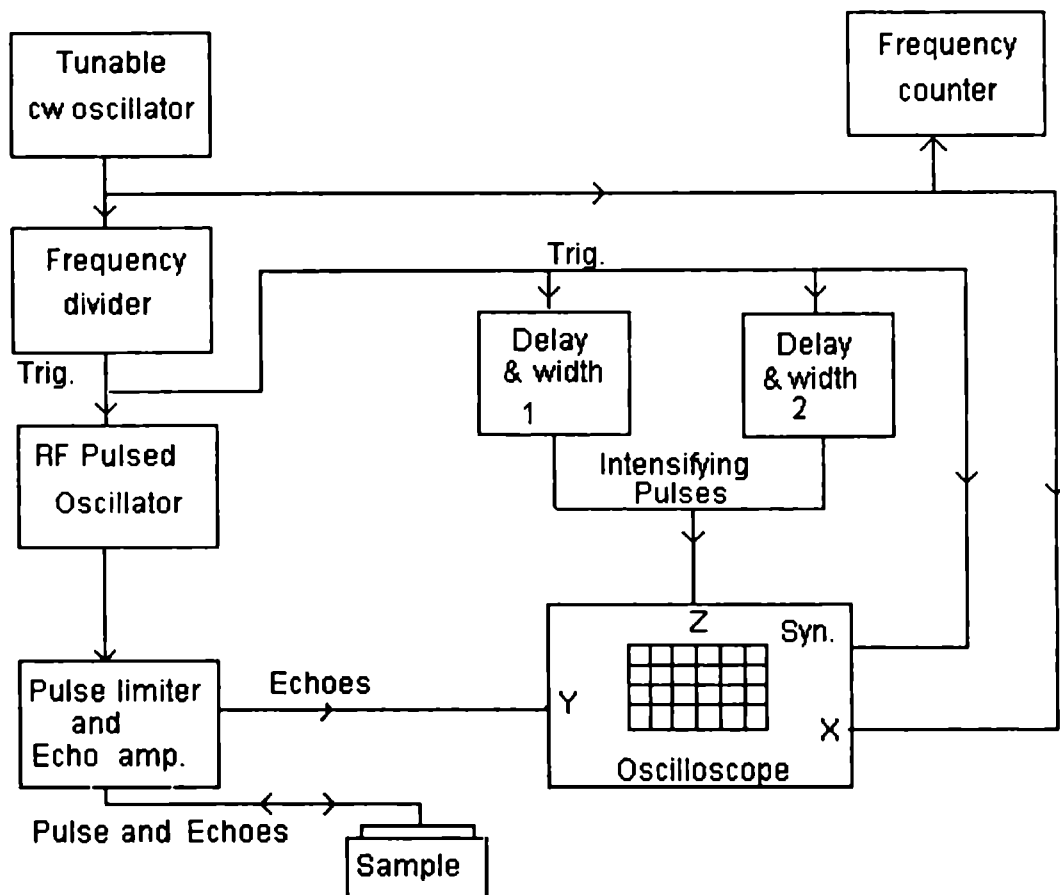
Fig. 2.5: The block diagram of the Pulse Echo Overlap method for measuring the travel time of the ultrasonic waves.

CRO to display the overlapped echoes on the CRO screen and frequency divider provides synchronous triggers for the pulsed rf oscillator and delay circuits. The frequency of CW signal can be measured with a frequency counter. The delay generator provides the two synchronised intensifying pulses of adjustable width and delay to permit the observation of two selected echoes by intensifying the CRO display at the two echoes of interest. The rf generator must be a pulsed oscillator which is triggered by the divided trigger generated from the CW oscillator. The rf pulse energises the piezoelectric transducer, which sends the ultrasonic signals into the sample and receives the echoes. After amplification the echo is sent to the Y input of the CRO. The diode pulse limiter protects the amplifier input from the high power rf pulses. When the CRO is in linear sweep mode, the X- axis sweep is triggered by the synchronisation input signal which is the same as the one triggering the rf pulsed oscillator. For jitter free overlap the signals of interest must be synchronised with the phase of the CW voltage. This condition is achieved by generating the repetition signal of the input rf pulse from the phase of CW voltage by frequency division. Division by large integer of the order of 100 or 1000 allows all the echoes from one pulse to be attenuated before the next pulse is supplied. The output of the frequency divider is the trigger signal synchronous with the phase of CW voltage. This trigger signal triggers a pulsed oscillator which is connected to the transducer. If the time base of the oscilloscope is properly set then all the echoes, with exponentially decaying amplitudes, along with the first rf pulse can be seen on the screen. The two echoes of interest between which the time delay is going to be measured can now be selected by positioning the intensifying pulses on them by adjusting the delay and width of the intensifying pulses. The approximate time interval between the echoes can be noted from the CRO to enable an initial frequency setting for the CW oscillator. When CRO is switched to x-y modes, the x-axis sweep is produced by the CW oscillator and a sweep is there corresponding to every echo. The echoes appear on the screen one after the other on successive sweeps. Due to the persistence of the vision, the echoes appear as if one is overlapped on the other by adjusting intensifying pulse amplitude and the two echoes of interest alone can be made visible in the overlapped condition. The overlap is exact, if the CW frequency is equal to reciprocal of the time interval

50

between the echoes. The cycle to cycle overlap of the echoes can be achieved by fine tuning the CW oscillator. The frequency of the CW signal can now be read on the frequency counter. The reciprocal of the CW frequency gives the round trip time of the echoes in the sample. By measuring the length of the sample the velocity can be calculated.

Due to the attenuation and the pulse distortion effects the number of rf pulses in the two selected echoes will be different and hence there is no easy way to find which cycle of the first echo should be overlapped with which cycle of second. In order to get correct cycle to cycle overlapping, a technique called McSkimin Δt criterion [18,19] is used.

2.5.1 The McSkimin Δt criterion

Consider the propagation of ultrasonic waves of single frequency echoing back and forth within the specimen. The specimen is bare on one end but has transducer bonded to the other end. The transducer is half a wavelength thick at its resonant frequency and the bond has finite thickness. The transducer is unbacked. We will consider the effect of the bond and transducer upon the phase reflected wave at the bonded end of the specimen in order to select the correct cycle to cycle matching of one echo with any subsequent echo. Fig. 2.6 shows the sketch of the specimen, bond and transducer. The phase angle γ which relate the reflected wave phase to incident wave phase is also shown in the fig.2.6. The phase angle is a function of acoustic impedance, the thickness of layers and frequency. The specific acoustic impedances are Z_s for the specimen, Z_1 for the bond, Z_2 for the transducer. The impedance looking into the termination from the specimen is Z_d, given by the transmission line theory as

$$Zd = jZe = jZi \left[\frac{(Z_1/Z_2)\tan\beta_1 l_1 + \tan\beta_2 l_2}{(Z_1/Z_2) - \tan\beta_1 l_1 \tan\beta_2 l_2} \right] \tag{2.7}$$

where β_1 and β_2 are the propagation constants in the bond and transducer and l_1 and l_2 are the thickness of the bond and transducer respectively. The propagation constants β_1 and β_2 are related to ultrasonic frequency f impressed upon the transducer by the rf pulse generator and also to the velocities v_1 and v_2 of the wave in the bond and
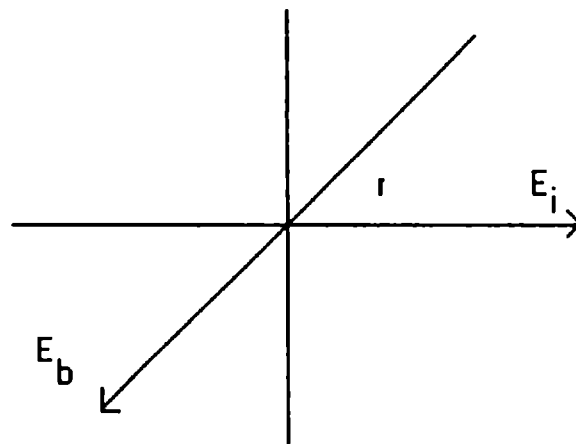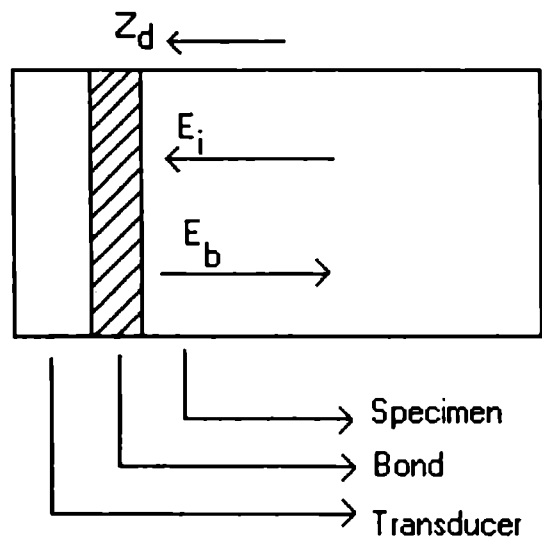
51

Fig. 2.6: Specimen geometry showing transducer, bond and sample.

transducer respectively. The relations are

$$\beta_1 = \frac{2\pi f}{v_1} \quad and \quad \beta_2 = \frac{2\pi f}{v_2} \tag{2.8}$$

Z_d can be used to derive the ratio of reflected to the incident pressure as

$$\frac{E_b}{E_i} = \frac{Z_d - Z_s}{Z_d + Z_s} \tag{2.9}$$

where Z_d is imaginary ($Z_d = jZ_e$). The real and imaginary parts of equation
(2.7) can be separated as

$$\frac{E_b}{E_i} = \frac{Z_s^2 - Z_i^2}{Z_i^2 + Z_s^2} - j\frac{2Z_e Z_s}{Z_e^2 + Z_s^2}, \tag{2.10}$$

from which the phase angle γ upon reflection is given by

$$\tan\gamma = \frac{-2Z_e Z_s}{Z_s^2 - Z_e^2} \tag{2.11}$$

In the above formulae, there is one unknown parameter, the bond thickness l_1 and one
running variable, the ultrasonic frequency f. By varying f one can change β_1 and β_2.
The phase angle γ is a measure of the effect of the transducer and bond on the reflected
wave.

McSkimin [18,19] has shown that the measured travel time t_M is made up of
true round trip time t plus some increments, given by

$$t_M = pt - (p\gamma/2\pi f) + (n/f) \tag{2.12}$$

Here p is the number of round trips in the measurement. The phase angle gamma
per reflection yields a fraction $\gamma/2\pi$ of a period of the rf, so that a time increment
$\gamma/2\pi f$ is generated per round trip. n is the number of cycles of mismatch in the overlap
measurement. The aim of mathematical analysis is to develop a method to make n = 0
and estimate the minimum of the residual γ value. From the above equations it is clear
that both γ and t_H are functions of frequency f. It is possible to utilise this dependence
of t_H on frequency to eliminate n, the cycle mismatch. For this, consider measurement
of t_M at high frequency f_H and a lower frequency f_L (for eg. at the resonant frequency
$f_H = f_r$ and $f_L = 0.9 f_r$). Then t_H is the measured time at f_H and t_L is the measured time

at f_L. ie,

$$t_H = pt - (p\gamma_H/2\pi f_H) + (n/f_H)$$

$$t_L = pt - (p\gamma_L/2\pi f_L) + (n/f_L) \tag{2.13}$$

where the same overlap condition has been maintained by shifting the repetition frequency slightly as the rf frequency is changed. Subtraction eliminates t and one gets the true travel time as

$$\Delta t_M = t_L - t_H = \frac{1}{f_L}\left(n - \frac{p\gamma_L}{2\pi}\right) - \frac{1}{f_H}\left(n - \frac{p\gamma_H}{2\pi}\right) \tag{2.14}$$

The above equation indicates that f_H, f_L, t_L and t_H are measured and γ_L and γ_H are computed from l_1, l_2, v_1, v_2, Z_1, Z_2 and Z_s using equations 2.6, 2.7, and 2.10, then there is one possible value for Δt_M when n $=$ 0, or we can say that if n $=$ 0 is set in the measurement, the measured value of Δt_M will agree with the value calculated theoretically

To apply McSkimin Δt criterion to pulse echo overlap technique one has to follow the following procedure. (i) With the ocilloscope in triggered sweep, find the approximate time between the echoes of interest from the graticule of the CRO and set the CW oscillator frequency to have that time as its period. (ii) Switch to the direct sync. sweep trigger mode and adjust the CW oscillator frequency to bring about a plausible overlap with the leading edges of the echoes nearly aligned and every cycle of the later echo smaller than the corresponding cycle of earlier echo because of the attenuation. (iii) Measure t_L and t_H of equation 2.13 at the frequencies f_L and f_H, usually $0.9f_r$ and f_r. (iv). Repeat step (iii) for several possible adjacent overlaps, for eg. three towards low CW repetition frequency and as many towards higher frequency. (v) Compute Δt_M of equation 2.14 for each of these sets of measurements. (vi) Compare Δt_M found experimentally with theory and choose the correct cycle for cycle match. Then t_H measured at $f_H = f_r$ will be t_M in equation 2.12 with n $=$ 0. This time t_M is the correct expression for the measured time before correction for phase shift due to bond. Comparison of Δt_M found experimentally with theory for selecting the correct overlap is not a straight forward procedure. This is due to the unknown bond thickness and

54

difficulty in computing a theoretical value of Δt_M for the comparison. To overcome this difficulty a graphical technique is often used. For this, bond thickness is assumed very thin, approximately less than a quarter of the acoustic wave length. This means that the bond phase $\beta_1 l_1$ expressed in degrees can be in the range 0 to 90 degrees. Using the equations presented above, the value of Δt_M can be computed (for n = 0 case) for measuring value of bond angle from 0 to 90 degrees   A plot of Δt_M vs. bond angle is then made. This gives a range of possible Δt_M values for the given transducer, bond and sample combination for the n = 0 case. By examining overlap case in measured values with calculated values for n = 0 case, the correct overlap case can be identified for n = 0. To find the correction factor, we need the value of unknown phase shift γ. All the parameters except the bond thickness are known for the computation of γ. The bond angle is then obtained from the plot as the angle corresponding to the measured value of Δt, which has fallen in the possible range. Thus the correction factor given by equation 2.14 can be estimated and the true round trip time t in the sample can be obtained. It may be noted that a graph has to be plotted for every measurement.

One expects a phase shift of $\pi/2$ radians from the face of the transducer to infinity. So the total diffraction contribution t_D of the travel time is always less than $\tau/4$, where τ is the period of the ultrasonic frequency. In equation 2.13 the diffraction delay time t_D must be added to t_M, the measured time, before the true travel time $t^{(T)}$ is calculated. Calling $t_M^{(T)}$ the corrected measurement, then

$$t_M^{(T)} = t_M + t_D \qquad (2.15)$$

and

$$t_M^{(T)} = pt^{(T)} - (\frac{p\gamma}{2\pi f}) + \frac{n}{f} \qquad (2.16)$$

This aspect is discussed at length by Papadakis [22].

2.5.2   Ultrasonic attenuation measurements

Ultrasonic attenuation α is measured as the logarithm of the ratio of the amplitudes of the ultrasonic waves at two distances along its propagation path. If one had a plain

wave and a linear sensor that could not perturb the wave. Then

$$\alpha = \frac{\ln (A_1/A_2)}{x_2 - x_1} \text{nepers/unitlength}$$

$$= 20 \frac{\log (A_1/A_2)}{x_2 - x_1} \text{dB/unitlength} \tag{2.17}$$

where A_1 and A_2 are the amplitudes of echoes sensed at positions x_1 and x_2. However, one never has plane waves and non perturbing sensors. So techniques have been developed to overcome these difficulties.

The method that is used for travelling wave attenuation measurement was introduced by Roderick and Truell in 1952 [32]. In the pulse technique a single piezo-electric plate which is bonded directly to the specimen is excited with rf pulses and it receives the echoes. To generate a useful quasi-planar wave, the transducer must be many wave length in diameter.

To minimise the perturbing effect of the transducer upon the echoes, the following conditions should be satisfied. 1. The rf burst should be at the fundamental or an odd harmonic of the resonance frequency of the piezo-electric transducer. This causes echo waves entering the transducer to return to specimen in phase with the portion reflected at the bond preventing destructive interference which would appear as excess attenuation. 2. The bond must be very thin to eliminate phase shift within it, which would have the same effect. 3. The electro mechanical coupling coefficient of the piezo-electric plate should be low to assure that little energy will be absorbed in the transducer. This absorption will appear as excess attenuation. 4. The electrical impedance of the transducer should be severely mismatched with respect to the electrical impedance of the receiving circuitry for the same reason. The use of quartz crystal plate (X-cut for longitudinal, Y-cut for shear) of high impedances operated from 50 or 93 ohms systems satisfy the above conditions.

Various methods have been used to find the amplitude of the echoes. Comparison of pulses running through an attenuation box and a delay line have been applied on alternate or chopped oscilloscope sweeps to find amplitude directly in decibels [32]. Another method employs displaying an electrically generated decaying exponential function curve and the echoes on alternate sweeps of an oscilloscope [33]. The decaying exponen-

tial is calibrated in decibels per microseconds. The slope of the decaying exponential can be varied so that the attenuation across any pair of echoes can be measured.

An automatic version of this attenuation measuring system has been developed by MATEC, USA. In this system, two gates with variable delays are set on the two echoes of interest to sample them. The amplitude of first echo is held constant by AGC circuitry and the amplitude of the second echo is sampled at its peak. Detected outputs obtained from a super-heterodyne system is used for this. A calibrated logarithmic amplifier converts the sampled amplitudes in decibels relative to the constant amplitude of the first echo. The decibel value is recorded on a built in strip chart that has several calibrated scales and a variable base line, which enables small changes in attenuation to be measured at various total loss levels. In addition to the strip chart, a direct readout meter also can be used.

2.5.3   The present experimental setup

The experimental setup used for the measurement of ultrasonic velocity using pulse echo overlap technique and attenuation by pulse comparison method consist mainly of the PEO system, a temperature and control unit, and an oven for high temperature measurements. The PEO system is assembled with the necessary units from M/s MATEC, Inc. (USA). The present equipments are MATEC model 7700 pulse modulator and receiver together with the 760V rf plug in, Model 110 high resolution frequency source, model 122B decade divider and dual delay generator, model 2470B attenuation recorder, model 70 impedance matching network, HIL model 2722 frequency cum period counter and HIL model 5022 dual trace oscilloscope. An oven for ultrasonic measurements from System Dimensions (INDIA) has been used for high temperature measurements.

The block diagram of experimental arrangement used is shown in Fig. 2.7. The tunable CW source is a highly stable oscillator and its output can be varied from 5 Hz to 50 MHz. This oscillator supplies the required low frequency CW signal for PEO by selectable frequency division with dual delay and divider unit which has dividers selectable as 10, 100 or 1000. The division factor 100 is quite suitable for most measurements, which means that next rf pulse is send to the sample only after a time
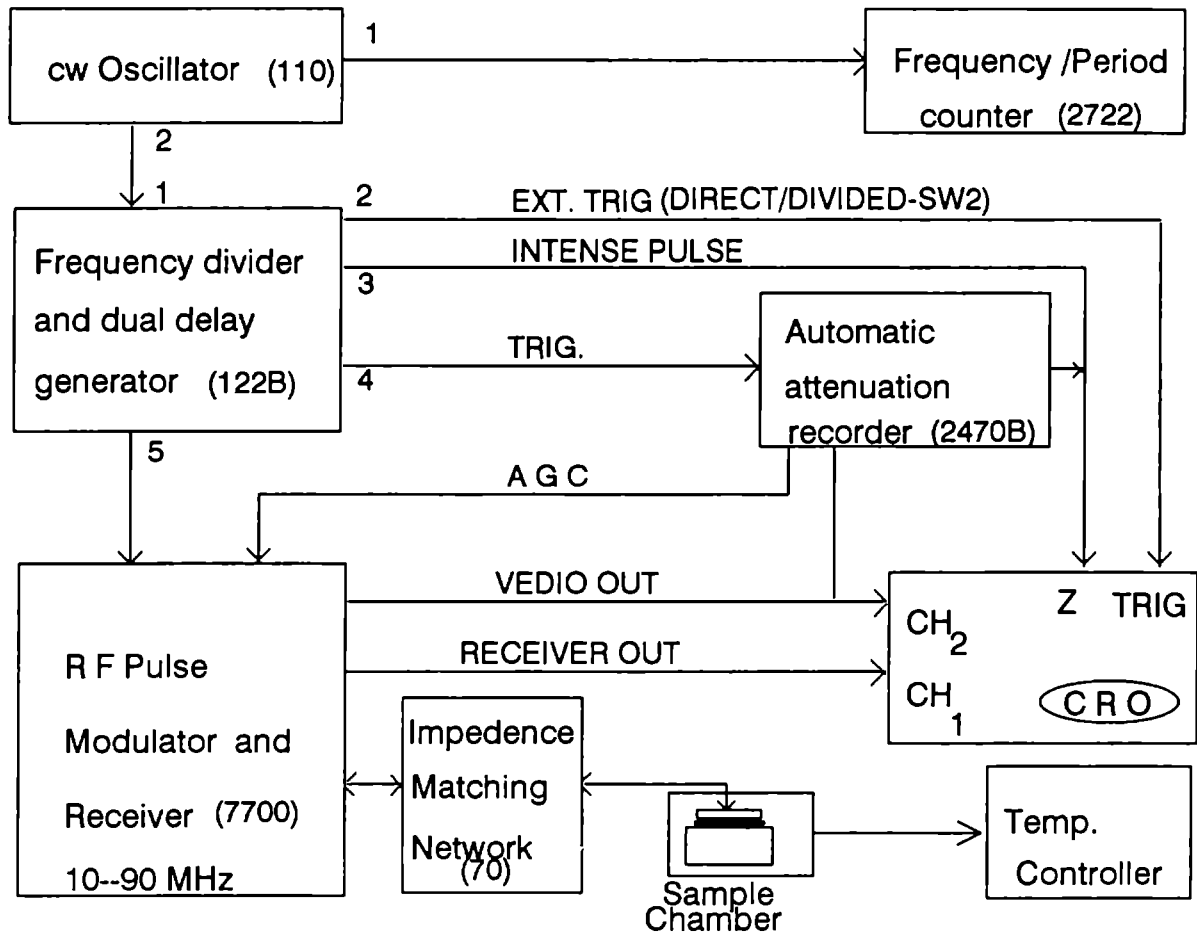
Fig. 2.7: Block diagram of the ultrasonic PEO setup used in the present experiments.

interval corresponding to 100. This division factor is quite suitable for most measurements, which means that next rf pulse is sent to sample only after a time interval corresponding to 100 echoes. The terminal 2 of this unit gives trigger pulses for the CRO. The CRO is always operated in the external trigger mode. By using a switch SW2 in 122B, the trigger at terminal 2 can be made direct trigger or divided trigger for observing the overlapped echoes or full echo pattern respectively. The dual delay generator in 122B can be adjusted for delay and width of the intensifying pulses for selecting two echoes of interest for overlap. These pulses are available at terminal 3 and are connected to the Z input of the CRO through the selector switch SW1.

The output of the dual delay and divider goes to the most important unit in the setup, the pulse modulator and receiver system (Model 7700 with rf plug - in model 760V). An rf pulse packet of peak power 1kw is obtained from the output when the unit is triggered at the input. For good pulse shape the unit is usually operated at full amplitude and amplitude reduction is achieved by using an rf attenuator (Allan attenuators) at the output. The high sensitive tunable superheterodyne receiver amplifies the received echoes from the sample and the amplified echoes are obtained at the video out terminal which is connected to the attenuation recorder and the Z axis input of the CRO. To get optimum signal to noise ratio in the amplification of weak echoes, an impedance matching network (Model 70) is connected before the quartz transducer.

For attenuation measurements, Model 2470B attenuation recorder is incorporated in the setup. The switch SW1 can be toggled to pole 2 for connecting the intensifying pulse output from the attenuation recorder to the Z input of the CRO. It provides the necessary AGC output to connect to the pulse modulator and receiver for keeping the amplitude of the first echo constant during measurements. The video output is applied to this. The calibrated logarithmic amplifier converts the amplitude of the two echoes to the corresponding attenuation in decibel values. The attenuation value can be recorded with maximum sensitivity either on a strip chart or on a panel meter. Offset adjustment of the attenuation enables one to measure small changes in attenuation of the order of 0.01dB. The transducer is bonded to the sample using proper

59

bonding medium. This transducer is connected to the pulse output of the modulator and receiver system through an impedance matching network in order to match the impedances of the cable and transducer for optimum power transfer. By using SW2 in 122B the trigger 2 can be made a divided trigger to observe the echo pattern on the oscilloscope screen. The dual delay generator in 122B can be adjusted for delay and width of the intensifying pulses for selecting two desired echoes of interest for overlap. Then switch SW2 in 122B is changed to direct position to overlap the selected echoes. By adjusting the frequency of the CW source, proper overlapping can be made. Now the frequency can be measured from the frequency counter from which the travel time can be determined. By taking the readings for six or seven overlapped condition and repeating the same for a lower frequency (0.9 f_r). McSkimin Δt criterion can be applied for getting the corrected velocity.

The video output is used to measure the attenuation with the attenuation recorder. By using intensifying signals from the attenuation recorder, we can select any desired echo pair. This enables to open a gate so that the amplitude of these two echoes can be sampled and attenuation can be read out or recorded on the chart recorder.

In order to make high temperature studies, a temperature controller (Lake Shore model 82C) is connected to the oven. This is a three mode controller (proportional, integral, derivative) and there is provision to use two temperature sensors. One is the control sensor and other is the sample sensor. Either platinum RTD or silicon diode sensors can be used with the system. Photograph of the equipment used for ultrasonic measurements is given in Fig. 2.8.

Paraffin oil, motor oil SAE40, nonaq stop cock grease, silicon grease etc. are found to be very good bonding materials for longitudinal measurement at room temperature as well as relatively high temperature. Silicon grease and nonaq stop cock grease are good for low temperature measurements. For transverse waves silicon grease is found suitable below $100^{\circ}C$ The acoustic impedance of paraffin oil and motor oil SAE40 are accurately determined by measuring ultrasonic velocity at 2MHz in them and density. It is found to be 11.67 Kg/m.sec. and 13.45 Kg/m.sec. Selection of bonding material is dependent very much on the sample.
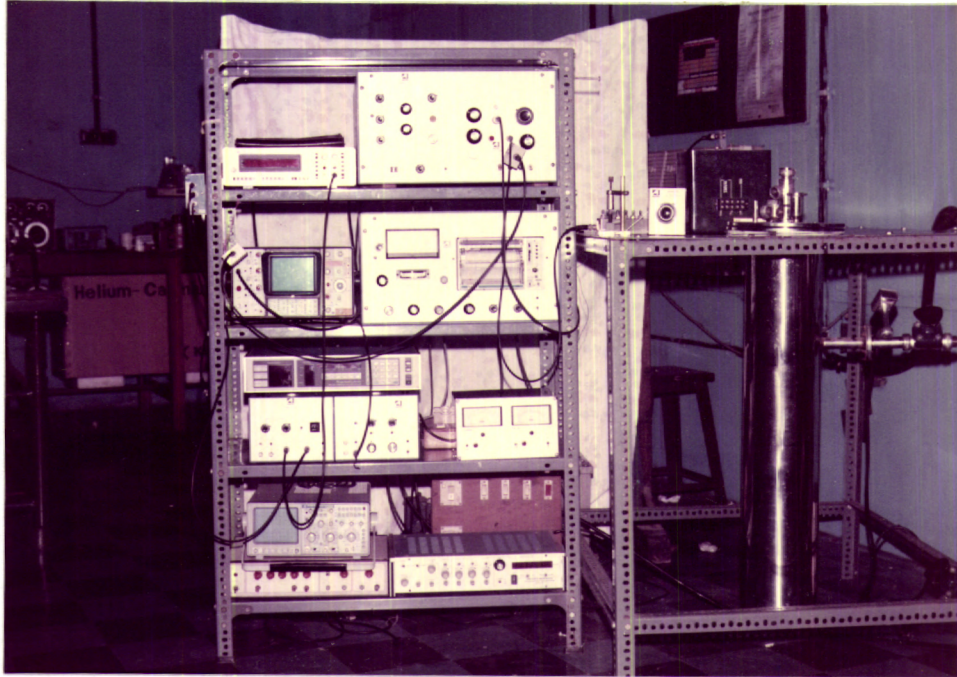
Fig. 2.8: Photograph of the equipment used for the ultrasonic measurements.

2.6 References

[1] A. C. Lynch,*Proc. IEEE* **104**, 359 (1957).

[2] A. C. Lynch, *Proc. IEEE* **112**, 426 (1965).

[3] D. F Gibbs and B. W Jone, *J. Phy. C (Solid State physics)* **2**, 1392 (1969).

[4] C. Ramasastry and Y. Syamasundara Rao, *J. Phys. E: Sci. Instrum.* **Vol. 12**, (1979).

[5] J. M. Ide, *Rev. Sci. instr.* **6** , 296 (1935).

[6] T. A. Read, C. A. Wert, M. Metzger, *In methods of Experimental physics*, **Vol. 6A**, ed: by K. Lark - Horovitz, V.A. Johnson (Academic press, New York 1974).

[7] W. P. Mason, *Piezo electric crystals and their applicationof ultrasonics* (Van Nostrand, Princeton (1950).

[8] G. Rupprecht, W. H. Winter,*Phys. Rev.* **155**, 1019 (1967).

[9] E. Schreiber, O. L. Anderson, N. Soga,*Elastic constants and their measurement* (McGraw-Hill, New York 1973).

[10] B. Luthi and W. Rehwald in *structral phase transistions* I (Eds: K.A.Muller and H. Thomas) springer verlag. Berlin (1981).

[11] D. I. Bolef in *Physical Acoustics* **Vol. IV, PtA**, (Eds.W.P.Mason and R.N.Thurston), Academic Press, New York (1966).

[12] D. I. Bolef and J. G. Miller in *Physical Acoustics* **Vol. VIII** (Eds. W.P. Mason and R.N. Thurston) Academic Press New York (1971).

[13] A. G. Beathe, H. B. Silsbee and E. A. Uchling, *Bull. Amer. Phys. Soc.* **7**, 478 (1962).

[14] G. A. Alers in *Physical Acoustics* **Vol. IV A** (Ed: W.P. Mason) Academic Press, New York (1976).

[15] F Birch, *J. Geophys. Res.* **65**, 1083 (1960).

[16] H. B. Huntington, *Phy. Rev.* **72**, 321 (1947).

[17] J. K. Gatt, *Phy. Rev.* **43**, 1460 (1948).

[18] H. J. McSkimin, *J. Acoust. Soc. Am.* **33**, 12 (1961).

[19] H. J. McSkimin and P. Andreatch, *J. Acoust. Soc. Am.* **34**, 609 (1962).

[20] H. J. McSkimin and P. Andreatch, *J. Acoust. Soc. Am.* **41**, 1052 (1967).

[21] E. P. Papadakis, *J. Acoust. Soc. Am.* **40**, 863 (1966).

[22] E. P. Papadakis in *Physical Acoustics* **Vol. XII**, (Eds. W.P.Mason and R.N. Thurston) Academic Press, New York (1976).

[23] N. P. Cedrone and D. R. Curran, *J. Acoust. Soc. Am.* **26**, 963 (1954).

[24] H. J. McSkimin and P. Andreatch, *J. Acoust. Soc. Am.* **22**, 413 (1950).

[25] P. L. M.Heydemann, *Rev. Sci. Instr.* **42**, 983 (1971).

[26] J. E. May Jr. *IRE Nat. Conv.* Rec. 6 **Pt 2**, 134 (1958).

[27] E. P. Papadakis, *J. Acoust. Soc. Am.* **42**, 1045 (1967).

[28] E. P. Papadakis, *J. Appl. Phys.* **35**, 1474 (1964).

[29] E. P. Papadakis in *Physical Acoustics* **Vol. XI**, (Eds. W.P.Mason and R. N. Thurston) Academic Press, New York (1975).

[30] E. P. Papadakis, *J. Acoust. Soc. Am.* **45**, 1547 (1969).

[31] E. P. Papadakis, *J. Acoust. Soc. Am.* **52**, 843 (1972).

[32] R. L. Roderick and R. Truell, On the measurement of ultrasonic attenuation in solids by the pulse technique. *J. Appl. Phys.* **23**, 267 (1952).

[33] R. Truell, C. Elbaum and B. Chick, *Ultrasonic methods in solid state physics.* Academic press New York and London (1969).

Chapter 3

Dielectric and elastic properties of $Ba_{2-x}Sr_x$ Ti_9O_{20} dielectric ceramics.

3.1 Introduction

Ceramics based on $Ba_2Ti_9O_{20}$ have been largely ignored over the past decade by manufacturers of high dielectric constant, temperature compensated materials for commerical wireless communications at microwave frequencies. When processed correctly, these ceramics yield properties that rival currently used materials except $ZrTiO_4$ based products. The ceramics based on $Ba_2Ti_9O_{20}$ received considerable attention and importance as a resonator as well as selective filters. These materials fall in the TiO_2 rich region of the BaO-TiO_2 phase diagram. Several workers faced difficulties in preparing these materials in single phase without adding a third phase like SnO_2 or ZnO_2 [1,2] which promotes the formation of the compound. Addition of small amount of SrO also has the same effect to promote the formation of the compound.

Due to the relevance of Sr doped $Ba_2Ti_9O_{20}$ ceramics as dielectric resonators, we have prepared and studied the dielectric properties of these materials. This work is presented in this chapter. Effect of SrO addition on their elastic properties is also important because the structural stability and Q of the material are strongly dependent on the elastic forces between atoms.

This chapter deals with measurements of the dielectric (upto 13MHz) and elastic properties of Sr doped $Ba_2Ti_9O_{20}$ ceramics. It is also essential to take a closer look at the imperfections commonly occurring in these dielectric ceramics during processing because they impose limits on the two most important properties of dielectric resonators

64

viz. high Q factor and low temperature coefficient of the resonance frequency. In view of the importance of temperature stability of these materials, we have also measured the temperature variation of elastic constants as well as dielectric constant of these materials.

Resonators are very important components in microwave communication circuits. They are used as filters and to select frequencies in oscillators, amplifiers and tuners. Bulky metallic cavity resonator based devices were used for frequency stabilisation during the initial period of operation of such devices. This resulted in instruments being very bulky as well as expensive. In the mid 1960s, when microwave integrated circuits (MIC) were developed, there were no devices with small size and weight suitable for integration in a miniature circuit to perform these functions. All these difficulties are being solved with the development of microwave dielectric resonators. The past 25 years have seen rapid developments in miniaturisation of microwave circuits which have accelerated the development of highly stable filters and compatible oscillators. A more recent advance in the miniaturisation of microwave circuits has been the phenomenal growth of satellite communication and cellular radio systems. A good number of reviews are available describing the properties and applications [2-9].

The dielectric resonator (DR) offers a means of miniaturising the device with compactness, light weight, stability with temperature and low cost. The dielectric resonators are widely used in such demanding applications like cellular telephones, microwave circuits, filters and in satellite communications. In satellite communications, microstrip and stripline resonators cannot be used because of their inherent high losses. Further more, carefully designed microwave oscillators which utilise dielectric resonators can equal the temperature stability of conventional microwave resonant cavities machined from invar.

In its simplest form, a ceramic dielectric resonator is a piece of unmetallised ceramic of relative permittivity ϵ sufficiently high for a standing electromagnetic wave to be sustained within its volume because of multiple total internal reflection at the dielectric air interfaces. Field inside a resonator stores energy at the resonant frequency where storage of electric and magnetic field energies occur. The magnetic field lines

of resonant mode $TE_{01\delta}$ in an isolated dielectric resonator are illustrated in Fig. 3.1. The shape of a dielectric resonator is usually a short solid cylinder but one can also make tubular, spherical and parallelopiped shapes. A commonly used resonant mode in cylindric resonators is denoted by $TE_{01\delta}$. When the relative dielectric constant is around 40, more than 90% of the stored electric energy of the $TE_{01\delta}$ mode as well as a great part of the stored magnetic energy are located within the cylinder. The remaining energy is distributed in the air around the resonator.

The materials used for dielectric resonators are required to have the following dielectric properties [4-11]: relative dielectric constant (ϵ_r) greater than 25; high Q value, greater than 3000 (at 10GHz) and very small temperature coefficient of resonant frequency (τ_f). These requirements have been chosen due to the following reasons. When most of the electromagnetic energy is stored within the dielectric region and losses other than the dielectric losses can be neglected, the resonator Q is approximately equal to the inverse of the dielectric loss tangent. Although Q values comparable to those of rectangular wave guide resonators (Q $\approx$ 8000 at 4GHz) are desirable, materials whose Q values exceed 3000 will have almost an order of magnitude advantage over other integrable resonators like microstrip resonators. Materials with ϵ_r values comparable to those of TiO_2 ($\epsilon_r = 100$) are highly desirable since they result in compact resonators which are convenient to use. Since copper waveguide resonators provide acceptable temperature stability ($\tau_f \approx 17\text{ppm}/^\circ\text{C}$) for many applications, a τ_f value comparable to or less than this is desirable.

The losses within the dielectric and the temperature dependence of the mechanical and electrical properties of the dielectric are of great significance because they impose limits on the two most important properties of dielectric resonators $viz.$ the high Q factor and the high temperature stability. An important temperature effect is the expansion of the material due to heating. It is an experimental fact that most solids expand linearly with increase in temperature. The relative expansion per degree centigrade is very small, of the order of 10^{-6} or 10^{-5} This coefficient will vary slightly as a function of temperature itself and result in a change in the resonant frequency. Magnitude of the change in resonant frequency can be computed using the
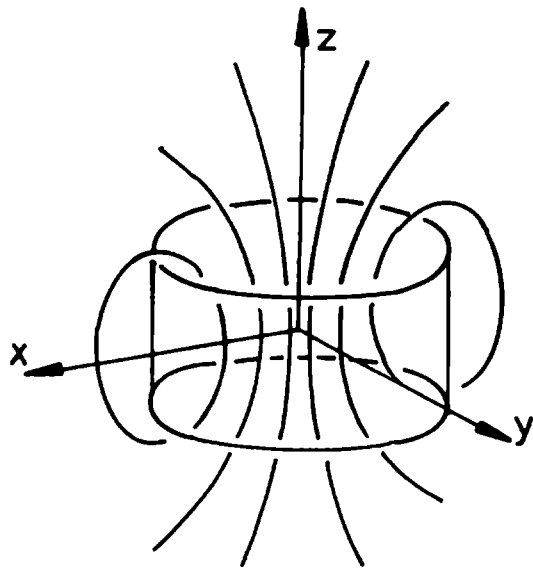
66

Fig.3.1: Magnetic field lines of resonant mode $TE_{01\delta}$ in an isolated

dielectric resonator

following equation

$$\frac{\Delta f}{f} = -\alpha \Delta T \tag{3.1}$$

where α is the linear coefficient of thermal expansion. The sign of $\Delta f/f$ is negative because an increase in temperature makes the resonator longer, causing its resonant frequency to decrease. The linear expansion of a solid material is the same in every direction in space unless the material has anisotropic expansion properties. The second effect of temperature of the resonant frequency of a microwave resonator comes from the fact that the relative dielectric constant ϵ_r also varies as a function of temperature. The change is, in general, linearly proportional to temperature. The temperature coefficient of the dielectric constant can be represented by

$$\frac{\Delta \epsilon_r}{\epsilon_r} = \tau_\epsilon \Delta T \tag{3.2}$$

As the temperature changes, the resonant frequency will shift for two reasons; linear expansion and change in dielectric constant. This change can be expressed as

$$\frac{\Delta f}{f} = \frac{\partial f}{f \partial L} \Delta L + \frac{\partial f}{f \partial \epsilon_r} \Delta \epsilon_r \tag{3.3}$$

Then the sensitivity of the resonant frequency to temperature, or the temperature coefficient of resonant frequency τ_f is expressed by

$$\frac{\Delta f}{f} = \tau_f \Delta T \tag{3.4}$$

The relation between coefficient of linear expansion, temperature coefficient of dielectric constant and temperature coefficient of resonant frequency is given by [3]

$$\tau_f = -(\alpha + \frac{1}{2}\tau_\epsilon) \tag{3.5}$$

The above equation suggests a method to achieve a temperature compensated resonator. Here τ_ϵ must have a sign opposite to α and have approximately double the magnitude. Since all solid materials expand with rising temperature, the dielectric material must exhibit a negative τ_ϵ in order to be suitable for temperature compensation.

High permittivity is the prerequisite for miniaturisation of dielectric resonators. For practical applications, the quality factor Q and the temperature coefficient

68

of resonant frequency τ_f of a DR are important parameters to be considered. During search for materials suitable for using microwave devices, Titania (TiO_2) first attracted attention because of its high relative permittivity ($\epsilon_r = 100$) and low loss (tan $\delta = 3x10^{-4}$). However, it is unsuitable because it has a $\tau_f \approx 350$ MHz/K. So interest turned to different titanats with high permittivity of which some have +ive and some -ive values for τ_f. Materials which showed promise were barium titanate based ceramics because the variation of dielectric characteristic of barium titanate ceramics with temperature, electric field strength, frequency and time vary with the substitution of minor amounts of other ions for Ba or Ti. Single crystal single domain $BaTiO_3$ has a relative permittivity of 230 at 20°C in polar direction and 4770 in perpendicular direction. Random orientation of axis would lead to permittivity of ≈ 1740 on the basis of Linchleneckers relation.

$$ln\epsilon_m = \Sigma Vf_i \, ln\epsilon_i \tag{3.6}$$

where V_f is volume of each single phase. The value of relative dielectric constant depend mainly on the method of preparation and large value of dissipation factor controlled mainly by domain wall motion. Thus an understanding of domain structure of ceramics greatly helps to control dielectric properties. The principal effects determining the properties are AO/BO_2 ratio which is the ratio of the total number of ions on Ba sites to the number on Ti sites. The effect of AO/BO_2 ratio varies with different substitutes and additives. The grain size of ferro electric ceramics has a marked effect on the permittivity on the size range 1-50 μm. Below about 1 μm, the permittivity falls with grain size. An important factor leading to this behaviour is the variation in the stress to which a strain is subjected as it cools through the curie point. The resulting stresses within the grain can be reduced by the formation of approximate arrangement of 90° domains, most of the stresses being relieved by this mechanism. As the grain size decreases the domains become smaller, with the domain width being roughly proportional to square root of the grain size. The number of domains per grain therefore decreases as the square root of grain size and smaller the grain the larger is the unrelieved stress. A reduction in 90° domain width can enhance permittivity because the domain wall area per unit volume of the ceramic increases [13].

69

The magnitude of applied field also has a marked effect on the dielectric properties. The solid solutions containing titanates like $Ba_2Ti_4O_9$ and $Ba_2Ti_9O_{20}$ have attracted the attenuation of many workers due to their peculiar properties. Single phase Ba_2 Ti_9O_{20} showed excellent results, when it is used as a dielectric resonator. But $Ba_2Ti_9O_{20}$ is not easy to process reproducibly because of the existence of wide range of BaO-TiO_2 phases, but is manufactured on commercial basis. The structure of $Ba_2Ti_9O_{20}$ can be most conveniently expressed as a hexagonal close packing of oxygen and barium atoms. It is similar to most of the phases of the system $BaTiO_3$-TiO_3. Here Ba atoms are participating with oxygen atoms in close packed arrangement having 12 co-ordination of oxygen atoms around them.

Single phase $Ba_2Ti_9O_{20}$ ceramic possess excellent dielectric properties such as high dielectric constant, low temperature coefficient of dielectric constant and low dielectric loss [14-16] which are used for low loss microwave dielectric resonators. The processing of these materials must be performed very carefully to form single phase material. Single phase $Ba_2Ti_9O_{20}$ ceramic is obtained by solid state reaction of TiO_2 with 18.2 mol% of BaO at 1300°C to 1400°C in binary composition. This was first performed by Jonker and Kwestroo [17] who suggested that the phase stability could be obtained only with a small percentage of SnO_2 or ZrO_2. The stability region of this phase in phase diagram is a narrow one. O' Bryan and Thomson [1] found it necessary to form some $Ba_2Ti_9O_{20}$ during calcination stage if a single phase $Ba_2Ti_9O_{20}$ ceramics has to be obtained during the sintering stage. But a single phase material could not be obtained within a reasonable time. Jackola, Usimaki and Leppavuori [12] found that a higher reaction temperature was required for the formation of $Ba_2Ti_9O_{20}$ within the reasonable time span in case of the mixture containing $BaCO_3$ and TiO_2. Faster reaction kinetics occur for the mixture $BaTiO_3$ and TiO_2, for which the reaction temperature for an equivalent reaction rate was lowered by over 250°C. This is because $BaTiO_3$ is closer to $Ba_2Ti_9O_{20}$ in Ti content than $BaCO_3$ and the diffusion distances involved to effect the solid state reaction are relatively short. Both O' Bryan *et al.* [1] and Jackola *et al.* [12] have highlighted diffusion as the main factor that affected the formation of $Ba_2Ti_9O_{20}$.

In addition to the above suggestion, Wu and Wang [18] have proposed that in addition to diffusion, nucleation of $Ba_2Ti_9O_{20}$ and strain energy involved in the formation of $Ba_2\ Ti_9O_{20}$ are important factors. O'Bryan et al. [19] reported that the unit cell structure of this compound is monoclinic with a theoretical density of 4.58 g/cc, whereas Tillmanns et al. [20] reported the unit cell as triclinic with a theoretical density of 4.61 g/cc and explained that monoclinic symmetry might be due to twinning which results from the symmetry of the distribution of the barium atoms over the closed packed positions and from the distribution of titanium atoms in the available octahedral interstices of the closest packing. Negas et al. [21] in their studies on the subsolidus phase relations in $BaTiO_3$ - TiO_2 system reported that the $Ba_2\ Ti_9O_{20}$ had temperature stability near 1300°C, while O'Bryan and Thomson [22,23] reported that the temperature stability was near 1400° C and above 1420°C it underwent a peritectoid decomposition. More recent work done by Guha et al. [24] confirmed that the peritectoid reaction results above 1400° C. Several metastable compounds have also been produced during the peritectoid reaction. $BaTi_5O_{11}$, $BaTi_6O_{15}$ and $BaTi_2O_5$ crystallises from the liquid whereas $BaTi_2\ O_5$ and $BaTi_5O_{11}$ also form as reaction intermediates during the solid state reaction.

While explaining the factors that affect the formation of $Ba_2Ti_9O_{20}$ phase, Wu and Wang [18] gave the phase development sequence as $BaTi_5O_{11}$ > $BaTi_4O_9$ > $BaTi_4O_{20}$ The structure and densities of $BaTi_4O_9$, $BaTi_4O_{20}$, $BaTi_5O_{11}$ have been reported elsewhere [35,36,37]. The basic structural elements of these compounds is the Ti - O octahedron. By sharing corners and edges of Ti - O octahedron and accommodating barium ions in interstitial positions between the Ti - O octahedron, the compounds $BaTi_4O_9$, $Ba_2Ti_9O_{20}$ and $BaTi_5O_{11}$ are formed. The connective state of Ti-O octahedral network of these compounds shows that Ti-O octahedral network is most connective in $Ba_2Ti_5O_{11}$ than $Ba_2Ti_9O_{20}$ and less connective in $BaTi_4O_9$. The relationship between the structures of these compounds can be seen easily if they are viewed as close packed oxygen ions with barium and titanium ions inserted into interstitial sites between oxygen ions. In addition to this, calculation of packing density of oxygen is also useful to compare the similarities of these compounds. Among the above group of titanates, it

71

is believed that $BaTi_5O_{11}$ is very close to rutile in Ti-O octahedral network than the other compound. $Ba_2Ti_9O_{20}$ should be formed next and $BaTi_4O_9$ should be formed last. But studies made by Wu and Wang [18] showed that $Ba_2Ti_9O_{20}$ is always the compound formed last. This indicates that some factors other than structural considerations should play an important role in the formation of $Ba_2Ti_9O_{20}$. They concluded that the nucleation is the main factor which controls the formation of $Ba_2Ti_9O_{20}$. Regarding the role of formation they pointed out that the high surface energy and interface energy might be the cause of this low rate of formation of $Ba_2Ti_9O_{20}$. Owing to the aforesaid facts the preparation of single phase $Ba_2Ti_9O_{20}$ through solid state reaction appeared to be quite challenging. Hence solution gel processing was recommended by Phule and Risbud [25] in their review article on the processing of electronic ceramic materials. Recently, single phase $Ba_2Ti_9O_{20}$ has been prepared by heating a solution gel derived precursor for 110 hours at 1200°C by Lu et al. [26].

Although the chemistry of $Ba_2Ti_9O_{20}$ seemed to be complex, efforts were made towards the improvement of the dielectric properties by suitable additives. For that $BaTi_4O_9/Ba_2Ti_9O_{20}$ composites containing substantial amounts of ZnO/Ta_2O_5 were introduced. Since cost of Ta_2O_5 is very high, Nb_2O_5 can be substituted, once the basics of the complex chemistry are understood. Jackola et al. [27] prepared Nd doped $Ba_2Ti_9O_{20}$ upto 10 wt% of Nd_3O_3 and studied the dielectric properties in comparison with the microstructure. They observed that Nd - rich phases increased the dielectric constant as well as temperature coefficient of resonant frequency (τ_f) and reduced the Q value. To avoid the lowering of the Q value, high purity TiO_2 and $BaTiO_3$ must be used with minor quantity of MnO_2 which is a crucial ingredient. Normura et al. [28] found that MnO_2 behaved as oxidising agent during sintering of $Ba_2Ti_9O_{20}$ and improved the unloaded quality factor.

Kwestroo and Paping [29] reported that a small quantity of SrO (upto 5 mol%) stabilised the $Ba_2Ti_9O_{20}$ phase. The effect of SrO substitution for BaO (upto 15 mol%) on the dielectric properties of $Ba_2Ti_9O_{20}$ were investigated by Chatterjee et al. [30] in the low frequency region (upto 13 MHz). However, neither, dielectric studies of complete solid solution in the system $Ba_{2-x}Sr_xTi_9O_{20}$ nor the elastic properties have

been reported. In this chapter, we describe the details of the preparation and the study of dielectric properties upto 13 MHz and elastic properties of $Ba_{(2-x)}Sr_xTi_9O_{20}$ ceramics for x ranging from 0 to 2. Since the structural stability of these ceramics is of great concern we report the temperature variation of their elastic constants and dielectric constant with the effect of SrO doping on the above properties.

3.2 Experimental details

3.2.1 Sample preparation

The conventional solid state synthesis method has been adopted for preparing $Ba_{2-x}Sr_xTi_9O_{20}$ ceramics. High purity electronic grade materials of $BaCO_3$, $SrCO_3$ and TiO_2 have been accurately weighed according to stochiometry with x ranging from 0 to 2. They are mixed in an agate mortar for about 60 minutes using acetone. The powder is then calcined at about 1200° C for 8 hours in platinum crucible. The calcined powder is then ground thoroughly for about 90 minutes. To the fine powder PVA is added as binder and again ground for 30 minutes. Then the powder is pressed at high pressure into cylinders of diameter 10 mm and thickness 7 -8 mm. The pellets are sintered at 1300 - 1350° C for 6 hours in air on platinum sheets. A cooling rate of 1°C/minute is given upto 1200°C. The sintering temperature increases with x. The sintered pellets are polished and annealed at 1000° C to eliminate any lattice strain which could adversely affect the quality factor.

3.2.2 X-ray and SEM analysis.

The XRD pattern of all the samples have been taken in a standard X-ray diffractometer (Regaku, Japan) using $CuK\alpha$ radiation. XRD patterns of the samples have enabled us to determine the phase constitution of the ceramic samples. The microstructures of the samples have been obtained by scanning electron microscopy (SEM) using JEOL (Japan). Highly polished and etched surfaces of the samples have been used for this. SEM studies show homogeneous nature of the sample.

73

3.2.3 Dielectric constant measurements

For low frequency dielectric constant measurements the samples are cut in to discs of diameter $\approx$ 10mm. Both the end faces are polished to precise dimensions to an accuracy of 0.1% or better. It is then placed in between two well polished copper electrode discs. A thin layer of high grade silver paint is applied on the surface of the sample in order to make good contact with the discs. The whole arrangement is kept in the home made dielectric cell whose temperature could be varied and controlled from liquid nitrogen temperature (77K) to 450K using a temperature controller.(Lakeshore cryotronics DRC-82C). A heating rate of 1° C/min has been used in the terminal connections of the dielectric cell for loss free measurements. It is better to have the lower electrode with larger area than the upper one so that the capacitance remains constant and positioning of the upper electrode is not very critical. In this experimental set up we have used a technique [30] to avoid fringe capacitance and lead capacitance. Offset adjustments provided in the impedance analyser (HP 4192A) are also helpful to some extent to minimise the error in the measured value due to spurious factors.

The dielectric inter electrode capacitance C for any electrode spacing can be determined from the equation $C=\frac{\epsilon A}{t}$ where ϵ is the dielectric constant, A is the area of the upper electrode and t is the spacing between the electrodes (thickness of the sample). The stray capacitance of the cell can be eliminated by offset adjustments of the impedance analyser. From the measured capacitance value the dielectric constant is determined   The measurements have been performed in the temperature range from 300K to 450K. In addition, the dependence of dielectric constant ϵ_r on doping has been measured by making measurements on different samples. The reliability of the experimental arrangement has been tested with standard samples before making measurements with the experimental samples.

3.2.4 Elastic constant measurements

Ultrasonic wave velocities in the ceramic samples have been measured by the pulse echo overlap (PEO) technique using Matec 7700 pulse modulator and receiver system [31] which has already been described in Chapter 2. Pelletised samples of diameter

10mm and thickness 6mm have been used for the present measurements. The faces of the samples are polished after making their faces parallel to each other. X cut quartz transducers of frequency 15MHz is mounted on the sample using silicon grease as the bond. It is placed inside a suitable enclosed chamber whose temperature can be varied and controlled from 300K to 450K with the help of a temperature controller. Y cut quartz transducer has been used to generate transverse ultrasonic waves of the same frequency.

The McSkimin Δt criterion [32] has been applied to correct for the phase lag due to bonding medium on RF echoes at room temperature. This technique helps to measure the ultrasound transit time in the sample to an accuracy of the order of a few parts per million The temperature dependence of the velocity of longitudinal and shear waves through the samples have been determined in the temperature range 300K to 450K. The measurements have been carried out at intervals of 5K. The elastic constants corresponding to longitudinal and transverse modes have been determined using the relation $C = \rho\, V^2$, where ρ is the density of the sample and V is the velocity of the corresponding mode. The bulk density has been determined by measuring the volume and weight of each sample accurately.

3.3 Results

The XRD pattern of the representative samples are shown in the Fig.3.2. XRD pattern of $Ba_2Ti_9O_{20}$ contain additional weak reflections corresponding to $BaTi_4O_9$ and TiO_2 in agreement with other reports [15,17,21]. The intensities of the reflection corresponding to $Ba_2Ti_4O_9$ and TiO_2 decreases gradually with increase in Sr concentration.

The SEM pictures of $Ba_2Ti_9O_{20}$, $Ba_{1.5}\,Sr_{0.5}Ti_9O_{20}$ are shown in the Fig.3.3. The microstructure contains polygonal grains of $Ba_2Ti_9O_{20} \approx 3\ \mu$ m and elongated grains corresponding to $BaTi_4O_9$ which are not seen in the Sr doped compositions.

Dielectric constant has been found to vary with Sr concentration as shown in Fig.3.4. It is found that the dielectric constant has a threshold maximum value at $x = 1.5$. On each sample, variation of dielectric constant with temperature and frequency have also been measured. It is found that the dielectric constant decreases with
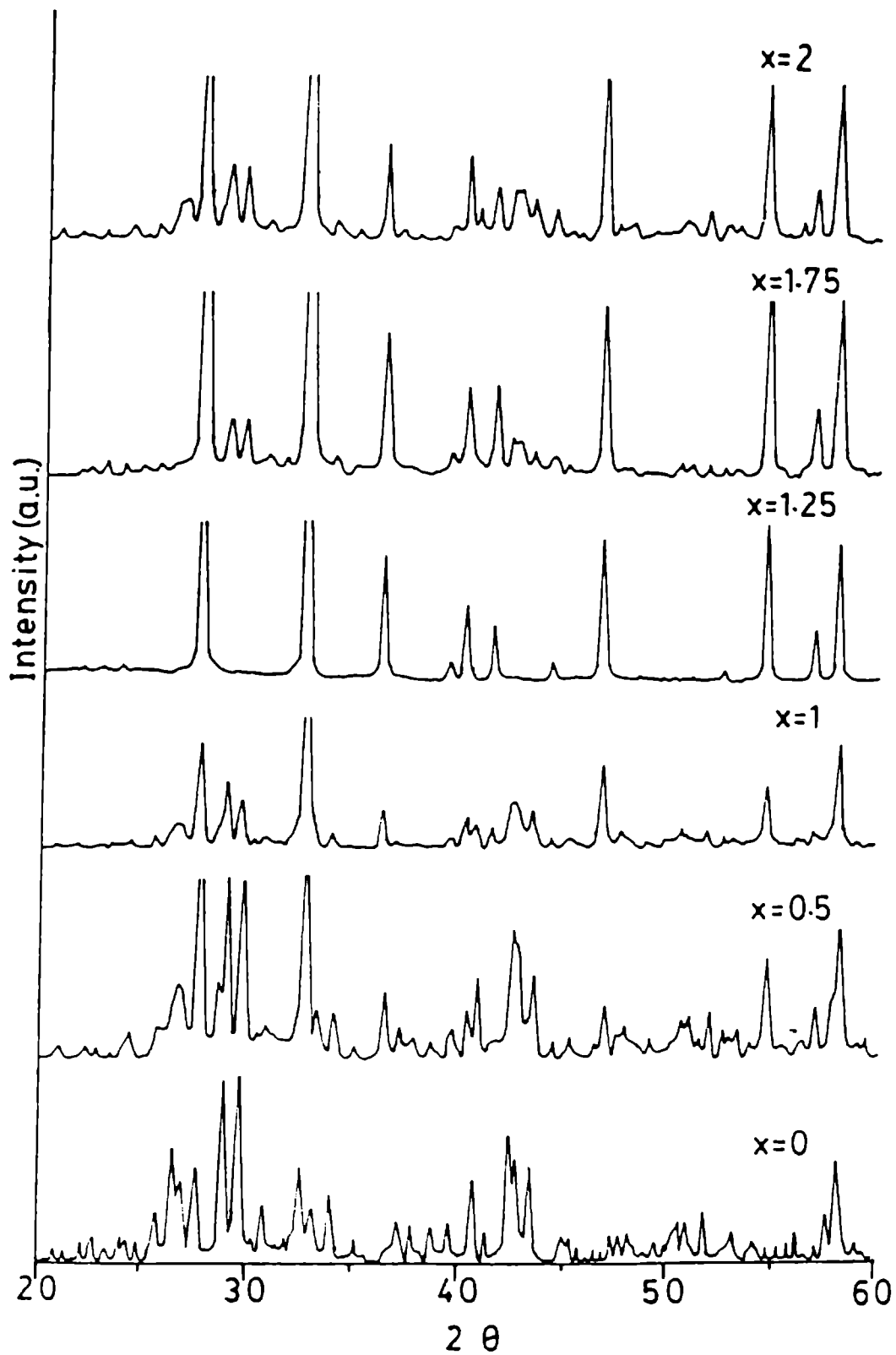
Fig.3.2: XRD pattern of $Ba_{2-x}Sr_xTi_9O_{20}$ ceramics

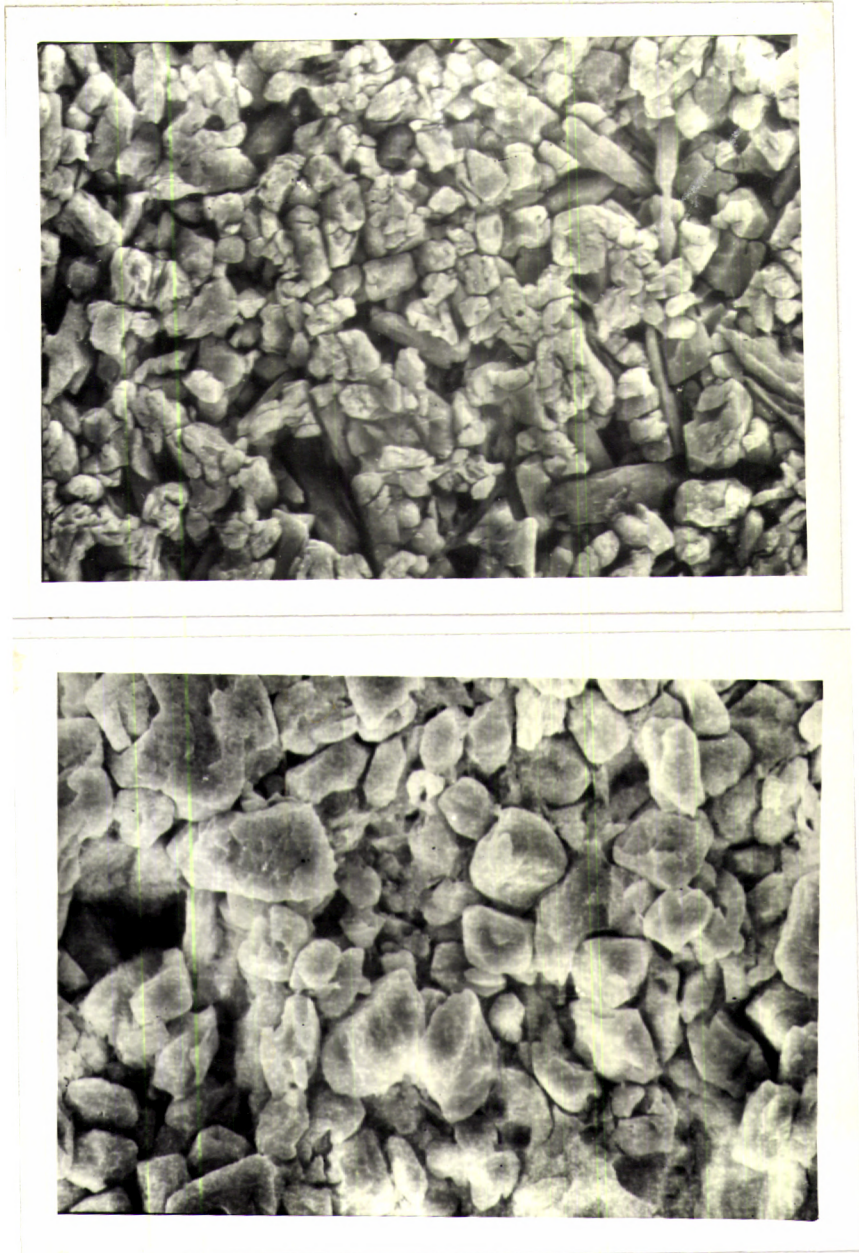Fig.3.3: SEM pictures of $Ba_2Ti_9O_{20}$ and $Ba_{1.5}Sr_{0.5}Ti_9O_{20}$ ceramics
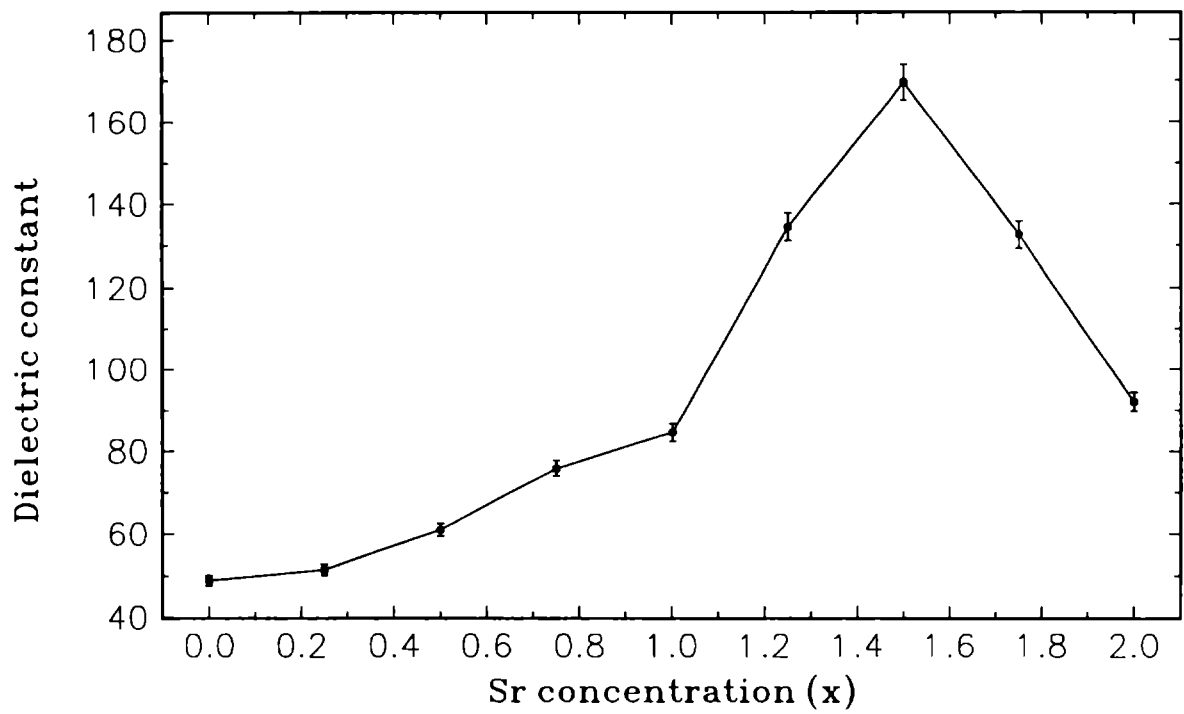
Fig.3.4: Variation of low frequency dielectric constant of $Ba_{2-x}Sr_xTi_9O_{20}$ ceramic with Sr concentration

increasing frequency   The variation of the dielectric constant with frequency is shown in Fig.3.5. The effect of temperature on dielectric constant on selected samples is shown in Fig.3.6. The decrease of the dielectric constant with frequency and temperature are due to the dielectric relaxation of the sample and is in tune with the behaviour exhibited by other dielectric ceramics. The measured longitudinal and transverse elastic constants plotted against Sr composition are shown in Fig 3.7. From these curves it can be seen that the elastic constants increase in general, with Sr doping and exhibits a threshold maximum at $x = 1.5$. The temperature variation of elastic constants of selected samples are shown in Fig. 3.8(a) and 3.8(b).

3.4   Discussion of the results

Grain size variation of pores, micro cracks and secondary phases are the factors which affect the quality of a ceramic dielectric resonator material. The Sr doped $Ba_2Ti_9O_{20}$ ceramics, which are dense and crack free have excellent dielectric properties. It has been seen that in these samples the temperature coefficient of resonant frequency, τ_f, vary with Sr doping more or less in the same way as the corresponding variation in low frequency dielectric constant [33]. The sample with $x = 1.5$ exhibits a maximum in the dielectric constant as well as in the τ_f value. The τ_f value becomes increasingly more positive as Sr concentration increases. It varies from -30ppm/$^{\circ}$C for undoped $Ba_2Ti_9O_2O$ sample to nearly +270ppm/$^{\circ}$C for the sample with $x = 1.5$ beyond which it decreases. Occurrence of threshold maxima in dielectric constant and τ_f carry the signature of a phase transformation in the sample as Sr doping increases. Also it has been found that the quality factor decreases slightly with Sr doping and is minimum again around $x = 1.5$.

The variation of the temperature coefficient of resonant frequency as well as dielectric constant with processing conditions are proposed as resulting from the variation in the relative amounts of the constituent phases in the sample [34]. One can apply the usually applied logarithmic mix-ture rule,
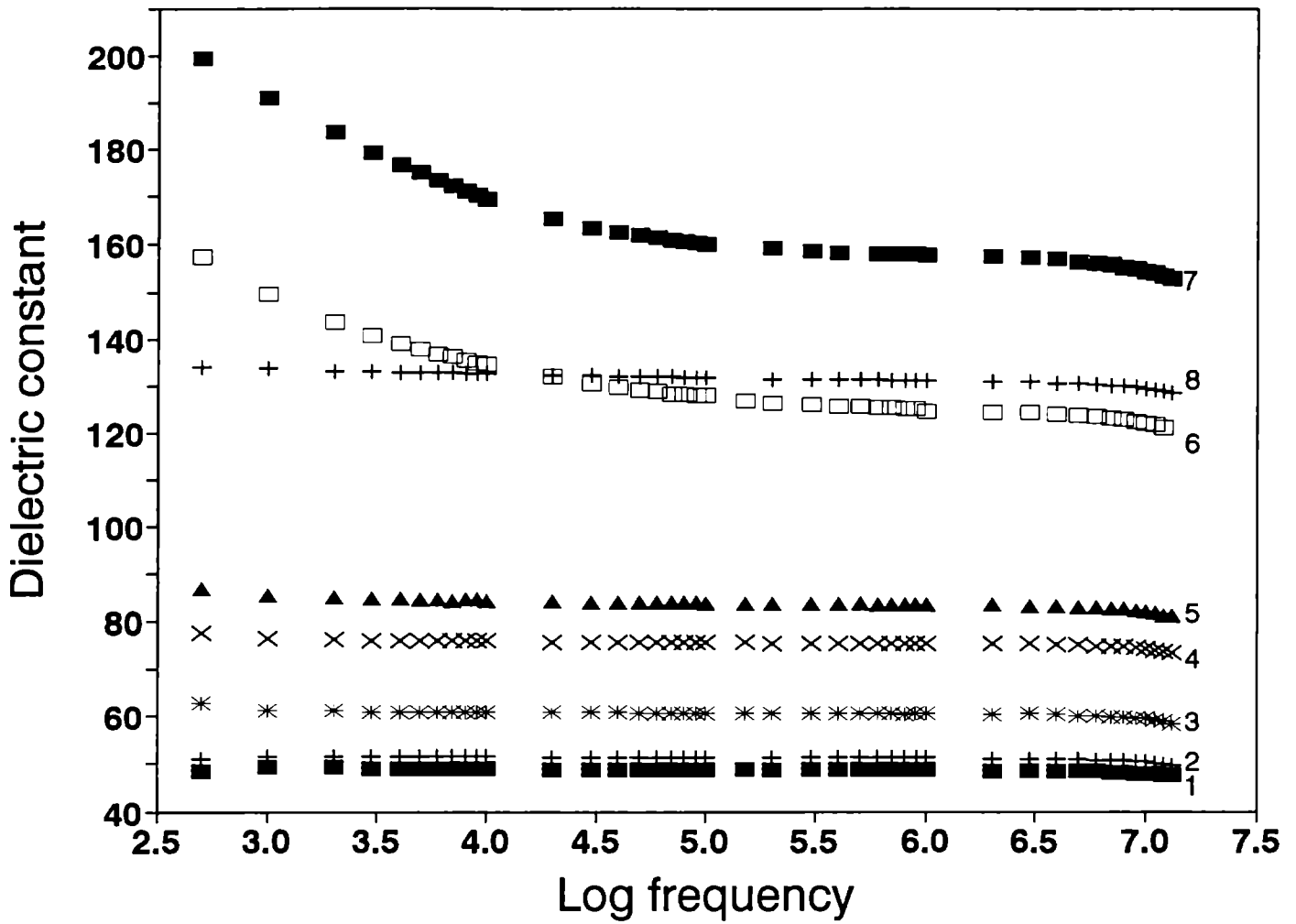
$$\log K = \Sigma v_i \log k_i \tag{3.7}$$

Fig.3.5: Variation of dielectric constant of $Ba_{2-x}Sr_xTi_9O_{20}$ ceramic with frequency, 1:$Ba_2Ti_9O_{20}$, 2:$Ba_{1.75}Sr_{0.25}Ti_9O_{20}$, 3: $Ba_{1.5}Sr_{0.5}Ti_9O_{20}$, 4: $Ba_{1.25}Sr_{0.75}Ti_9O_{20}$, 5: $Ba_1Sr_1Ti_9O_{20}$, 6: $Ba_{0.75}Sr_{1.25}Ti_9O_{20}$, 7: $Ba_{0.5}Sr_{1.5}Ti_9O_{20}$, 8: $Ba_{0.25}Sr_{1.75}Ti_9O_{20}$
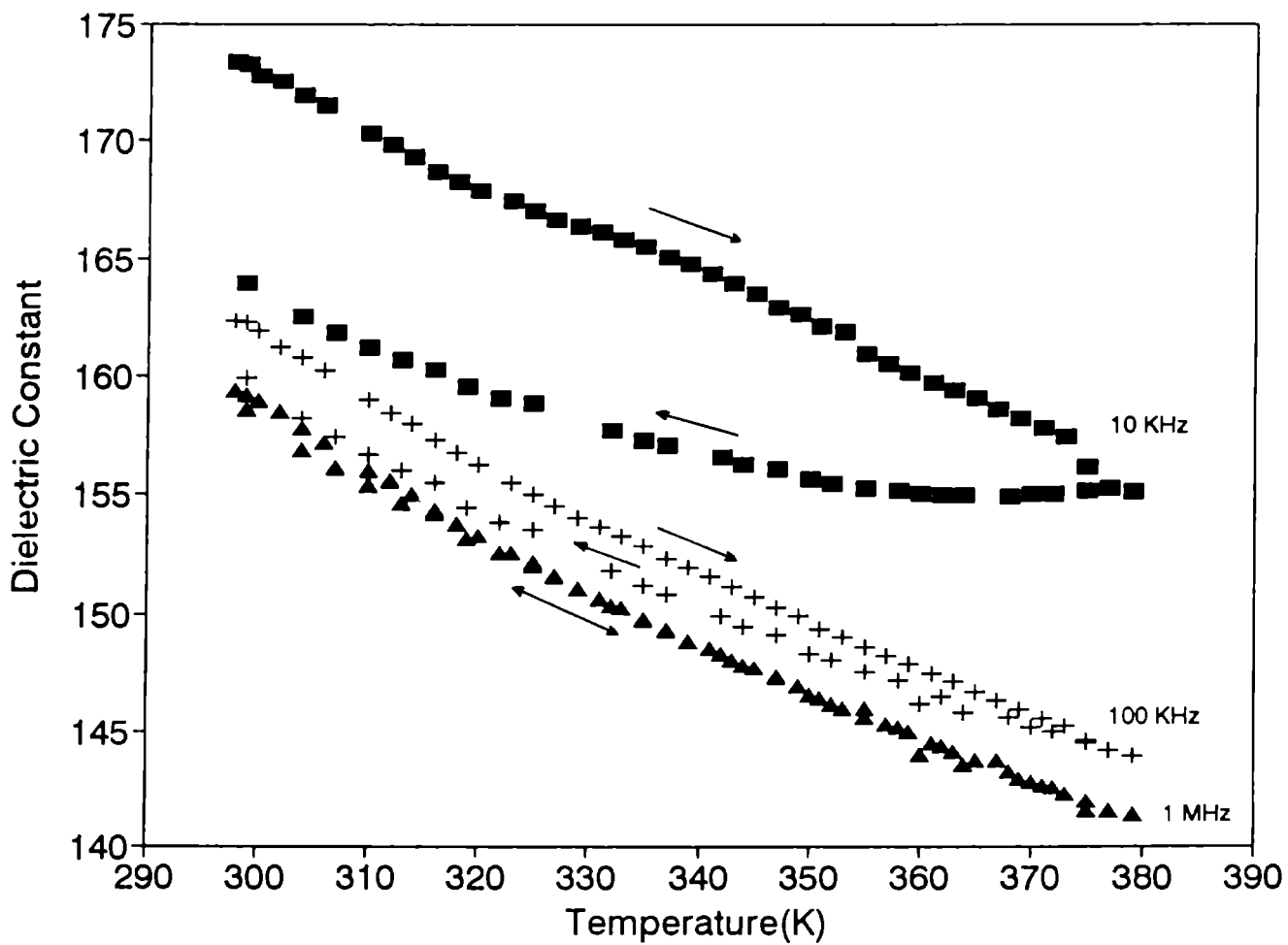
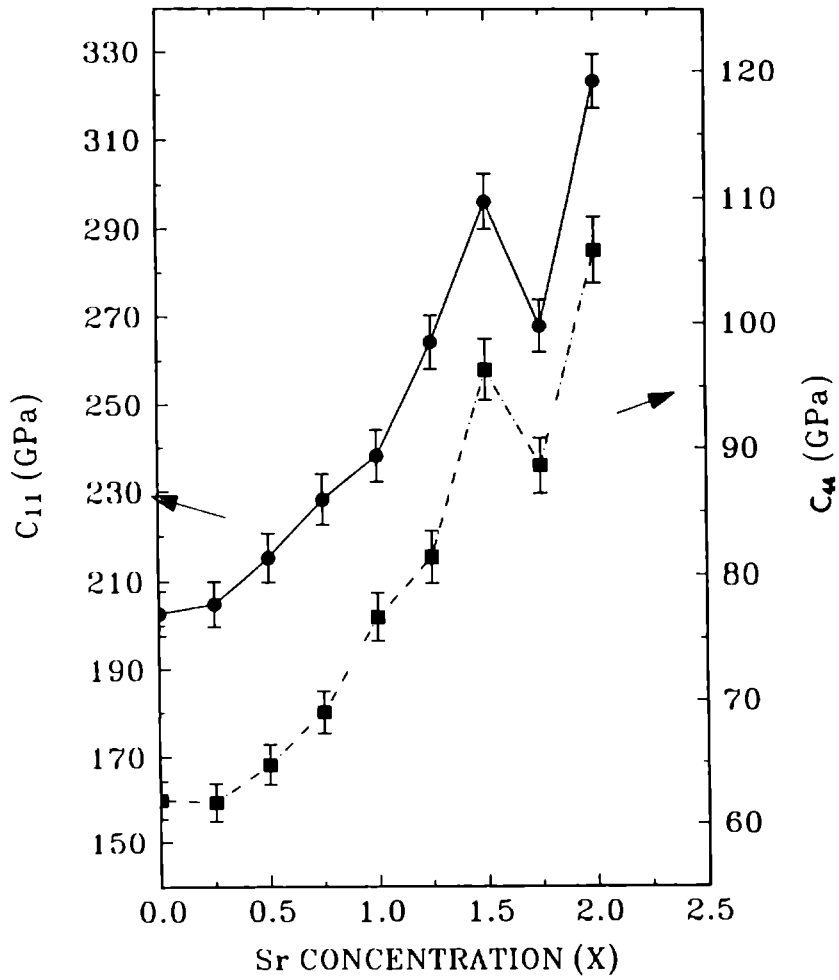Fig.3.6: Variation of dielectric constant of $Ba_{0.5}Sr1.5Ti_9O_{20}$ with temperature at different frequencies.

Fig.3.7: Variation of elastic constants C_{11} and C_{44} of $Ba_2Ti_9O_{20}$ ceramics with Sr Concentration.
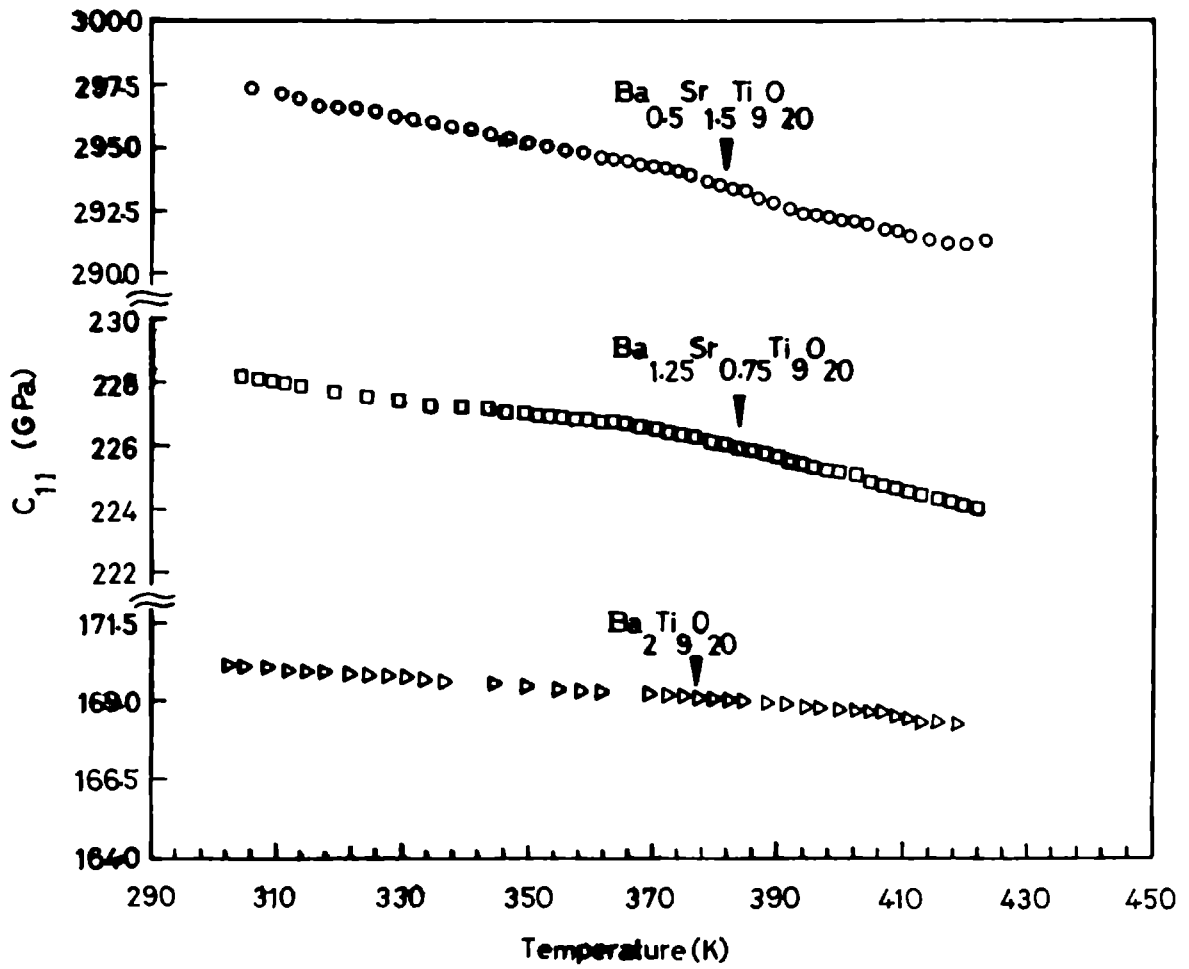
Fig.3.8(a): Variation of elastic constant C_{11} of$Ba_2Ti_9O_{20}$, $Ba_{1.25}Sr_{0.75}Ti_9O_{20}$ and $Ba_{0.5}Sr_{1.5}Ti_9O_{20}$ with temperature

83
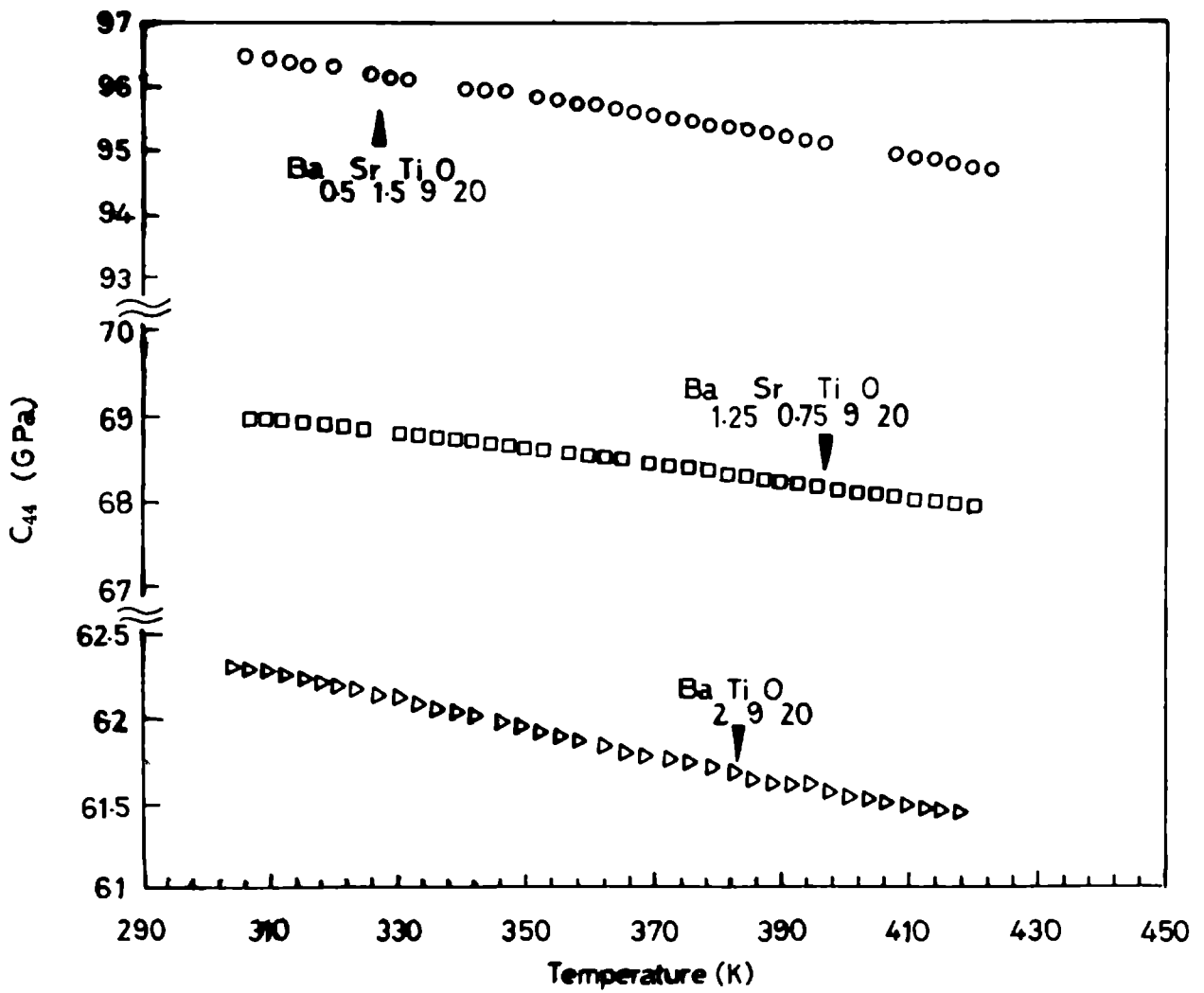
Fig.3.8(b): Variation of elastic constant C_{44} ofBa$_2$Ti$_9$O$_{20}$, Ba$_{1.25}$Sr$_{0.75}$Ti$_9$O$_{20}$ and Ba$_{0.5}$Sr$_{1.5}$Ti$_9$O$_{20}$ with temperature

where K and k_i are relative dielectric constant of the resultant sample and the individual phase i respectively and v_i is the volume fraction of phase i to the present system. Our results indicate that our samples undergo a change in the phase at around $x = 1.5$. For $x < 1.5$, the system is in a Ba rich phase which changes into a Sr rich phase as x increases beyond 1.5. A balance of the competition between these two phases at $x = 1.5$ is probably responsible for the threshold maxima in the values of dielectric constant and temperature coefficient of resonant frequency.

Since ours is one of the first measurements of elastic constants of ceramic dielectric resonator materials, we could not make any comparison with any of the already published data in this regard. Composition dependence of elastic constants shown in Fig. 3.7 indicate that the material, in general, becomes mechanically more rigid as Sr concentration increases, with maximum strength for the composition with x = 1.5. This again is a consequence of the phase transformation occurring at this composition in the system. Optimum bonding between atoms in the network probably make it maximum rigid at this composition.

As can be seen from Fig.3.8 (a) and 3.8 (b), the elastic constants decrease with temperature as for most other solids. The temperature coefficient of elastic constants is of the order of -0.03 GPa/K for longitudinal constant C_{11} and -0.01 GPa/K transverse constant C_{44} respectively. These values are comparable to those exhibited by other normal solids. The temperature variation studies also indicate that these samples do not exhibit any elastic anomaly between room temperature and 420K.

Our results indicate that the addition of Sr is effective in enhancing the dielectric constant as well as elastic constants. Sample with $x = 1.5$ shows maximum value of dielectric and elastic constant in this category. The results showing temperature variation of dielectric constant are indicative of the dielectric relaxation in these samples and the samples do not undergo any elastic anomaly in the temperature range investigated.

3.5 References

[1] H. M. O'Bryan Jr., J. Thomson,*J. Am. Ceram. Soc.* **57** **(12)**, 522 (1974).

[2] W Wersing, *Electronic Ceramics* Edited by B. C. H. Steele, Elsevier pub.co.Inc **67**, (1991).

[3] Darko Kajfez and Pierre Guillon, *Dielectric Resonators*, Artech Publishing house Inc. (1986).

[4] J. K. Plourde and C. Ren, *IEEE Trans. Microwave Theory Tech.* MTT **29**, 754 (1981).

[5] R. Freer, *Silicates Industriels* **9-10** , 191 (1993).

[6] S. Nomura, *Ferroelectrics* **49**, 61 (1983).

[7] K. Wakino, T. Nishikawa Y. Ishikawa and H.Tamura, *Br.ceram. Trans J.* **89**, 39 (1990).

[8] K. Wakino, H.Tamura, *Ceram. Trans.* **15**, 305 (1990).

[9] Y. Konishi, *Proc. IEEE* **79(6)**, 726 (1991).

[10] S.Nomura, K.Tomaya and K.Kaneta,*Jap. J. Appl. Phy.* **21**, L 624 (1982).

[11] A. J. Moulson and.J. M. Herbert, *Electroceramics* (Chapman and Hall 1990).

[12] T. Jaakola, A. Unsimaki,S. Leppavuori, *Int. J. High Technol. Ceram.* **2**, 195 (1980).

[13] G. Arlt, D. Hennings and G. De With, *J. Appl. Phy.* **58** **(4)**, 1619 (1985).

[14] J. K. Plourde, D. F. Linn, H. M. O' Bryan and J. Thomson, *J. Am. Ceram. Soc* **58**, 418 (1975).

[15] H. M. O'Bryan Jr., J. Thomson Jr. and J. K. Plourde,*J. Am. Ceram. Soc.* **57**, 450 (1974).

[16] J. K. Plourde and C. Ren, *IEEE Trans. Microwave Theory Tech.* **MTT 29**, 754 (1981).

[17] G. H. Jonker and W. K. Kwestroo, *J. Am. Ceram. Soc.* **41**, 390 (1958).

[18] J. M. Wu and H. W Wang, *J. Am. Ceram. Soc.* **71**, 869 (1988).

[19] H. M. O'Bryan Jr., W. H. Grodkiewicz, and J. L. Bernstein *J. Am. Ceram. Soc.* **63**, 309 (1980).

[20] E. Tillmanns, W. Hofmeister and W. H. Baur, *J. Am. Ceram. Soc.* **66**, 268 (1983).

[21] T. Negas, R. S. Roth, H. S. Parker and D. Minor, *J. Sol. State Chem.* **9**, 294 (1974)

[22] H. M. O'Bryan Jr., J. Thomson, *J. Am. Cerm. Soc.* **66**, 66 (1983).

[23] Idem, *J. Am. Ceram. Soc.* **57 (12)**, 522 (1974).

[24] J. P. Guha, *J. Am. Ceram. Soc.* **60**, 246 (1977).

[25] P. P. Phule and S. H. Risbud, *J. Mat. Sci.* **25**, 1169 (1990).

[26] H. S. Lu, L. E. Burkhart, G. L. Schrader,*J. Am. Ceram. Soc.* **74(5)**, 968 (1991).

[27] T. Jaakola, J. Mottonen, A. Unsimaki, R. Rautioaho and S. Leppavuori, *Ceram. Int.* **13**, 151 (1987).

[28] S. Nomura, K. Tomaya and K. Kaneta, *Jap. J. Appl. Phy.* **22**, 1125 (1983).

[29] W. Kwestroo and H. A. M. Paping, *J. Am. Ceram. Soc.* **42**, 292 (1959).

[30] C. Chatterjee, A. N. Virkar and A. Paul, *J. Mat. Sci. Lett.* **9**, 1049 (1990).

[31] E.P.Papadakis: *Physical Acoustics* (eds. W.P.Mason and R.N.Thurston; Academic press, New York) **12**, 277 (1976).

[32] H. J. McSkimin, *J. Accoust. Soc. Am.* **33**, 12 (1961).

[33] H.Sreemoolanadhan, Johney Issac, Peter Koshy, M.T.Sebastian and P.Mohanan:to be published in Br. Ceram. Trans. J.

[34] J. M. Wu and M. C. Chang, J. Am. Ceram.Soc. **73**, 1599 (1990).

[35] E. Tillmanns and W. H. Baur,*Acta Crystallogr.* **B.26**, 1645 (1970).

[36] B. D. Burbank and H. T. Evans Jr.,*Acta Crystallogr.* **1(6)**, 330 (1948).

[37] E. Tillmanns, *Acta Crystallogr.* B **25(8)**, 1444 (1969).

Chapter 4

Dielectric and elastic properties of Hf doped $(Zr_{0.8}\ Sn_{0.2})TiO_4$ dielectric ceramics

4.1 Introduction

During the last few decades, the most significant developments in the field of microwave communications have been the development of dielectric resonators with preassigned properties and a number of materials have been developed [1-8]. The desirabale properties of such microwave resonator ceramics are high dielectric constant, low dielectric loss or high Q value and very small temperature coefficient of resonant frequency. These dielectric resonators replace wave guide filters in such demanding applications as satellite communications where microstrip and stripline resonators can not be used because of their inherent high losses. Further more, carefully designed microwave oscillators which utilise dielectric resonators can equal the temperature stability of conventional microwave resonant cavities.

Ceramic materials used as dielectric resonators must have a very low loss tangent and controllable temperature stability. There are groups of materials which have been found to offer a combination of properties which are suitable for the fabrication of microwave dilectric resonators. Various processes have been developed for the preparation of better dielectric resonator materials [4]. Higher demands are imposed on the operating reliability of devices based on these materials. New classes of dielectric resonator materials have been developed which posses special properties and broader field of application has been found for them The new materials serve as the basis for recently developed microwave devices like cellular telephones, microwave filters etc. In

89

order to get a clear insight into the material characteristics that lead to the desirable properties, it is necessay to study the physical properties of these materials.

Commercially useful dielectric resonators require enhancement in dielectric and mechanical properties as well as thermal stability with sufficient quality factor. This can be achieved by proper doping or substitution of selected elements. At the same time, dielectric loss and temperature coefficient of resonant frequency should lie as minimum as possible. Several reports on the investigation of the effects of various dopants and methods to improve dielectric and mechanical properties have appeared in the last two decades [1,6,9-15]. During processing different phases develop inside the material. The interfaces between these phases are regions in which changes in lattice orientation occur. As a result it is very difficult to predict the properties of the ceramics. Studies on single crystal properties of the principal components provide valuable information. However, the growth of single crystals is usually difficult and time consuming The dielectric properties of mixed ceramics with many phases depend on the distribution of these phases [16]. In reducing the effective dielectric properties of mixtures, the concept of connectivity is useful in classifying the type of the mixture [17].

One essential requirement of a dielectric resonator, $\tau_f=0$, is satisfied only by a limited number of single phase materials. An alternate method of providing zero τ_f is to combine different materials having positive and negative τ_f values. This concept has been developed from Lichteneekers's rule and is used to control the permittivity of mixtures [18]. But this type of relation do not hold good for improving Q values.

A number of groups of materials with desirable properties have been developed over the years. All series of complex perovskite compounds have been prepared in which two B sites of the lattice are shared by the ions of different valencies [17-22]. Zirconium titanate and their modifications gained considerable interest as materials for high Q dielectric resonator in microwave devices with low dielectric loss and temperature coefficient of resonant frequency. These materials have got widespread applications and they have been in use as temperature stable dielectric materials for ceramic capacitors for a long time. The additions of Sn alone and coupled substitution with Tallium and Aluminium are found to be effective in increasing the dielectric properties and

periodicity without affecting the quality factor. The coupled substitution of Al^{3+}/Ta^{5+} on Zirconium titanate ceramics is found to have all ordering transformation that leads to an increase in the periodicity of the parent cell [11].

The compound $ZrTiO_4$ has been investigated by many workers [24-30]. The high temperature structure of $ZrTiO_4$ has been related to that of α-PbO_2 having a random distribution of Zirconium and Titanium ions in available octahedral cation sites [31,32]. Agreement exist among many workers on orthorhombic structure of the phase and existence of phase transition at temperature $< 1200°C$ [27-29]. The reported phase transition is accompanied by a slight decrease in the length of the longest unit cell (c-axis). The low temperature form has an ordered arrangement of atoms characterised by incommensurate super structure diffractions along the a-axis. Within the transition temperature, mixed phases are observed with either the high or low temperature form of $ZrTiO_4$ dominant, depending on the prior heat treatment of the specimen. The variation in a and b dimensions are essentially unchanged by the phase transition[31].

Zirconium tin titanate (ZTS) which is a solid solution of ZrO_2, TiO_2 and SnO_2, offers the best properties and ease of processing [33,34]. A number of papers have appeared in literature reporting the structure, range of existence and dielectric properties of ZTS [27-29]. The crystal structure has been identified as that of α-PbO_2 having orthorhombic symmetry and space group Pbcn. The Zr^{4+}, Ti^{4+} and Sn^{4+} ions are randomly distributed in the lattice, each surrounded by slightly distorted oxygen octahedra. $(Zr_{1-x}Sn_x)TiO_4$ with upto 20 at. % of Zr replaced by Sn have been in use for specific device applications. Substitution progressively increases Q from 2000-5000 for $x = 0$ to 6000- 10000 for $x = 0.2$ [1,35].

Several attempts have been made to replace the different elements in $ZrTiO_4$ ceramics Wolfram et al. [1] reported that Sn substitution decreases the dielectric constant of $(Zr_xSn_yTi_z)$ solid solution. This decrease can be attributed to small polarisability of Sn^{4+} containing oxygen octahedra. In compounds containing oxygen octahedron with Ti and Zr central ions, ϵ_r seems to stem from the hybridisation of the oxygen p with d states of the transition metal ion [36]. As Sn is lacking d-valence states, oxygen octahedra with Sn^{4+} ions are less polarisable and contribute less to the dielectric con-

stant than Ti^{4+} and Zr^{4+} containing octahedra. It has also been found that the addition of ZnO-B_2O_3-SrO_3 commercial glass to (Zr Sn)TiO_4 [23] shows more than 20% higher density than that of pure material sintered at the same temperature. The Q value is also found to improve with glass addition.

There have been considerable improvement in the mechanical properties of $ZrTiO_4$ with the addition of Sn. Sn substitution inhibits Zr-Ti ordering transformation that Zirconium titante undergoes at a temperature below 1200°C [37 38]. Sn can be substituted to differing degrees for either Zr or Ti or for both [39]. Here substitutional tin is apparently effective in stopping the transformation by stabilising the random nature of the high temperature structure against cation ordering. The useful dielectric properties associated with the solid solutions may result from this stabilisation phenomenon. The relation between electrical properties and composition is rather complex. In general, as TiO_2 increses at the expense of ZrO_2, ϵ_r increases, while increasing SnO_2 at the expense of ZrO_2 increases Q, but has little effect upon ϵ_r. The more interesting feature that has been observed in Sn doped $ZrTiO_4$ samples is the existence of homogeneous solid solution.

Commercial ZTS ceramics are processed with sintering additives like La_2O_3, ZnO, Fe_2O_3 and CoO_3 [40]. Without the sintering aid, densities > 90% theoretical values have proved almost impossible to achieve by conventional routes and therefore dielectric properties can not be reliably related to those of a pure dense ceramic. It was thought that the additives act by forming a liquid phase at the grain boundaries during sintering and aid densification through rapid transport of matter through the liquid phase. There are a number of publications and patents which report the efficiency of a variety of sintering aids and dopants [1,2,40]. The most commonly used sintering aid for ZTS system is ZnO. But the presence of grain boundary phase due to ZnO added to achieve adequate densities may be assumed to cause significant deviation from the properties of a pure dense material. Therefore it is difficult to seperate the intrinsic behaviour of ZTS from the influence of additives.

Considerable improvement in the dielectric properties of ($ZrSnTiO_4$) ceramics have been reported with addition of NiO as sintering agent by Wakno et al [6]. They

support lattice vibration theory which predicts that impurities or lattice defects in ionic crystals cause deterioration of the Q value.

The effect of ionic substitution on the thermal expansion of $ZrTiO_4$ ceramics have attracted almost as much attention as their structural changes. Titanium in $ZrTiO_4$ can be substituted by combining $3^-/5^+$ cations. The expansion of some of these $Zr(Me^{3+}/Me^{5+})O_4$ solid solution is low and highly anisotropic with contraction in the direction of basis during heating. Extended microcrack formation occurs in the samples with large grains because of their highly anisotropic expansion behaviour [41]. In the case of $HfTiO_4$,thermal expansion is low but highly anisotropic. It has been found that substitution of Sn^{4+} for Ti strongly decrease the thermal expansion of $ZrTiO_4$ while it has practically no effect on $HfTiO_4$. Substitution of trivalent cations such as Al, Ga,Fe in combination with Ta^{5+} for titanium in $ZrTiO_4$ and $HfTiO_4$ was succesful but not with Cr, Sn, In or Y. It is true also for the coupled substitution of Me^{3+}/Nb. One of the main interesting phenomena is that the thermal expansion is lowered considerably by substitution with Fe^{3+}/Ta^{5+} and with Al^{3+}/Ta^{5+}

Several studies have been done to improve the dielectric properties of $ZrTiO_4$ by suitable dopants. Ikawa et al. [38] studied the behaviour of the substitution in $ZrTiO_4$ system and it was found that the behaviour is exactly similar to that of Sn substitution. Moreover, volume of Hf substituted material is found to be larger than pure $ZrTiO_4$ and order-disorder transformation is prominent only at low Hf contents. Hence the Hf and Sn substitution are clearly effective in suppressing the driving force for the long range cation ordering reaction because this reaction play an important role in determining the dielectric properties Zirconium titanates.

Though all the above cited additions are succesful to some extent in improving the dielectric resonator properties of ZTS, nobody has investigated the effect of Hafnium doping on their elastic properties. In an attempt to understand the chemical and structural factors that control elastic and dielectric properties of the system, we have investigated the effect of Hf substitution on the stability and geometry of the ordered structure. Hafnium is similar to titanium in valency. We have carried out x-ray powder diffraction studies on the ceramic with the formula $(Zr_{0.8} Sn_{0.2}) (Ti_{1-x} Hf_x)O_4$

with different values of x. In this chapter we report the result of our measurements on the longitudinal and shear elastic modulii of ZTS and the effect of Hf substitution on these parameters. The temperature variation of the elastic modulii have also been measured and reported. The low frequency dielectric constant and its variation with Hf concentration have also been measured and reported. The temperature vatriation of the dielectric constant at different frequencies have also been investigated.

In the following sections we outline the details of sample preparation, experimental techniques used, results obtained and a discussion of the results.

4.2 Sample preparation and characterisation

4.2.1 Sample preparation

Solid solution compounds of $(Zr_{0.8} Sn_{0.2}) (Ti_{1-x} Hf_x)O_4$ with x=0, 0.2,0.4,0.6,0.8 and 1 have been prepared by the conventional solid state ceramic prepartion method. Accurately weighed quantities of ZrO_2 (99.9% Aldrich, USA) SnO_2 (99.9 % Aldrich, USA), TiO_2 (Electronic Grade, Automere, USA) and HfO_2 (99.9% Aldrich, USA) have been mixed in an agate mortar and calcined at 1250 to 1300°C for 4 hours. The calcined powders are thin ground, compacted into cylinders under a presssure of 225 MPa. These compacted discs are then sintered at 1420 to 1480°C for 4 hours The sintering temperature is increased with increase of Hf content. The sintered compacts have been polished and used for characterisation and further investigations.

4.2.2 X ray and SEM analysis

All the samples prepared have been subjected to X ray diffraction analysis in a standard X ray diffractometer (Regaku Japan) using $CuK\alpha$ radiation. XRD patterns of the samples have enabled us to determine the phase constitution of the ceramic samples.

The microstructure of the samples have been obtained by scanning electron microscopy (SEM) using JEOL (Japan) machine SEM photographs have been taken using polished and etched surfaces of the sample discs. The single phase nature of the ceramics are evident from the pictures. Crystal structure of $(Zr_{0.8} Sn_{0.2}) (Ti_{1-x} Hf_x)O_4$

94

is reported as orthorhombic.

4.3 Low frequency dielectric constant measurements

For the low frequency dielectric constant measurements, the samples are cut into thin discs of diameter ≈10mm and thickness ≈ 1mm. Both the end faces are polished to precise dimensions to an accuracy of 0.1% or better. It is placed between two well polished copper electrode discs. Silver point is applied on the surfaces of the sample to ensure good electrical contact with the copper electrodes. The whole arrangement is kept in a home made dielectric cell whose temperature could be varied and controlled from liquid nitrogen temperature (77K) to 450K using a temperature controller (Lakeshore Cryotronics DRC-82C). The heating rate used has been 1K/min. Four probe method has been used in terminal connections of the dielectric cell for loss free measurements. It is better to have the lower electrode with larger area than the upper one so that the capacitance remains constant and positioning of the upper electrode is not very critical.

The inter-electrode capacitance C for any electrode spacing can be determined from the equation $C = \frac{\epsilon A}{t}$ Where ϵ is the dielectric constant, A is the area of the upper electrode and t is the spacing between the electrodes. The stray capacitance of the cell can be eliminated by offset adjustments of the impedance analyser. The fringe capacitance can be eliminated by finding the slope [42]. The measurements have been performed in the temperature range 300K to 430K. The composition dependence and frequency dependence of the dielectric constant have been measured for all samples of the Hf doped ZTS system.

4.4 Measurement of elastic constants

Ultrasonic wave velocities in the ceramic samples have been measured by the Pulse Echo Overlap method (PEO) using Matec 7700 pulse modulator and receiver system [43]. Pelletised samples of diameter ≈ 10mm and thickness ≈ 6mm have been used for these measurements. The end faces of the samples have been polished after making

them parallel to each other. X cut quartz transducer of frequency 15MHz is mounted on the sample using silicon grease as the bond. It is placed inside a suitable enclosed chamber whose temperature can be varied and controlled from 300K to 450K with the help of the temperature controller. Y cut quartz transducer has been used to generate transverse ultrasonic waves.

McSkimin. Δt criterion has been applied to correct for the phase lag due to bonding medium on RF echoes [44]. This technique helps to measure the ultrasound transit time in the sample to an accuracy of the order of a few parts per million. The temperature dependence of the velocity of the longitudinal and shear waves through the samples have been determined in the temperature range 300K to 450K. The longitudinal and shear elastic constants C_{11} and C_{44} for all the samples have been determined from their corresponding velocities using the relation $C_{ij} = \rho\, V^2$ where ρ is the density of the sample. The density has been determined by measuring the volume and the weight of each sample accurately.

4.5 Results and discussions

All the solid solution compositions show homogeneous dense appearance with relative density greater than 92% of the theoretical density for which the crystal structure is known. This is an indication of the best performance of additives used for sintering the samples. Fig.4.1 shows the XRD patterns obtained from representative samples. It can be seen from the XRD patterns that the different $(Zr_{0.8}Sn_{0.2})$ $(Ti_{1-x}\, Hf_x)O_4$ compositions have been obtained as single phase materials within the sensitivity limit of the XRD. The patterns obtained for $x < 0.6$ are in good agreement with that of undoped $(Zr_{0.8}Sn_{0.2})TiO_4$ (JCPDS) [34-33]. The reflections have been indexed based on the orthorhombic symmetry of $(Zr_{0.8}\, Sn_{0.2})TiO_4$ for $x = 0.2$ and 0.4. The lattice parameters have been evaluated for these composition and are indicated in the figure. It can be seen from the figure that the x-ray patterns obtained for $x > 0.6$ are different from that of the orthorhombic one. This is indicative of a structural change occuring in the system as a result of Hf substitution. The orthorhomic symmetry is lost when 60% or more Hf is substituted at the Ti site of $(Zr_{0.8}Sn_{0.2})TiO_4$.

$(Zr_{0.8} Sn_{0.2})(Ti_{1-x} Hf_x)O_4$

x=1

x=0·8

x=0·6

Intensity (arb. units)

(111)   a=4.8057, b=5.4393, c=5.0767

(110)

(020) (002) (200)
       (021)
                              (220) (202)
                                    (221)   x=0·4
                              (022)
              (121)(112)   (131)

a=4.7891, b=5.4313, c=5.0379

x=0·2

20   30   40   50   60

2θ (deg)
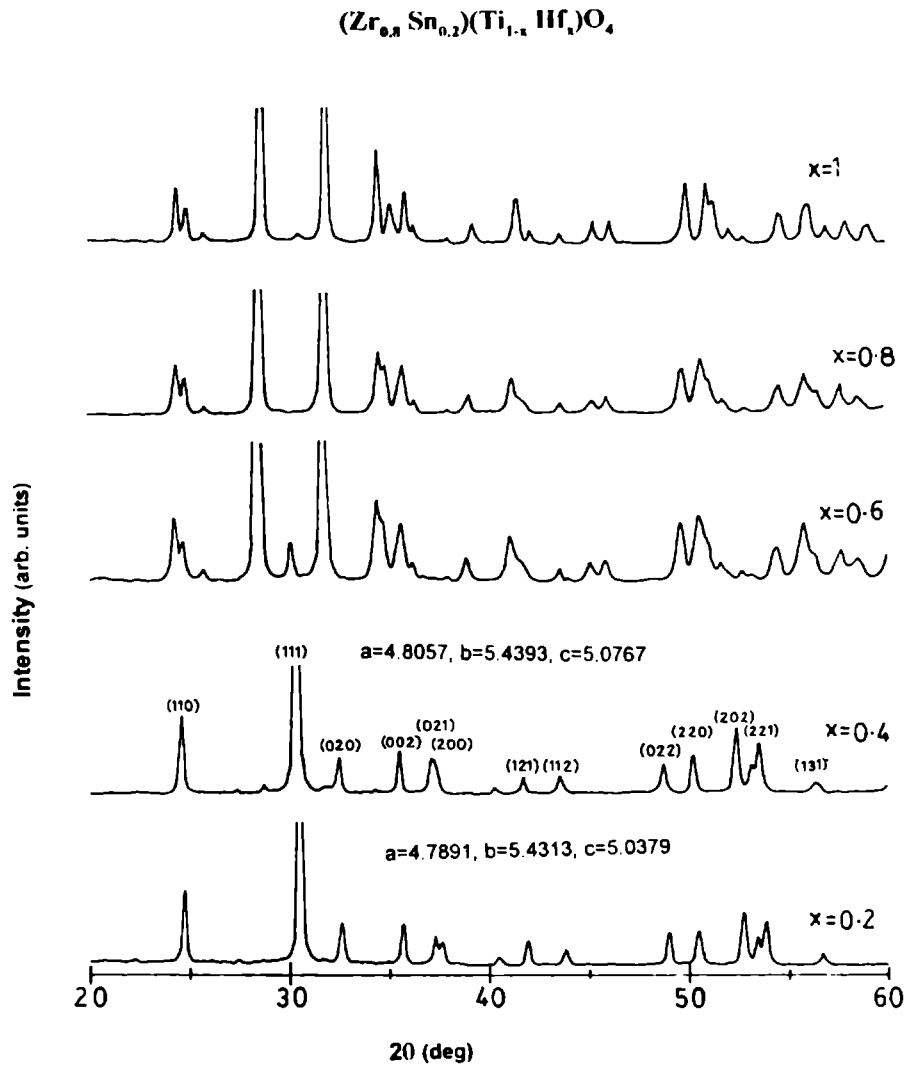
Fig.4.1: Powder XRD patterns of $(Zr_{0.8}Sn_{0.2})$ $(Ti_{1-x} Hf_x)O_4$ ceramics obtained using CuKα radiation

97

Typical SEM photographs showing the microstructures of the pure and Hf doped samples are shown in Fig.4.2. Analysis of the SEM pictures show that $(Zr_{0.8}Sn_{0.2})$ $(Hf_{0.5}Ti_{0.5})O_4$ grains are about $5\mu m$ size whereas $(Zr_{0.8}Sn_{0.2})HfO_4$ grains are relatively smaller in size. Fig.4.3 shows the variation of the low frequency dielectric constant with Hf concentration. It can be seen that the dielectric constant increases first and then decreases when Ti ions are replaced by Hf ions. We have measured the frequency and temperature dependence of low frequency dielectic constant up to 13MHz and 430K respectively for each of the samples. The variation of the low frequency dielectric constant with temperature at two different frequencies for the samples $(Zr_{0.8}Sn_{0.2})$ $(Ti_{0.8}Hf_{0.2})O_4$ is shown in the fig.4.4. It can be noted that the dielectric constant exhibits a broad peak around 360K which is indicative of phase transformations taking place in these materials at high temperature.

The variations of the longitudinal and shear elastic modulii, C_{11} and C_{44}, with Hf concentrations are shown in Fig. 4.5. It can be seen that, in general, both the elastic modulii decrease as Hf concentration increases. The temperature variation of the longitudinal modulus C_{11} has been measured as a function of temperature from room temperature to 420K. This variation in the case of $(Zr_{0.8}Sn_{0.2})$ $(Ti_{0.8}Hf_{0.2})O_4$ sample is significant which is shown in Fig. 4.7. This curve shows a minimum between 360K and 370K indicating the possibility of a diffuse phase transformation around this temperature. A temperature hysteresis of about 10K is found for this transformation between the heating and cooling cycles. Other samples exhibit similar kind of behaviour. The curves for the other samples $(Zr_{0.8}Sn_{0.2})$ $(Ti_{0.95}Hf_{0.05})O_4$ and $(Zr_{0.8}Sn_{0.2})$ $(Ti_{0.6}Hf_{0.4})O_4$ are shown in figures 4.6 and 4.8 respectively.

The objective of these investigations has been to understand the effect of substituting titanium ions with hafnium in $(Zr_{0.8}Sn_{0.2})$ TiO_4 ceramics. Hafnium ion has larger ionic radius than titanium ion. Consequently, one can expect an increase in cell volume with increase in x which is in agreement with experimental observations found in elastic constant measurements. The density of the sample increases as the heavier Hf content increases. Our interest has been to see whether the dielectric properties and elastic properties improve with Hf substitution It is found that replacement of
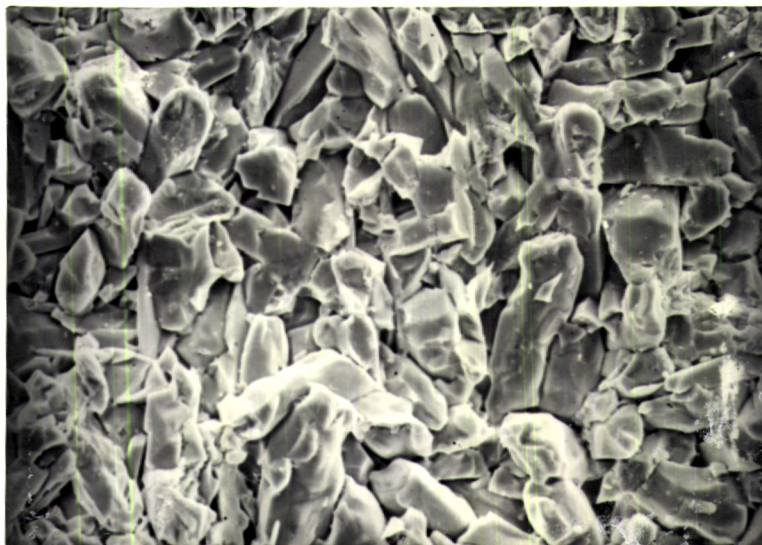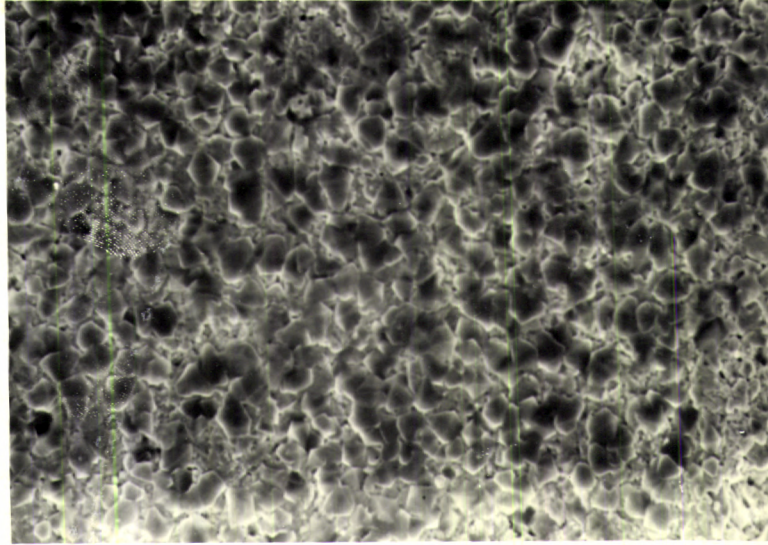
Fig.4.2: SEM photograph of $(Zr_{0.8}Sn_{0.2})$ Hf O_4 and $(Zr_{0.8}Sn_{0.2})$ $Ti_{0.5}Hf_{0.5}O_4$ ceramics
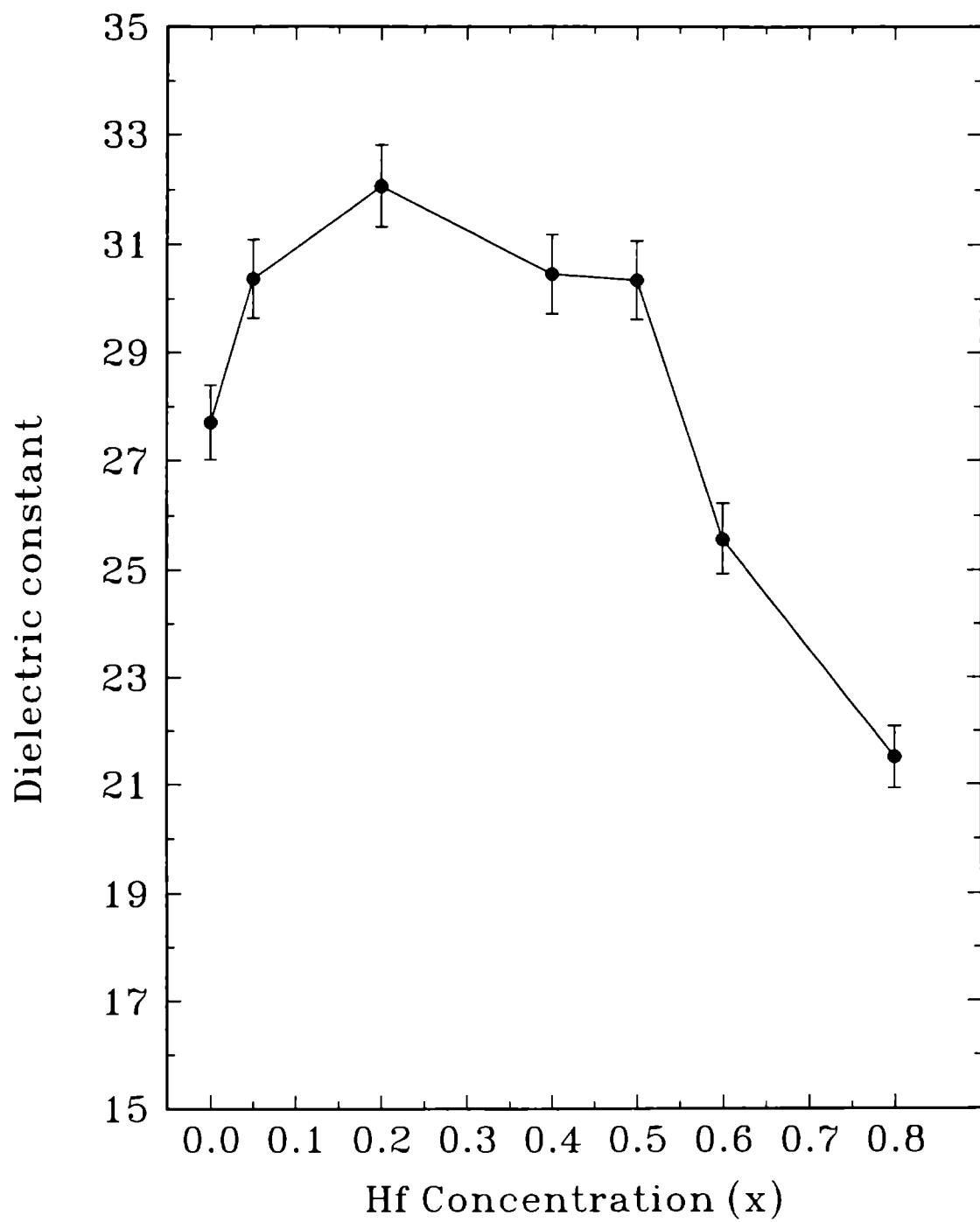
Fig.4.3: Variation of low frequency dielectric constant with Hf content (x) of $(Zr_{0.8}Sn_{0.2})$ $(Ti_{1-x}Hf_x)O_4$ ceramics
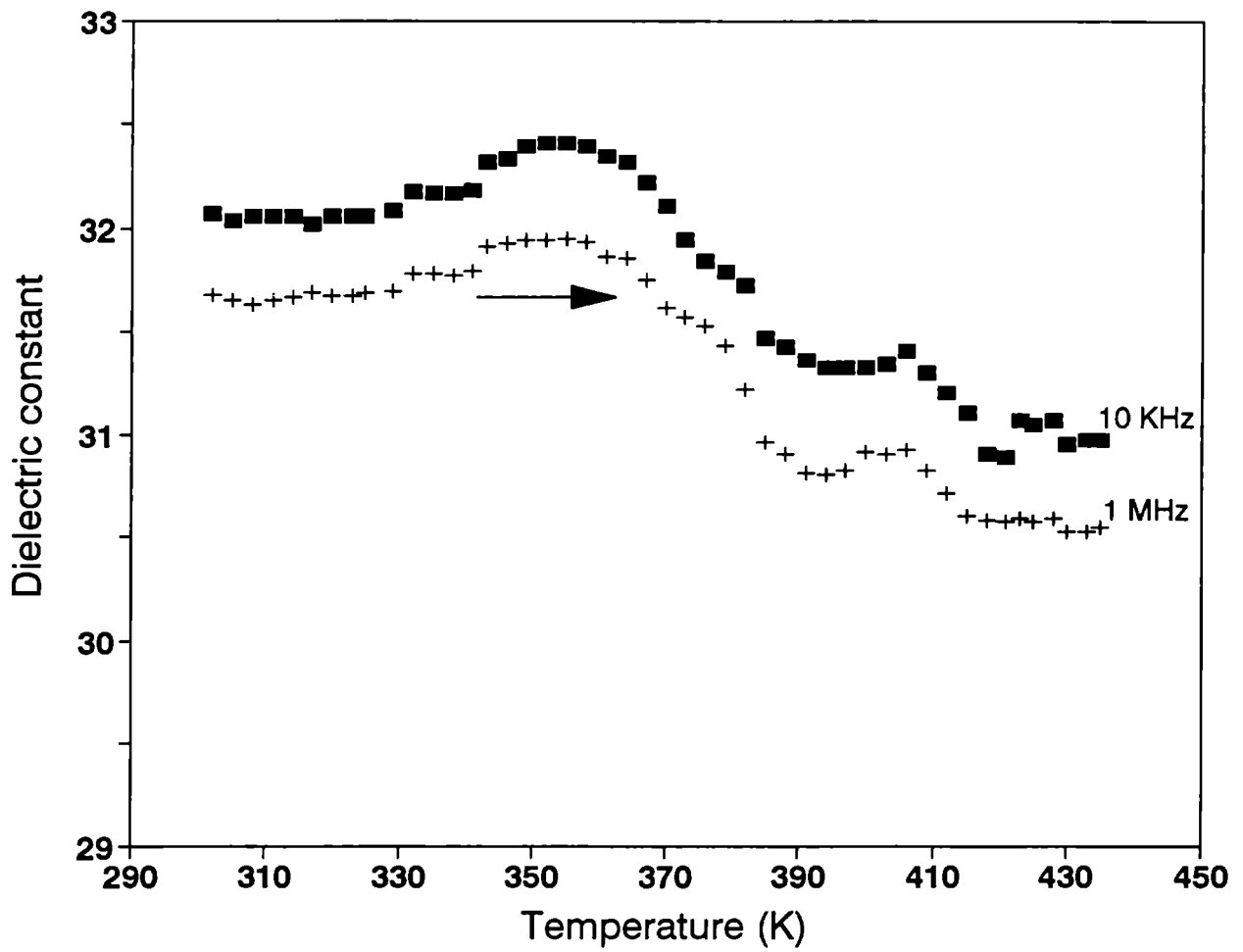
Fig.4.4: Variation of dielectric constant of $(Zr_{0.8}Sn_{0.2})$ $Ti_{0.8}Hf_{0.2}O_4$ ceramic
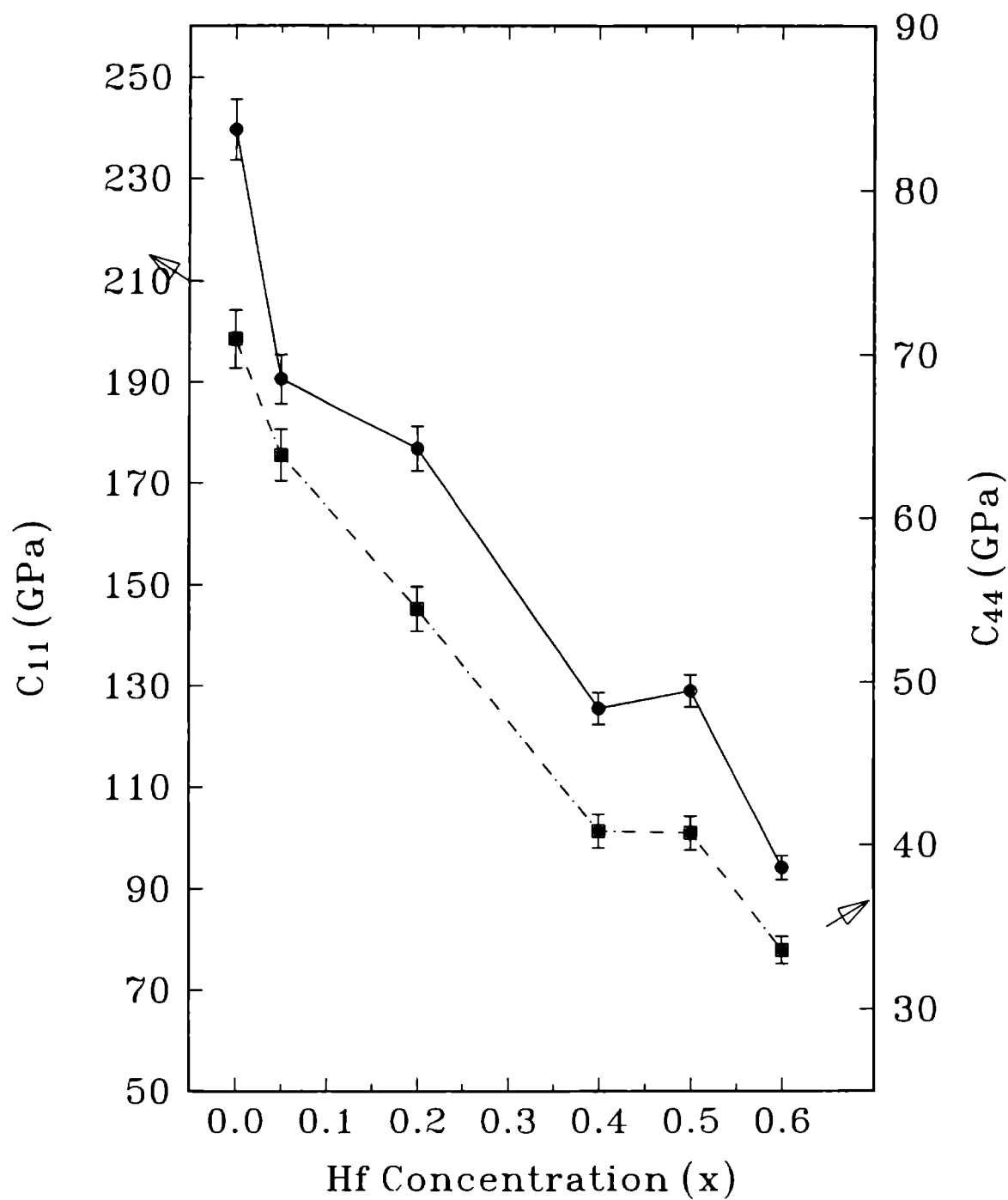with temperature at 10 KHz and 1 MHz

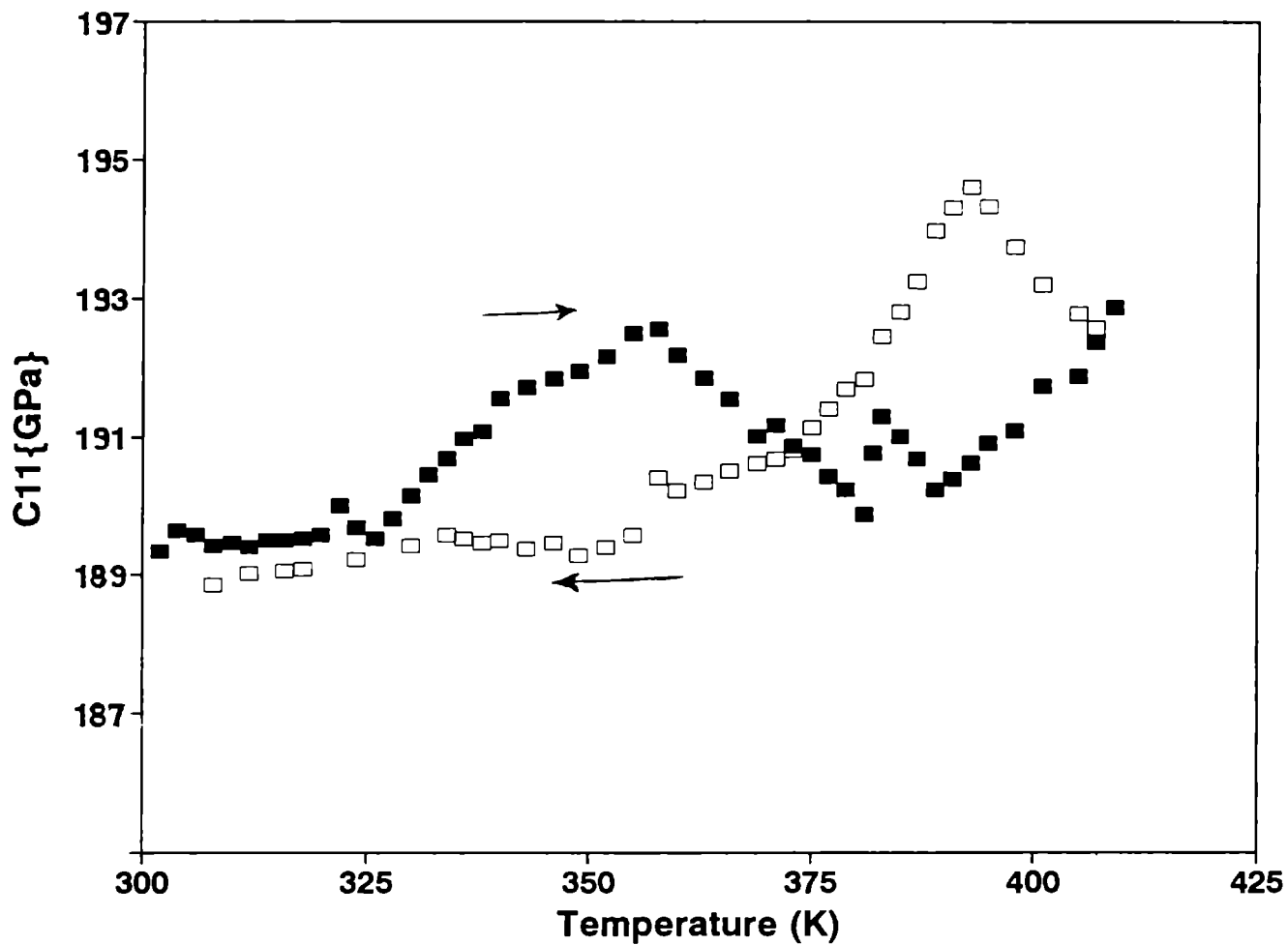Fig.4.5: Variation of C_{11} and C_{44} of $(Zr_{0.8}Sn_{0.2})$ $(Ti_{1-x}Hf_x)O_4$ ceramics with Hf concentration

Fig.4.6: Variation of longitudinal elastic constant C_{11} of $(Zr_{0.8}Sn_{0.2})$

$(Ti_{0.95}Hf_{0.05})O_4$ ceramic with temperature
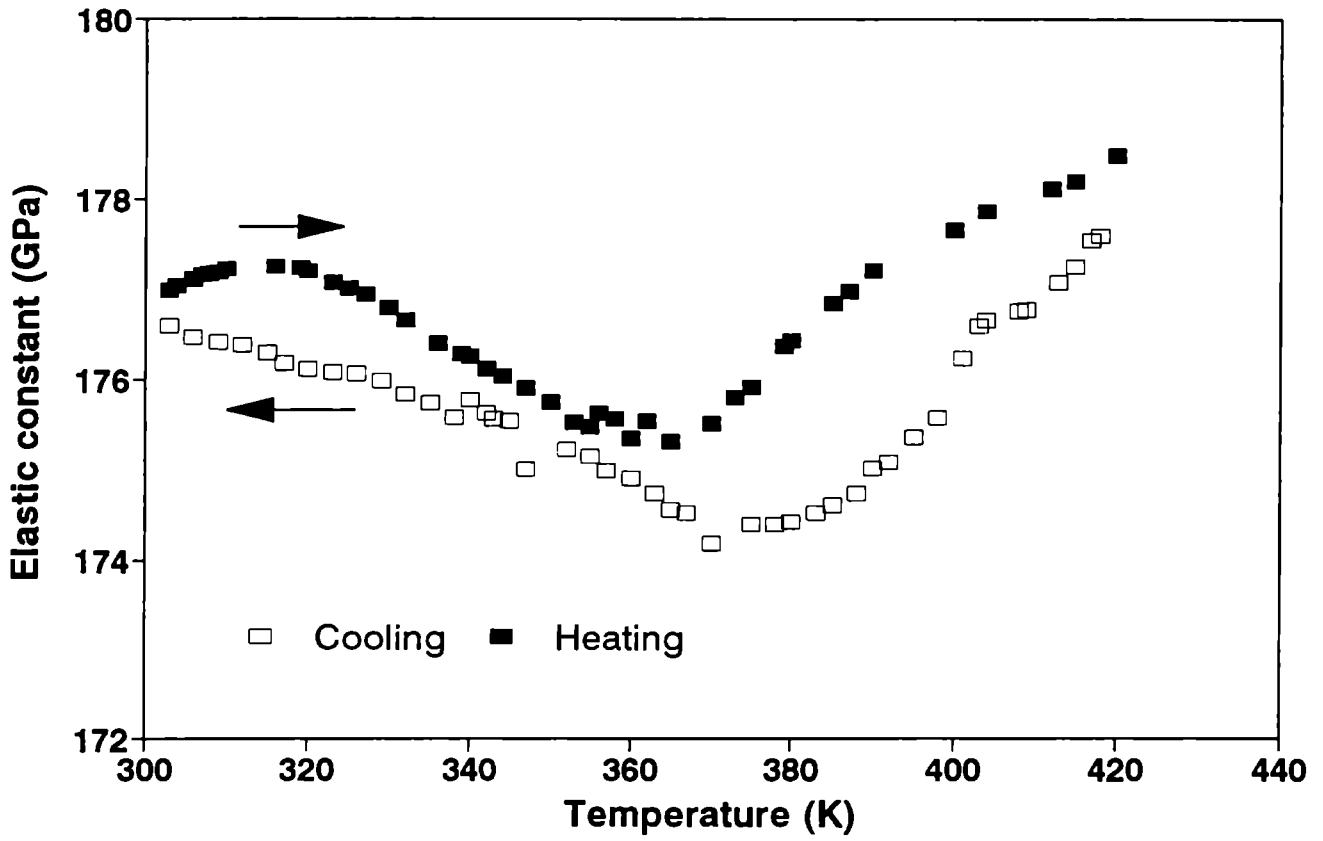
Fig.4.7: Variation of longitudinal elastic constant C_{11} of $(Zr_{0.8}Sn_{0.2})$

$(Ti_{0.8}Hf_{0.2})O_4$ ceramic with temperature
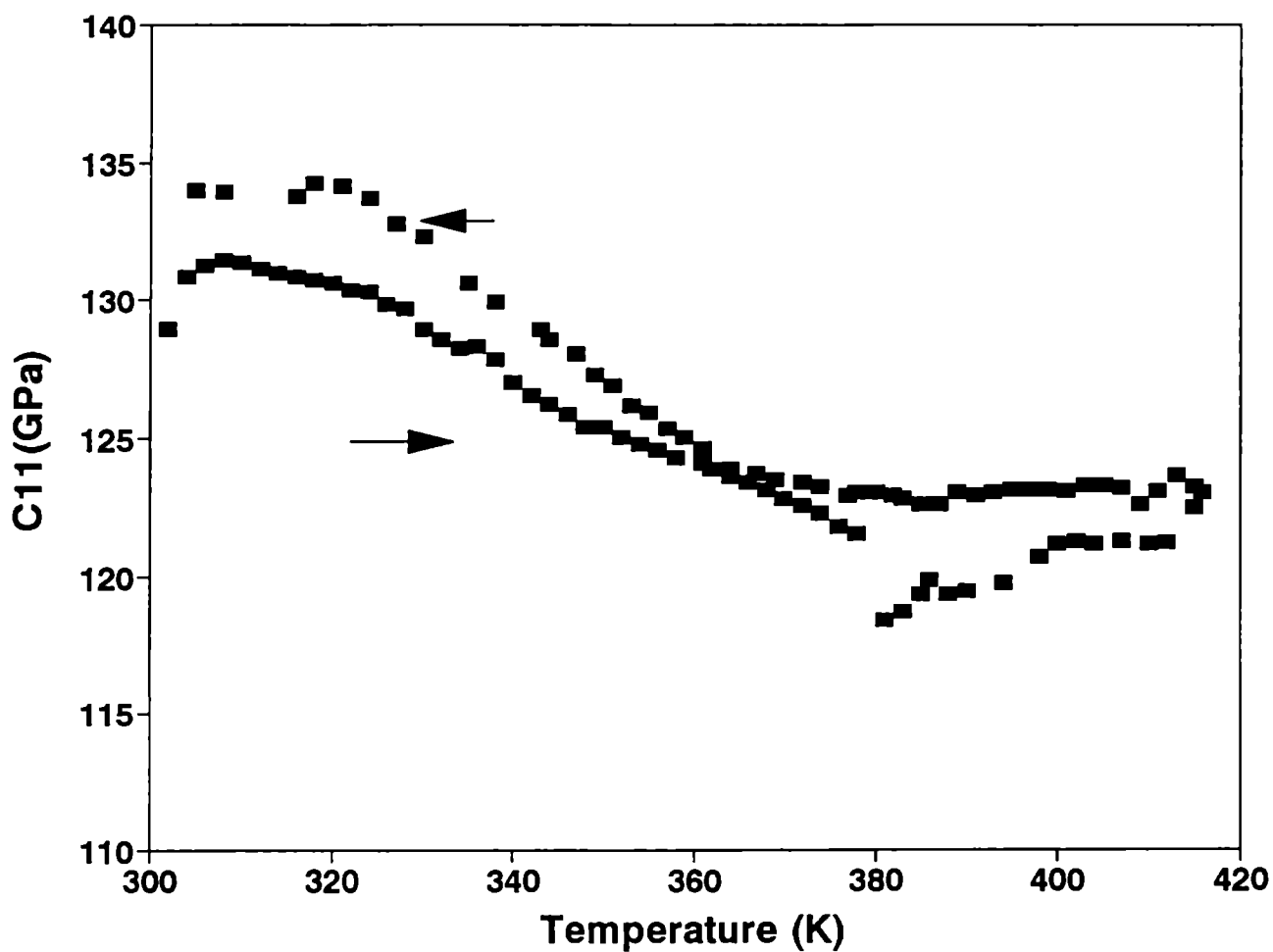
Fig.4.8: Variation of longitudinal elastic constant C_{11} of $(Zr_{0.8}Sn_{0.2})$ $(Ti_{0.6}Hf_{0.4})O_4$ ceramic with temperature

Ti ions with Hf ions lead to deterioration of the dielectic properties ie, ϵ_r decreases. But for small values of x, the material shows a very small (nearly zero) variation of the τ_f which is of great significance for practical applications for this material. The interesting result of Hf substitution is that the material undergoes a structural change for values of $x > 0.6$ as is evident from the X ray patterns. Further studies on the nature of this phase transformation is proposed to be done at a later time. The diffuse phase transformation occuring in these samples around 360K should be taken into account while using these materials as dielectric resonators.

The variation of dielectric constant with temperature on the sample, $(Zr_{0.8}Sn_{0.2})$ $(Ti_{0.8}Hf_{0.2})O_4$, shown in Fig. 4.4 is a typical curve. Other samples are found to exhibit similar behaviour. The decrease of dielectric constant with temperature is due to the dielectric relaxation of the sample. This factor also should be taken into account while attempting to use these materials at elevated temperatures.

4.6 References

[1] G. Wolfram and E. Gobel, *Mater. Res. Bull.* **16**, 1455 (1981)

[2] K. Wakino, K. Minai and H. Tamura, *J. Am. Ceram. Soc.* **67**, 278 (1984).

[3] D. Kolar, S. Gaberscek, Z. Stedler and D. Suvorov, *Ferro electric* **27**, 269 (1980).

[4] S. Kawashima, M. Nishida, I. Ueda and H. Ouchi, *J. Am. Ceram. Soc.* **66**, 42 (1983)

[5] G. Wilson and F. P. Glasser, *Br. Ceram. Trans. J.* **88**, 69 (1989).

[6] K. Wakino, K. Minai and H. Tamura, *J. Am. Ceram. Soc.* **67**, 278 (1984).

[7] R. Freer, *Silicate Industrials* **9-10**, 191 (1993).

[8] D. Kolar, Z. Stadler, S. Gaberscek and D. Suvorov, *Ber. Deutsch. Keram, Ges.* **55**, 346 (1978).

[9] R. H. Arendt, J. H. Rosolowski and J. W. Szymaszek, *Materi: Bull.* **14**, 703 (1979)

[10] S. H. Cho and J. V. Biggers, *J. Am. ceram. Soc.* **66**, 743 (1983).

[11] Y. Zhang and P. K Davies, *J. Am. Ceram. Soc.* **77**, 743 (1991).

[12] R. W. Lynch and B. Morosin, *J. Am. Ceram. Soc.* **55(8)**, 409 (1972).

[13] R. Ruh, G. W. Hollenberg, E. G. Charles, and V A. Palel, *J. Am. Ceram. Soc.* **59**, 495 (1976).

[14] F. Khairulla and P. P. Phule, *Mater. Sci. D. Eng* **B12**, 327 (1992).

[15] W E. Courtney, *IEFE Trans. Microwave theory Tech* **MTT -18**, 476 (1970).

[16] D. M. Iddles, A. J. Bell and A. J. Moulson, *J. Mat. Sci.* **27**, 6303 (1992).

[17] M. T. Anderson, K. B. Grenwood and G.A. Taylor,*Prog. Solid. State. Chem.* **22**, 197 (1993).

[18] F. Galasso, *Structive, properties and preparation of perovskite type components* (Pergamon press 1969.)

[19] R. Roy, *J. Am. Ceram. Soc.* **37**, 581 (1954)

[20] T. Nakamura and J. H. Choy, *J. Solid. State Chem.* **20**, 233 (1977).

[21] J. B. Goodenough and J. M. Longo, *Crystallographic and Magnetic properties of Pervoskite and Perovskite-related compounds*, Landolt- Bornstein New series Group III: Springer- Verlag, **Vol.4a.**, 126.

[22] B. M. Goldschmidt, *Skrifter Norske Videnskaps- Akad. Mater. Naturvid* **Kl. No.4**, (1928).

[23] T. Takada, S. F. Wang, S. Yoshikawa, S. J. Jang and R. E. Newnham,*J. Am. Ceram. Soc.* **77**, 743 (1994).

[24] H. Ikawa and T. Yamada, *J. Am. Ceram. Soc.* **74(6)**, 1459 (1991).

[25] R. Kudesia, A. E. McHale and R. L. Snyder, *J. Am. Ceram. Soc.* **12**, 3215 (1994).

[26] JCPDS Reference cards **34-31** to **34-33**.

[27] L. W. Coughanour, R. S. Roth and V.A. DeProsse, *J. Res. Nat. Bur. stand* **52**, 37 (1954).

[28] R. E. Newnham, *J. Am. Ceram. Soc.* **50(4)**, 216 (1967)

[29] R. W. Lynch and B. Morosin, *J. Am. Ceram. Soc.* **55(8)**, 409 (1972).

[30] H. Stetson and B. Schwartz, *J. Am. Ceram. Soc.* **44(8)**, 420 (1961).

[31] A. E. McHale and R. S. Roth, *J. Am. Ceram. Soc.* **66**, C-18 (1983).

[32] Phase diagrams for Ceramists, **Vol. 1975**, Fig.4452.

[33] G. Blasse, *Z. anorg. allg. chem.* **345**, 222 (1966).

[34] O. Muller and R. Roy, *Crystal chemistry of Non-Matallic Materials* Vol.4, (Springer-Verlag, New York 1974).

[35] S. Sr. Hirano, T. Hayashi and A. Hattori, *J.Am. Ceram. Soc.* **74**, 1320 (1991).

[36] R. Migom, H. Bilz and D. Banerli, *Phy. Rev. Lett.* **37**, 1155 (1976).

[37] A. E. McHale and R. S. Roth, *J. Am. Ceram. Soc.* **66** (2), C-18 (1983).

[38] H. Ikawa, A. Iwai, K. Hiruta, H. Shimojima, K. Urabe and S. Udagawa, *J. Am. Ceram. Soc.* **71** (2), 120 (1988).

[39] R. Christofferson, P. K Davies and X Wei, *J. Am. Ceram. Soc.* **77** , 1441 (1994).

[40] F. A. Kroger and H. J. Vink in *Solid State Physics* **Vol.3** edited by F. Seitz and D. Turnbull (Academic press New York) 307 (1981).

[41] G. Bayer, M. Hofman and L. Gaukler, *J. Am. Ceram. Soc.* **74**, 2205 (1991).

[42] C. Ramasastry and Y. Syamasundara Rao, *J. Phys. E: Sci. Instrum.* **Vol.12**, (1979).

[43] E. P. Papadakis in *Physical Acoustics* **Vol.12** ed: W. P. Mason and R. N. Thurston. (Academic press, New York) (1976).

[44] H. J. McSkimin, *J. Acoust. Soc. Am.* **33** (1961).

Chapter 5

Dielectric and elastic properties of $BaLn_2Ti_5O_{14}$ dielectric ceramics

The growing importance of ceramic dielectrics for the application as high dielectric constant capacitors, PTC resistors and microwave integrated circuits have led to the development of a number of dielectric ceramic systems. Because of the growing number of applications for these compounds, information on the preparation and properties of different materials are of great interest. Ceramics based on the $Ba_2Ti_9O_{20}$, $Zr_xTi_ySn_zO_4$ ($x+y+z=2$) and $Ba(Zn_{1/2}, Ta_{2/3})O_3$ are typical dielectric ceramics having high Q factor, high temperature stability and low temperature coefficient of resonance frequency. But these compounds have only moderate dielectric constant value ($\epsilon_r < 45$) and could not be used in devices operating at high microwave frequencies because of large size required to satisfy the resonance condition. This necessitated the development of dielectric materials with higher dielectric constant values for such applications. Material scientists have been continuously trying to prepare new ceramic compounds with new and improved properties. In spite of extensive research on material synthesis, work on the structure and properties of these materials are limited for the design of new dielectric materials with desired preassigned properties. Basic understanding of the reasons for desirable properties like low temperature coefficient of resonant frequency, high Q factor, and high temperature stability in some materials are still lacking.

Most ceramic dielectrics developed so far for microwave applications composed of mixed phases consisting of different compounds. Usually the mixed phase dielectrics are prepared by conventional solid state reaction of mechanically mixed powders. The inevitable inhomogeneity inherent in the compound inhibits the compositional and mi-

crostructural properties of fired products. Therefore it is important to study quantitatively the factors that control the compound with optimized and reproducible dielectric properties. In order to do this, the dielectric properties of different phases constituting a complex dielectric material and quality of the constituent phases should be studied. The dielectric as well as elastic properties of fired products are related to the physicochemical characteristics of the materials from which they are prepared.

Dielectric materials may be classified into several groups according to their ϵ_r and Q values. The highest dielectric constant materials with ϵ_r around 90 and Q factor = 5000 are TiO_2 based ceramics such as the $BaO-Re_2O_3-TiO_2$ system (Re = Rare earth). In this ternary ceramic system, substitution of lanthanide cations has been found to be very effective to design a dielectric material with preassigned properties. Eventhough the parent material is the same, the variation in their physical and chemical properties mainly depend on the ionic size of substituent elements. In ternary system $BaO-LnO_3-TiO_2$, extensive substitution studies have been reported with every lanthanides.

The ternary dielectric ceramics based on the system $BaO-TiO_2-Ln_2O_3$ (Ln = La, Y., Pr , Sm,Nd , Gd , Tb , Dy and Er) and their structural and chemical properties have been a subject of extensive study for many years [1,2]. Among the various compositions reported in these systems, those occurring in TiO_2 rich region are particularly important, because they exhibit combination properties such as high dielectric constant and low losses with small temperature coefficient of resonant frequency which make them very attractive for a multitude of applications [3,4]. Investigations on these materials have revealed that the enhancement of dielectric properties is mainly due to the formation of ternary compounds, $BaLn_2Ti_3O_{10}$ and $BaLn_2Ti_5O_{14}$. Although the existence of these compounds and their favourable influence on the ultimate properties of the ceramic have been established, considerable ambiguity still persists regarding the correct chemical composition of these compounds, particularly the one with $BaO:Ln_2O_3:TiO_2$ ratio of 1:1:5 [5,6].

Another interesting compound in the same system is the 1:1:4 compound. It is found that the 1:1:4 isotypical compounds are formed with other rare earth oxides from La_2O_3 to Gd_2O_3 [14]. With decreasing rare earth ionic radius the range of existence of

$Ba_1.2Re_{8+2/3x}$ $Ti_{18}O_{54}$ becomes narrower. For Nd and Pr, $0 < x < 2.25$, for Sm and Er, $0 < x < 1.5$ and for Gd, $x = 0$ which is $Ba_6Gd_8Ti_{18}O_{54}$. Matreeva et al. [28] reported the solid solution formula $Ba_{3.75}Re_{9.5}Ti_{18}O_{54}$ for $x = 0.5$. These solid solutions contain divalent Ba^{2+} ions replaced by two R^{3+} cations. To maintain the electrostatic stability, three Ba^{2+} ions should be replaced by two R^{3+} ions and one vacancy. Therefore in this region of phase diagram a marked change in behaviour occurs due to the substitution of $2R^{3+}$ for $3Ba^{2+}$ ions. Thus there exist two kinds of sites occupied by the large cations. One is similar to A site of ABO_3 Perovskite type structure which is occupied by a maximum of ten Ba^{2+} ions and M^{3+} in the unit cell. Another is a pentagonal-channel cavity which is formed among the perovskite like columns which is occupied by a maximum of four Ba^{2+} ions or vacancies in the unit cell. If the large sites are fully occupied, the formula $Ba_2M_8Ti_{18}O_{54}$ should be detained as the end member. Thus the derived formula for the solid solution are $Ba_{6-3n}M_{8+2x}Ti_{18}O_{54}$ and $BaM_2Ti_4O_{12}$ corresponding to $x = 0.5$.

Ceramics with the general formula $BaLn_2Ti_5O_{14}$ belonging to the BaO-Ln_2O_3-TiO_2 ceramic system have been investigated in this work. For convenience they are represented as 1:1:5 compounds. The dielectric constants of $BaLn_2Ti_5O_{14}$ ceramics increase with the ionic radius of lanthanide ions (Although the trend for Pr and Nd is the reverse). This phenomenon can be explained by considering that the lattice expand with the increase of the ionic radius of the rare earth material. The ϵ value 90 is obtained for the system containing La (1.14Å) which has the largest ionic radius among the rare earth elements. The calculated ϵ_r value $BaLn_2Ti_5O_{14}$ ceramics show much deviation from the measured values which may be due to the presence of secondary phases, deviation from the entire enviornment ionic conductivity etc. It is found from microwave dielectric constant measurement that τ_f of these ceramics can change from the positive value to negative value with cation substitution and it is even possible to get zero τ_f by combining appropriate stoichiometry of Ln^{3+} compounds.

XRD pattern of these ceramics show that TiO_2 and $Ba_2Ti_9O_{20}$ remain as secondary phases. The $BaLn_2Ti_5O_{14}$ ceramics have orthorhombic structure with 4 molecular formulae per unit cell. Microstructures of typical $BaLn_2Ti_5O_{14}$ ceramics (BLT) have been reported earlier [8]. In order to estimate the effect of the rare earth on BLT

ceramics, Fukuda et al. [9] measured the fourth order dielectric constant of these materials. They found that the fourth order constant, which lead to the anharmonicity of the ceramics, increase with rare earth content. The same parameter is responsible for the decrease of experimental Q value.

A very exciting value of dielectric constant was reported in the BaO-Nd_2O_3-TiO_2 system. It is found that the ceramic compound in the ternary system with Nd shows a relatively high permittivity in the range 70-90 a temperature coefficient of permittivity about -100ppm/K and a low dielectric loss [1]. Among the different compositions, the best properties were achieved with the composition BaO: Nd_2O_3: TiO_2 in the ratio 1:1:5 and 1:1:4. Subsequent work in the same system showed that the composition 1:1:5 is not a single phase one [6,10], where as 114 compound [11,12] belongs to the broad solution region located between $BaTiO_3$ and $Nd_2Ti_3O_9$ (non existent).

According to Varfolomeev et al. [13] a solid solution described by the general formula of pseudo-ternary system $BaLnO_{1.5}$-TiO_2 shows maximum stability in the composition of Ba_{6-x} $Ln_{2x/3}$ Ti_{18} O_{54} where value of x corresponds to $0<X<3$ for La, $0 < x < 2.25$ for Pr and Nd, and $0<x<1.5$ for Sm and Gd. Studies on the thermal evolutions of the dielectric permittivity on these system with Ln = La, Pr, Nd and Sm show similar behaviour, ϵ_r goes through a maximum in the range 860-940K at 10kHz except for the Pr compound and the temperature of this maximum is shifted towards low temperature. Besides, for both frequencies the temperature at which these maxima occurs increase almost linearly with the decreasing ionic radius of the lanthanide [14,15].

Substitution of Nd at the lanthanide site in the $BaLn_2Ti_5O_{14}$ ceramics causes tremendous change on their crystal structure. Kolar et al. [16] studied the crystal chemistry of $BaNd_2Ti_5O_{14}$ ceramics. It was found that the structure of the crystal is orthorhombic with a = 22.346 ± 0.0002 Å, b = 12.201 ± 0.0001 Åand c = 3.8404 ± 0.003 Åhaving possible space group of Pbam and Pba2. Very interesting results on the mirostructures of BNT5 ceramics have been reported [17]. It is found that microstrucre of BNT5 ceramics vary significantly with the sintering temperature. Nearly equiaxial fine crystals were observed in the BNT5 ceramics sintered at 1340°C. But samples sintered at 1370°C indicate homogeneous columnar crystals. At moderately high tem-

perature, major phase of the BaO-Nd$_2$O$_3$-5TiO$_2$ (BNT5) ceramics is orthorhombic and micro phase is found to be obtained above a critical sintering temperature while associated binary phases like BaTi$_4$O$_9$ and Nd$_2$TiO$_7$ reduce in amount and disappear at this range of temperature.

Regarding the densification behaviour of BNT5 ceramics [18], the bulk density is found to increase as the temperature increases and it reaches a maximum value at 1360°C. At sintering temperature above 1360°C, no more densification is obtained due to the development of columnar structures. Moreover, plastic deformation and sticking occur in the sample at these temperatures.

Various studies have been made to analyse the methods to improve the quality factor of these ceramics. Among the various factors, sintering condition is found to be the one which affects the quality factor most. The relation between Q factor and the sintering condition seems to be linked to oxygen loss during sintering and to re-orientation during cooling. High Q values are achieved in BNT5 ceramics with homogeneous fine structure because oxidation can easily penetrate the fine grains. Since oxidation is difficult to penetrate large grains, significant quality factor degradation is found to occur in BNT5 ceramics with discontinuously grown crystals sintered at high temperatures.

Among the several studies made on the BNT5 ceramic system, Takahashi et al.'s [19] work on these systems by modified precipitation method attracted considerable attention. Eventhough several workers have put forward numerous structure formula for correct composition for a single phase in BaO- Nd$_2$O$_3$- TiO$_2$ system, chemical composition of single phase compound has not yet been identified.

In addition to the substitution of Nd^{3+} ions on these ceramic compounds, substitution with various (rare earth) lanthanide cations have also been tried by many workers. In the case of Pr$^+$, Sm$^+$ substitution, ceramic compound becomes dense and show similar structure upon sintering in the temperature range 1350-1370°C. They had different dielectric properties eventhough the chemical properties of these rare earth oxides are very similar. The x-ray diffraction study of single crystal Pr compound confirmed the symmetry and unit cell dimension as orthorhombic with a = 22.36 ±

0.007Å, b $= 12.181 \pm 0.004\text{Å}$ and c $= 3.83 \pm 0.004\text{Å}$. The structural formula of single phase in Pr compounds have been verified by x-ray specrtoscopic analysis and found the chemical composition as $Ba_{3.75}$ $Pr_{9.5}$ Ti_8O_{54}.

Another interesting ceramic compound in $BaO\text{-}Gd_2O_3\text{-}TiO_2$ system is Gd based compound $Ba_{4.5}$ $Gd_9Ti_{18}O_{54}$. This type of compounds have got potential application due to their negative τ_f and therefore can be used as high permittivity additive for suppressing τ_f in systems with positive τ_f. The amount of toxic and volatile additives like Bi_2O_3, PbO required for this purpose can be completely substituted by $Ba_{4.5}Gd_9Ti_8O_{54}$ addition without affecting the permittivity and quality factor. Valent et al. [20] successfully used the BGT ceramics for the complete suppression of τ_f in ceramics based Bi doped BNT compound [4]. The ceramic compounds with La, Y Tb Dy and Er show more or less similar properties as other lanthanides explained above.

The objective of our work is to investigate the effect of lanthanides, La, Sm, Nd, Pr, Y , Tb , Dy and Er on the dielectric and elastic properties of TiO_2 rich region of the system $BaO\text{-}Ln_2O_3\text{-}TiO_2$. Since the dielectric constant, quality factor, dielectric loss and structural stability of ceramics are interconnected parameters, it is essential to know about the elastic instability occuring in the system, which is closely related to structure stability. Any anomaly in elastic properties of the system can be analysed by measuring the velocity of ultrasonic waves through the medium. To study the dielectric properties we have measured the dielectric constant in the low frequency ($<$13MHz) region for each lanthamide substitution. Since the TiO_2-rich BLT ceramics are found to be suitable for the manufacture of multilayer monolithic capacitors due to its low dielectric loss at 10 MHz and low temperature coefficient of capacitance.

The dielectric constant ϵ at GHz frequencies is nearly 10% lower than at 1MHz, and the temperature coefficient of resonant frequency is correlated to temperature coefficient of relative permittivity τ_K by the relation $\tau_f = -(\alpha_l + \tau_K/2)$ where α is the linear thermal expansion coefficient and τ_K is the temperature coefficient of relative permittivity. For $\tau_f = 0$ ppm/K, τ_K should be $\approx -2\alpha_l$. For $\alpha_l \approx 10.10^{-6}\text{K}^{-1}$, $\tau_K = -20$ ppm/K. By this analysis, one can easily produce the materials with $\tau_f = 0$. Since the

115

loss factor increases with frequency, proper combination of rare earth elements in 1:1:5 compound solid solution in additives are used for the improvement of Q and ϵ.

Our present work is on the measurement of low frequency dielectric constant and longitudinal and transverse elastic constants of $BaLn_2Ti_5O_{14}$ ceramic and their variation with temperature. In the following sections we describe the details of experimental technique used, including sample preparation, results obtained and a discussion of the results.

5.1 Experimental method

5.1.1 Sample preparation

High purity $BaCO_3$, TiO_2, La_2O_3, Pr_2O_3, Nd_2O_3, Er_2O_3, Gd_2O_3, Sm_2O_3, Tb_2O_3, Dy_2O_3 and Y_2O_3 were mixed in the molecular proportions BaO Ln_2O_3 TiO_2 = 1:1:5 with distilled water for 30 min. in an agate mortar. The powders were calcined in alumina crucible at 1120-1200°C for 4 hours with intermediate grinding, then mixed with PVA binder, and ground for 1hour. They were pressed in to 10mm diameter compacts at 350 MPa and subsequently sintered in air at 1300-1350°C for 4 hours. The density of sintered compacts are determined from the dimensions. The compacts have been polished and used for characterisation and further investigations.

5.1.2 X-ray and SEM analysis

The powder XRD patterns of all the prepared samples have been taken using $CuK\alpha$ radiation. The patterns are in agreement with earlier reports [12,26] TiO_2 and Ba_2 Ti_9 O_{20} remain as major phase in the ceramic system. XRD patterns of two samples are shown in Fig 5.1. The diffraction peaks of TiO_2 and Ba_2 Ti_9 O_{20} are marked in the figure. The Ba Ln_2Ti_5 O_{14} ceramics have orthorhombic crystal system with 4 molecular formula per unit cell.

Microstructures of $BaLn_2Ti_5$ O_{14} ceramic system have been obtained using scanning electron microscopy (SEM). The columnar grain corresponds to the 1:1:5 compound and grey coloured polygonal grains corresponds to $Ba_2Ti_9O_{20}$ [27]. The
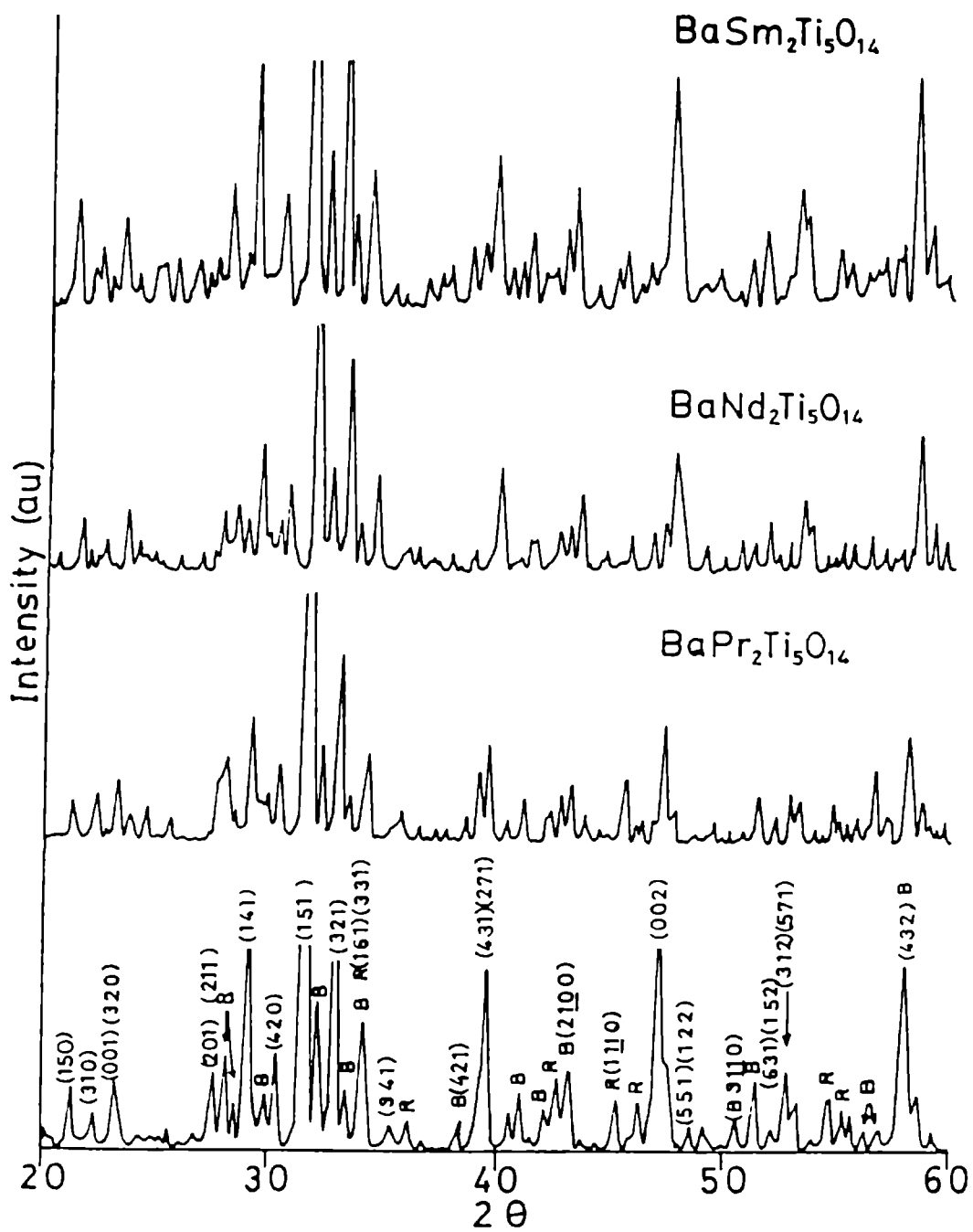
Fig.5.1: XRD pattern of $BaLa_2Ti_5$ O_{14}, $BaPr_2Ti_5$ O_{14}, $BaNd_2Ti_5$ O_{14} and $BaSm_2Ti_5$ O_{14} ceramic samples.

117

length of the columnar grains is approximately equal to 10 μm. SEM patterns of few samples are shown in Fig 5.2.

5.1.3 Low frequency dielectric constant measurement

The dielectric constant of all the samples have been measured using the capacitance technique after placing them inside the home made dielectric constant cell. The capacitance of a capacitor with sample acting as the dielectric has been measured accurately using an HP 4192A impedance analyser as already outlined. Variation of the dielectric constant with temperature has been measured in all samples using the same set up under temperature control. To make good electrical contact, high grade silver paint has been applied on the surface of the sample. To eliminate the fring and lead capacitance, we have adopted the same technique as did in the preceeding chapters.

5.1.4 Elastic constant measurements

Pelletised samples in the form of cylindrical discs have been cut so as to have parallel end faces. The diameter of the samples are of the order of 10mm and sample lengths are of the order of 8mm. The sample faces have been made flat and parallel by hand lapping and polishing. The sample lengths have been measured to an accuracy better than 0.1%. X-cut transducer having resonance frequency 10MHz has been bonded to the sample under spring loading. A suitable bonding material such as silicon grease has been applied between the transducer and sample so that the generated longitudinal ultrasonic waves get transmitted in to the sample. The waves get multiply reflected across the sample faces producing an exponentially decaying echo pattern. The transducer is excited in the pulsed mode so that the same transducer is used for transmission and reception on time sharing basis.

We have used pulse echo overlap (PEO) technique to measure velocity of longitudinal and transverse ultrasonic waves accurately [30,31,32]. The technique enables one to measure velocity to an accuracy better than 1%. Moreover, we have applied the McSkimin Δt criterion to correct for the phase changes introduced by the bond [33,34]. A Matec model 7700 pulse modulator and receiver along with associated
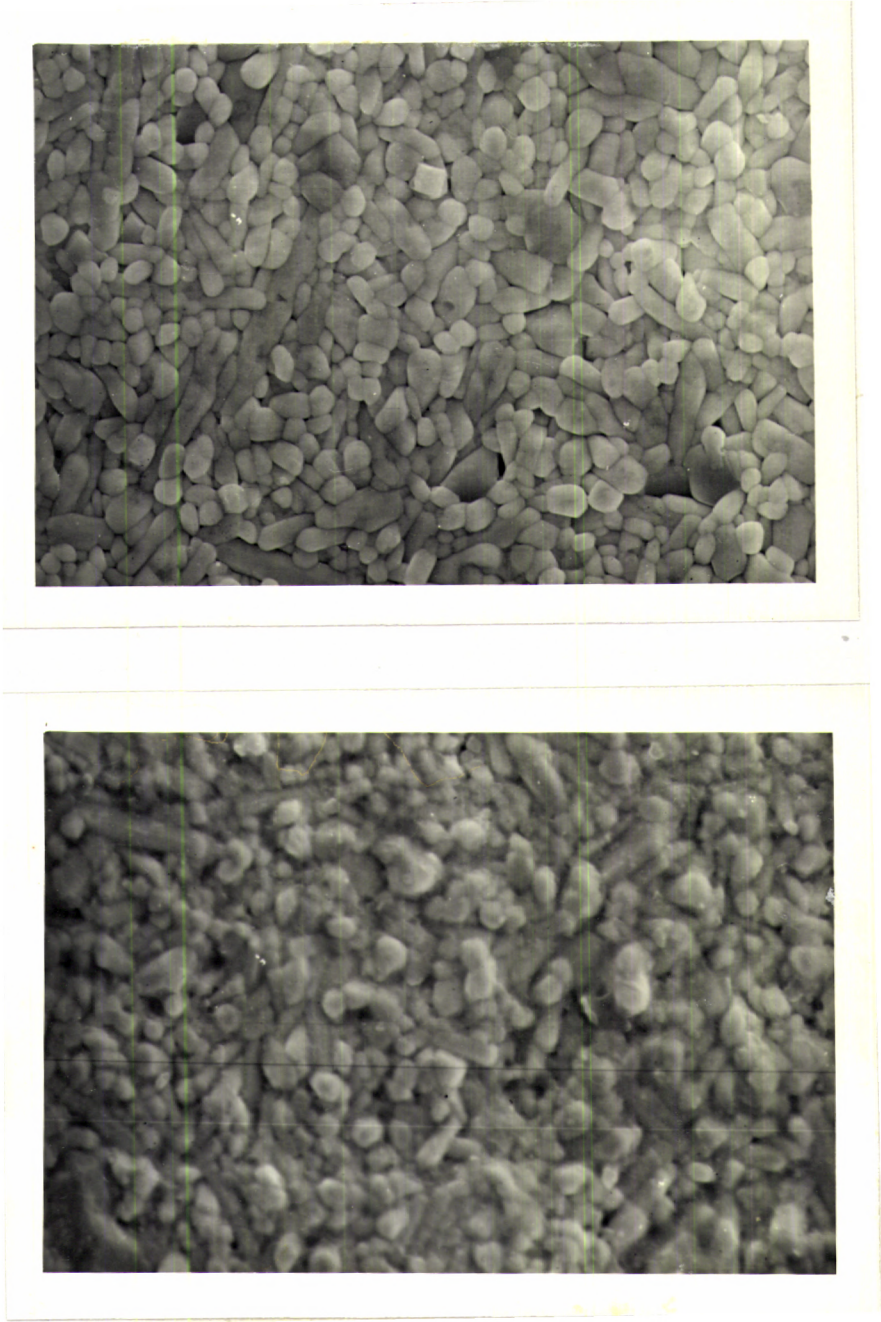
Fig.5.2: SEM pictures of BaNd$_2$Ti$_5$ O$_{14}$ and BaSm$_2$Ti$_5$ O$_{14}$ ceramic samples.

accessories have been used for measurements as already described in chapter 2. Once the velocity v is determined, the corresponding elastic constant can be calculated from the relation $C_{ij} = \rho v^2$ where ρ is the density of the sample. The temperature variation of only longitudinal modulus C_{11} has been measured in these samples as the quality of the echoes with transversewaves are not found to be good to carry out temperature variation measurements.

5.2 Results

There are a great number of compound ceramics with lanthanides at their cation site in the system $BaO\text{-}Ln_2O_3\text{-}Ti\ O_2$. In the majority of cases, the structural transition coincides with the anomaly in dielectric constant values. This has not been tested in dielectric ceramics with high dielectric constant and Quality factor so far. Since ultrasonic measurements provide valuable information about the class of phase transition occurring in solids, we have measured the temperature dependence of longitudinal elastic constant of this class of ceramics with each lanthanides cations substituted in the cation site of these systems. The dielectric constant and longitudinal elastic constant C_{11} for all the samples measured at room temperature are presented in Table 5.1.

From the temperature dependence of elastic constants one can determine the point at which phase transition occurs. To correlate the anomaly in ultrasonic measurements with corresponding dielectric constant variation we have measured the temperature dependence of dielectric constant also for all the samples.

Fig 5.3(a) shows the temperature dependence of the elastic constants of La substituted ceramic system while Fig 5.3(b) shows the corresponding dielectric constant data. From these curves one can easily determine the temperature coefficient of elastic constant and dielectric constant.

Another interesting lanthanide compound in the system is the Pr substituted ceramic $BaPr_2Ti_5O_{14}$. Since no ultrasonic studies have b een performed in this system, we have measured longitudinal ultrasonic velocity with temperature and plotted it
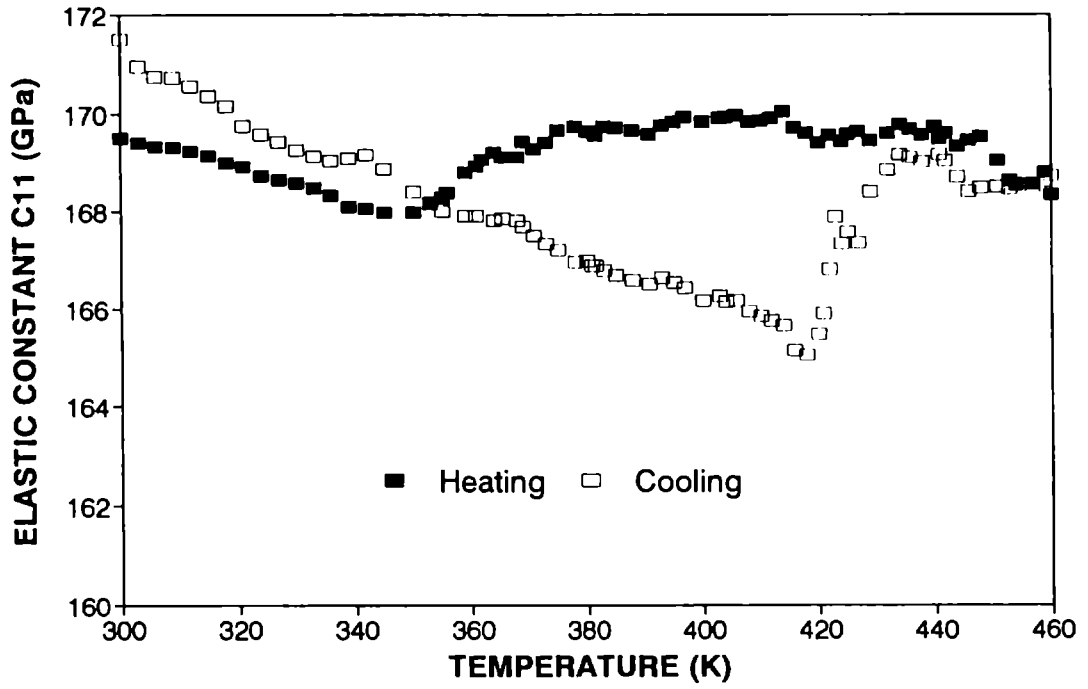
120
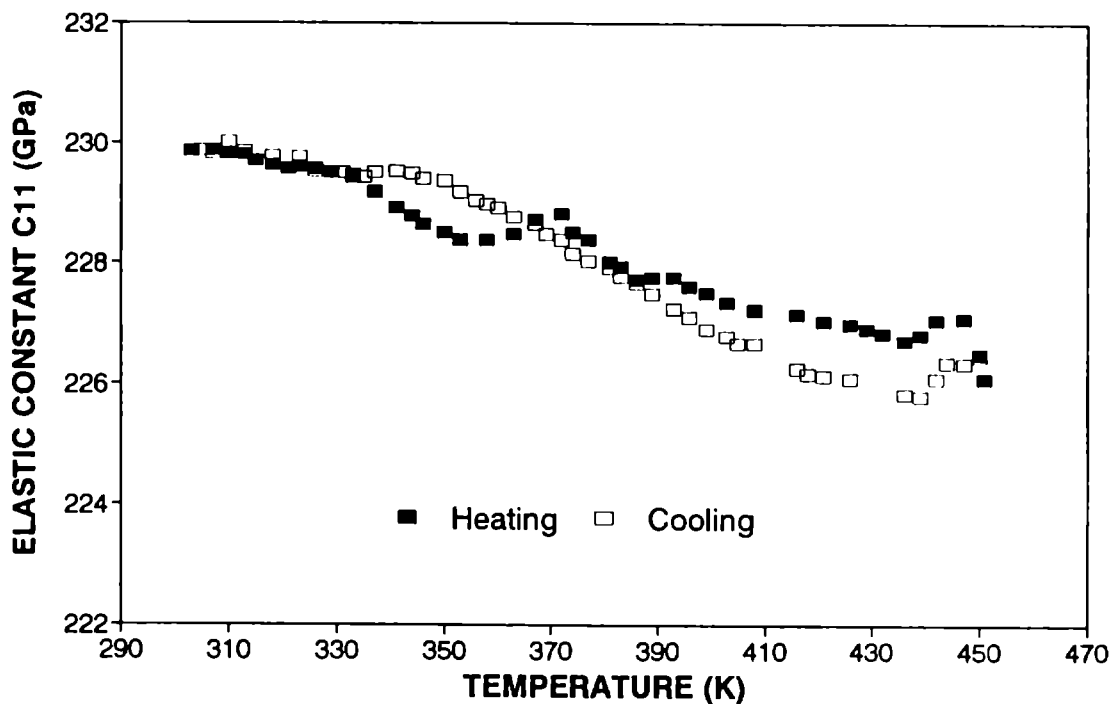
Fig.5.3(a): Temperature variation of longitudinal elastic constant C_{11} of $BaLa_2Ti_5O_{14}$ ceramic
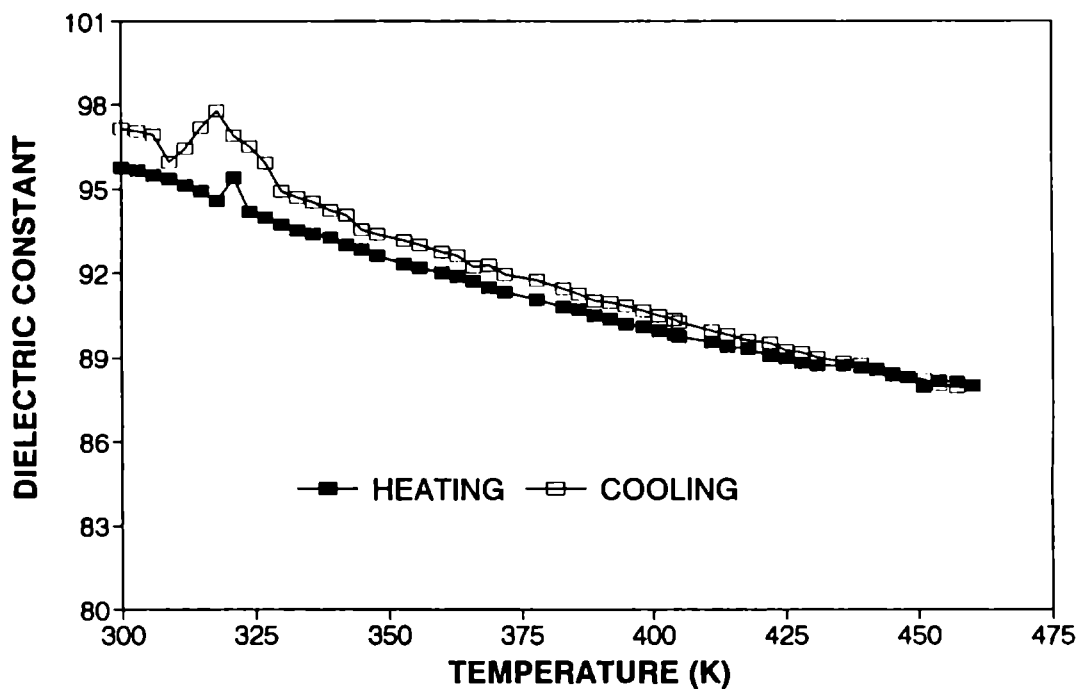
Fig.5.3(b): Temperature variation of dielectric constant of $BaLa_2Ti_5O_{14}$ ceramic

against temperature. This is shown in Fig 5.4(a). The temperature dependence of dielectric constant of the sample has been measured which is shown in Fig 5.4(b). Nd substituted ceramic system has received much attention because of their peculiar properties. The temperature variation of the longitudinal modulus C_{11} has been measured as a function of temperature from room temperature to 450K. This variation is shown in Fig 5.5(a). The temperature dependence of dielectric constant of this sample is shown in Fig 5.5(b).

The next lanthanide cation in this group is Sm^{2+} The effect of Sm^{2+} cation substitution in the same ceramic system is very interesting. So we have measured temperature dependence of elastic and dielectric constants of this ceramic system. These results are plotted in Fig 5.6(a) and 5.6(b) respectively. In addition to these we have carried out measurements on ceramics substituted with cations Gd^{2+}, Tb^{2+}, Dy^{2+}, Y^{2+} and Er^{2+} to analyse the dependence of elastic and dielectric constants on ionic radius. The variation of elastic constant of Gd substituted ceramic system with temperature as shown in Fig 5.7(a) and the corresponding dielectric constant variation Fig 5.7(b).

Another interesting lanthanide ceramic compound is $BaTb_2Ti_5O_14$ system. Fig 5.8(a) shows the variation of the longitudinal elastic constant of the Tb substituted system with temperature. The variation of dielectric constant with temperature is shown in Fig 5.8(b). Besides these we have carried out measurements on the other ceramic samples with Dy, Y and Er cation substitution on the same parent material. The longitudinal elastic constant values of these samples with temperature are shown in figures 5.9(a), 5.10(a) and 5.11(a) respectively. The temperature dependence of dielectric constant of these samples are shown in the figures 5.9(b), 5.10(b) and 5.11(b) respectively.

5.3   Discussion and conclusion

In Table 5.1, where we have tabulated the room temperature values of the elastic and dielectric constants for various materials studied along with the corresponding ionic radii of the cations, it can be noted that there is no direct correlation between the cation radii and elastic or dielectric constants. But one can make a general statement

Fig.5.4(a): Temperature variation of longitudinal elastic constant C_{11} of $BaPr_2Ti_5O_{14}$ ceramic.
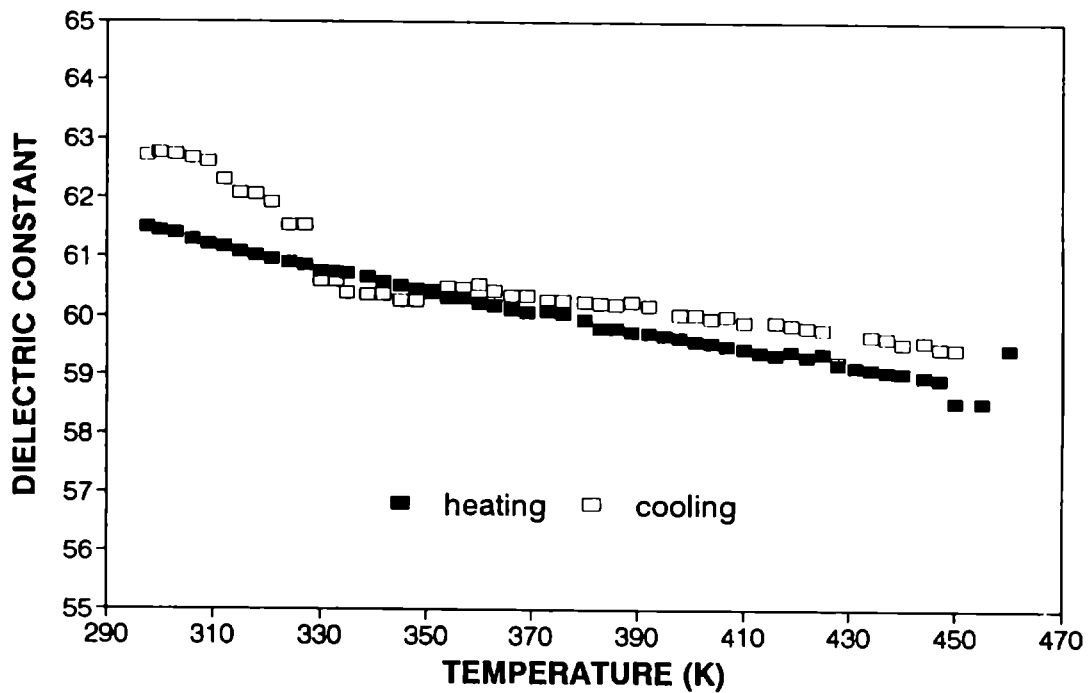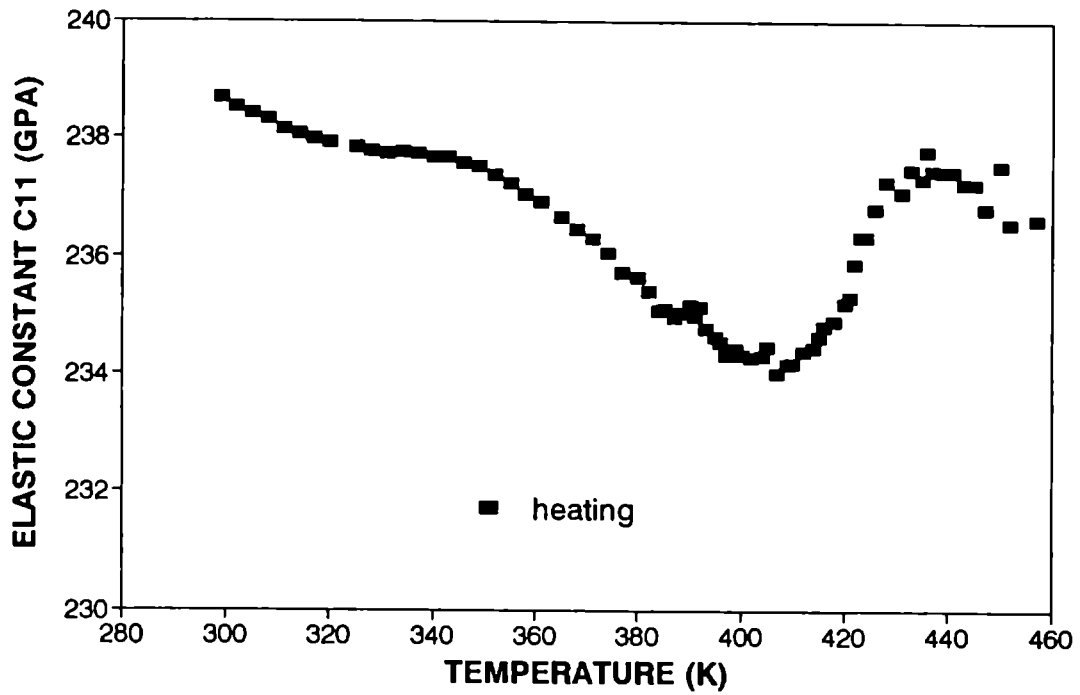

Fig.5.4(b): Temperature variation of dielectric constant of $BaPr_2Ti_5O_{14}$ ceramic.

Fig.5.5(a): Temperature variation of longitudinal elastic constant C_{11} of $BaNd_2Ti_5O_{14}$ ceramic.
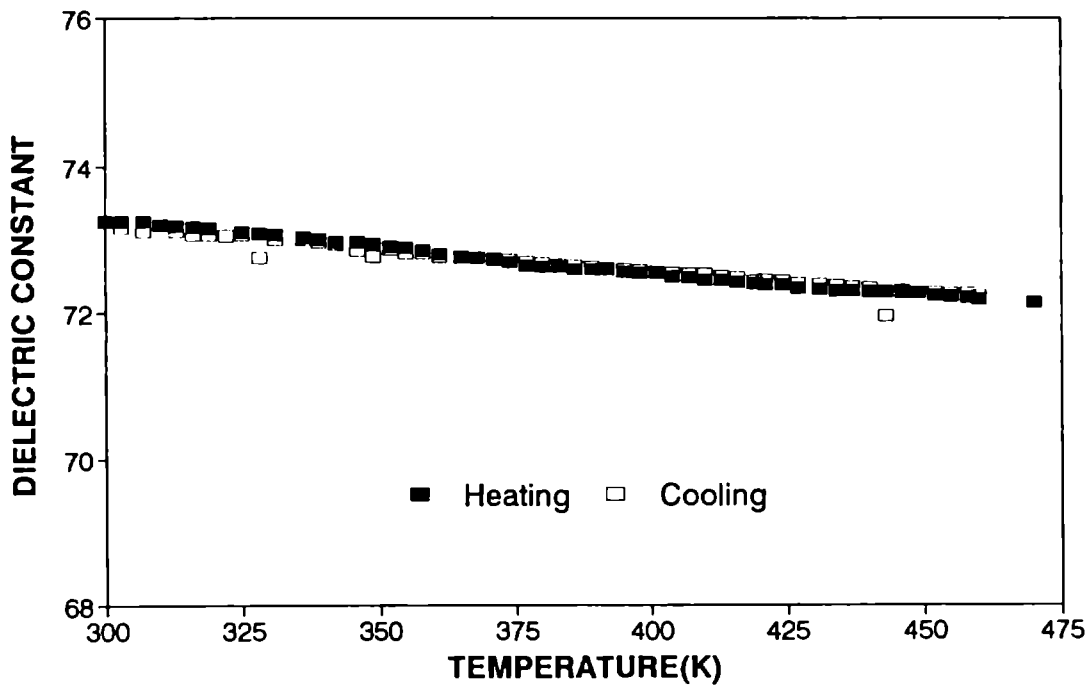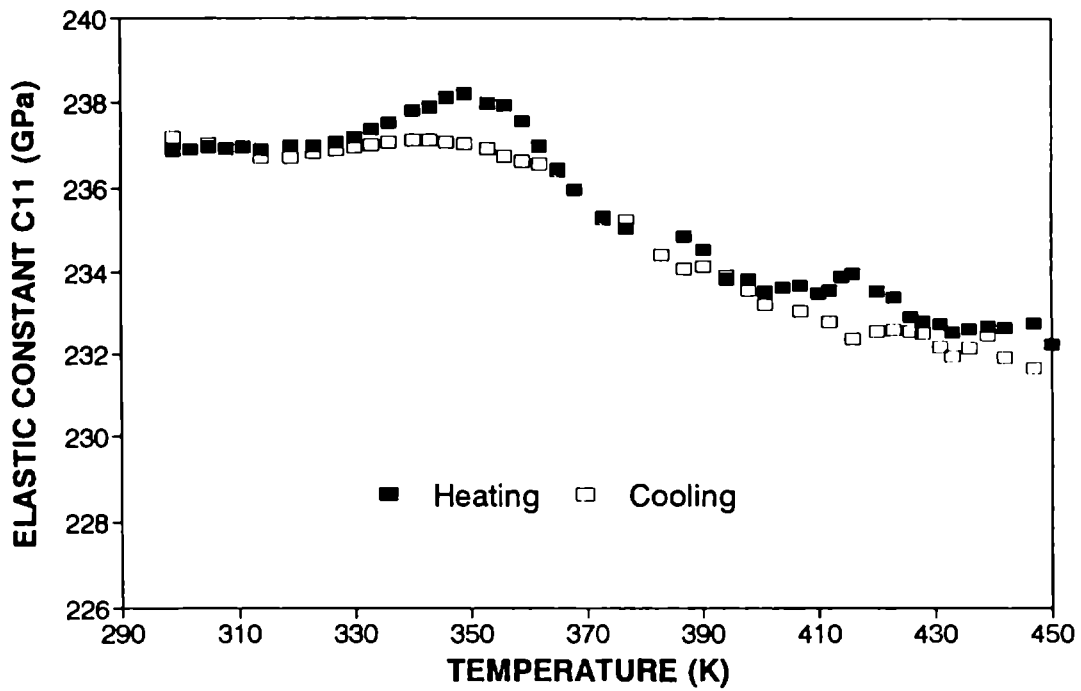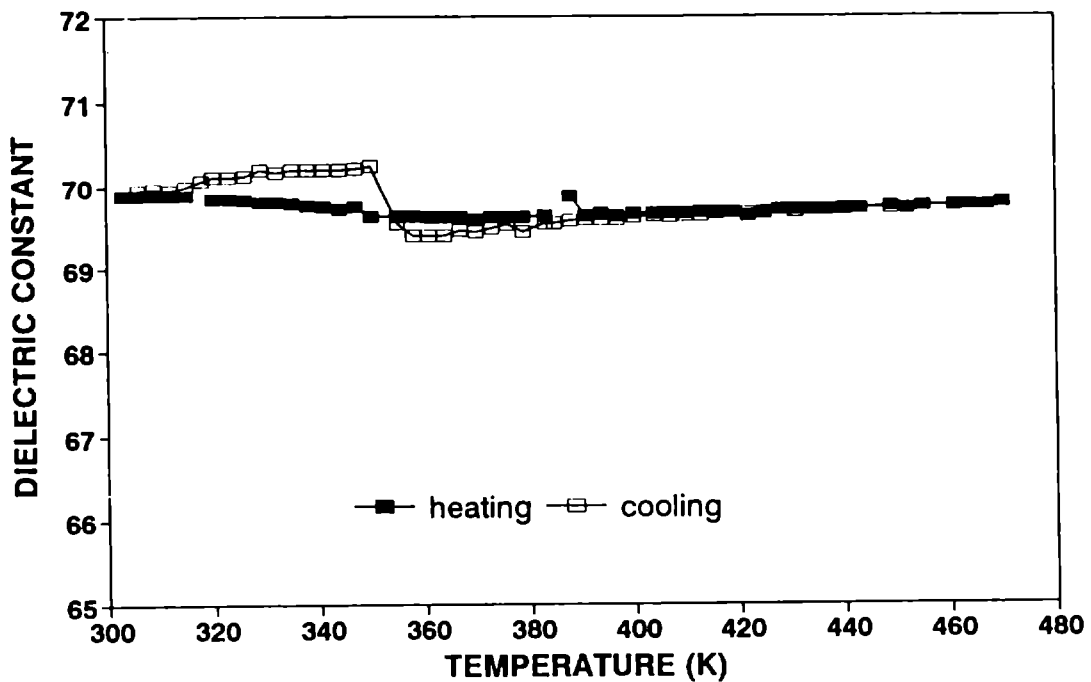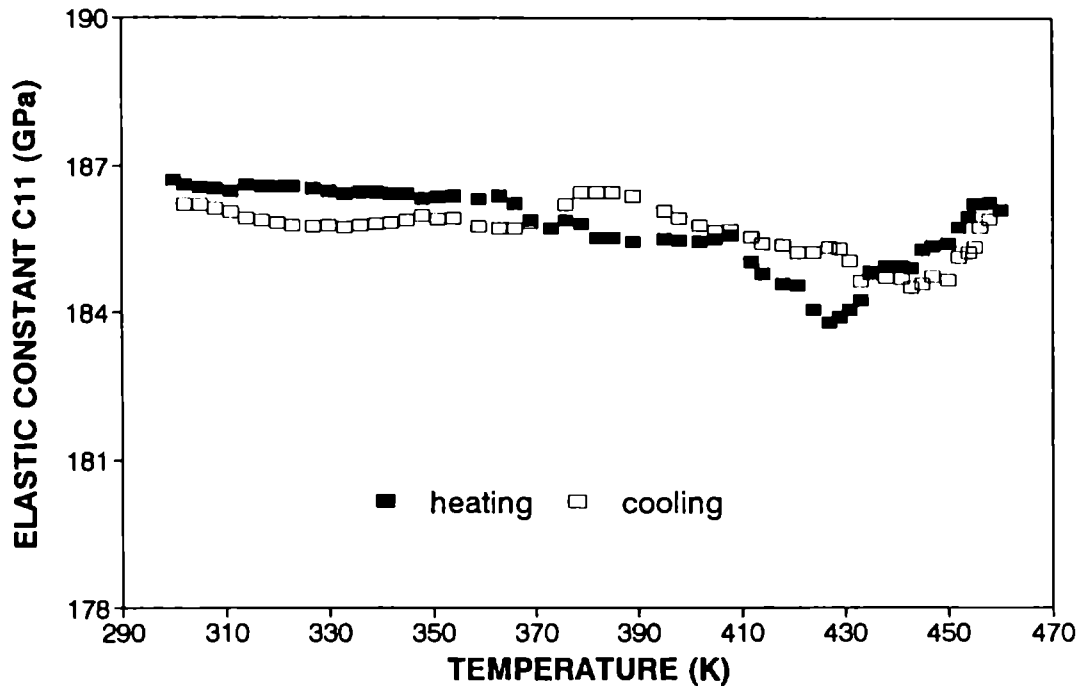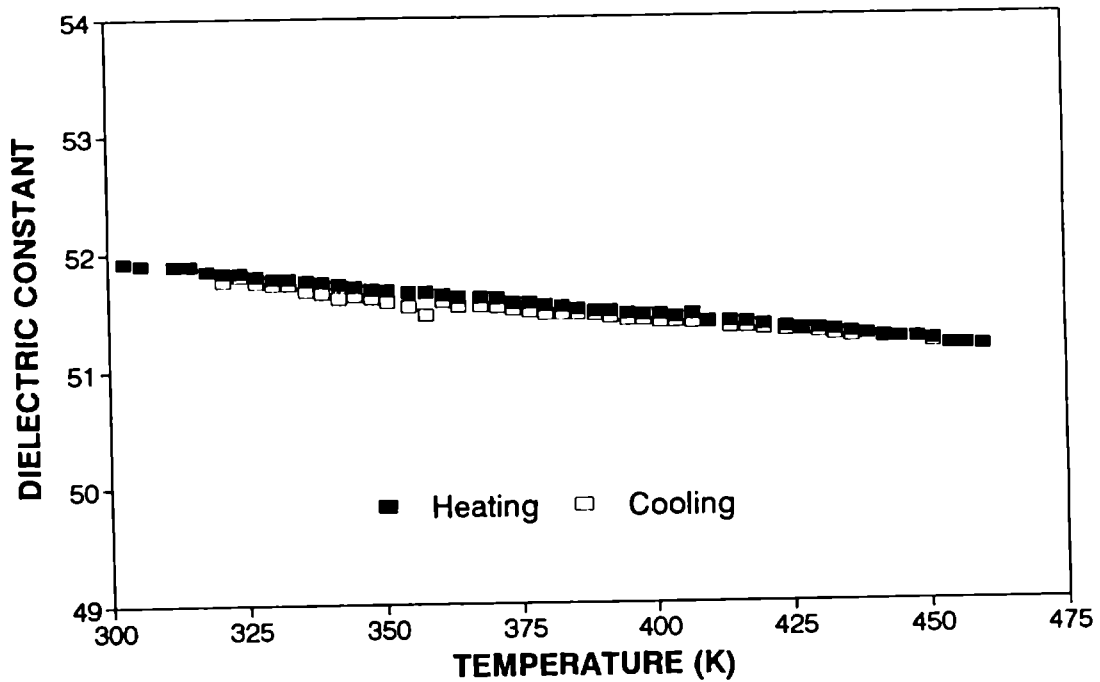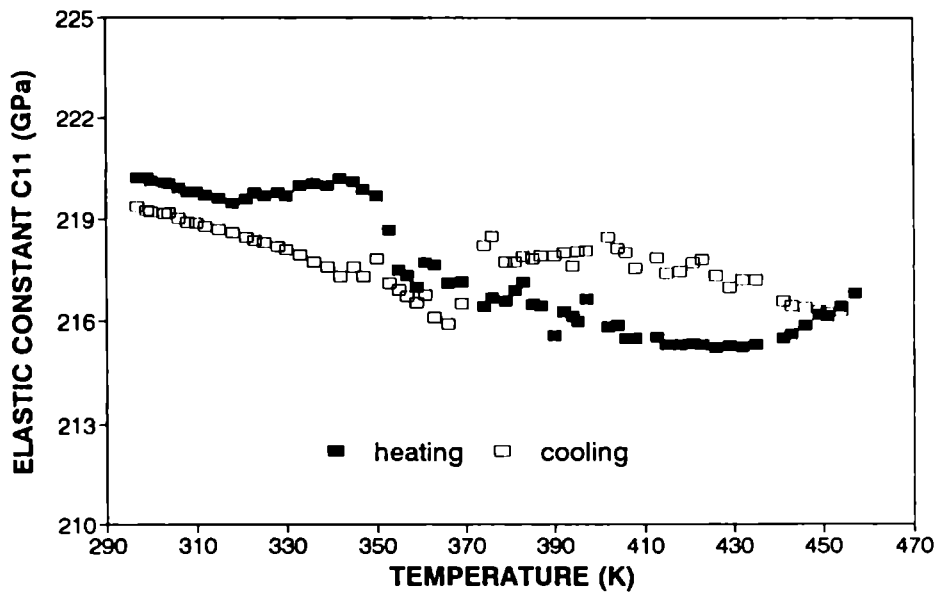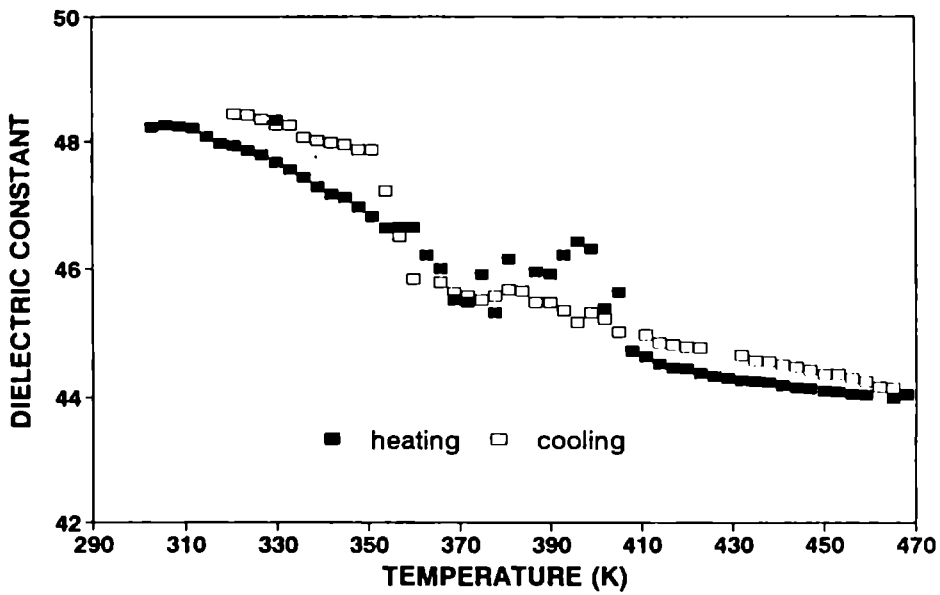

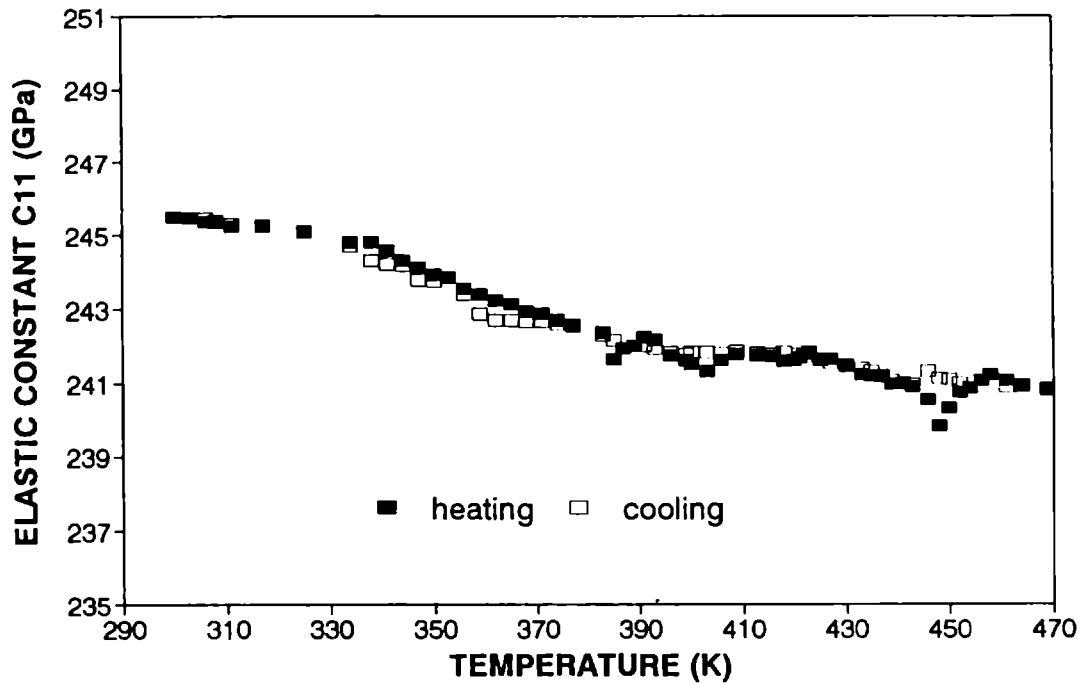**Fig.5.5(b): Temperature variation of dielectric constant of $BaNd_2Ti_5O_{14}$ ceramic.**

Fig.5.6(a): Temperature variation of longitudinal elastic constant C_{11} of $BaSm_2Ti_5O_{14}$ ceramic.

Fig.5.6(b): Temperature variation of dielectric constant of $BaSm_2Ti_5O_{14}$ ceramic.

Fig.5.7(a): Temperature variation of elastic constant C_{11} of $BaGd_2Ti_5O_{14}$ ceramic.
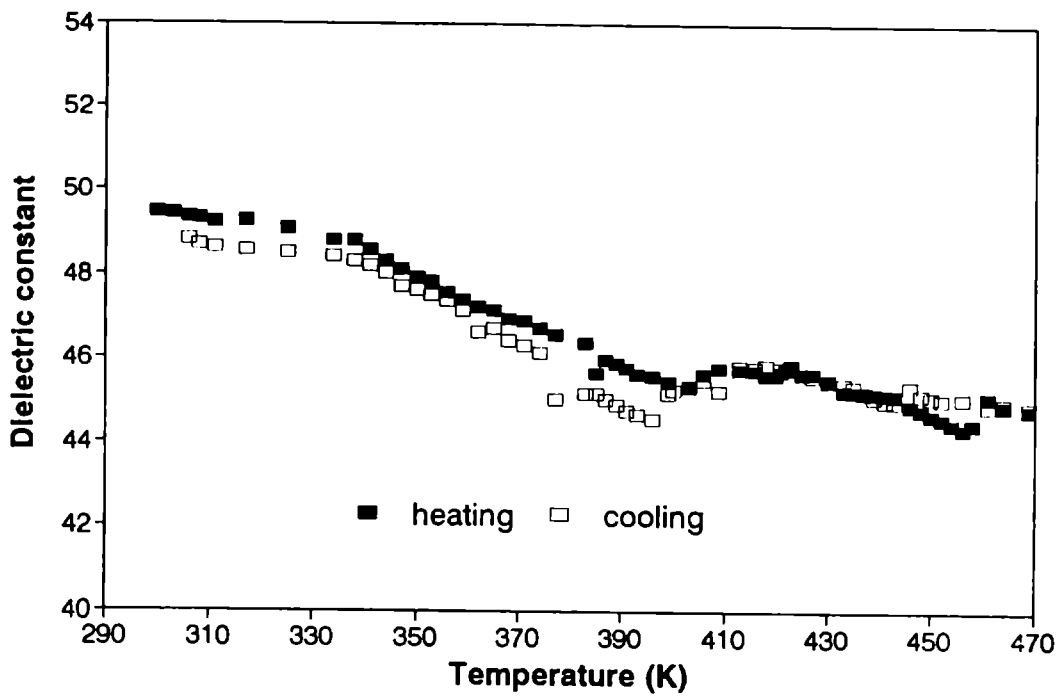

Fig.5.7(b): Temperature variation of dielectric constant of $BaGd_2Ti_5O_{14}$ ceramic.

Fig.5.10(a): Temperature variation of elastic constant C_{11} of $BaY_2Ti_5O_{14}$ ceramic.

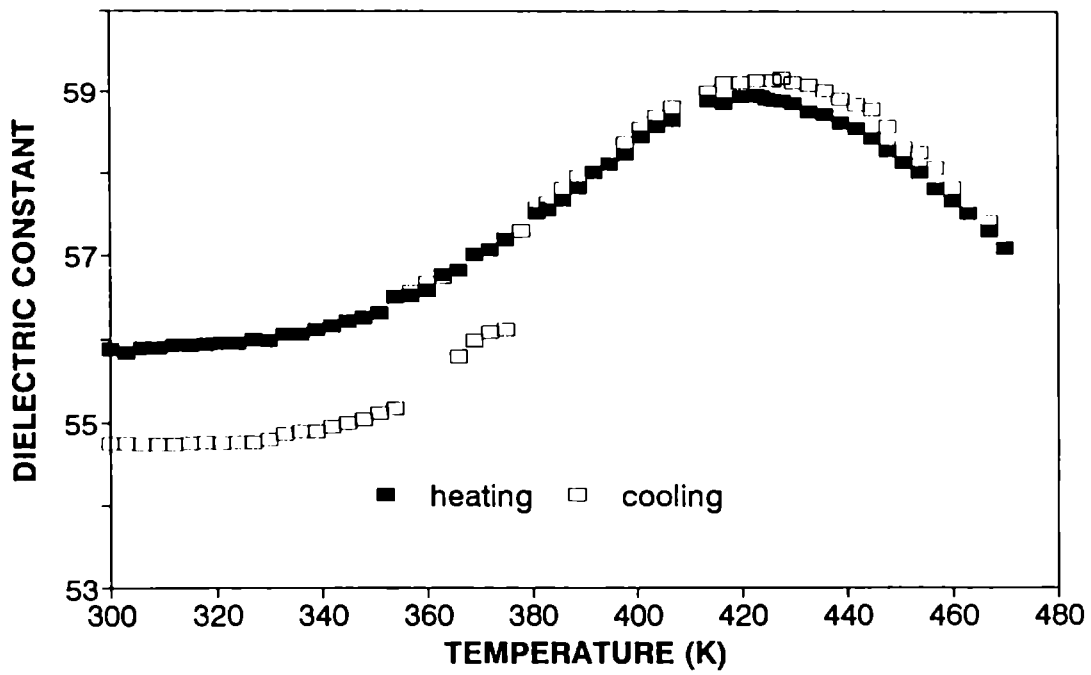Fig.5.10(b): Temperature variation of dielectric constant of $BaY_2Ti_5O_{14}$ ceramic.

127

Fig.5.9(a): Temperature variation of elastic constant C_{11} of $BaDy_2Ti_5O_{14}$ ceramic.

Fig.5.9(b): Temperature variation of dielectric constant of $BaDy_2Ti_5O_{14}$ ceramic.

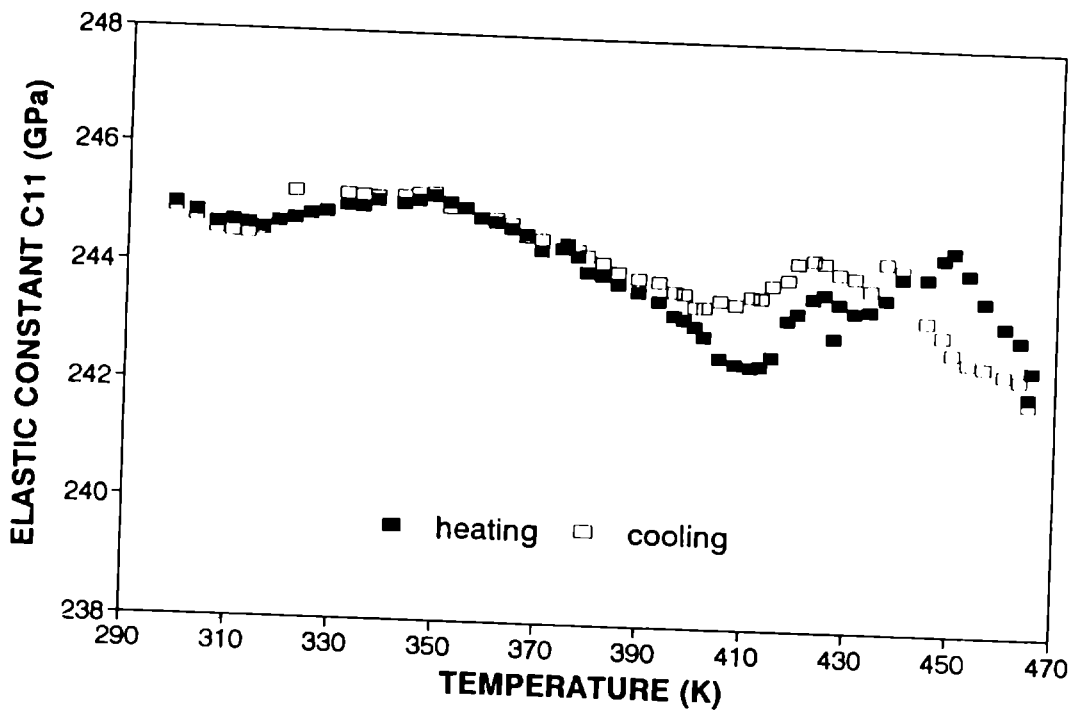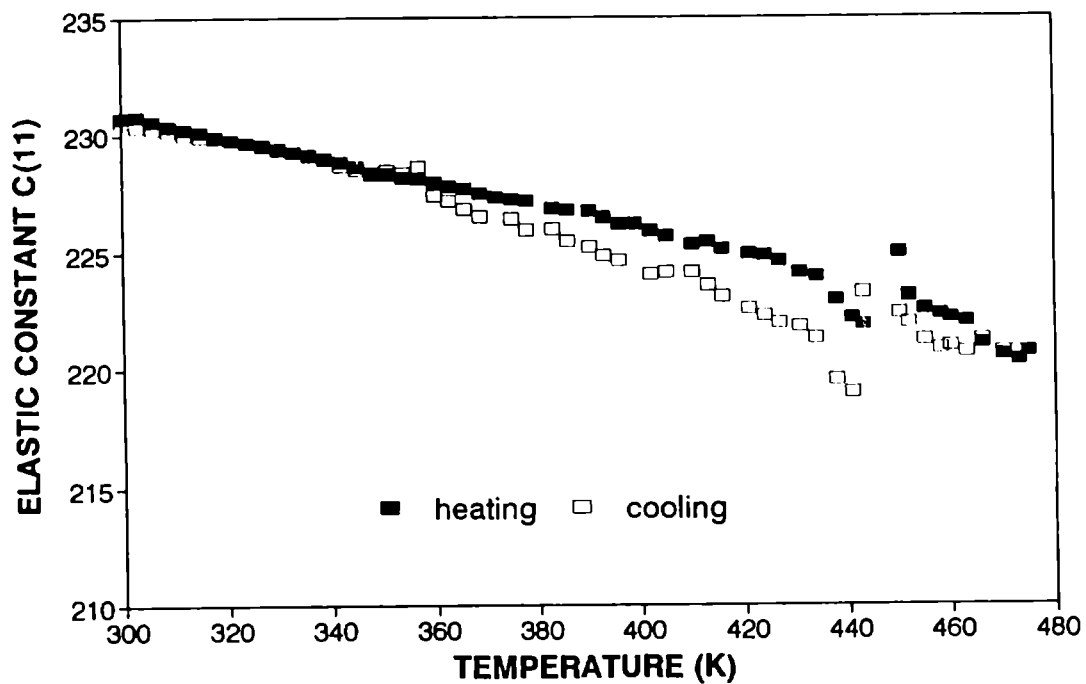Fig.5.8(b): Temperature variation of dielectric constant of $BaTb_2Ti_5O_{14}$

Fig.5.8(a): Temperature variation of elastic constant of $BaTb_2Ti_5O_{14}$ ceramic.

Fig.5.11(a): Temperature variation of elastic constant C_{11} of $BaEr_2Ti_5O_{14}$ ceramic.
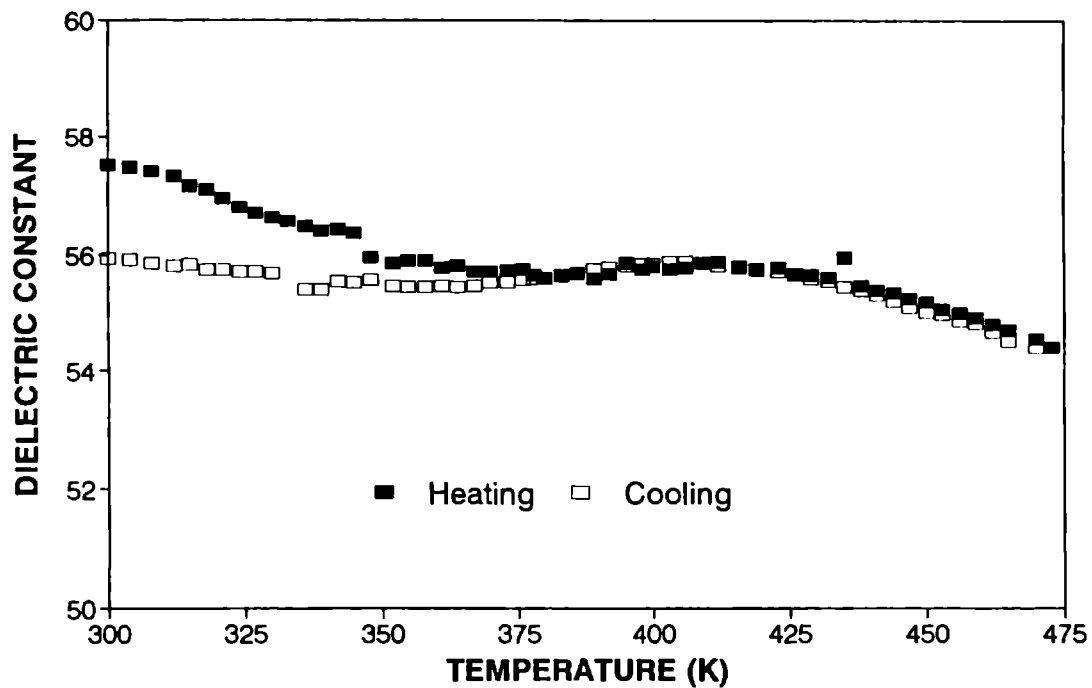

Fig.5.11(b): Temperature variation of dielectric constant of $BaEr_2Ti_5O_{14}$ ceramic.

that the dielectric constant is lower for materials with smaller ionic radii. the compound $BaLa_2Ti_5 O_{14}$ has the highest dielectric constant value. Moreover, its elastic constant or dielectric constant do not undergo any significant anomaly as the temperature increases.

It can be noted from the figures that some of the materials exhibit significant variations in elastic constant with temperature with minima in the range of 400-430K. These are indicative of very weak elastic anomalies in these compounds. The materials are not driven into any elastic instability. Since all the compounds contain rare earth ion, one can expect a coupling between atomic vibrations and the electronic states of the 3d and 4f orbitals. In single crystalline systems in which such coupling is strong the system is known to undergo structural instability and phase transition. The effect known as the Jahn-Teller effect is exhibited by rare earth and transition element containing compounds such as $PrAlO_3$ and $TmVO_4$. In our systems since the material is ceramic with multiphase structure, the system is not driven into a structural instability but the coupling is manifested in the temperature variation of elastic constant. Again, due to the complexity of the multiphase structure, it is not easy to work out the exact nature of the coupling quantitatively.

If not for the anomaly and minima exhibited by C_{11}, it decreases with temperature, in general, in all materials. Moreover, the elastic constants do not show any significant hysteresis in its variation with temperature and returns to its original value upon cooling the sample back to room temperature.

The dielectric constant of the materials do not exhibit any significant variation with temperature. As has been seen in almost all ceramics with high dielectric constant values that the dielectric relaxation times are rather long. Upon cooling back to room temperature, the material does not regain the original dielectric constant value immediately. If the material is left undisturbed for a few hours, then it regains the original dielectric constant value.

The results of investigations presented in this chapter help to understand the elastic and dielectric properties of dielectric ceramics with the general formula $BaLn_2Ti_5O_4$ where Ln is a rare earth ion. The effect of different ions on the elastic

131

and dielectric properties are revealed and the temperature dependence of those properties are reported.

Table 5.1 Dielectric and elastic properties of $BaLn_2Ti_5O_{14}$ dielectric ceramics.

Name of cation Ln	ionic radius 10^{-12}m	ϵ_r	Elastc constants C_{11} (GPa)	Elastic constants C_{44} (GPa)
Y	103.2	48± 2	221± 5	71± 2
La	120	96 ± 5	230±6	77± 2
Pr	115	62± 3	149± 3	49± 2
Nd	113.5	73± 4	239± 6	79± 2
Sm	110	70± 4	238± 6	75± 2
Gd	107	52± 3	187± 4	60± 2
Tb	106.3	56± 3	245± 6	82± 2
Dy	105	59± 3	245± 6	82± 2
Er	102.1	58± 3	231± 5	81± 2

5.4 References

[1] D. Kolar, Z. Stadler, S. Gaberseek and D. Suvorov, *Ber: Dtsch-Keram Ges* **55(7)** 346 (1978).

[2] D. Kolar, S. Gaberseek, B. Volavasek, H. S. Parker and R.S. Roth, *J. Solid State Chem.* **38(2)** 158 (1981).

[3] K. Wakmo, K. Minai and H. Tamura, *J. Am. Ceram. Soc.* **67(4)** 278 (1984).

[4] D. Kolar, S. Gaberseek, Z. Sladler and D. Suvorov, *Ferroelectrics* **27** **(1/4)** 269 (1980).

[5] R. C. Matveeva, M. B. Vapolomeev and L. S. Il'yuschenko, *Russ. J. inorg. chem.* **29 (1)** 31 (1984).

[6] T. Jaakola, A. Vusimaki, R. Rautioaho and S. Leppavuori, *J. Am. Ceram. Soc.* **69(10)** C 234 (1986).

[7] E. S. Razgon, A. M. Geus, M. B. Varfolomeev, S. S. Korovin and U. S. Kostomaro, *Zh. Neogan. Khim* **25(8)** 2298 (1980).

[8] H. Sreemoolanathan and M. T. Sebastian, *Br. Ceram. Trans. J.* **95(2)** 79 (1996).

[9] K. Fukuda, I. Fujii, R. Kitoh,Y. Cho and I. Awai, *Jpn. J. Appl. Physics* **32** 1712 (1993).

[10] J. Takahashi, T. Ikegami and K. Kageyamma, *J. Am. Ceram. Soc.* **74 (8)** 1868 (1991).

[11] E. S. Razgon, A. M. Gens, M. Varzolomeev, S. S. Korovin and V. S. Kostomarov, *Zh. Neorgam. Khim* **25 (6)** 1701 (1980).

[12] L. P. Mudrolubova & et. al. *Neorgan Mat.* **17(4)** 683 (1981).

[13] M. B. Varfolomeev, A. S. Mironov, V. S. Kostomarov, *Zh. Neogan. Khim* **33(4)** 1070 (1988).

[14] J. P. Mercurio, M. Manier and B. Frit, *Ferroelectrics* **127** 35, (1992).

[15] R. D. Shannon and C. T. Prewitt, *Acta. cryst.* **B25** 925 (1969).

[16] D. Kolar, S. Gaber Seal and Volavsek, *J. of Solid State Chemistry* **38** 158 (1981).

[17] X. M. Chen, Y. Suzuki, N. Sato, *Jourl. of Mat. Sc. Materials in Electronics* **6** 10 (1995).

[18] X. M. Chen, Y. Suzuki and N. Sato, *Materials letters* **16** 75 (1993).

[19] J. Takahashi, T. Ikegam and K. Kageyama, *J. Amer. Ceram. Soc.* **74** 1868 (1991).

[20] M. Valant, D. Suvorov and D. Kolar, *Proc. Conf. Euro Ceramics* (RWTH Ed: Waser et al) (1994)

[21] J. E. May Jr., *IRE Natl. Commu. Rec* **6** pt2 134 (1958).

[22] E. P. Papadakis, *J. Appl. Phy.* **35** 1474 (1964).

[23] E. P. Papadakis in *Physical Acoustics*, **Vol, 12** ed: W. P. Mason and R. N. Thurston, (Academic press NewYork 1976).

[24] H. J. McSkimin, *J. Acoust. Soc. Am.* **33** 12 (1961).

[25] H. J. McSkimn and P. Andreatch, *J. Acoust. Soc. Am.* **34** 609 (1962).

[26] J. M. Wu, M. C. Chang and P. C. Yao, *J. Am. Ceram. Soc.* **73(6)** 1599 (1990).

[27] X. M. Chen, Y. Suzuki and N. Sato, *Mater. Lett.* **16** 75 (1993).

[28] R. G. Matveeva, M. B. Varfolomeev and L. S. Il'yushcenko, *Zh. Neogan. Khim*, **29(1)** 31 (1984).

Chapter 6

Elastic properties of $Ba_{5-x}Sr_xNb_4O_{15}$ ceramics

6.1 Introduction

The perovskite type materials possess excellent properties that make them potentially useful for catalytic, electronic and ion exchange applications [1]. The crystal structure of a series of perovskite type materials $R_5M_4O_{15}$ (R = Ba, Sr; M = Nb, Ta) have been studied by Galasso and Katz [2,3]. They reported that $Ba_5Nb_4O_{15}$ has a hexagonal structure (space group Psm1) with one molecular unit per crystallographic unit cell whereas the strontium analogue could not be formed from other members of the group.

The ideal perovskite structure having cubic symmetry with one ABO_3 formula per unit cell is shown in Fig.6.1. The A cations are at the corners, B cation at the body centre and O^{2-} ions at the face centre positions of the cube. Many perovskite materials have symmetry different from cubic at room temperature, but assume cubic symmetry at high temperatures [4,5]. Several reviews are available in the literature about the structure and properties of the perovskites [2,5,6,7]. The microscopic as well as macroscopic properties can be adjusted to some extent according to the requirement by suitable cationic substitution in A, B or both sites of $A^{2+}B^{4+}O_3$ perovskites. Symmetry of the perovskites has a crucial role on their physical properties. The symmetry is mainly affected by number of factors like tolerance factor and perovskite parameter. Goldschmidt [8] made number of studies on the dependence of these factors on the properties of several perovskite system and defined the tolerance factor to account for the limit of the size of the cations to form perovskite structure.
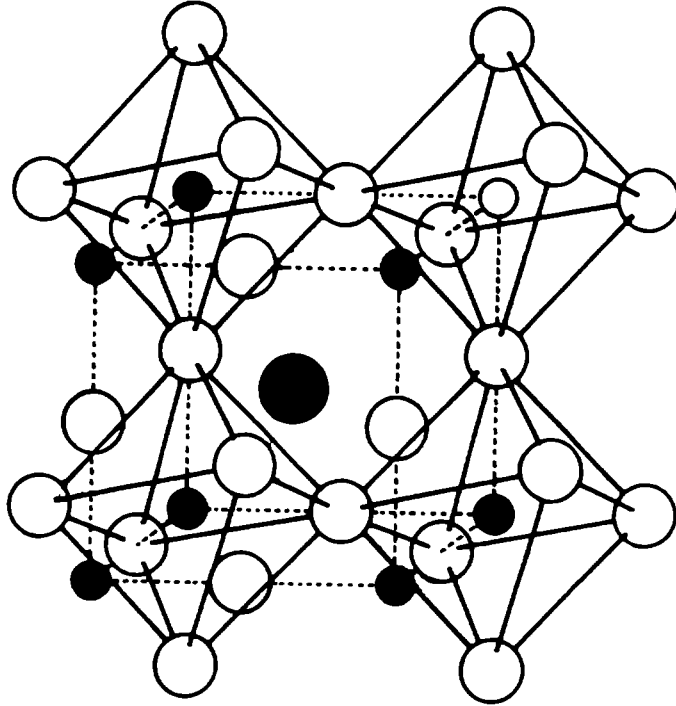
135

Fig.6.1: The ideal cubic perovskite structure of ABO_3. A cation at the centre showing the octahedral frame work.

One interesting property of perovskites is that they can accommodate more than one type of element for both A and B sites. Such combinations can be represented as A $(B'_x B''_y)O_3$ and are referred to as complex perovskites. The B' and B'' are two elements in different oxidation states and $x + y = 1$. Roy [5] has studied the the possible multiple ion substitutions in perovskites. The Ba ($B'_{1/2} Nb_{1/2})O_3$ ceramics come under the A $(B'_{1/2} B''_{1/2})O_3$ perovskites where B' is a trivalent ion and B'' is a pentavalent ion.

A (B' B'')O_3 compounds show the phenomenon of order-disorder depending on the size and charge of the B cations. In the disordered structure lattice can be represented as stacking of one layer of B' ions followed by another layer of B'' ions in the B site along (111) plane. The ordering behaviour of B site cations in the A(B' B'')O_3 type complex perovskite is important, because the order - disorder transition influences the structural as well as dielectric properties of these compounds. Ordered $A(B'_{1/2}B''_{1/2})O_3$ compounds adopt the structure shown in Fig.6.2. The ordered distribution of the B ions is most probable when a large difference exists in either charges or ionic radii [3]. The mininmum difference in ionic size that results in ordered A(B' B'')O_3 compound is $(r_{B'} - r_{B''})/r_{B'} \approx 0.09$. Depending upon the B site cations, the extent of ordering differs in $A(B'_{1/2} B''_{1/2})O_3$ perovskites.

Structural differences in perovskites between one phase and another are so small that it is extremely difficult to carry out a precise structural determination [9,10]. Megaw [11] showed that the factors determining structures could be broken into various factors such as tilting of octahedra, displacement of the cations and distortion of the octahedra. The tilting of the anion octahedra is the most important factor which establishes the overall space group and symmetry of particular perovskite [9]. Another important consequence of the tilting is to double certain cell axes. The tilting causes the B cation-anion bonds of one octahedron to rotate in an opposite direction to that in a neighbouring octahedron, which gives rise to a doubling of the distances perpendicular to that little axis [12,13]. There are 23 possible tilt systems in perovskite [9,10]. The relative pseudo cubic subcell parameters and the space groups for all the tilt systems have been worked out by Glazer [10]. Since tilting of the octahedra causes a doubling of the unit cell axis, extra reflections are produced in addition to the ordinary reflections
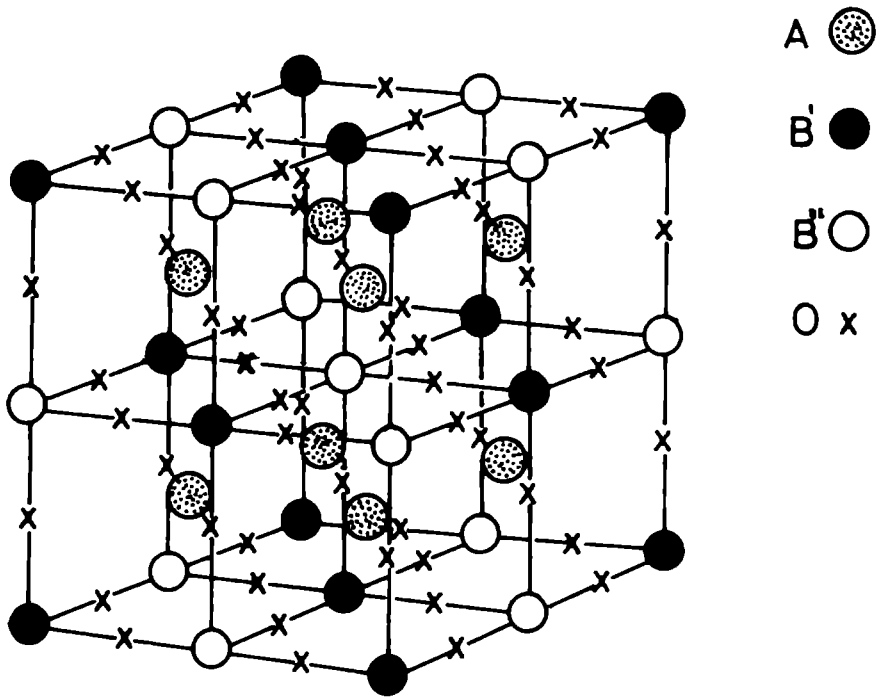
137

Fig.6.2: Ordered structure of $A(B'_{1/2} B''_{1/2})O_3$

which lie in the half integral reciprocal lattice planes. So special attention must be made to record very weak difference reflections which helps to analyse the perovskite structure with more accuracy. In the past perovskite structures have been determined by comparing the observed x- ray powder patterns with those of already known structures. But this procedure leads to incorrect structure determination [9,10].

A considerable amount of work has been done on the $A(B'_{1/2} B''_{2/3})O_3$ type ceramics, but only little attention has been paid to the elastic properties of $A(B'_{1/2} B''_{1/2})O_3$ type complex ceramic system. Several authors prepared and studied the structure and properties of $A(B'_{1/2} B''_{1/2})O_3$ perovskites [15,16,17].

In this chapter, our interest is to study the elastic properties of $Ba_{5-x}Sr_xNb_4O_{15}$ ceramics at different compositions of Sr. Hutchmison et al [14,15] had studied the polytypism of $Ba_5Nb_4O_{15}$. However Wiedan et al [12] prepared $Sr_5Nb_4O_{15}$ material and reported that its structure is monoclinic (space group $A_{2/m}$) with two molecular units per crystallographic unit cell. Several studies have been made on the structure of $Ba_5Nb_4O_{15}$ ceramics and established it to be hexagonal structure. As unit cell consists of a fine layer stacking of Ba^{2+} and O^{2-} ions with Nb^{5+} occupying the octahedra sites in between the layers. $Ba_5Nb_4O_{15}$ is isostructural with $Ba_5Ta_4O_{15}$ and $Sr_5Ta_4O_{15}$. The structure is commonly known as AO_3- layer structure with perovskite type arrangements. To prevent edge sharing of NbO_6 octahedra, one Nb ion is missing between the 3rd and 4th layers in the unit cell. The $Ba_{5-x}Sr_xNb_4O_{15}$ ceramic system has been found to be a very good dielectric resonator in microwave applications.

Vibrational analysis made on the $Ba_{5-x}Sr_xNb_4O_{15}$ ceramic system by Ratheesh et al.[11] showed that both the lattice parameters a and c increase initially upto $BaSr_3Nb_4O_{15}$ and then decrease. Dielectric properties and lattice parameters show a nonlinear variation with x. This variation may be due to the occurrence of a phase transformation at this composition. In addition to this, the Sr^{2+} ion is large in size and having high polarisability compared to Ba^{2+} ion. So c axis elongation increases unit cell polarisation which causes a nonlinear variation in ϵ and τ_f values. Although they had studied the Raman and IR spectrum of these materials to observe any effect due to phase change, satisfactory explanation has not been obtained. Our main interest has

been to probe the phase transition occurring in this system using ultrasonic technique, which has not been attempted before.

6.2 Experimental method

6.2.1 Sample preparation

$(Ba_{5-x} Sr_x) Nb_4O_{15}$ ceramics were prepared by the conventional solid state route with x ranging from 0 to 5 at an interval of 1. Starting materials were high purity $BaCO_3$, $SrCO_3$ and Nb_2O_5. The stoichiometric mixtures, after wet mixing, were calcined in the temperature range 1250 - 1375°C for 4 hours depending on the strontium content (x). These powders were thoroughly ground and were then sintered at 1400 -1450°C for 4 hours. Sintered pellets had diameter of 9-10 mm and thickness 5-6 mm. All the compositions showed densification except x=5 compound ceramic which do not densify even after firing at 1600°C However, addition of 1wt% Y_2O_3 after calculation is found to be very effective in densifying the x = 0 ceramics. XRD patterns were taken using powder samples.

6.2.2 X ray diffraction analysis

X-ray diffraction analysis of all the prepared samples have been made with X ray diffractometer (Regaku,Japan) using CuKα radiation. Fig.6.3 shows a typical pattern of XRD of these samples. The pattern of $Ba_5Nb_4O_{15}$ is in agreement with earlier reports. The indexing of patterns that obtained from the XRD analysis have been made in accordance with hexagonal system.

6.2.3 Elastic constant measurements

For the elastic constant measurements using ultrasonic technique, we have used the same experimental set up and procedure already outlined in earlier chapters.
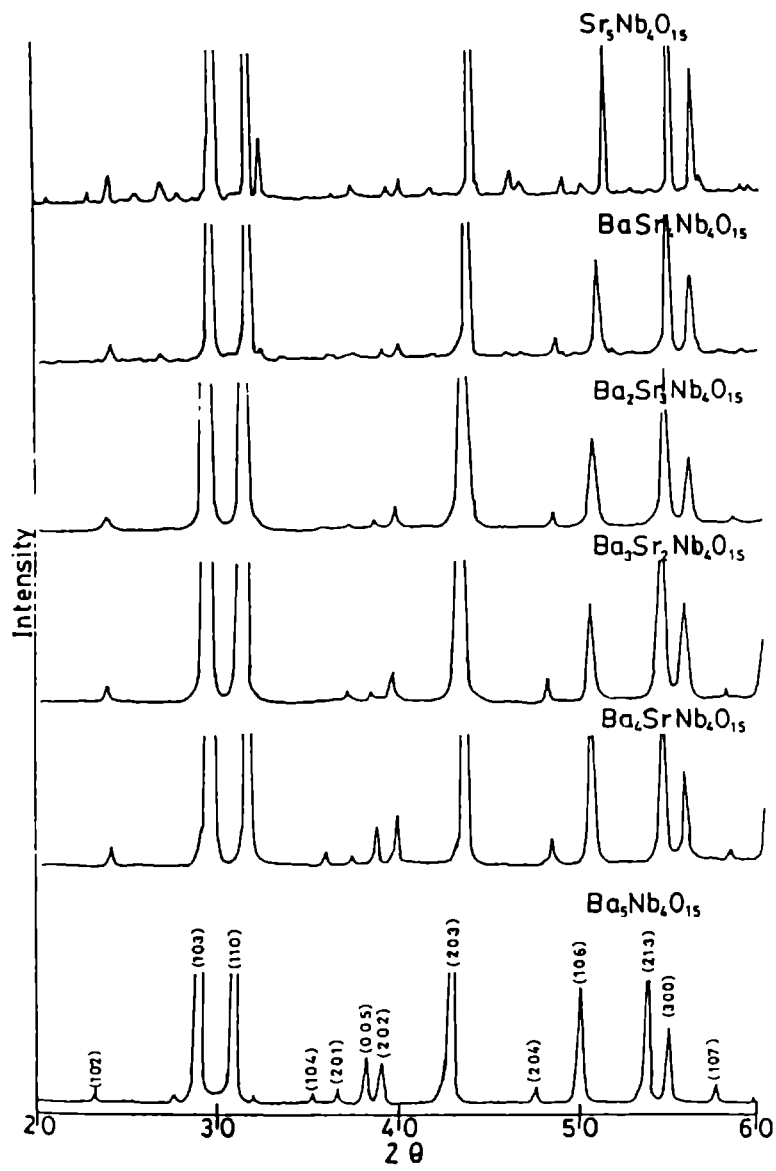
Fig.6.3: XRD pattern of $Ba_{5-x}Sr_xNbO_{15}$ ceramics

141

6.3 Results

We have measured longitudinal ultrasonic velocities in different compositions of the $Ba_{5-x}Sr_xNb_4O_{15}$ ceramics with x ranging from 0 to 0.5. Since these are highly attenuating samples, tranverse velocity could not be measured. The longitudinal elastic modules C_{11} for all samples have been determined and plotted as a formation of x. The results are shown in Fig. 6.4   We have also measured the temperature variation of C_{11} for the samples $Ba_5Nb_4O_{15}$, $(Ba_2\ Sr_3)\ Nb_4O_{15}$ and $Sr_5\ Nb_4O_{15}$ between room temperature and 450K. The results are plotted in figures 6.5,6.6 and 6.7 respectively.

6.4 Discussion

The results on elastic constant values indicate that, in general, elastic constant is lower for samples doped with strontium. So one can see that Si doping decreases the mechanical strength of these samples. Among the doped samples, $(Ba_2\ Sr_3)\ Nb_4O_{15}$ has a maximum value for C_{11}. This is attributed to the composition dependent structural change in the samples. This may be due to abrupt change in the length of the C-axix which results the rotation of NbO_4 octahedra due to the comparatively large Ba^{2+} ions in the third and fourth layers. It is known from the Raman and IR spectral studies made on the same ceramic compound that the structure of the system improved with Sr substitution. This change is manifested in our result that $(Ba_2\ Sr_3)\ Nb_4O_{15}$ shows a peak in the value of C_{11}.

The results on the temperature variation of C_{11} for the three samples shown in figures 6.5, 6.6 and 6.7 indicate that these samples have very long relaxation times. Initially C_{11} value increases indicating that the samples become more rigid upon heating. After the completion of the temperature cycle, the samples do not return to the original elastic state. They return to a state with a C_{11} value which is larger by nearly 5% of the initial value. It is found that the original C_{11} value is regained if the sample is kept undisturbed for several hours. This has been verified experimentally. This effect is one which repeats in all the samples. We can conclude that the samples become elastically
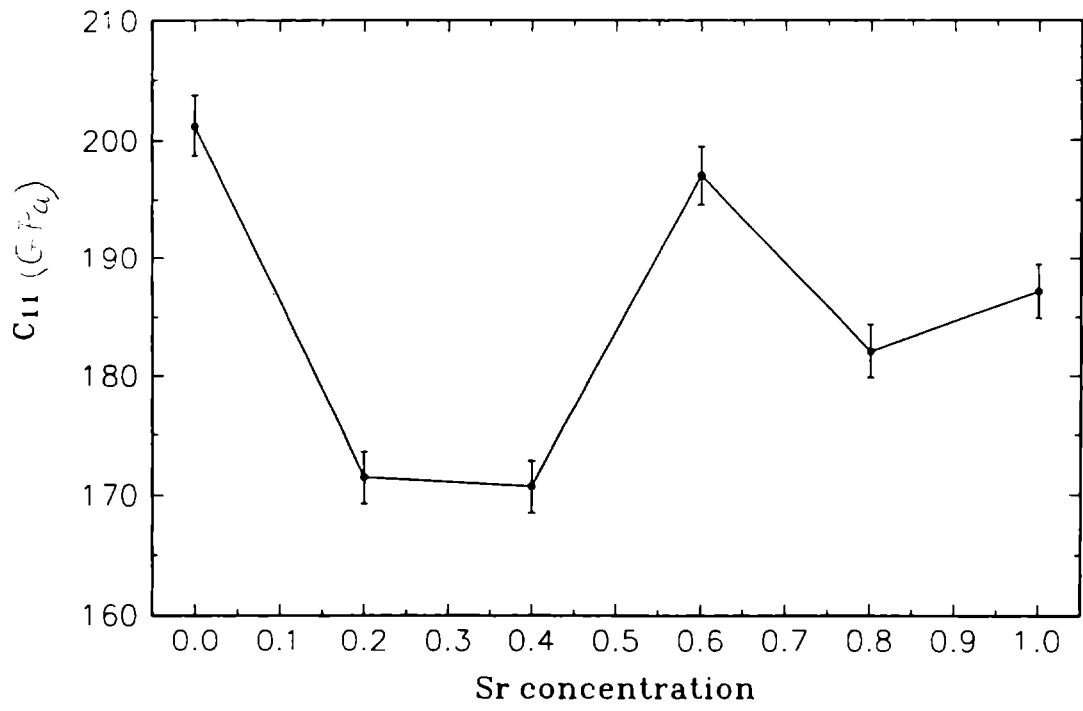
142

Fig.6.4: Variation of longitudinal elastic modulus C_{11} with Sr doping in $Ba_{5-x}Sr_xNb_4O_{15}$ ceramics
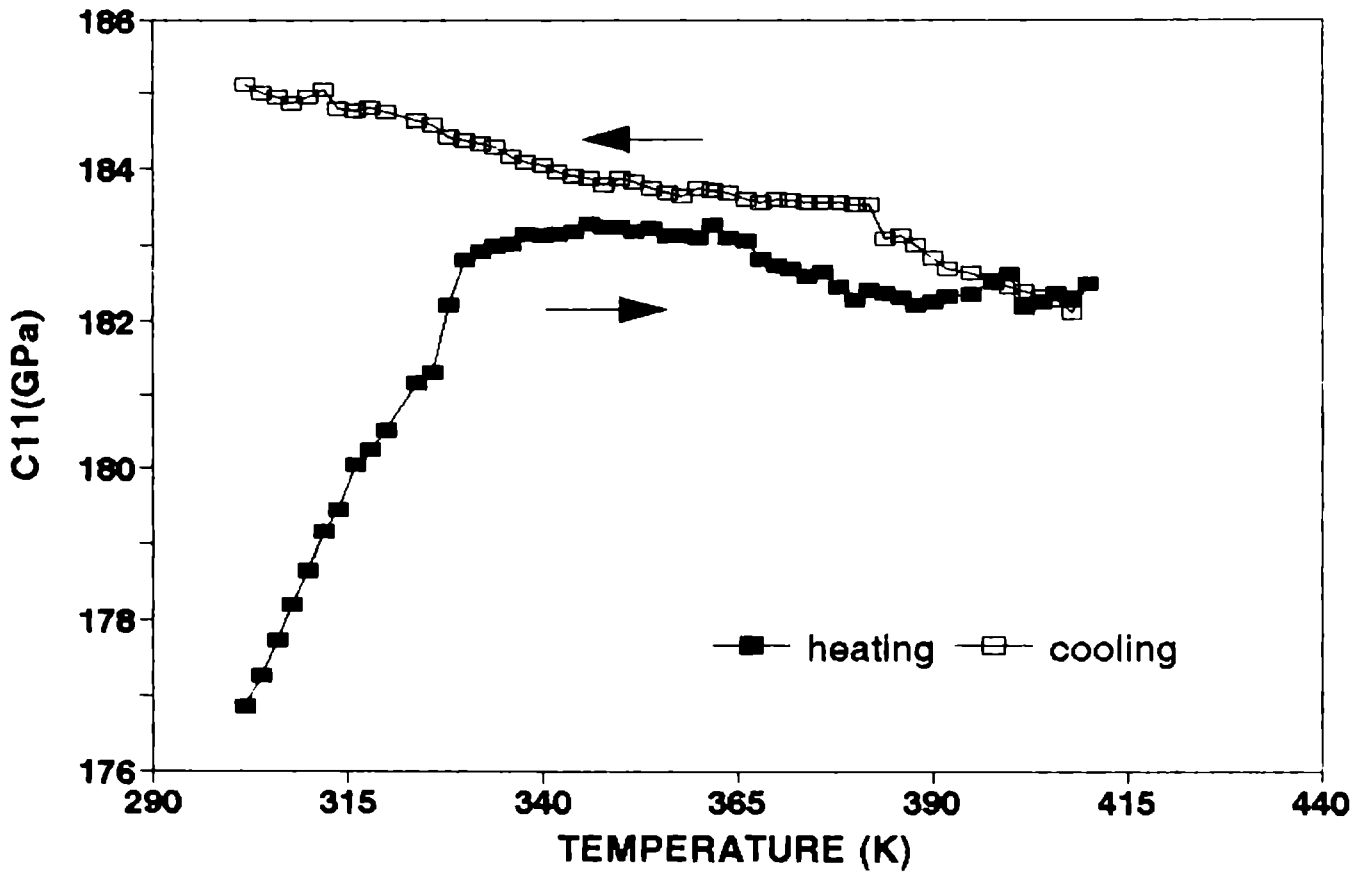
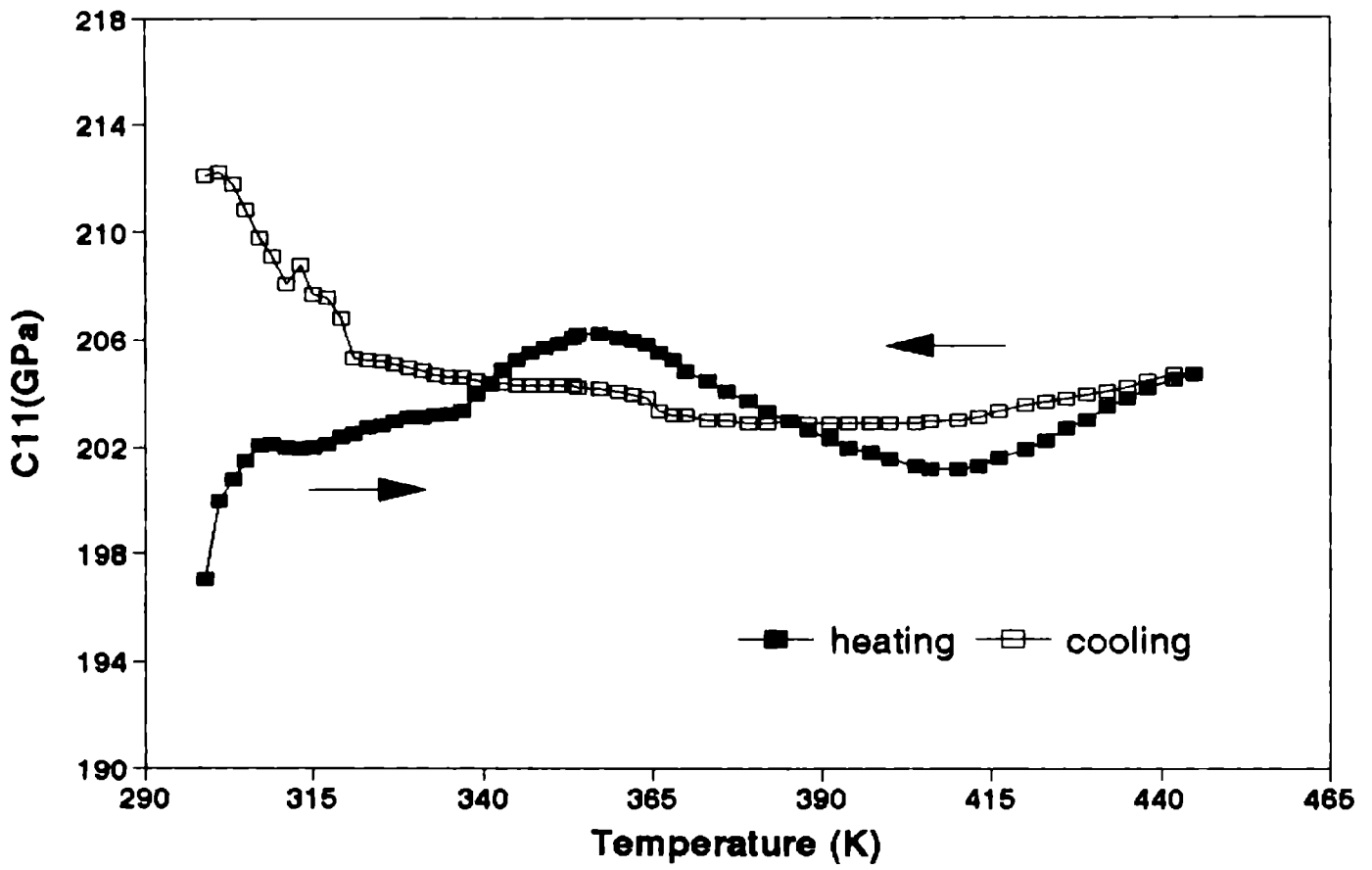Fig.6.5: Temperature variation of C_{11} for $Ba_5Nb_4O_{15}$ ceramic

Fig.6.6: Temperature variation of C_{11} for $Ba_2Sr_3Nb_4O_{15}$ ceramic during heating and cooling cycles
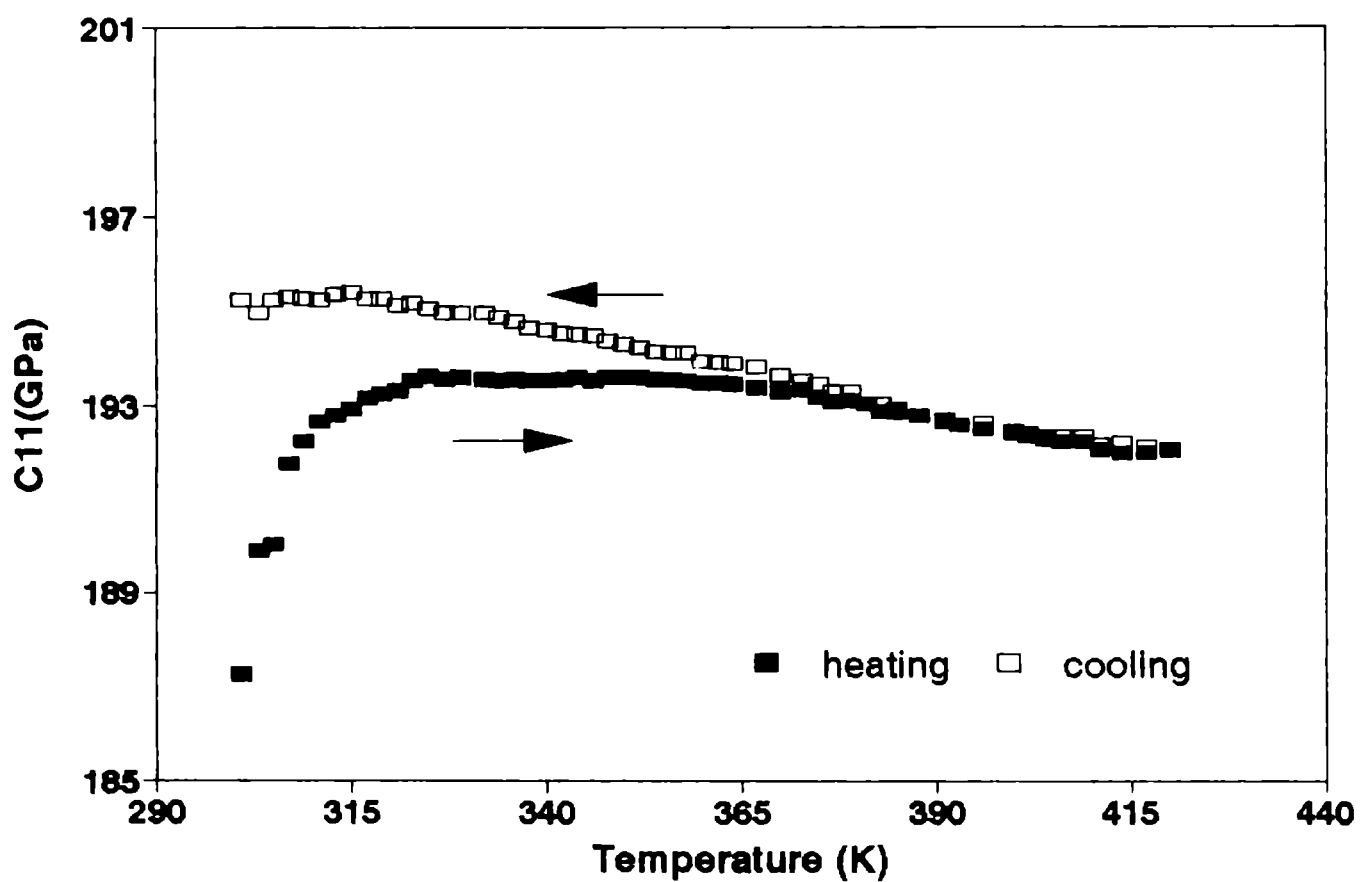
Fig.6.7: Temperature variation of C_{11} for $Sr_5Nb_4O_{15}$ ceramic during heating and cooling cycles

more stiff when they are heated and they relax slowly upon cooling to regain the initial state.

It can also be noted in figures from 6.4 to 6.6 that the temperature variation of C_{11} for $Sr_5Nb_4O_{15}$ and $Ba_5Nb_4O_{15}$ are smooth without any anomaly whereas for (Ba_2Sr_3) Nb_4O_{15}, C_{11} starts decreasing at around 360K and has a minimum value around 415K during the heating cycle. The nature of this minimum is indicative of a slow structural change in this sample. This decrease can be attributed to a diffuse phase transformation taking place in the system. It may be noted that this is the composition in which the structural change from hexagonal to an yet unidentified structure (more probability in tetragonal) take place. Moreover, this feature is absent during cooling cycle indicating that the temperature induced slow structural change also has very long relaxation times. This is evident from the fact that the same cycle repeats if the sample is kept for a long time at room temperature. These factors should be taken in to account while using these samples for any application.

6.5 References

[1] G. T. Stanford and R. A. Condrate Sr.,*J. Mater Sec. Lett* , **3** 303 (1984).

[2] F Galasso and Lkatz, *Acta Cryst.* **14** 647 (1961).

[3] F. S. Galasso, *structure and properties of inorganic solids*, Pergamon press (1970).

[4] R. M. Hazen, *Sci. Am.* **74** (1988).

[5] R. Roy,*J. Am. Ceram. Soc.* **37** 581 (1954).

[6] M. T. Anderson, K. B. Greenwood, G. A. Taylor, K. R. Poeppelmeire, *Prog. Sol. State Chem.* **22** 197 (1993).

[7] T. Nakamura and J. H. Choy, *J. Sol. State Chem.* **20** 233 (1997).

[8] B. M. Goldschmidt, *Skrifter Norske Videnskaps-Akad. Mat. Naturvid* **Kl. No.4** (1928).

[9] A. M. Glazer, *Acta Cryst.* **B 28** 3384 (1972).

[10] A. M. Glazer, *Acta Cryst.* **A 31**, 756 (1975).

[11] H. D. Megaw, *Proc. Phys. Soc.* **58** 133 (1946).

[12] M. Weiden, A. Granel, J. Norwig, S. Horn and F. Stegtich, *J. Alloy and compounds* **218** 13 (1995).

[13] R. Ratheesh, H. Sreemoolanath and M. T. Sebastian (to be publised).

[14] J. L. Hutchmison and A.J. Jacobson *Acta Cryst.* **B 31** 442 (1975).

[15] J. L. Hutchmison, *Chem. Scripta* **14** 181 (1978-79).

Chapter 7

Dielectric and elastic properties of $(Bi_2O_3)_{1-x}(CuO)_x$ Glasses.

7.1 Introduction

The elastic and dielectric behaviour of glasses differ from their crystalline counterparts in many different ways. In general, ultrasonic and dielectric absorption are greatly enhanced in glasses. The vibrational excitations in a glass, which determine all phonon related properties such as heat capacity, thermal conductivity, elastic constants, ultrasonic absorption etc., cannot be described with respect to the underlying lattice by means of the Bloch formalism with the result that the phonon wavevector is no longer a good quantum number. Consequently, the selection rules obeyed by the wavevector in any interaction of the phonon in a crystalline solid are related in a glass and therefore the description of vibrational excitations in terms of the dispersion curves become inappropriate. Moreover, disorder scattering reduces the lifetimes of vibrational excitations and they may become spatially localized giving rise to effects that are not found in crystalline solids. These aspects are discussed in detail in several books and articles [1,2,3]

Oxide glasses are the oldest and most common among all glasses and they find a wide variety of applications. Some 70 years ago, it was believed that the only glass forming materials were oxides, of which only five oxides SiO_2, GeO_2, B_2O_3, As_2O_3 and P_2O_5 formed glasses by themselves. While some oxides of the type AO and A_2O_3 do not form glasses, the question 'why do certain chemical composition of materials form glasses more easily than others' remains one of the great unsolved mysteries of

glass science. So a comprehensive theory of glass formation in oxides is needed before catagorical answers to the questions surrounding semiconducting glass forming ability can be given.

According to Zachariasen [4], the interatomic interaction in both amorphous and crystalline phases would be very similar in certain regards. He assumed, therefore, that oxygen polyhedra found in oxide crystals (triangular, tetrahedral or octahedral) would also occur in glasses; the only difference being that relative orientation of polyhedra should be variable in glasses giving rise to a nonperiodic structure. From Zachariasen's approach to glass formation, a continuous random network (CRN) can be constructed in which the approach of the atoms closer than a normal bond length can be avoided. This will minimise repulsive energies and hence total internal energy.

It is well known that glass formation is generally favoured for compositions at which there is a deep eutectic. Composition near the eutectic favour glass formation since the melting point is depressed and so the liquid is less supercooled at the glass transition T_g, thereby reducing the possibility of crystallisation. This is also true for metallic glass system as it is for inorganic materials. A more detailed theory regarding the influence of eutectic formation on glass-forming ability has been proposed by Rawson [11] by modifying the earlier suggestions made by Sun [12]. It has been verified earlier that crystallisation involves substantial atomic arrangement and consequent rupture of bonds. Since oxide materials have high bond strengths, they should be less prone to crystallisation and hence better glass formers. Rawson suggested that the amount of thermal energy available at the melting temperature has also got significant importance. The lower the thermal energy available for breaking bonds, the more the difficulty should be for crystallisation and hence more easy for a supercooled melt to transform in to glass. A parameter (B/T_m), ratio of the single bond strength (B) to the melting point (T_m), can be related to ease of the glass formation. Therefore 'easy' glass formers such as B_2O_3 or SiO_2 have higher values of B/T_m than incipient network formers (Bi_2O_3, TiO_2, TeO_2) and considerably higher values than those of modifiers like CuO, MgO and CaO. Thus one can easily understand the reason why the V_2O_5- PbO system should be glass forming in the vicinity of the eutectic composition, although V_2O_5 by itself is not

a glass former.

Profound consideration of the nature of glass formation fades in to insignificance when faced with question like which chemical composition is to be used in order that semiconducting property of a glass is facilitated. Frequently, and particularly in technological applications, small amounts of additive are found to be necessary so that semiconducting glass nature is improved in some materials having no glass forming tendency.

The study of oxide glasses is one of the major frontier of research in the glass system especially with transition metals. Generally transition metal oxide glasses show semiconducting behaviour because of the transition metal ions. Semiconducting oxide glasses with transition metals are currently attracting considerable scientific interest for its potential use for the manufacturing of switching and memory devices, cathode ray tube materials, ferrites, fast photonic switches etc.

Many kind of binary oxides with transition elements are well known to posses semiconducting properties. So the parameters that determine their physical properties such as thermal conductivity, specific heat, elastic constants, dielectric constant etc. should be known to high degrees of accuracy. Eventhough the thermal conductivity and heat capacity of different oxide glasses have been measured over wide ranges of temperatures from the mK range to several hundred K, data on elastic constants are comparatively less. The lack of crystalline periodicity give rise to short rage order in glasses resulting in isotropic elastic properties so that there are only two independent elastic constants. These are the longitudinal and transverse elastic constants C_{11} and C_{44} respectively.

Because of their interesting electrical transport and switching properties, a number of oxide glasses with metallic oxides as additives have been prepared. Many of these glasses are semiconducting and exhibit threshold switching properties. The electrical and dielectric properties of various oxide glasses have recently been reviewed by Buchanan [5]. The Bi_2O_3 glass is a popular member of the oxide glass family whose physical properties are well documented and reported in literature. In recent years attempts have been made to modify properties of oxide glasses to suite various applications by

151

incorporating various additives into the glass network. The electrical conductivity of a number of oxide glasses have been measured by adding different additives such as alkali oxides and metallic oxides [5]. The electrical conductivity and dielectric constant of Bi_2O_3 glass with different concentrations of CuO have recently been measured as a function of temperature [6]. It has been reported that conductivity increases with CuO content and the results have been interpreted in terms of non adiabatic hopping of electrons through the network.

In this chapter we report one of the first measurements of the effect of addition of a metallic oxide on the elastic properties of an oxide glass. We have determined the longitudinal and transverse elastic constants of $(Bi_2O_3)_{1-x}$ $(CuO)_x$ glasses as a function of x with x varying from 0 to 0.5 by measuring the corresponding ultrasonic velocities. Variation of elastic constants with temperature have been measured from room temperature to 450 K. Ultrasonic attenuation has also been measured as a function of temperature in all the glasses. Other related elastic properties such as the Debye characteristic temperature, Young's modulus and Poisson's ratio have also been determined. The low frequency dielectric constant and its variation with temperature have been measured in all the glasses and reported. The experimental techniques used, results obtained and a discussion of the results are given in the following sections.

7.2 Experimental Method

7.2.1 Sample preparation

$(Bi_2O_3)_{1-x}$ $(CuO)_x$ glass samples with x ranging from 0 to 0.5 in steps of 0.1 have been prepared by mixing appropriate amounts of Bi_2O_3 and CuO (Annular grade chemicals). A homogeneous mixture of the two powders are prepared by firing it in a fire clay crucible at 1000°C for several hours in a temperature controlled muffle furnace. The thoroughly mixed molten mixture is quenched by pouring it into appropriate openings cut into highly conducting metallic blocks. Cooling rates of the order of 10^6K/sec. are easily realised following this technique which is sufficient to form good glasses for the present system. The samples have been cut into cylindrical shapes with diameter

$\approx$ 10mm and length 10mm. The ends have been cut with a diamond wheel saw and polished by hand lapping so as to have plane parallel faces which are necessary for ultrasonic measurements. The nonparallalism of the end faces is estimated to be well within one degree. Thin slices of the samples with thickness $c \approx$ 1mm have also been cut from the same ingot for dielectric constant measurements.

The amorphous nature of the glasses have been checked by the X-ray diffraction method. The XRD pattern shows a broad maximum at a particular value of 2θ which indicates the amorphous character of the samples.

7.2.2 Ultrasonic velocity and attenuation measurements

Velocities of longitudinal and transverse ultrasonic waves propagating along each of the glass samples have been measured using the pulse echo overlap (PEO) technique using the MATEC 7700 pulse modulator and receiver system [7] as described earlier. X and Y cut quartz ultrasonic transducers with resonant frequency 15MHz have been bonded to the samples with silicon grease as the bond for generating longitudinal and transverse ultrasonic waves respectively. The sample has been placed inside a suitable temperature controlled oven to vary the temperature from room temperature to 500K. For measuring variation of velocity with temperature, the temperature has been increased in steps of 2 degrees while keeping the temperature steady during measurements.

The Mc Skimin Δt criterion [8] has been applied to correct for the phase lag due to the bonding medium on RF echoes while making room temperature measurements on each sample. Once the correct overlap of echoes is identified at room temperature, variations in travel time can be monitored continuously as the temperature is varied. The PEO techniqe enables one to measure ultrasound transit time in the sample to an accuracy of a few ppm. Once the transit time is measured, the velocity can be evaluated knowing the length of the sample. The overall accuracy in measured velocity values is of the order of 1%. Once the longitudinal and tranverse velocities are measured, the corresponding elastic constants are determined from the relation $C_{ij}=\rho V^2$ where ρ is the density of the sample. The ultrasonic attenuation in each sample has been measured by the pulse comparison technique from the exponentially decaying pulse

pattern using the MATEC 2470B automatic attenuation recorder.

In addition to longitudinal and transverse modulii of $(Bi_2O_3)_{1-x}$ $(CuO)_x$ glasses, other moduli like Bulk modulus (K), Young's modulus E and Poisson's ratio σ have been evaluated from the measured velocities of each sample by using the standard expressions of elasticity theory [13] for an isotropic medium.

These expressions are

$$
\begin{aligned}
\text{Bulk modulus K} &= \frac{\rho(3V_l^2 - 4V_s^2)}{3} \\
\text{Young's modulus E} &= \frac{\rho V_s^2(3V_l^2 - 4V_s^2)}{(V_l^2 - V_s^2)} \\
\text{Poisson's ratio } \sigma &= \frac{(V_l^2 - 2V_s^2)}{2(V_l^2 - V_s^2)}
\end{aligned}
\tag{7.1}
$$

where ρ, V_l and V_s are the density, longitudinal velocity and shear velocity respectively.

Debye temperature θ_D is a very important physical constant for a solid. It enters into evaluation of a very large number of solid state parameters such as specific heat, electrical resistivity, diffuse X-ray reflection, scattering of thermal neutrons etc. on account of its direct relationship with lattice vibrations. The importance of this parameter has led to the development of methods by which it could be evaluated from a knowledge of elastic properties.

According to Debye's theory of specific heats, the characteristic temperature θ_D is related to the Debye cut off frequency ν_D of the lattice as

$$
\theta_D = \frac{h\nu_D}{K_B}
\tag{7.2}
$$

where h is the Plank's constant and K_B is the Boltzmann's constant. The cut off frequency ν_D depends on the elastic wave velocities in the solid given by

$$
\nu_D = V_m \left(\frac{3N}{4\pi V}\right)^{1/3}
\tag{7.3}
$$

where N is the number of atoms per unit volume and V_m is the mean velocity of propagation of plane waves averaged over all directions in the crystal. For isotropic solids like

glasses, the mean velocity V_m in terms of longitudinal and shear wave velocities reduce to

$$V_m = \frac{1}{3}\left(\frac{2}{V_s^3} + \frac{1}{V_l^3}\right)^{-1/3}$$
(7.4)

Debye temperature of the glass system is then given by

$$\theta_D = 251.4\left(\frac{p\rho}{M}\right)^{1/3} V_m$$
(7.5)

where V_m is expressed in km s^{-1} and numerical factor arises from the physical and numerical constants in the preceding equations.

7.2.3 Dielectric constant measurements

The dielectric constants of all the samples have been measured using the capacitance technique after placing the sample inside the home made dielectric constant cell. The capacitance of a capacitor with the sample acting as the dielectric has been measured accurately using an HP 4170 impedance analyzer. Variation of the dielectric constant with temperature has also been measured in selected samples using the same set up under temperature control.

7.3 Results

The room temparature values of density, elastic constants C_{11} and C_{44} and dielectric constant for different glasses investigated are tabulated in Table 7.1.

The XRD patterns of the some of the $(Bi_2O_3)_{1-x}$ $(CuO)_x$ glasses have been analysed The variation of longitudinal and transverse elastic constants, C_{11} and C_{44}, of $(Bi_2O_3)_{1-x}(CuO)_x$ glasses with $x$are shown in Fig.7.1. (p. 166) The uncertainties in the data plotted, including uncertainties in density measurement, is less than 4%. As is evident from Fig.7.1, the elastic constants do not vary significantly with the addition of CuO. The values tend to increase with CuO content. The variation of related elastic parameters, the Debye characteristic temperature, Youngs'modulus and Poisson's ratio with CuO concentration are plotted in Fig.7.2(a) and 7.2(b) respectively. As can be expected,
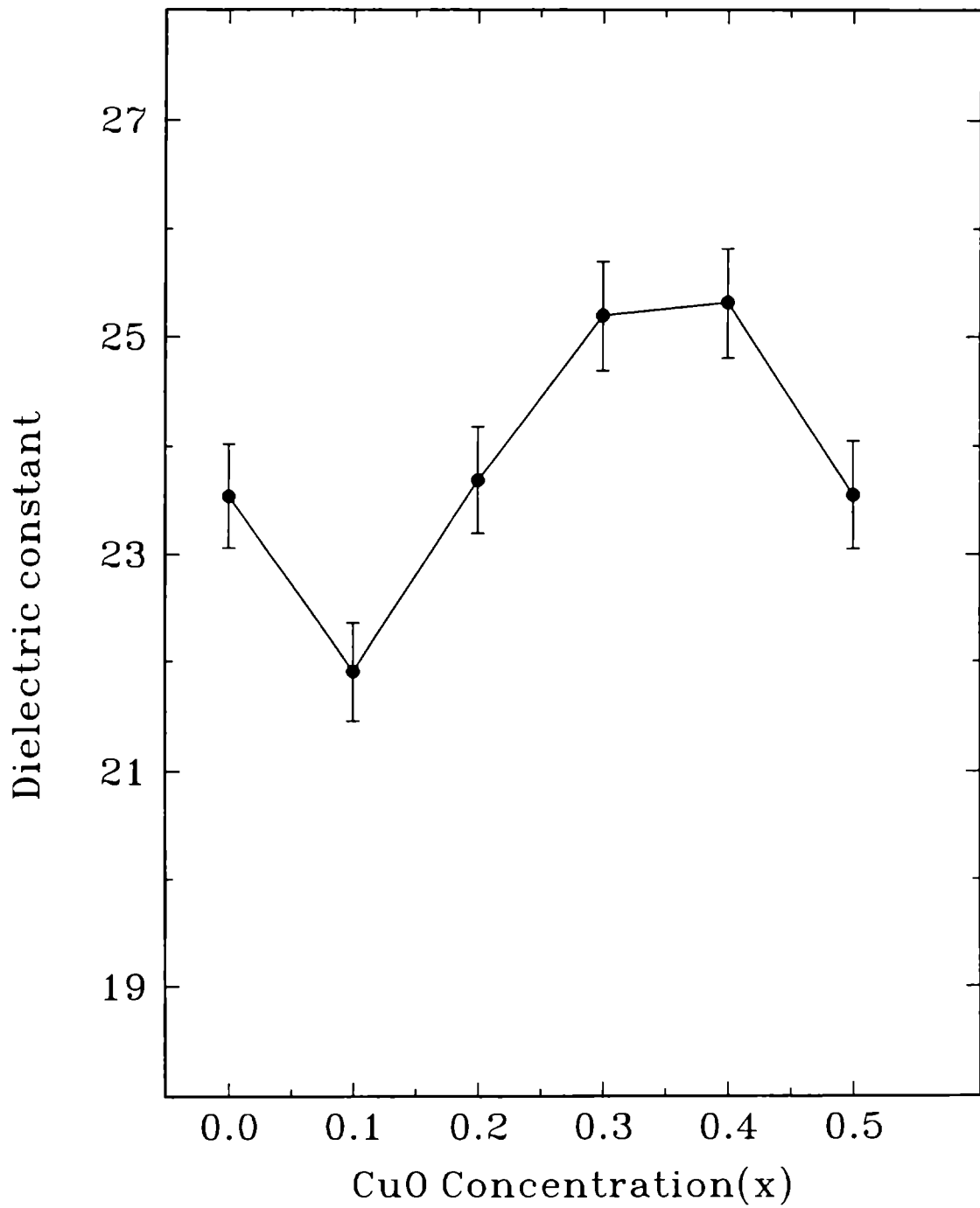
155

Fig.7.9 : Variation of dielectric constant (10 MHz)of $(Bi_2O_3)_{1-x}(CuO)_x$
glasses with CuO concentrations

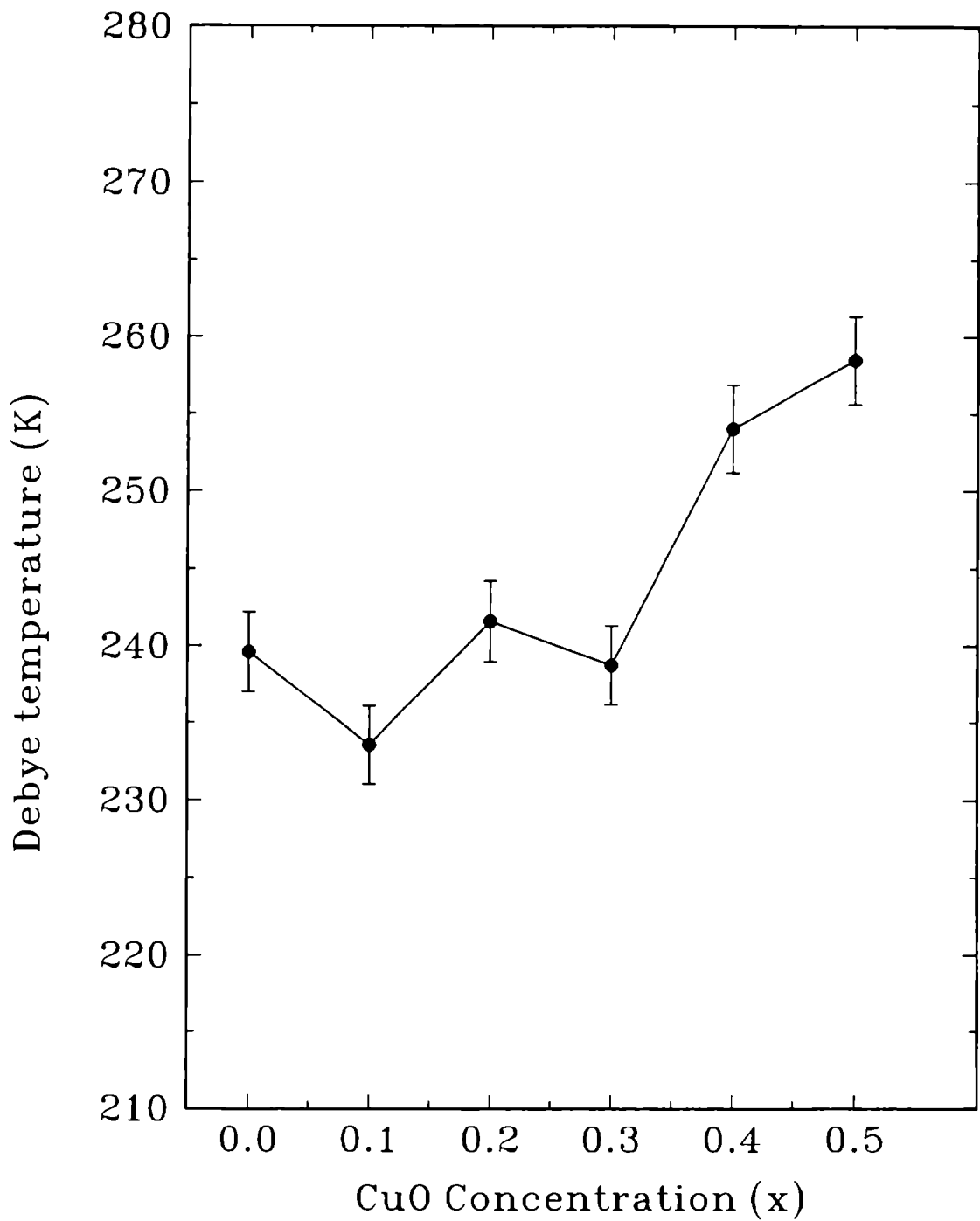Fig.7.2(a): Variation of Debye chracteristic temperature of
$(Bi_2O_3)_{1-x}(CuO)_x$ glasses with CuO concetrations

157

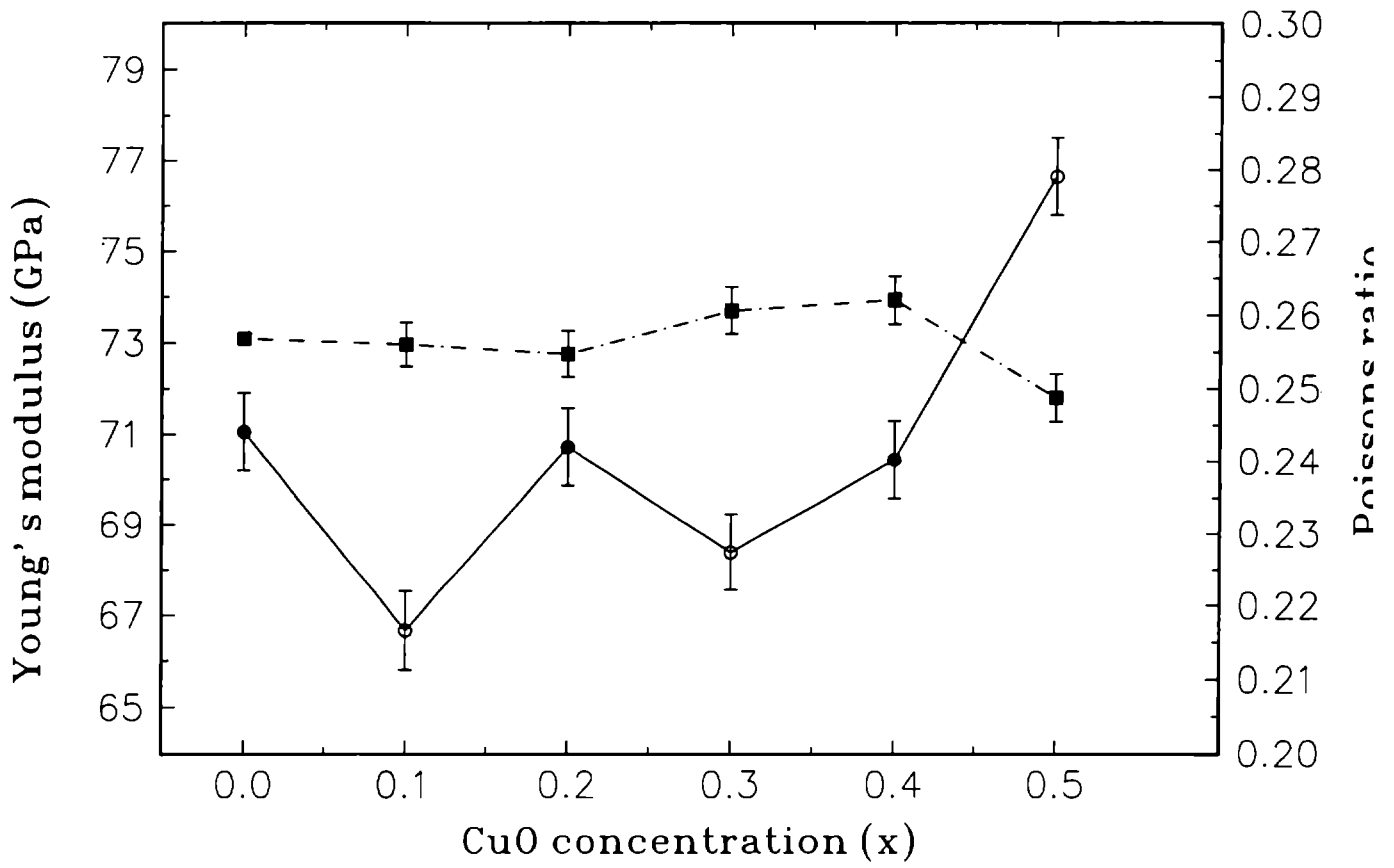**Fig.7.2(b): Variation of Young's modulus and Poisson's ratio of $(Bi_2O_3)_{1-x}(CuO)_x$ glasses with CuO concetrations**

Table 7.1 Room temparature values of density, elastic constants and dielectric constant

Sample	Density (Kg m^{-3})	Elastic Constant C_{11} (GPa)	Elastic Constant C_{44} (GPa)	Dielectric Constant (ϵ)
'Bi_2O_3	6551	86	28	23
$(Bi_2O_3)_{0.9}$ $(CuO)_{0.1}$	6641	81	27	22
$(Bi_2O_3)_{0.8}$ $(CuO)_{0.2}$	6516	86	28	24
$(Bi_2O_3)_{0.7}$ $(CuO)_{0.3}$	6608	84	27	25
$(Bi_2O_3)_{0.6}$ $(CuO)_{0.4}$	6152	86	28	29
$(Bi_2O_3)_{0.5}$ $(CuO)_{0.5}$	6283	92	31	24

the variation of these parameters follow the corresponding variations of the two basic elastic constants. The temperature variation of longitudinal elastic constant C_{11} in glasses with $x = 0$ (pure Bi_2O_3), $x = 0.1$, $x = 0.2$, $x = 0.3$, $x = 0.4$ and $x = 0.5$ are shown in figures 7.3, 7.4, 7.5, 7.6, 7.7. and 7.8 respectively. In Fig. 7.6, 7.7 and 7.8 we also plot the temperature variation of ultrasonic attenuation in glasses with $x = 0.3$, 0.4 and 0.5 respectively. Attenuation curves for glasses with $x = 0$, 0.1 and 0.2 do not exhibit any anomalous variations with temperature whereas glasses with $x = 0.3$, 0.4 and 0.5 show anomalies around 435 K. The elastic constant (or the corresponding velocity) shows a minimum and attenuation exhibits a maximum around this temperature. No definite correlation is found to exist between the temperature at which attenuation maximum or velocity minimum occurs and the corresponding x value. In samples with $x = 0.3$ anomalies in velocity and attenuation occur around 440K.

In Fig 7.9 we plot the variation of low frequency dielectric constant with CuO concentration. As in the case of elastic constants, there is no drastic change in dielectric constant with x value. In general, dielectric constant increases with increase in CuO concentration. It increases with x up to $x = 0.3$, and shows a decrease for
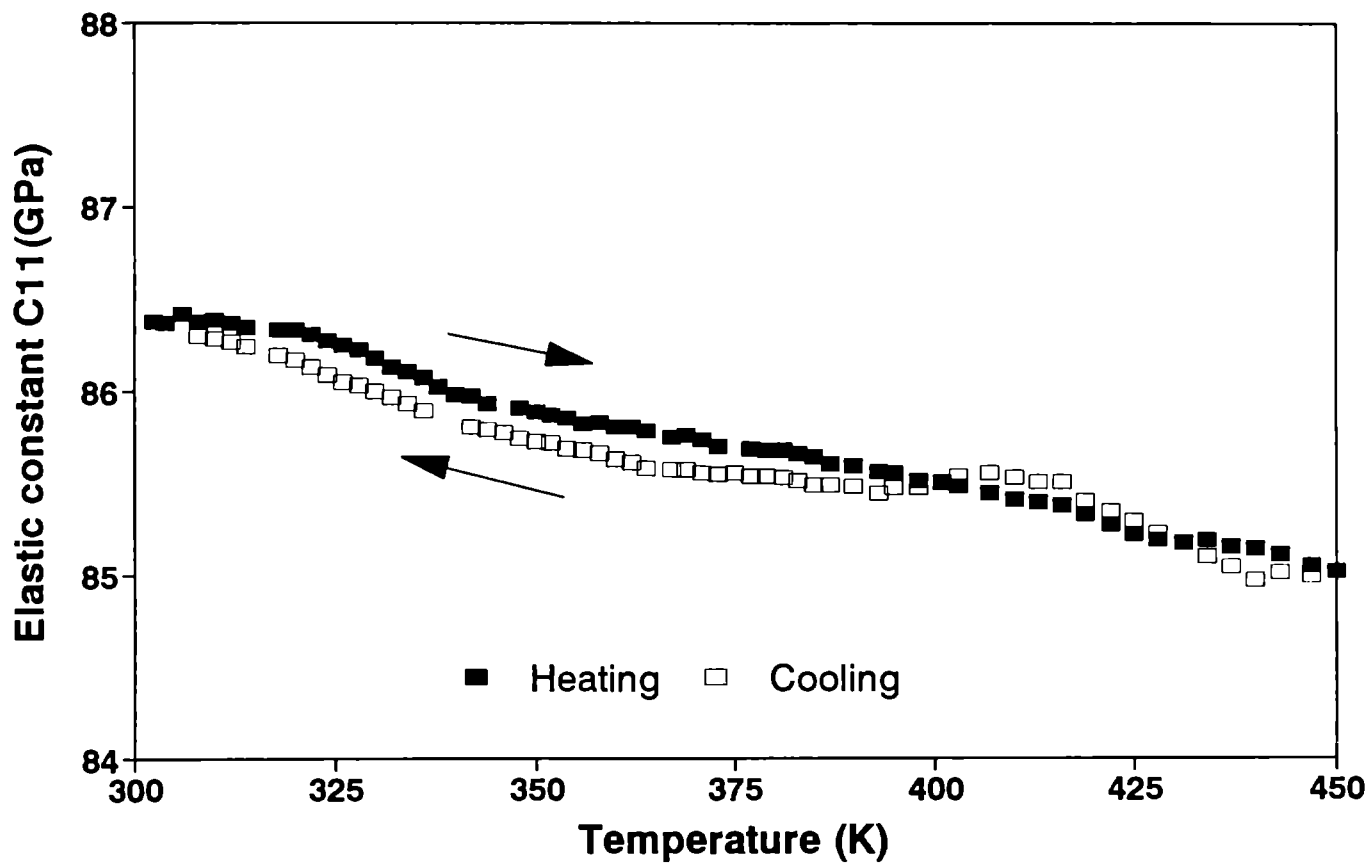
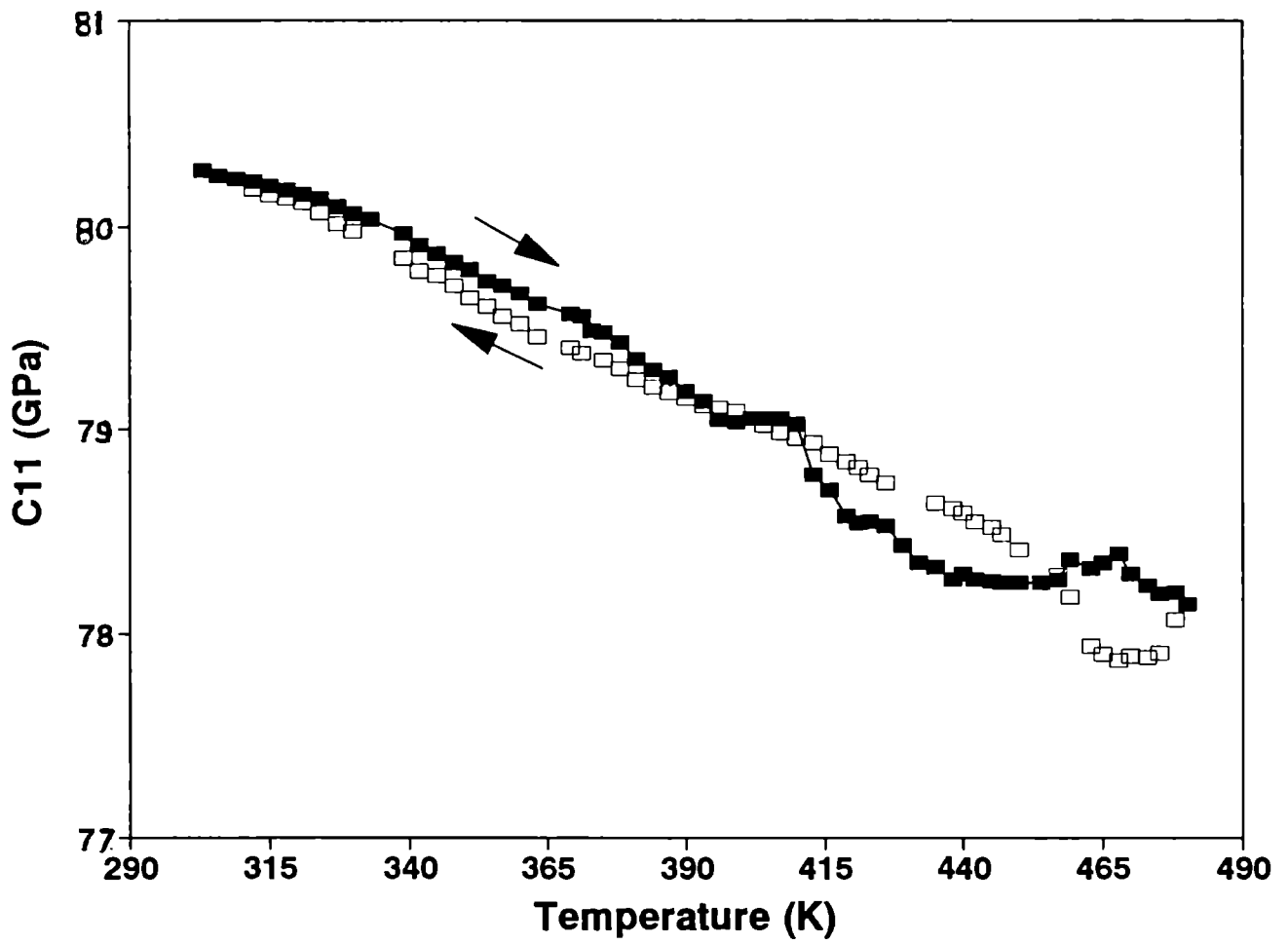Fig.7.3: Temperature variation of longitudinal elastic constant C_{11} of Bi_2O_3 glass

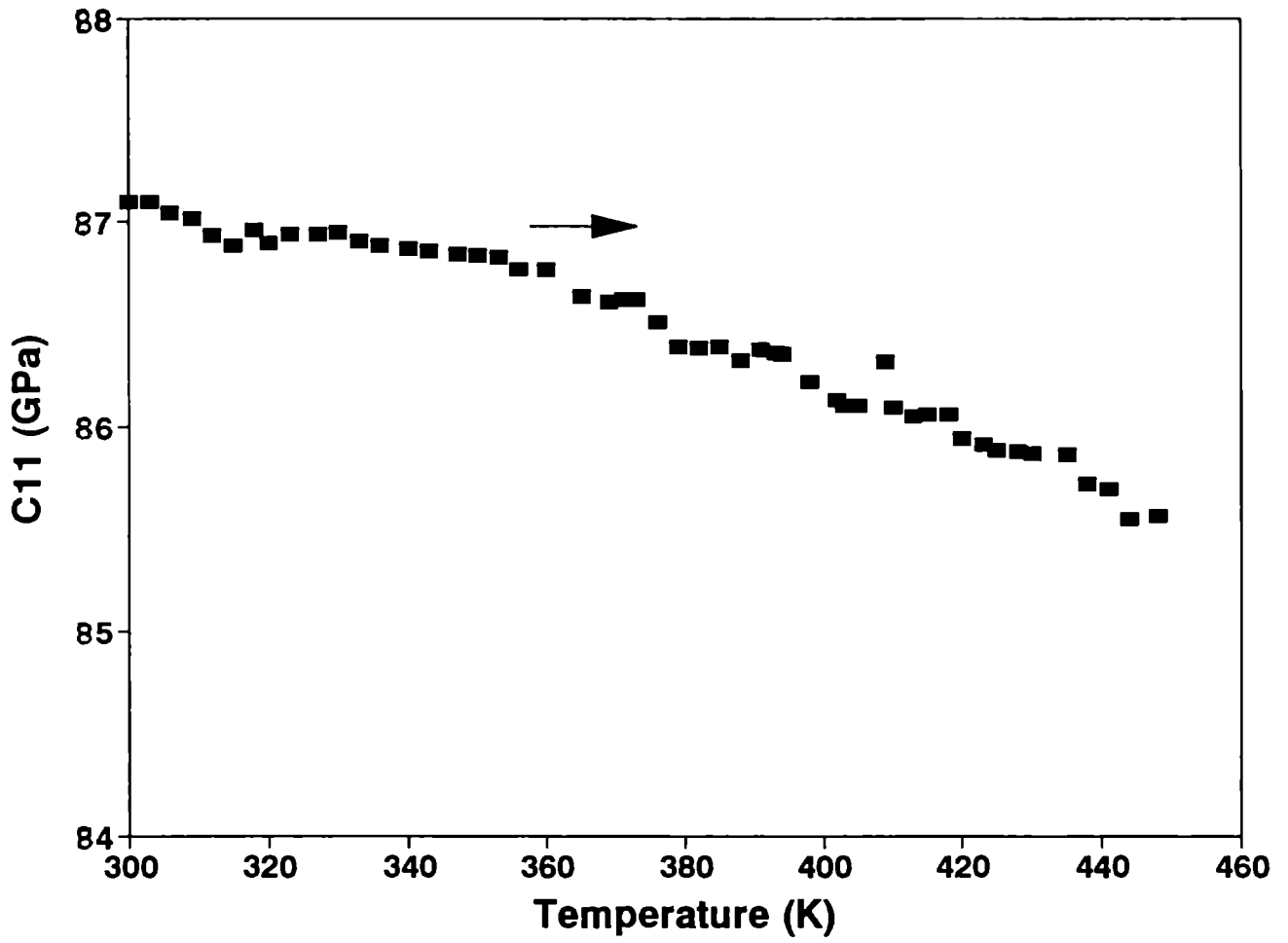Fig.7.4: Temperature variation of longitudinal elastic constant C_{11} of $(Bi_2O_3)_{0.9}(CuO)_{0.1}$ glass

Fig.7.5: Temperature variation of longitudinal elastic constant C_{11} of
$(Bi_2O_3)_{0.8}(CuO)_{0.2}$ glass
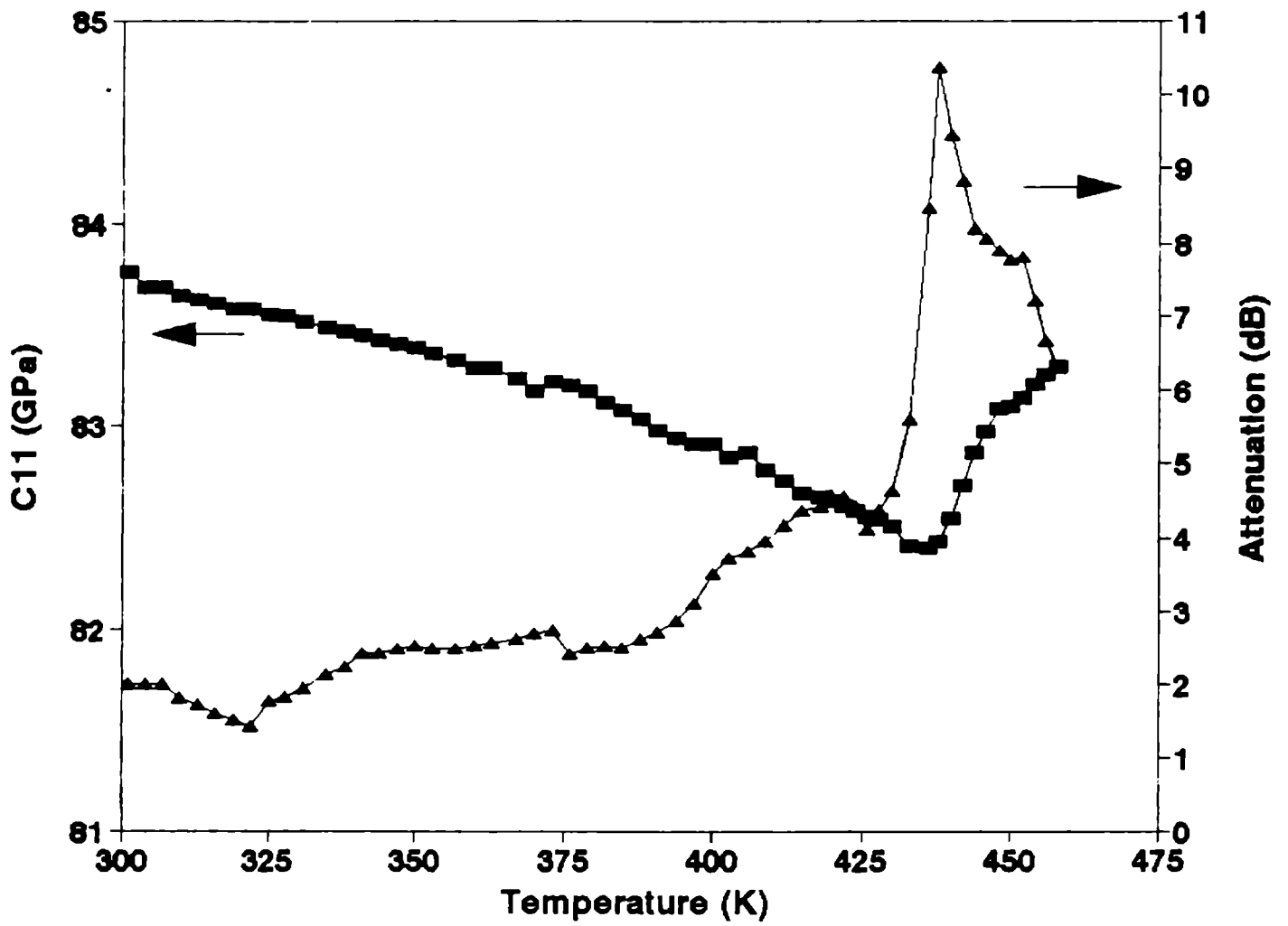
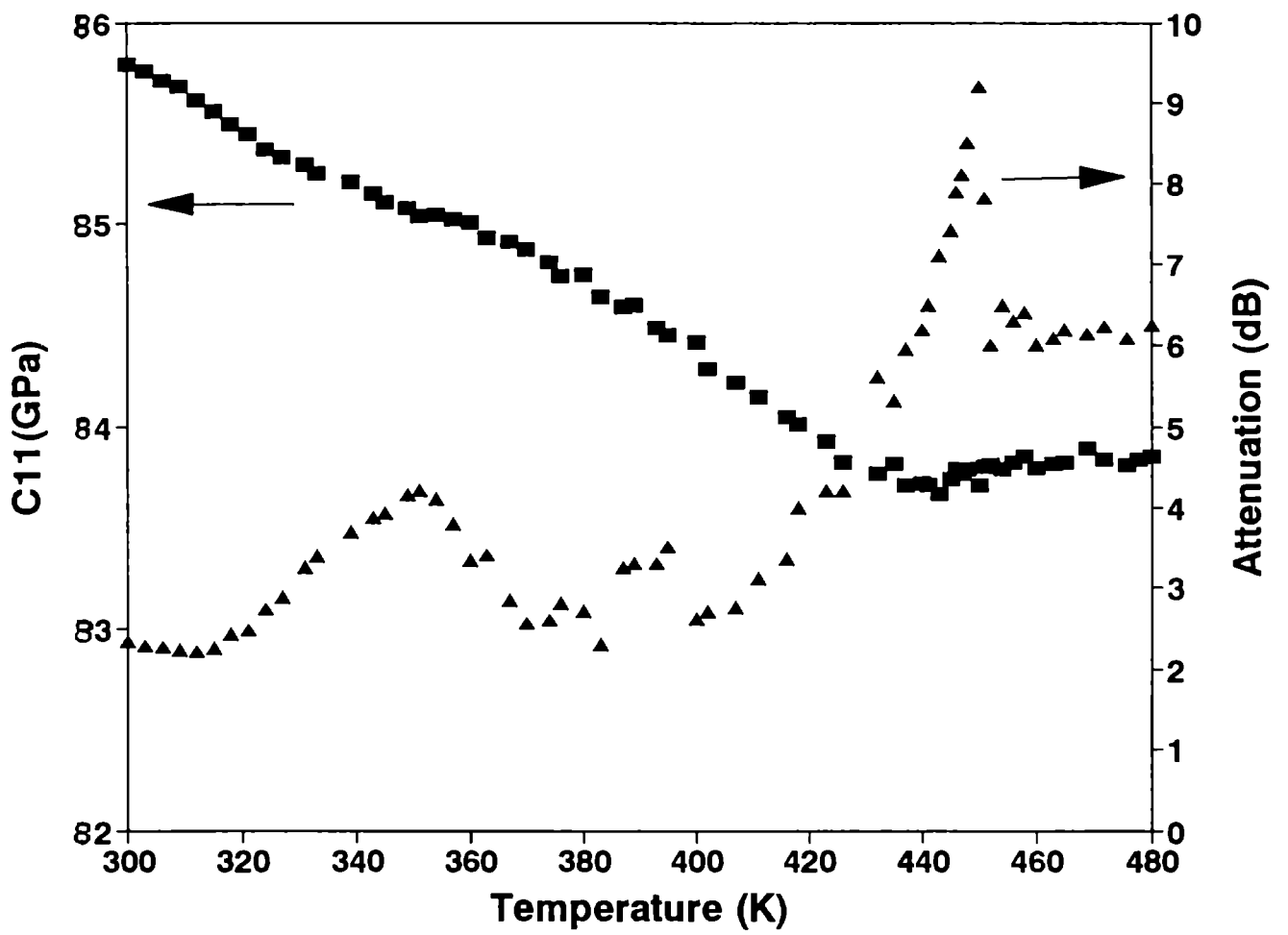Fig.7.6: Temperature variation of longitudinal elastic constant C_{11} of
$(Bi_2O_3)_{0.7}(CuO)_{0.3}$ glass

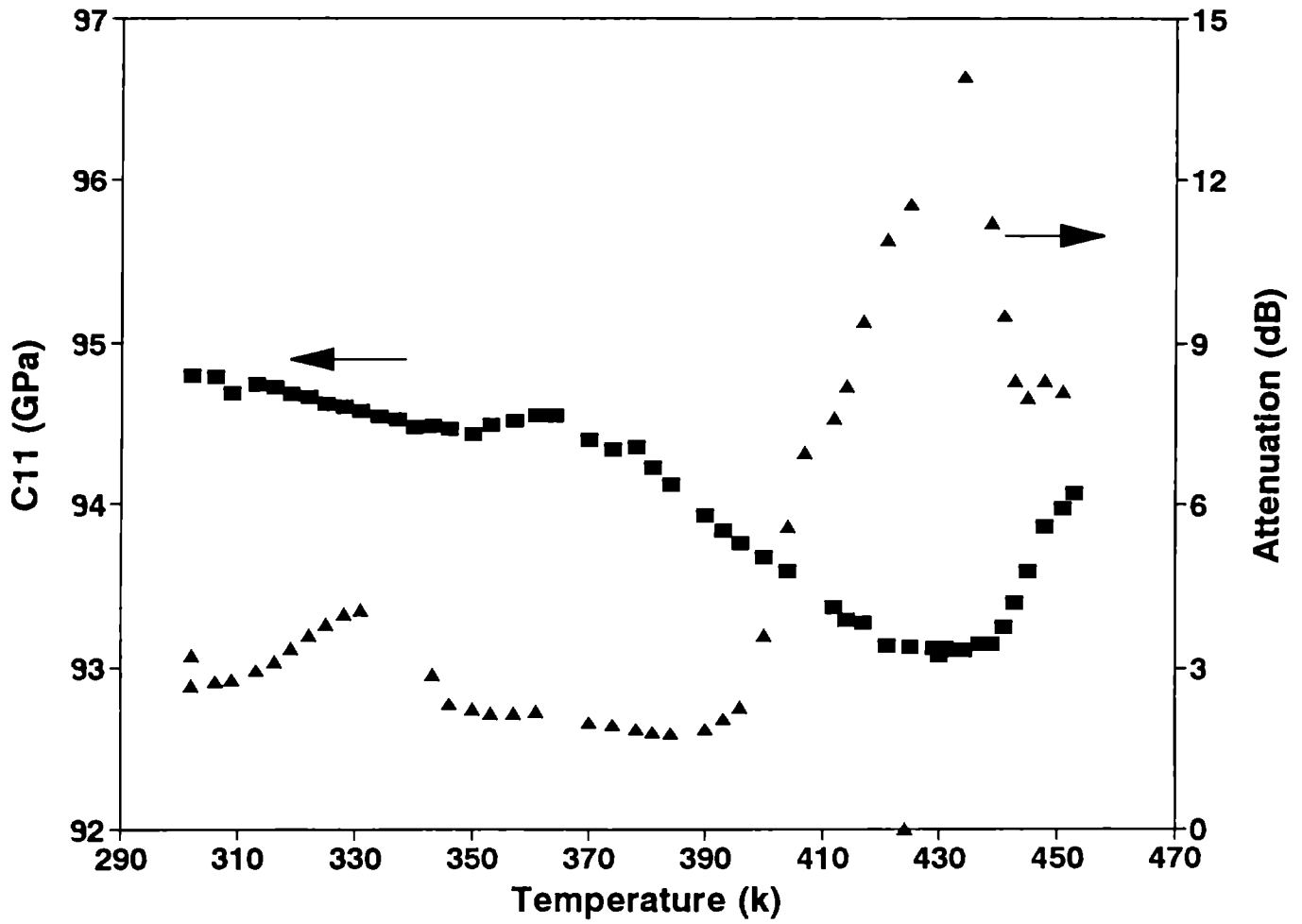Fig.7.7: Temperature variation of longitudinal elastic constant C_{11} of $(Bi_2O_3)_{0.6}(CuO)_{0.4}$ glass

Fig.7.8: Temperature variation of longitudinal elastic constant C_{11} of $(Bi_2O_3)_{0.5}(CuO)_{0.5}$ glass
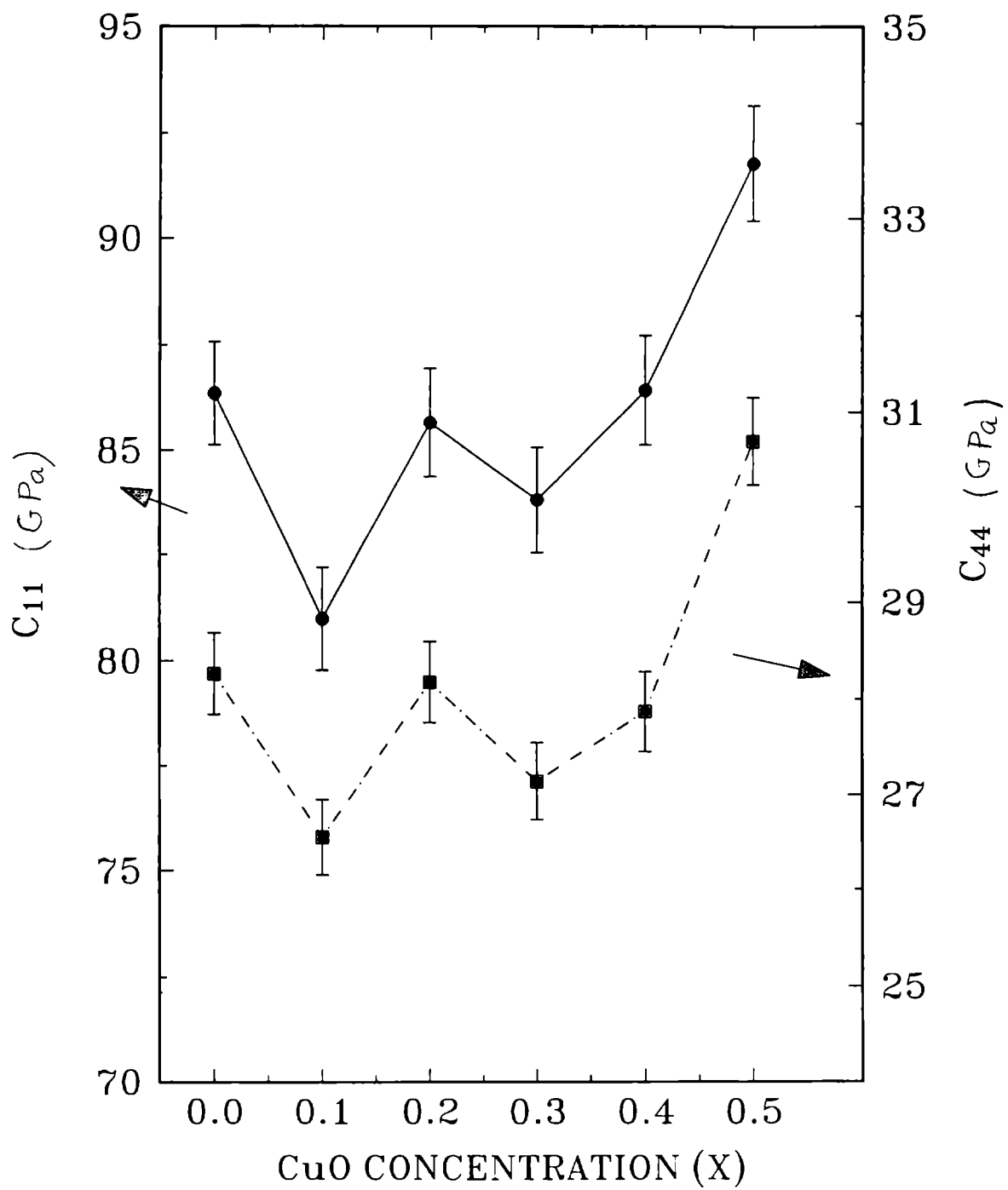
Fig.7.1: Variation of longitudinal and transverse elastic constant of $(Bi_2O_3)_{1-x}(CuO)_x$ glass with CuO concetrations

values of $x > 0.4$. Essentially, dielectric peaks around $x = 0.3 - 0.4$. The dielectric constant is found to increase with temperature in all samples as shown in Fig. 7.10 and 7.11 for glasses with $x = 0.3$ and $x = 0.5$ at different frequencies. It can be noted that dielectric constant does not undergo any anomalous change at the temperature at which ultrasonic velocity and attenuation exhibit anomalous variations. Dielectric constant curves for other samples are not shown as they are quite similar to those shown in Fig. 7.10. It may be noted that the dielectric constant does not get back to the initial value immediately after cooling. It takes a few hours for the dielectric constant to reach the original value after the sample has been taken through the heating cycle.

7.4   Discussion and Conclusion

Our results indicate that the elastic properties of $(Bi_2O_3)_{1-x}(CuO)_x$ glasses marginally improve as CuO concentration increases. In these glasses Bi_2O_3 is the network former and CuO is a network modifier. During fusion of the glass mixture, a structural readjustment takes place such that the Bi-O-Bi bonds are broken and the bridging oxygens are converted into nonbridging oxygens. Such a rearrangement of atoms can be represented as

$$Bi - O - Bi - + Cu - O \rightarrow Bi - O - Cu - O - Bi$$
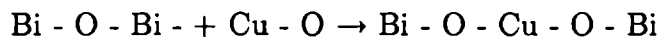
As the bond energy of Cu-O bonds is more than that of Bi-O bonds, the network becomes more rigid with addition of CuO giving rise to the observed increase in elastic constants

As more Cu atoms are added to the glass, fewer and fewer oxygens remain. As is evident from Fig.7.6, network with $x = 0.3$ undergoes a structural softening at around 440K. Similar behviour is shown by all glasses with $x \geq = 0.3$. This structural softening can be correlated to the number of nonbridging oxygens or Cu-O bonds present in the network. Our experiments show that the onset of the critical structure with optimum number of nonbridging oxygens occur for values of x lying between 0.2 and 0.3. As x increases, we can say that the network coherence decreases and it become easier for the metal ions to move through the network. When the network coherence e goes below

167

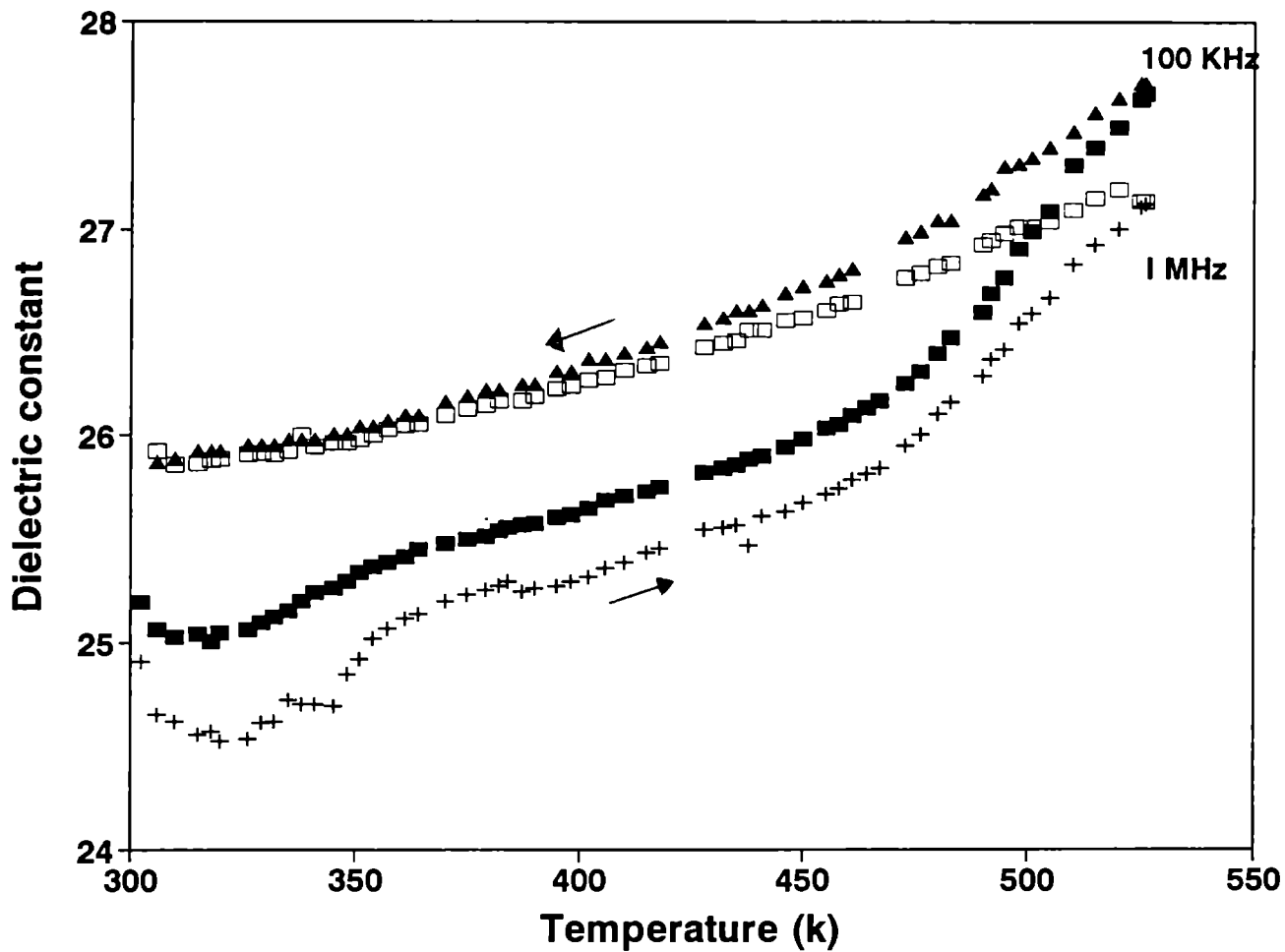Fig.7.10: Temperature variation of dielectric constant of $(Bi_2O_3)_{0.7}(CuO)_{0.3}$ glass at two different frequencies

168
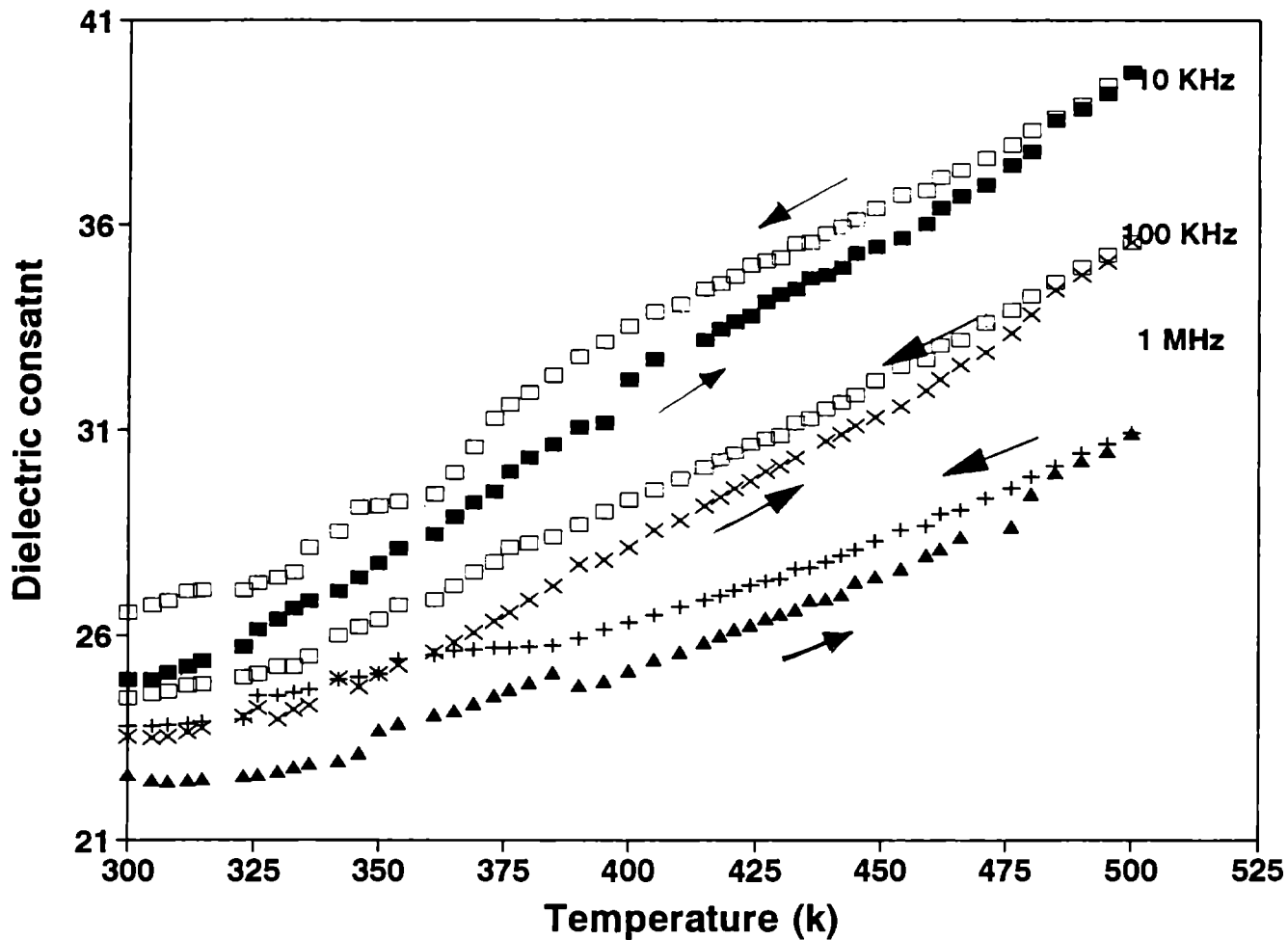
Fig.7.11: Temperature variation of dielectric constant of $(Bi_2O_3)_{0.5}(CuO)_{0.5}$ glass at three different frequencies

a critical value corresponding to a value of x between 0.2 and 0.3, the structure is such that it undergoes a softening at around 435K. A more detailed structural analysis and modelling would be required to confirm this and to give a quantitative footing for the above arguments. Besides the above, there is a chance for the occurence of phase seperation as transition metal ions could preferentially get segregated in the minor discontinuous phase. Such an effet is reflected in the dielectric constant as well as elastic constant values.

The observed tendency of the dielectric constant to decrease with increasing CuO content can be correlated to the increase in conductivity of the sample with the number of metal ions in the structure. The conductivity of oxide glasses is generally explained in terms of polaron hopping in the non-adiabatic approximation [9,10] and is found to increase with increase in the number of metallic ions [6].The dielectric constant of glasses, as expected, decreases with increasing frequency However, the variation over the wide range of frequencies is quite small. In general, ϵ increases slightly with increasing density of glasses. This is attributed to the fact that ϵ is a direct measure of the polarizability per unit volume and that for a denser glass there are more electrons and ions to polarise. The increase in dielectric constant with temperature again follows the corresponding decrease in conductivity with temperature. In addition to this, at elevated temperatures the glassy network relaxes and ionic motion becomes easier. This increase is also expected to be more pronounced at low frequencies because ions have more time to participate in the motion.

One important observation to be made in the temperature variation of dielectric constant is that it does not exhibit any anomaly around 435K where ultrasonic velocity and attenuation exhibit anomalies. This indicates that the structure of the network is the origin of the anomaly in elastic properties seen in glasses with $x \geq 0.3$. Probably a structural rearrangement of the network is taking place at this temperature which is reflected in ultrasonic properties.

In conclusion, we report the variation of the longitudinal and transverse elastic constants with CuO addition in $(Bi_2O_3)_{1-x}(CuO)_x$ glasses. Ultrasonic velocity and attenuation are found to exhibit anomalies around 435K in glasses with $x \geq 0.3$. We

also report the low frequency dielectric constants in these glasses and their variation with temperature.

7.5 References

[1] S. R. Elliot, *Physics of amorphous materials* (2nd ed. Longman Scientific & Technical) (1990).

[2] W. A. Phillips (ed), *Amorphous Solids* (Topics in Current Physics,) **Vol.24**, Springer-Verlag (1981).

[3] J. Jackle, L. P. liche, W. Arnold and S. Hunklinger, *J Non-Cryst. Solids* **20** 365 (1976)

[4] W. H. Zachariasen, *J. Am. Chem. Soc.* **54**, 3841 (1932)

[5] R. C. Buchanan, *Ceramic materilas for electronics* (University of Illinois Press, 1991)

[6] D. K. Burghate, S. G. Moke, W. J. Gawande, S. V. Pakade and S. P. Yawale *Ind. J. Phys. 68A* 141 (1994)

[7] E. P. Papadkis in *Physical Acoustics* **Vol. 12** ed: W. P. Mason and R. N. Thurston (Academic Press, New York 1976).

[8] H. J. Mc Skimin, *J. Acoust, Soc. Am.* **33** 12 (1961)

[9] I. G Austin and N. F. Mott, *Advances in Phys.* **18** 41 (1969)

[10] N. F Mott, *J. Non-Cryst. Solids* 1 1 (1968)

[11] H. Rawson *Inorganic Glass- Forming Systems* (Academic Press, New York, 1967)

[12] K. H. Sun *J. Am. Ceram. Soc.* **30** 277 (1947).

[13] E. Schreiber, O. L. Anderson and N. Soga, *Elastic constants and their measurements* (Mc Graw - Hill, New York) (1973).

Chapter 8

Elastic properties and ultrasonic attenuation of $Ba_{1-x}K_xBiO_{3-\delta}$ glasses

8.1 Introduction

Complex perovsikite type oxide glasses, for many years, have been of considerable interest owing to their peculiar properties and composition dependent ability of these properties. Over 90% of the natural metallic elements of the periodic table form perovskites with formula ABO_3. This wide range of cations coupled with the possibility of partial substitution, mainly at electronically sensitive B cation site, results in an abundant diversity of behaviour ranging from semiconductivity to even superconductivity. Perovskites have normally been regarded as alloys which shows ferroelectric and metal-insulator transitions. The interesting properties exhibited by perovskite oxide glasses are not common in either covalent or semiconducting oxide glasses. The phase transitions in perovskite type compounds is very interesting because they are often associated with a change in ferroelectric properties. In this phenomenon chain and layer structures of the lattice have vital role and their contributions are noteworthy. Since the atoms in most perovskite compounds are arranged in a layer manner, replacement of atoms in the parent lattice with foreign atom often influence their macroscopic as well as microscopic properties.

Study of phase transitions in perovskite oxide glasses using ultrasonic technique can provide valuable information about the nature of the transition, order parameter involved and coupling of the order parameter to different material parameters. The basic ideas of propagation of acoustic waves in glasses have been discussed by

172

many workers and are summarised by Landau and Lifshitz [1]. A considerable number of reports dealing with proagalion of acoustic waves in different kinds of glasses have been discussed in several books and articles [2,3,4,]. Generally, most of the glasses posses glass transition and crystallisation at different temperatures and some of them exhibiting semiconducting to metal transition at still another temperature. Even superconductivity in particular stoichiometry has been observed in some of them [5,6,7,8,9]. One can vary the value for the above temperatures by adding proper dopants atoms to the glass. To get a glass with superconducting properties, they should posses property such as phase purity, absence of defects, high density, chemical stability and oriented micro structured [10]

Besides these, the doping of foreign atoms at the electronically sensitive B site of the perovskite glass has dramatic effect on their electrical and structural properties [11]. This also causes change in the density of carrier localization which determine the nature of the semi conductor metal semi conductor as well as super conducting transition[12]. Several articles related to the structural, elastic and light scattering properties of oxide glasses during the last decade [2]. The Ba BiO$_3$ glass is a popular number of the perovskite glass family whose preparation, characterization and physical properties have already appeared in literature [5,13 ,14]. According to Cox and Sleight [22,16] the crystalline form of BaBiO$_3$ becomes rhombohedral at temperature below about 700K and monoclinic below 400K. The Monoclinic space group is C$_{2h}^3$ (C2/m). orthorhombic.

Because of their interesting electrical and structural properties, a number of glasses with different metals like K, Li, Rb as additives have been prepared. It has been reported that Pb doped BaBi O$_3$ glass with the formula BaPb$_{1-x}$Bi$_x$O$_3$ first in this group[6] (B). This system shows semi conducting properties only at high values of x (x>0.3). In the low value side (x<0.3) the system shows superconducting properties over the range x = 0.05 - 0.3 in the 20K temperature range. This behaviour has been explained successfully with the concept of Anderson localization. Usually Anderson localization occurs only when the density of localized carriers exceeds a critical value. The trend in the increase of charge localization is due to the presence of oxygen vacan-

cies. Suzuki etal have studied the effect of oxygen vacancies on carrier localization in $BaPb_{1-x}Bi_xO_3$ [13].

In another report, the reasons of semiconducting properties has been explained with electronic band structure calculation [14] which predict a single broad conduction band for $BaPb_{1-x}Bi_xO_3$ system,. This band originates from strong σ-antibonding combinations of Pb-Bi (6s) and O(2p) states.

This band is gradually filled in a rigid-band manner with increasing x until it is half filled in $BaBiO_3$. The strong coupling of the electronic states at ϵ_F to O band-stretching displacements lead to a commensurate charge density wave distortion. In this distortion O octahedra that surround neighbouring Bi sites are alternately expanded or compressed. This breathing type displacement of O octahedra opens a semiconductor gap over the Fermi surface which account for the semi conducting properties of $BaBiO_3$.

Another interesting system in this class is Ba_{1-x} Li_x $BiO_{3-\delta}$ glasses [15] These glasses are found to show very interesting semiconductor- metal-semiconductor transition above room temperature. This behavior has been attributed to the orientational motion of BiO_3/BiO_6 structural units present in the glasses. This rigid rotation is expected to produce small band shifts and splitting in the energy bands and anomaly in their specific heat values [14]. These phenomena possessed by this material leads to interesting ferroelectric, metal insulator, and even super conducting properties for it[14,15].

Several studies related to the dielectric and electrical conducting properties of such glasses have been carried out during last few years [12,15,17]. Among the $Ba_{1-x}K_xBiO_{3-\delta}$alloys is a notable one in the rapidly growing family of perovskite type compounds. From the early studies, it has been reported that [6] the unit cell structure of Ba BiO_3 perovskite is orthorhombic with a = 4.343Å, b = 4.358Å, and C = 4.333 Å. But Mattheiss et al [5] reported later that the structure of $BaBiO_3$ is monoclinic. Doping of K on the $BaBiO_3$ has drastic effect on its structural as well as electrical properties. According to Hinks et al [7] the system occurs in the degenerate orthorhombic structure with lattice parameters a = b = 6.117 Åand c = 8.647 Åat low concentration values of K. This structure is similar to the I2/m mono clinic cell of $BaBiO_3$ (which is

pseudotetragonal) orI 4/mcm tetragonal cell of super conducting $BaPb_{1-x}Bi_xO_3$. But at the high concentration values of K ($x > 0.25$), $Ba_{1-x}K_xBiO_{3-\delta}$occurs only in a cubic perovskite phase which is stable at $< 600°c$. Within this cubic phase the sample shows even superconductivity range in the 30K temperature range.

In a significant study made by Cava et al, $Ba_{1-x}K_xBiO_{3-\delta}$system has been obtained in a single phase form with reproducibility [8] from X ray diffraction results, it has been found that the lattice parameters of $Ba_{1-x}K_xBiO_3$ perovskite system are significantly smaller than that of $BaBiO_3$ and found to increase on annealing from 425°c (a_o =4.292 Å) to 475°C (a = 4.292 Å) due to an increased up take of oxygen at higher temperatures.

Most of the work on $Ba_{1-x}K_xBiO_{3-\delta}$glass (BKB glasses) have been carried out either at room temperature or at very low temperature. Since there is no data on elastic properties available at either low or high temperatures, it is thought worthwhile to investigate the elastic behaviour of the $Ba_{1-x}K_xBiO_{3-\delta}$glasses with different values of x.

In this chapter we report the results of our measurement of the elastic constants and ultrasonic attenuation in the range of temperatures at which semiconductor-metal- semiconductor (SMS) transition take place in these materials. A systematic study of the elastic behaviour of three glass compositions of the BKB system have been undertaken from 150K to 350K. To the least of our knowledge there is no other data available on the elastic properties of BKB glasses.

We have measured the longitudinal and transverse elastic constants of $Ba_{1-x}K_xBiO_{3-\delta}$glasses as a function of x, by varying x at the intervals of 0.2 from 0 to 0.4. The temperature variation of longitudinal ultrasonic velocity and attenuation at 10 MHz have also been measured in all the three samples from 150K to 350 K. Details of the experiment, results obtained and a discussion of the results are outlined below.

175

8.2 Experimental method

8.2.1 Sample preparation

The $Ba_{1-x}K_xBiO_{3-\delta}$ glasses were prepared by the quick quenching method. Appropriate amounts of $BaCO_3$, K_2CO_3 and Bi_2O_3, all of purity 99.99% (or better) were well mixd for each composition and then first sintered at 500°C for 10h. The sintered sample was melted at 1200°C for 1h (for each sample). The melt thus obtained was quickly quenched between two steel blocks at room temperature. The amorphous character of all the glasses were tested by X ray diffraction (XRD) method.

8.2.2 Elastic constants measurements

For the low temperature ultrasonic velocity and attenuation measurement a specially designed doubled walled crystal has been used. Liquid nitrogen has been used as cryogen for the low temperature measurements. The double wall portion of the cryostat is usually kept at moderate high vacuum in order to reduce the heat exchange from the surroundings from the sample chamber.

The size of the samples used in the measurements is approximately $1cm^3$ [cylindrical shape]. It is necessary that the cooling rate of the sample be small in order to avoid the cracking of the sample. Besides, if the cooling rate is high there will be temperature gradient within the sample which can cause many other distortions in the measurements. Thus a slow and uniform cooling necessary to get accurate readings.

To generate longitudinal and transverse waves X and Y cut quartz transducers with resonance frequency 10 MHz have been used. The transducers are gold plated with a annular ring type separation between the two electrodes. So that one can easily take both connections from its top side neglecting the thickness of the gold plating, there is only a thin layer of bond between the transducer and sample and this makes the bond correction technique in very effective. We have used silicon grease as the bonding material to carry out ultrasonic velocity measurement at low temperature up to 150K. For transverse velocity measurement at room and low temperatures, salol is found to be more effective.

176

Velocity of longitudinal and transverse ultrasonic waves propagating along at each of the glass samples have measured using the pulse echo overlap (PEO) technique using a MATEC 7700 pulse modulator and receiver system [18] as already described. The McSkimin Δt criterion [19] has been applied to correct for the phase lag due to the bonding medium on R F echoes. From the measured transit time, the velocity is evaluated knowing the length of sample. The overall accuracy in measured velocity values is of the order of 1%. From the measured longitudinal and transverse velocities, the corresponding elastic constant are determined from the relation $C_{ij} = \rho V^2$ where ρ is the density of the sample[23]. The density of the sample is determined from their mass and bulk volume. The ultrasonic attenuation in each sample has been measured by the pulse comparison technique from the decaying pulse pattern using the MATEC 2470B automatic attenuation recorder. Attenuation measurement have been carried out with longitudinal waves in the same temperature range as velocity.

8.3 Results

The concentration dependence of transverse elastic constants for $Ba_{1-x}K_xBiO_{3-\delta}$ glasses is shown in the Fig.8.1. The density and elastic moduli at room temperature for the samples studied are in Table 8.1.

The temperature variation of longitudinal elastic constant and attenuation of $Ba_{1-x}K_xBiO_{3-\delta}$ with x = 0, x = 0.2 and x = 0.4 between 150K and 350K are shown in the figures 8.2, 8.3 and 8.4. Elastic constant curve as well as attenuation curves show anomalies at particular temperatures for each specimen. The elastic constant shows a minimum value while attenuation shows a maximum value around this temperature. Even though the anomalies in elastic constants are very weak and difficult to notice, the changes in attenuation are sharp and show a peak at specific temperature.

8.4 Discussion

The room temperature elastic constant of $Ba_{1-x}K_xBiO_{3-\delta}$ are comparable to those of oxide glasses. But as the concentration of K increases, the values of elastic constants
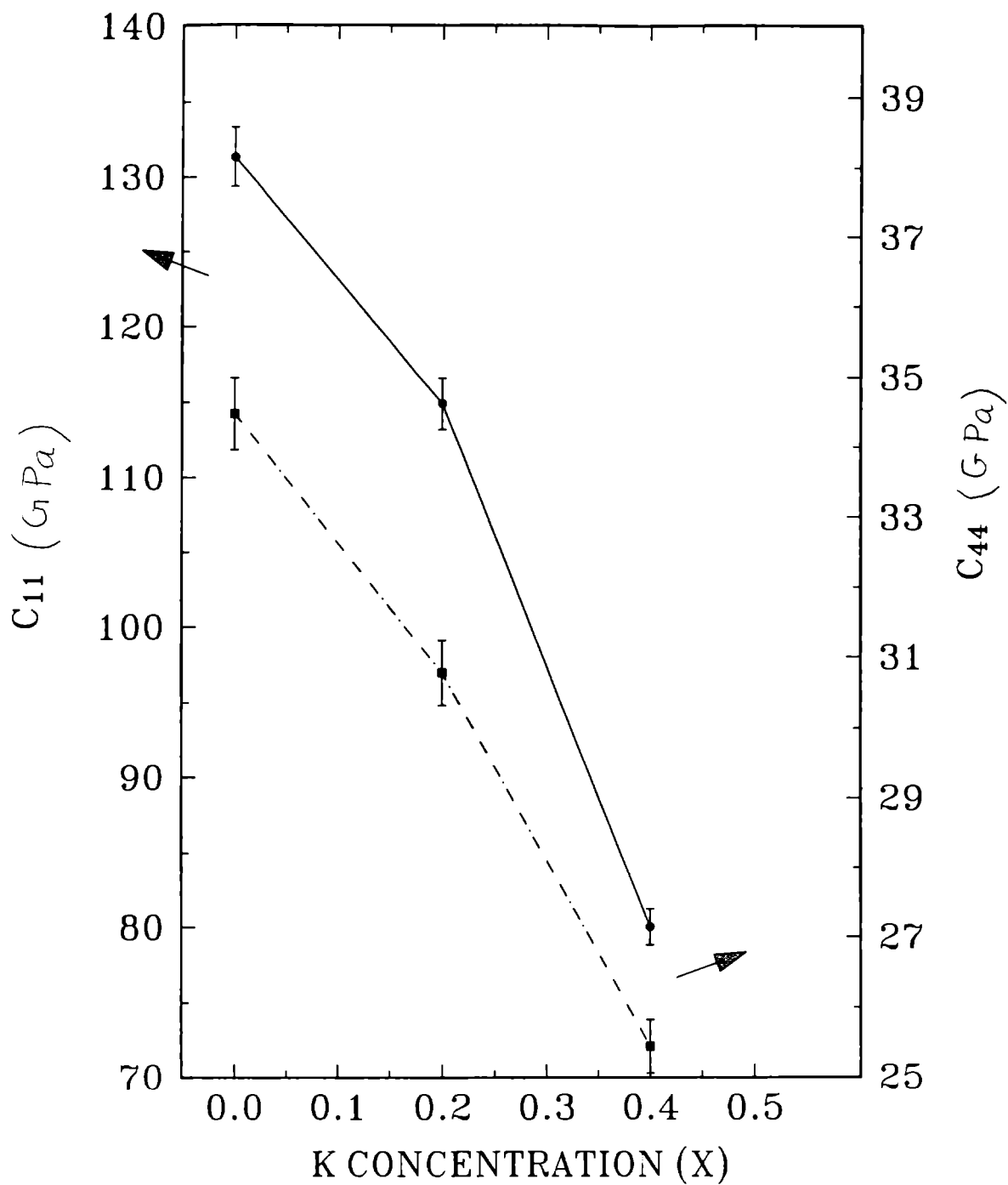
Fig. 8.1: Elastic constants C_{11} and C_{44} of three $Ba_{1-x}K_xBiO_{3-\delta}$ glasses with $x = 0$, 0.2 and 0.4
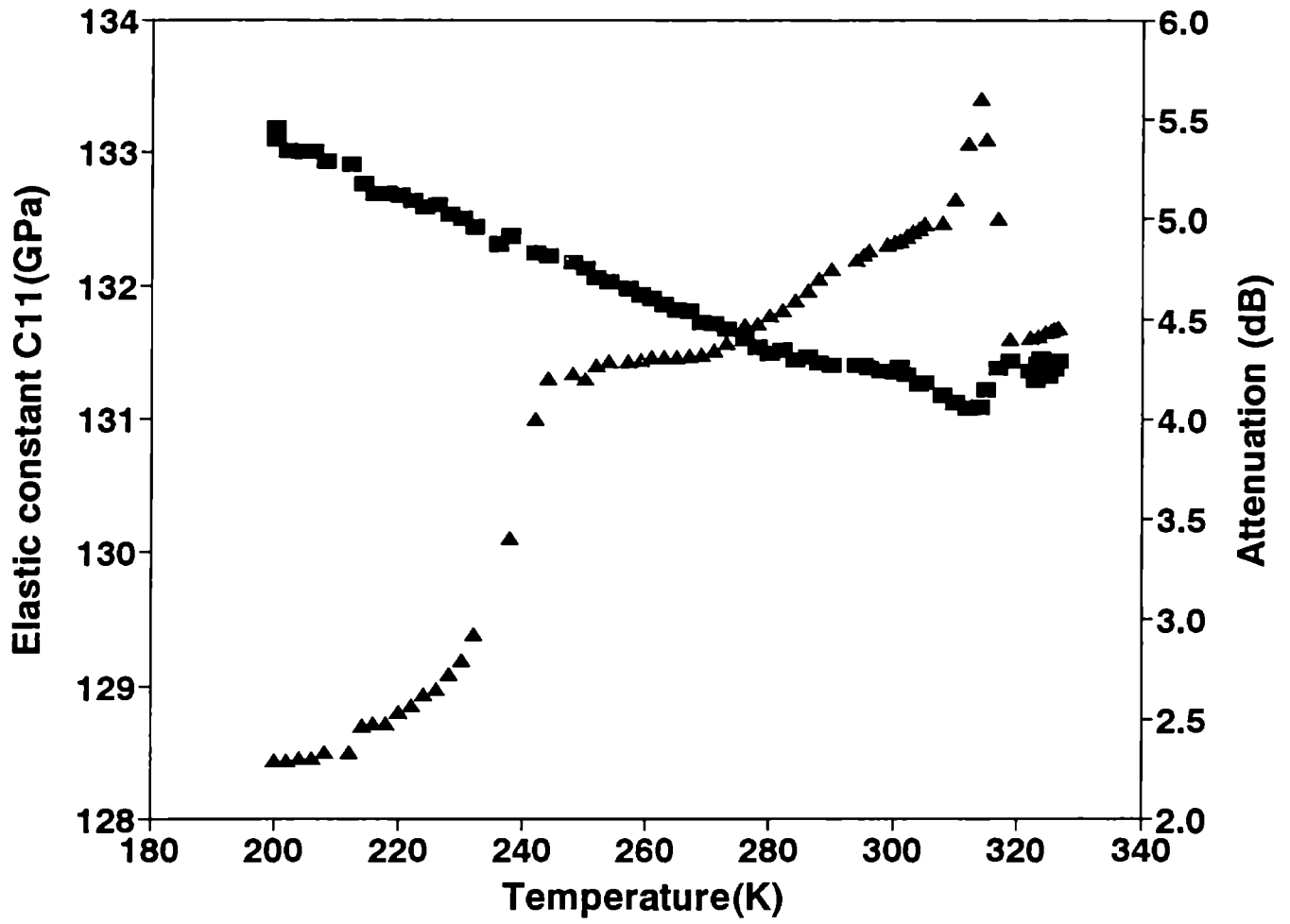
Fig. 8.2: Temperature variation of longitudinal elastic constant C_{11} and ultrasonic attenuation in Ba $BiO_{3-\delta}$ system
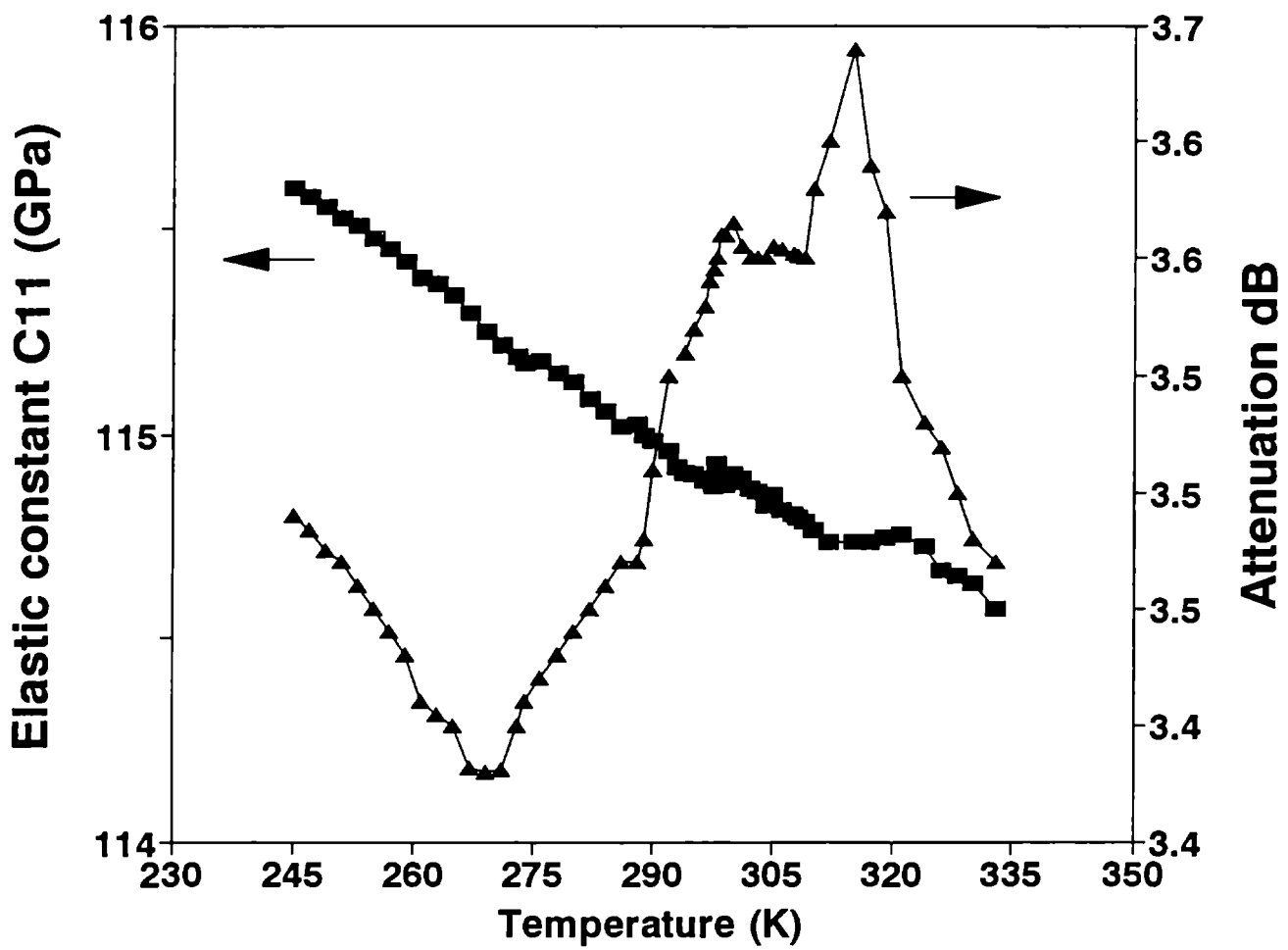
Fig. 8.3: Temperature variation of elastic constant C_{11} and ultrasonic attenuation in $Ba_{0.8}K_{0.2}BiO_{3-\delta}$ glass
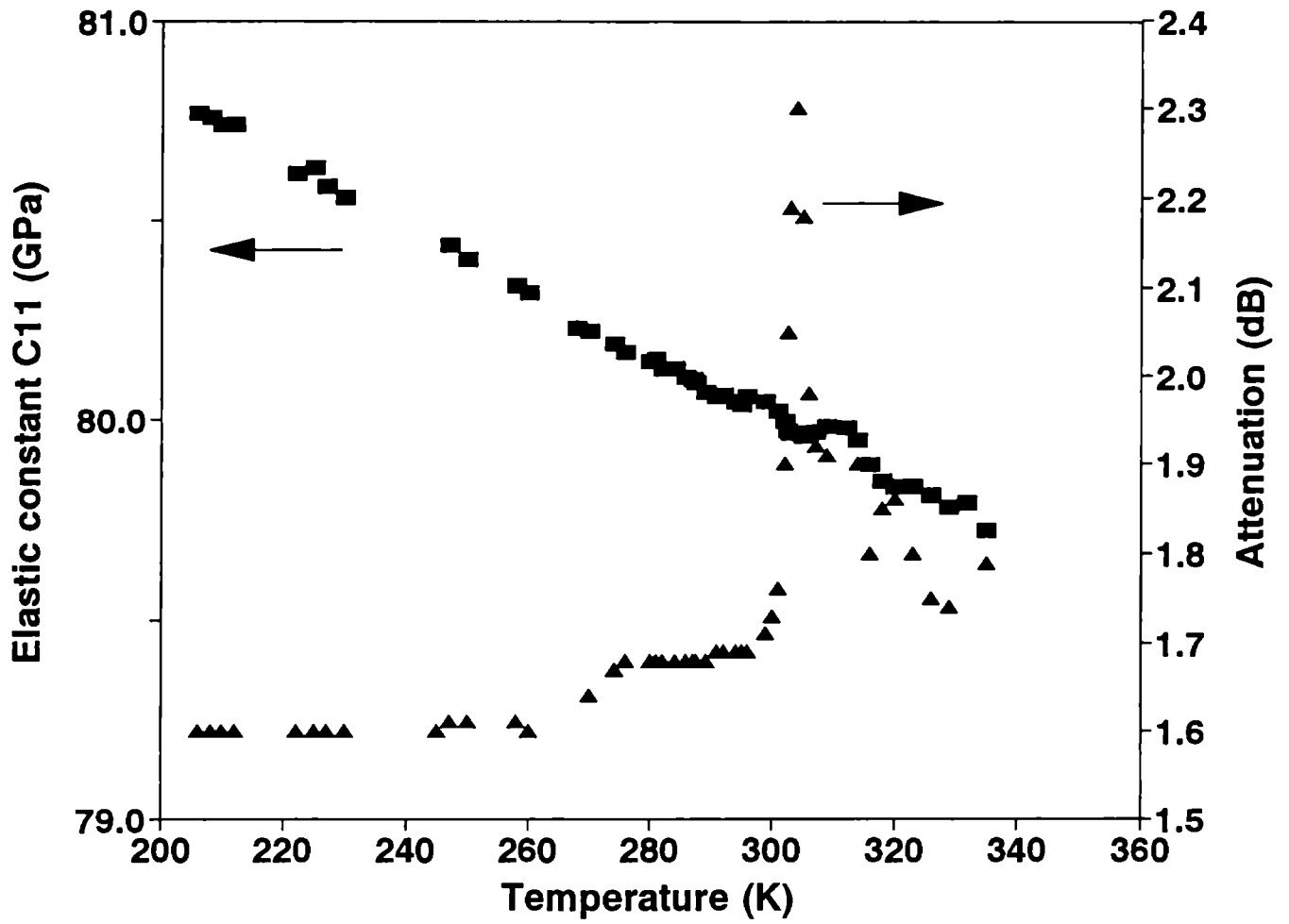
Fig. 8.4: Temperature variation of elastic constant C_{11} and ultrasonic attenuation in $Ba_{0.6}K_{0.4}BiO_{3-\delta}$ glass

decrease appreciably. It has been verified that the structure of single phase pure $BaBiO_3$ as monoclinic doping of K on this system causes considerable reduction in the density of the material which may be due to reduction in metallic species and a corresponding increase in the lattice parameters. Moreover, the strength of the interatomic forces decrease and the contration of potassium increase causing a corresponding reduction in the velocity of ultrasonic waves. A combined effect of the two is a substantial reduction in the values of the elastic constants as the x value increases.

A small dip in the elastic constant curve and a high peak in the attenuation curve for the three samples around 310K provide indications for structural transformation in these glasses. The values of transition temperature in each sample are in good agreement with the results obtained from dielectric constant and conductivity studies made by the other workers [12]. The reason of small anomaly in the temperature variation of elastic constant may be due to the weak coupling for the elastic strain to the order parameter. This coupling is very weak compared to a ferroelastic phase transition.

It has been proposed from different experimental results that the ordering quantity in the transition exhibited by BKB glasses is the rotation of the BiO_6 octahedra or the BiO_3 tetrahedral units around the transition temperature T_p. The rotational or orientationnal motion of the Bi_2O_3 structural units mentioned above give rise to structural instability of the glass network (as in ferroelectric crystals) in the presence of strong electron-phonon interaction in such a system. It has been pointed out that such an ionic or molecular motion can be responsible for lattice distortion leading to interesting ferroelectric, metal insulator, or even super conducting behaviour.

When a lattice distortion involving rotation of molecular or ionic groups occur which is coupled to the lattice strain, one can expect an elastic instability leading to the elastic constant tending to zero and ultrasonic attenuation tending to infinity [20] since the coupling here is weak, the decrease in elastic constant is not so significant, but the attenuation is still strong near T_p. In the case of BKB glasses it has been pointed out that there is an unusual local anisotrophy for the nonlinear electron-phonon interaction arising from the orientational motion of the ions or molecular units. This anisotropy leads to the reduction of a three-dimensional system to a pseudo-one dimensional system

182

as only one axis is lattice-dynamically relevant for the evolution of the polar state for a perovskite structure. The same nonlinear electron-phonon coupling plays an important role in driving the system to the super conducting state at low temperature. This aspect has not been considered in this work. Our results show that the BKB glasses is a good system which exhibit interesting transitions in which lattice distortion caused by orientational motion of the ions play an important role.

Table 7.1 Elastic constants C_{11}, C_{44} and density of three $Ba_{1-x}K_xBi_2O_{3-\delta}$ with x=0, 0.2, and 0.4

Glass composition	Density (Kg m^{-3})	Elastic Constant C_{11} (GPa)	Elastic Constant C_{44} (GPa)
$BaBiO_{3-\delta}$	8220	131	35
$Ba_{0.8}K_{0.2}BiO_{3-\delta}$	6886	115	31
$Ba_{0.6}K_{0.4}BiO_{3-\delta}$	4560	80	25

8.5 References

[1] L. D. Landau and E. M. Lifshitz, *Theory of Elasticity* (Pergamon Press, Oxford and NewYork) (1986).

[2] S. R. Elliot, *Physics of amorphous materials* 2nd ed. (Longman scientific & technical) (1990).

[3] W.A. Phillips (ed), *Amorphous solids* (Topics in current physics, vol. 24 Springer-Verlag) (1981)

[4] R. Zallen *The physics of amorphous solid* John Wiley & sons, NewYork (1983).

[5] L. F. Mattheiss, E. M. Gyorgy, and D. W. Johnson Jr., *Phy. Rev.* **37** 3745 (1988).

[6] A. W. Sleight, J. L. Gillson and P. E. Bierstedt *Solid State Commun.* **17** 27 (1975).

[7] D G. Hinks, B. Dabrowski, J. D. Jorgensen,A. W. Mitchell, D. R. Richards, Shiyou Pei and Donglu Shi *Nature* **333** 836 (1988).

[8] R. J. Cava, B. Batlogg, J. J. Krajewski, R. Farrow, L. W. Rupp Jr, A. E. White, K. Short, W. F. Peck and T. Kometani, *Nature* **332** 814 (1988).

[9] S. Mollah, K. K. Som, K. Bose and B. K. Chaudhuri, *J. Appl. Phy.* **74** 931 (1993).

[10] J. S. Luo. D. Michel and J. P. Chevalier, *Appl.Phys. Lett.* **55** 1448 (1989).

[11] F. S. Galasso *Structure, Properties and Preparation of Perovskite Type Compounds* (Pergamon Press New York) (1969).

[12] S. Mollah, A. K. Bera, S. Chakraborty and B. K. Chaudhuri, *Phy. Rev.* **B 49** 15017 (1994).

[13] M. Suzuki and T. Murakami, *Solid State Commun.* **53** 691 (1985).

[14] L. F. Matheiss and D. R. Hamann, *Phy. Rev.* **28** 4227 (1983).

[15] G. Banerjee, M. Sadhukhan, A. K. Bera, M. Karar and B. K. Chaudhuri,*Jourl. of Mat. Sci. Lett.* **15** 2008 (1996).

[16] D. E. Cox and A. W. Sleight, *Acta. Crystallogr.* sect. B **35** 1 (1979).

[17] A. K. Bera, G. Banerjee, A. K. Ghosh, D. K. Modak, S. Banerjee and B. K. Chaudhuri, *Phase Transitions* **51** 217 (1994).

[18] E. P. Papadakis in *Physical Acoustics* **12** ed W.P. Mason and R.N. Thurston (Academic press, NewYork) 1976.

[19] H. J. McSkimin *J. Acoust. Soc. Am.* **33** 12 (1961).

[20] K. A. Muller and H. Thomas *Structural Phase Transitions* (Spring- Verlag New York) (1981).

[21] R. Sreekumar, *Ph.D thesis*, Cochin University of Science and Technology (1993)

[22] D. E. Cox and A. W. Sleight, *Solid state Commun.* **19**, 969 (1976).

[23] B. A. Auld, *Acoustic fields and waves in solids* **Vol. 1** (John Wiley & Sons, New York 1973).

Chapter 9

Conclusions

In this thesis we have presented the work that has been carried out on the dielectric and elastic properties of few selected dielectric ceramics and oxide glasses. Eventhough ceramics are polycrystalline in nature, they are basically disordered and in that sense both the systems of samples we have investigated belong to the catagory of disordered solids. Eventhough microwave dielectric properties of these ceramics have been studied extensively, not much work has been done on their elastic properties, which determine the mechanical strength and stability of these materials. As a matter of fact, ours is the first series of measurements of the elastic constants and their variation with temperature reported on ceramic materials, which are extensively used as dielectric resonators at microwave frequencies.

Oxide glasses have been studied extensively during the past 60 years. The elastic as well as dielectric properties of different oxide glasses have been widely investigated. But recent work has shown that certain oxide glasses, particularly Bi_2O_3 glasses doped with transition metal oxides, rare earths oxides etc., show many interesting properties such as metal- semiconductor-metal transition and superconducting transition at low temperatures. Eventhough electrical transport as well as dielectric properties of many such glasses have been reported, no data could be found on the elastic constants of glasses such as $(CuO)_x$-$(Bi_2O_3)_{1-x}$ and $Ba_{1-x} K_x BiO_{3-\delta}$ in literature. Temperature variation of elastic constants and ultrasonic attenuation reported in this thesis throw light upon the transitons that these materials undergo upon heating.

We have prepared a variety dielectric ceramics following the conventional solid state reaction route in collabration with another research group. Considerable efforts

186

have been made to prepare well known ceramics with suitable additives to modify their properties. The work carried out on Sr doped $Ba_2Ti_9O_{20}$ and Hf doped $(Zr_{0.8} Sn_{0.2})TiO_4$ ceramics are good examples for this. Similarly, work has been done on Ba Ti_5O_{14} ceramics doped with different rare earths. The elastic properties of $(Ba_{5-x} Sr_x)Nb_4O_{15}$ ceramics in chapter 6, show a dependence of change in lattice parameter with Sr concentration which results in the rotation of NbO_6 octahedra. Our studies show that these materials have high dielectric constants and vary with different dopents and their concentration. Dielectric constant do not, in general, undergo any anamalous changes upon heating, but show significant hysteresis upon taking the sample through a temperature cycle. This has been attributed to the long dielectric relaxation times in these systems.

The absolute values of elastic constants are not so significant in the case of ceramics as these can vary with densification and packing efficiency. But, temperature variation of elastic constants reflect lattice instabilities and phase transformations that these materials undergo as temperature changes. Our results indicate that many of the ceramics undergo very weak phase changes upon heating which are reflected in ultrasonic velocity measurements. We have attributed this to phase change caused by coupling of the electronic states to the lattice strain.

Our work on the two oxide glass systems is even more significant as our measurements reveal clear phase changes in some of them at elevated temperatures. These are more predominant in ultrasonic attenuation measurements. The reults of our measurements would be very useful while modelling the structure of these glasses. In all the samples investigated in this thesis, the information provided would be very useful while selecting these materials for specific applications.

Only very limited data is available on the elastic properties of dielectric resonator ceramics. Since this data would be valuable from the application point of view, measurement of the elastic properties of other known ceramics need to be done. Another property that has not been investigated systematically is the thermal conductivity of these materials. Since thermal properties are related to elastic properties, both being related to atomic vibrations, systematic studies of these properties would be valuable for materials scientists and technologists. Further work in these directions would be

very useful.

Oxide glasses doped with different additives still remain mysterious owing to their anamalous properties. Elastic properties of only very few have been reported and there is plenty of scope for doing further work in this direction. The information collected from measurement of elastic constants and ultrasonic attenuation would provide valuable information in modelling of the structure of these materials and hence in understanding the mechanisms responsible for the anomalous properties such as metal-semiconductor and superconducting transitions exhibited by them. Moreover, oxide glasses are finding increasing number of applications. An understanding of the elastic and dielectric properties would be useful while selecting materials for specified applications. Preparation of newer and better materials is another challenging area of work. So there is plenty of scope for doing very exciting further work on oxide glasses as well.